# Optimization of the sizing and the energy management for a hybrid fuel cell vehicle including fuel cell dynamics and durability constraints

Ramon, Naiff Da Fonseca

Numéro d'ordre : Année 2013

# P H D THESIS

*to obtain the title of*

**Ph.D of Science**

**of the Institut National des Sciences Appliquées de Lyon-INSA Lyon**

Doctoral School: Electronics, Electrical, Automatic
Speciality: Energy and Systems

*defended by*

**Ramon Naiff da Fonseca**

---

# Optimization of the Sizing and Energy Management Strategy for a Hybrid Fuel Cell Vehicle Including Fuel Cell Dynamics and Durability Constraints

---

Defended in October 2013

Jury :

| | | |
|---|---|---|
| **Alexandre TROFINO** | Prof. UFSC Brazil | Reviewer |
| **Christophe TURPIN** | HDR, LAPLACE Lab. | Reviewer |
| **Rachid OUTBIB** | Prof., LSIS Lab. | Reviewer |
| **Eric BIDEAUX** | Prof., Ampère Lab. | Supervisor |
| **Mathias GERARD** | Ph.D, CEA-LITEN | Supervisor |
| **Luc LORON** | Prof., IRENA Lab. | Examinator |
| **Denis CANDUSSO** | Ph.D C.H., IFSTTAR-FCLAB | Examinator |
| **Bruno JEANNERET** | Research Engineer, IFSTTAR | Invited |
| **Matthieu DESBOIS-RENAUDIN** | Engineer, CEA-LITEN | Invited |
| **Ali SARI** | Ph.D MdC, Ampère Lab. | Invited |
| **Loic BOUILLO** | Engineer, Zodiac Aerospace | Invited |

«I believe that water will one day be employed as fuel, that hydrogen and oxygen which constitute it, used singly or together, will furnish an inexhaustible source of heat and light, of an intensity of which coal is not capable»

*Jules Verne, The Mysterious Island (1874)*

# Acknowledgements

Despite all the knowledge acquired and the results obtained, a doctoral work is not only constructed from the theories, equations, hypotheses and tests. During the three years of thesis, the collaboration and the friendly atmosphere with people and groups do not bring only scientific knowledge, but also personal contributions. Therefore, I would like to thank everyone that somehow allowed me to reach the end of this doctoral cycle.

Firstly to my supervisors: Mr. Eric Bideaux, Mr. Mathias Gerard, Mr. Bruno Jeanneret, Mr Matthieu Desbois-Renaudin et Mr. Ali Sari. Thank you for believing in my potential and to share with me your wisdom from the first discussions until the final stages of this thesis. I would like to emphasize that the obtained results were possible thanks to the generosity of each one to contribute with your experiences.

I also thank the members of the jury that allowed me part of their time to understand the developments proposed in this document and lead me to improve it with their questions, comments and relevant observations.

Afterwards, I would like to highlight that during these three years of thesis I had the opportunity and the pleasure to be part of the three different laboratories workgroups: Ampère, LTE and LIGE. The presence in each one brought me not only technical-scientific knowledge, coming from the brilliant people who integrate them, but rather brought me friends that I will take with me forever.

Even though I can not name everyone who participated of my thesis (I apologize in advance to those who were not mentioned), I could not avoid to thank the friendship of my office friends at the Ampère Laboratory: Lu Hao and Ahmed Redha.

I also thank the friends I made during my period in CEA. My friend Hortense Laforet that is strongly responsible for my current French level. Besides, I would like to thank my squash and happy hour fellows: Pascal Martin, Anthony Barre, Yanick Meynet and Christophe Robin. Their friendship allowed me feel welcomed in their country as if I was in mine.

I could not forget the two people of the LTE that are fundamentally important during my doctoral life. First of all a special thanks to Pascal Gastineau for the important

discussions about work and the most important yet about football, talking parrots and French administration!! And a «huge» thanks to my friend in this doctorate and for the rest of the life, Felicitas Mensing. The path up to this final point was not easy, but her singular support and her extreme knowledge about «Paint» made everything more enjoyable!! And what I can tell you Feli is «bref on a fait une thèse».

I want to make an important acknowledgement to my friends Jun Young Bae and Betul Aydin, who started this French journey with me in 2008 and that always showed a unique friendship.

Finally, I take this opportunity to thank the persons who are the most important not only in this PhD, but in my whole life that are my family. Therefore, I apologize to the reader for the change of language, but this acknowledgement would not have the real meaning if it is not presented in the form that they could understand:

Muito obrigado ao meu pai Lucival Rodrigues da Fonseca e minha mãe Eleonora Maria Naiff da Fonseca pelo apoio incondicional às decisões difíceis que tomei, pela criação fundamentada no caráter exemplar de vocês e pelo carinho que nunca foi pouco. Ao meu irmão e melhor amigo não somente agradeço pelo seu apoio e exemplo de força, personalidade, caráter e amizade, mas afirmo que este agradecimento reflete a divida de gratidão fundada nestas qualidades que quero manter pra sempre, quero ser sempre grato à você!! Deixo também um agradecimento à toda minha família (tios, tias, primos, primas, avô e avós) que sempre estiveram ao meu lado onde quer que eu estivesse, em especial à grande amiga Cristiane Pereira de Jesus Naiff e à minha prima e cúmplice Fabíola Simões Fonseca.

Finalmente, obrigado à Deus por me permitir realizar os meus sonhos, pois sem ele não seria possível.

# Résumé

L'hydrogène à travers de l'utilisation des piles à combustible (PAC), est de plus en plus considéré comme une option énergétique possible au secteur des transports grâce à ces caractéristiques fonctionnelles. Cependant, la technologie liée à la mise en œuvre de véhicules alimentés par une pile à combustible n'a pas encore atteint le niveau de maturité requis. Ainsi, ce travail propose de traiter certaines de ces limitations qui existent encore. Plus précisément, trois thèmes représentent les objectifs de ce travail:

- Le dimensionnement optimal des éléments présents dans un véhicule hybride à pile à combustible.
- La gestion d'énergie optimale pour les applications en temps réel et intégrant les contraintes dynamiques du système PAC.
- Inclusion de la durabilité de la pile à combustible dans la gestion d'énergie du véhicule.

Le premier thème est abordé à travers l'élaboration d'une méthodologie de dimensionnement adapté à un véhicule hybride à la pile à combustible. Dans une approche systématique, le dimensionnement proposée combine les exigences de performance présents dans les spécifications techniques du véhicule, les algorithmes d'optimisation, l'analyse de la mobilité de la population et la viabilité économique de la conception.

Le deuxième objectif établi a été développé à l'aide d'une approche d'optimisation de la répartition de puissance entre la batterie et le système PAC. Par l'adoption d'une méthode d'optimisation globale combinée à une stratégie de commande prédictive et l'inclusion de la dynamique du système PAC, un algorithme de gestion d'énergie pour des applications de temps réel a été conçu.

Enfin, la durabilité de la pile à combustible a été incluse dans ce travail par l'intégration de sa dynamique de dégradation dans le problème d'optimisation lié à la gestion d'énergie. Cette dynamique représente une contrainte à prendre en considération lors de la répartition de puissance entre le système PAC et la batterie.

# Abstract

The hydrogen, through the use o fuel cell stacks (FC), has been increasily considered as an energy possible option for the transport sector. Nevertheless, the technology related to its implementation in fuel cell vehicles has not reached the required maturity level. Therefore, this work intends to deal some of these existing limitations. More precisely, three topics represent the objectives of this work:

- The optimal sizing of the element present in the fuel cell hybrid vehicle
- The development of an optimal energy management strategy oriented for real time applications and including the dynamic constraints of the FC system.
- The inclusion of the fuel cell durability in the vehicle energy management strategy.

The first topic is tackled by the development of a sizing methodology adapted to the fuel cell hybrid vehicle application. Using a systematic approach, the proposed sizing method combine the performance requirements present in the vehicle's technical specifications, optimization algorithms, population mobility behavior and the economic viability of the design.

The second assigned objective was developed using an optimization approach for the power split between the battery and the FC system. Through the adoption of a global optimization method allied with a predictive control strategy and the inclusion of the FC system dynamics, it was created an energy management algorithm oriented for real time applications.

Finally, the fuel cell durability was included in this work by the integration of its degradation dynamics in the optimization problem, which is related to the vehicle's energy management. Such dynamic represents a constraint that should be taken into account in the power sharing between the FC system and battery

# Synthèse du travail

Le modèle énergétique actuel basé sur l'utilisation de sources d'énergie non renouvelables est économiquement et écologiquement discutables et fait l'objet de discussions au cours de ces dernières années. L'augmentation de la consommation d'énergie et donc les émissions de polluants, démontrent les limites de ce modèle énergétique et ne peut donc pas être soutenu à moyen et long terme sans impact majeur sur l'environnement et le développement mondial.

Dans ce contexte, le secteur des transports, qui est responsable d'une importante part de la consommation énergétique mondial 27 % [67], étudie activement depuis ces 20 dernières années, des solutions propres et durables pour augmenter le mixte énergétique. La présence de véhicules hybrides, à propulsion électrique et à l'éthanol dans le marché automobile sont des exemples réussis de cette recherche. Néanmoins, ces différentes solutions sont destinées à des marchés de niche et ne sont adaptées à certains environnement socio-économiques.

L'hydrogène comme vecteur d'énergie pour le transport, et valorisé par des piles à combustible (PAC), est mis en évidence de plus en plus comme une solution prometteuse en raison de ses caractéristiques fonctionnelles, de performance (rendement supérieur à 50 %) et environnementales (aucune émissions de polluants par le véhicule).

Cependant, l'introduction de l'hydrogène dans le secteur des transports à travers des véhicules à pile à combustible est toujours confrontée à diverses contraintes telles que le coût (du système pile à combustible du véhicule et de l'hydrogène) mais surtout des infrastructures nécessaires pour la production, le transport et la distribution de l'hydrogène. En outre, la technologie liée à la mise en œuvre de véhicules propulsé par une pile à combustible n'a pas encore atteint le niveau de maturité que d'autres solutions du secteur des transports. Certaines différences notables peuvent être observées à travers la durabilité et le coût du système pile à combustible.

Selon le DOE (Department of Energy des USA) [92], le véhicule à pile à combustible (VPAC) doit être compétitif par rapport aux technologies concurrentes présentes dans les moyens de transports actuels. Par conséquent, des objectifs de commercialisation à

atteindre dans le processus de l'élaboration du VPAC ont été établis. A titre d'exemples, la PAC devant atteindre un coût de $30\,\$/kW$ en 2017 et une durée de vie de 5000 heures (équivalent à 241.000 km). A titre de comparaison, afin d'amorcer le marché, les constructeurs visent un prix d'un VPAC similaire à un véhicule hybride diesel.

Pour atteindre ces objectifs et améliorer les performances du véhicule, les constructeurs automobiles adoptent des architectures hybrides contenant système PAC et batterie. La présence de cet élément de stockage (batterie) apporte un degré de liberté dans l'utilisation de la PAC et permet de contrôler certaines conditions défavorables au fonctionnement de la PAC : performances (consommation d'hydrogène) et durabilité. Cependant, l'hybridation apporte une complexité du contrôle de puissance entre les deux éléments (SPAC et batterie), qui doit être résolu par une stratégie de gestion d'énergie embarquée dans le véhicule.

Afin de contribuer à l'avancement de cette technologie présente dans les véhicules hybrides à pile à combustible (VHPAC), ce document vise à proposer des solutions pour répondre à certaines limitations de cette technologie. Plus précisément, trois thèmes constituent les objectifs de ce travail:

- Le dimensionnement optimal des éléments de la chaine énergétique présents dans un véhicule hybride à pile à combustible.

- La gestion d'énergie optimale pour les applications en temps réel et intégrant les contraintes dynamiques du système PAC.

- La prise en compte de la durabilité de la pile à combustible dans la gestion d'énergie du véhicule.

En raison de ces objectifs, il est tout d'abord nécessaire de présenter une description des élements importants du VHPAC et de l'hybridation, puis d'élaborer des modèles de ces élements du véhicule adaptés à nos objectifs et à l'utilisation des méthodes d'optimisation pour la synthèse de la stratégie de gestion de l'énergie.

Ainsi, le type de VHPAC est mis en oeuvre présenté à travers de ses principales caractéristiques, puis les modèles et les méthodes d'optimisation utilisées dans les tâches de dimensionnement, de gestion d'énergie et de gestion de la durabilité sont présentés. Finalement, ces différentes contributions sont décrites afin de montrer les principales caractéristiques des solutions proposées.

# VHPAC: caractéristiques et fonctionnalités

Dans le processus d'hybridation d'un système PAC et d'une batterie dans un véhicule, il est necéssaire de choisir un type d'architecture et les prestations et fonctionnalités désirées. Il existent différents types d'architecture de véhicule hybride (série, parallèle et série-parallèle). Celle qui est la plus souvent adoptée pour un VHPAC est l'architecture hybride série (figure 0.1).

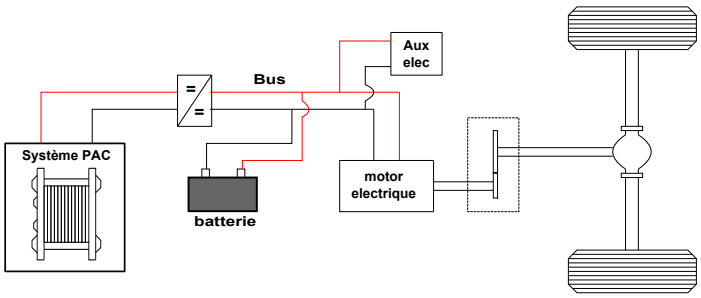


**Figure 0.1**: Architecture série pour un véhicule hybride à pile à combustible

Une architecture hybride série possède qu'un élément de traction (moteur électrique dans le cas d'un VHPAC). Pendant la phase de freinage, la puissance mécanique est convertie en puissance électrique par le moteur électrique et est stockée dans la batterie. Tandis que pendant la traction, la puissance électrique demandée est fournie par le système PAC et/ou batterie. Cette gestion de la puissance doit être faite dynamiquement pour profiter au maximum de l'énergie de freinage et de la meilleure région de rendement du système PAC.

Une caractéristique importante de cette architecture vient du découplage entre la dynamique de puissance imposée par le véhicule et la dynamique du système PAC. Cet aspect permet à la PAC de travailler dans son meilleur domaine de performance tandis que les batteries donnent la composante dynamique de la puissance suivant des contraintes de taux maximales de charge et décharge et des états de charge minimals et maximals.

Concernant les fonctionnalités possibles pour ce type d'architecture, il y existe six différentes fonctionnalités: μhybrid, mild-hybrid, full-hybrid, plug-in hybrid et range extender. Notre travail s'est concentré sur une fonctionnalité full hybrid du véhicule. Le full-hybrid apporte des modes de fonctionnement comme le "start/stop", le "power boost" et en plus autorise que la puissance de traction soit fournie uniquement par la batterie. Néanmoins, comme dans cette fonctionnalité la batterie ne peut pas être rechargé par le réseau électrique, il est imposé en mode d'assistance électrique où l'état d'énergie d'une batterie doit être le même (ou proche) au début et à la fin d'un cycle de roulage.

Le choix de l'architecture et des fonctionnalités ayant été retenus, les éléments qui composent cette architecture sont maintenant présentés.

## Chaîne de traction

Comme illustré dans la figure 0.1, la chaine de traction du véhicule est composée d'un moteur électrique et d'un réducteur. Une machine synchrone a été choisie dans ce travail et le réducteur est considéré comme un élément de conversion de puissance avec un rendement constant.

## Batterie et système pile à combustible

Concernant les composants responsables de la fourniture de la puissance électrique, les technologies considérées comme les plus adaptées pour les application véhicules sont les batteries $LiFePO_4$ et les piles à combustible PEMFC (Polymer Electrode Membrane Fuel Cell).

### Batteries $LiFePO_4$

Les batteries $LiFePO_4$ possèdent un compromis intéressant entre densité de puissance et densité d'énergie (pouvant être déchargés à $10\,C$ et chargés à $-3\,C$) et la sécurité [49]. En plus, la caractéristique en tension de ces batteries donne une grande région de stabilité (peu de variation avec les changements de courant, température et état d'énergie).

### Système PAC

Le système pile à combustible est composé de sous systèmes. En effet le stack de la PAC doit être en permanence allimenté par les gaz réactifs et refroidi. Les sous systèmes sont le groupe air, le groupe hydrogène, le groupe thermique et le groupe gestion électrique. La figure 0.2 donne une vision générale de ce système.

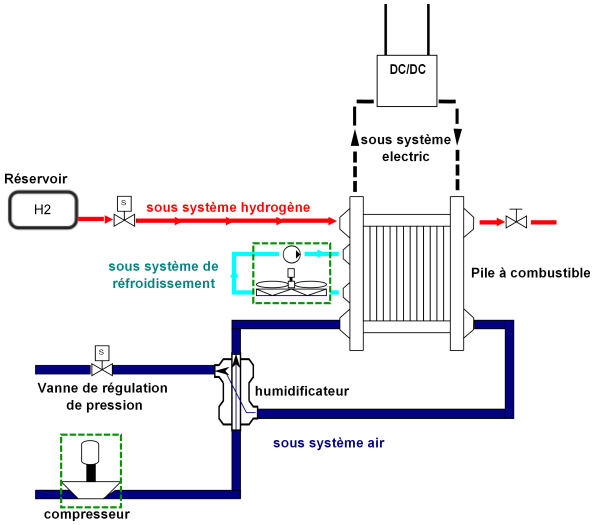


**Figure 0.2:** Système pile à combustible

**Pile à combustible** Le principe de fonctionnement d'une pile à combustible est basé sur des réactions d'oxydation et de réduction au sein de la pile (1). Les réactions entre l'hydrogène $H_2$ et l'oxygène $O_2$ se produisent par une réaction électrochmique pour créer de l'électricité, de l'eau $H_2O$ et de la chaleur.

$$\begin{aligned} Anode: \quad & H_2 \longleftrightarrow 2H^+ + 2e^- \\ Cathode: \quad & \tfrac{1}{2}O_2 + 2H^+ + 2e^- \longleftrightarrow H_2O \\ \cdots\cdots & \cdots\cdots\cdots\cdots\cdots\cdots\cdots\cdots\cdots\cdots \\ & H_2 + \tfrac{1}{2}O_2 \longleftrightarrow H_2O \end{aligned} \tag{1}$$

La structure élémentaire est composée de couches actives (anode et cathode), d'une membrane et de couches de diffusion. L'ensemble est nommé Assemblage Membrane Electrode (AME).

La réponse en tension de la pile est fonction de la demande de courant et de ses conditions de fonctionnement en termes de ses variables d'état (pressions, température, stoechiométrie et humidité) (2).

$$U_{PAC} = f\left(p_{cath}, p_{an}, St_{O_2}, St_{H_2}, T_{PAC}, H_r\right) \tag{2}$$

Par conséquent, le pilotage de ces variables a un effet important sur la réponse de la PAC, justifiant l'intérêt de l'étude des sous systèmes autour de la PAC. L'architecture des sous systèmes retenus dans ce travail est :

**Sous système hydrogène** L'objectif principal de ce sous système est de contrôler et de réguler le débit (stoechiométrie $St_{H_2}$) et la pression ($p_{an}$) de l'hydrogène dans la cellule. Ceci se fait à partir du pilotage entre les deux valves présentes dans le circuit (fig. 0.2).

**Sous système air** Comme dans le cas du sous système hydrogène, ce sous système contrôle et régule le débit (stoechiométrie $St_{O_2}$) et la pression ($p_{cath}$) de l'air dans la cellule. Les éléments qui composent ce circuit sont, les plus souvent, un compresseur d'air, un humidificateur et une vanne de régulation de pression. Le contrôle du débit d'air est effectué par le compresseur, tandis que la vanne de régulation de pression en sortie pilote la pression de la cathode. L'humidificateur est utilisé pour humidifier l'air à l'entrée de la cathode afin d'augmenter les performances et durabilité de la pile. Dans cette étude un humidificateur passif par diffusion de l'eau de l'air humidifié en sortie via l'air sec en entrée est utilisé.

**Sous système de refroidissement** Comme la réaction électrochimique de la PAC est exothermique, un circuit de refroidissement est nécessaire pour réguler la température et évacuer le flux de chaleur créé. Ce circuit est normalement composé d'un radiateur, d'une vanne thermostatique et d'une pompe à eau. La régulation de température de la pile est faite à partir de la vanne et d'un ventilateur au niveau du radiateur.

**Sous système électrique** Ce sous système constitue l'interface entre le bus électrique et la PAC. Un convertisseur DC/DC irréversible est utilisé pour cette interface et permet la régulation de courant.

Après avoir présenté les principales caractéristiques du VHPAC, la section suivante présente les modèles et les méthodes d'optimisation utilisés dans chaque partie de ce travail.

# Modèles et méthodes d'optimisation utilisés

Chaque objectif de ce travail nécessite d'outils et des modèles adaptés aux problèmes posés. Dans cette section, nous allons maintenant présenter les outils (modèles et algorithmes d'optimisation) utilisés dans la suite du mémoire.

## Outils pour le dimensionnement optimal du VHPAC

Dans la méthode de dimensionnement du véhicule, les différents éléments de la chaine de traction et des sources de puissance (système PAC et batterie) sont soumis à des

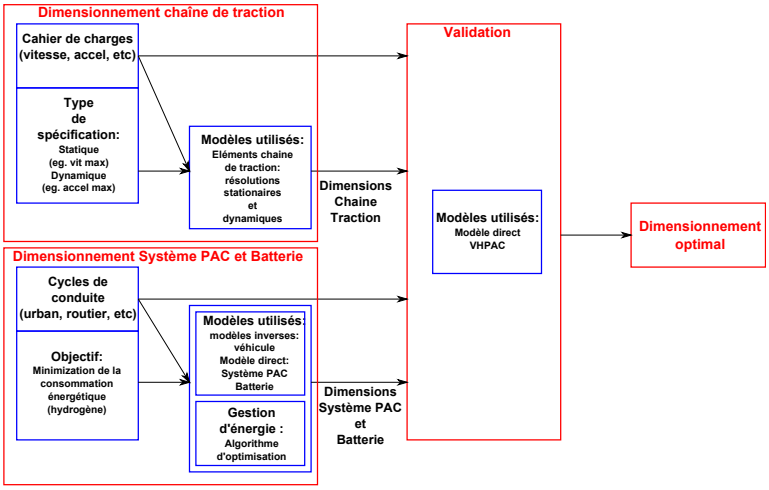


**Figure 0.3**: Méthode de dimensionnement du VHPAC

contraintes et critères afin d'obtenir le dimensionnement optimal pour l'application. Des modèles et algorithmes spécifiques sont donc nécessaires. Par exemple, les éléments de la chaîne de traction sont dimensionnés pour atteindre les performances établies par un cahier des charges et des spécifications techniques comme la vitesse maximale, l'accélération maximale, tandis que les sources de puissance doivent respecter des critères d'optimisation permettant de déterminer le taux d'hybridation présentant le meilleur choix en termes de réduction de consommation d'hydrogène par exemple.

La figure (0.3) synthétise le processus de dimensionnement à partir des outils requis à chaque étape.

**Modèles pour le dimensionnement de la chaîne de traction** Le schéma de la figure (0.3) montre que pour le dimensionnement de la chaîne de traction, nous allons utiliser les spécifications caractéristiques de performance stationaire et dynamique, ce qui nécessite des modèles directes du véhicule et de la chaîne de traction.

Dans notre cas, on appelle modèle direct des modèles qui ont à l'entrée la demande du conducteur (ou cycle de conduite) et comme sortie la vitesse et/ou accélération du véhicule.

Par conséquent, les modèles du véhicule, réducteur et moteur électrique ont été construits à partir de la dynamique associée à chaque élément. La dynamique du véhicule permet d'aboutir à l'équation (3). D'autre part, le réducteur est modélisé par un gain avec un rendement fixe et le moteur électrique par une représentation quasi-statique qui combine une cartographie de pertes avec une inertie mécanique.

$$\frac{dv}{dt} = \frac{F_{traction} - F_{resistance}}{M} \tag{3}$$

**Modèles et algorithmes pour le dimensionnement du système PAC et batterie**
La définition du taux d'hybridation (dimensionnement du système PAC et batterie) se base sur un modèle inverse du véhicule et les caractéristiques énergétiques/puissance des systèmes PAC et batterie.

Contrairement au modèle directe, le modèle inverse a pour entrée le profil vitesse du véhicule et comme sortie la puissance électrique demandée pour que le véhicule suivre la trajectoire imposée. Le modèle du véhicule et des éléments de la chaîne de traction sont donc simplifiés (dynamique simplifié) en vue de l'inversion.

A partir de la puissance électrique demandée ($P_{vehicule}$) calculée par le modèle inverse, l'optimum du taux d'hybridation est determinée en utilisant un algorithme d'optimisation qui évalue la répartition de puissance optimale entre le système PAC et batterie. Le critère appliqué cherche à trouver la répartition qui minimise la consommation d'hydrogène pour un cycle de conduite.

Comme l'objectif de cette optimisation est dédié aux aspects énergétiques, et donc les modèles du système pile et batterie peuvent être simplifiés sont simplifiés (les dynamiques étant considérés comme négligeables) tout en conservent l'information de consommation énergétique.

Concernant l'algorithme d'optimisation, la méthode de la programmation dynamique [122, 106, 39] a été choisie pour cette tâche de dimensionnement. Dans cette méthode, l'optimisation est faite par la résolution numérique d'un graphe qui réprésente le problème d'optimisation. La problématique spécifique du VHPAC peut être défini par le problème d'optimisation suivant (4):

$$\begin{cases} Minimisation\,du\,critère: \\ \\ \mathbf{J}\left(P_{PAC}^{*}\right) = min_{P_{PAC}^{*}} \int_{0}^{t_f} g\left(P_{PAC}\left(t\right)\right).dt \\ \\ P_{PAC}^{*} = argmin\mathbf{J}\left(P_{PAC}\left(t\right)\right) \\ \\ \hline \\ Contraintes: \\ \\ P_{batt\,min}\left(-3C\right) \leq P_{batt} \leq P_{batt\,max}\left(10C\right) \\ \\ P_{PAC\,min} \leq P_{PAC} \leq P_{PAC\,max} \\ \\ SoE_{min}\left(40\%\right) \leq SoE \leq SoE_{max}\left(80\%\right) \\ \\ Condition\,limite: \\ \\ SoE\left(0\right) = SoE\left(t_f\right) \end{cases} \tag{4}$$

La résolution de ce problème vise à déterminer le profil de la puissance du système PAC $P_{PAC}^{*}$ qui minimise le critère de consommation d'hydrogène $g\left(P_{PAC}\left(t\right)\right)$ sur un cycle de conduite. Néanmoins, la solution du problème doit prendre en compte certaines contraintes et conditions limites liées aux éléments et aux fonctionnalités du véhicule. Par exemple, l'état énergétique ($SoE$ - State of Energy) de la batterie doit respecter certaines limites et conditions représentatives du mode d'assistance électrique choisi comme $SoE\left(0\right) = SoE\left(t_f\right)$.

Malgré le temps de calcul important, la quantité de mémoire nécessaire et le besoin de connaitre à priori le cycle, la programmation dynamique permet un calcul déterministe de l'optimum global, requis par l'approche de dimensionnement. Elle est donc adaptée à ce problème d'optimisation hors ligne.

**Validation du dimensionnement** Les outils utilisés dans cette partie du processus de dimensionnement sont les modèles de chaque composant du véhicule. Comme l'objectif de cette étape est de vérifier si le dimensionnement déterminé permet d'atteindre les spécifications techniques, un modèle dynamique direct est adopté.

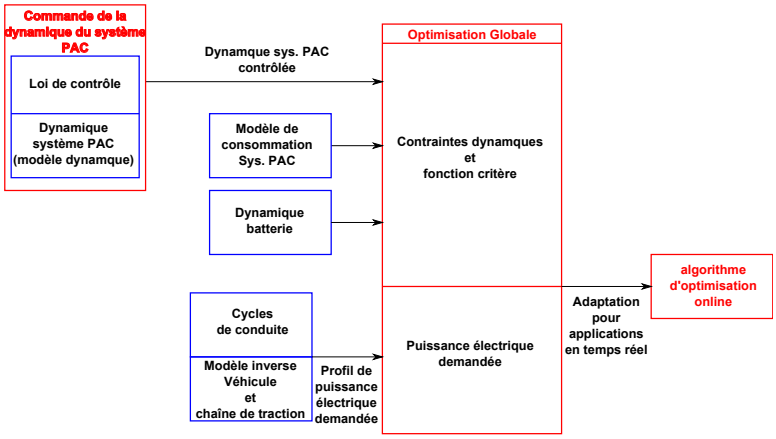


**Figure 0.4:** Structure pour le développement de la gestion d'énergie en ligne

## Outils pour le développement de la loi de gestion d'énergie temps réel

Le deuxième objectif de ce travail vise à proposer une loi de gestion d'énergie optimale pour une application en temps réel. La figure (0.4) résume les outils utilisés pour cet objectif.

Comme ce travail propose comme noveauté l'intégration de la dynamique du système pile à combustible comme une contrainte du problème d'optimisation, permettant d'adapter la répartition de puissance en fonction de la dynamique du SPAC, cette dynamique doit être, premièrement définie et stabilisée par une commande locale. Un modèle dynamique du système pile à combustible est donc utilisé pour valider les lois de commande afin d'observer l'évolution dynamique des variables d'état de la pile à combustible.

L'autre partie du schéma de la figure 0.4 illustre la démarche d'optimisation globale en temps réel. Cette étape n'utilise pas la programmation dynamique. En effet le calcul d'optimisation doit être rapide et utiliser moins de mémoire et accepter facilement l'introduction d'autres contraintes dynamiques. De plus, nous désirons que la solution puisse être mise sous une forme analytique pour simplifier l'implémentation dans un système réel. Pour effectuer une optimisation gloable au même titre que la programmation dynamique, le Principe du Maximum de Pontryaguine (PMP) [39] est appliqué.

Le PMP fait partie des méthodes variationnelles utilisées pour optimiser un processus. En termes d'implémentation, la minimisation du critère **J** pour un système avec une dynamique $\dot{x} = f\left(x\left(t\right), u\left(t\right), t\right)$ est faite en utilisant un co-état $\lambda_i$ pour chaque dynamique. Une représentation avec un Hamiltonien (5) permet de résoudre le problème d'optimisation en appliquant les conditions données en (6).

$$\mathcal{H}(x,u,\lambda,t) = \lambda.f(x,u,t) - g(x,u,t) \tag{5}$$

$$\mathcal{H}_u(x,u,t) = 0\,;\ \dot{x} = \mathcal{H}_\lambda\,,\ \dot{\lambda} = -\mathcal{H}_x \tag{6}$$

En utilisant une fonction de consommation d'hydrogène quadratique comme proposé par Bernard et al. [21] ($g(P_{PAC}) = a_1 P_{PAC}^2 + a_2 P_{PAC} + a_3$), le bilan de puissance du véhicule ($P_{vehicule} = P_{PAC} + P_{batt}$) et de la dynamique d'état d'énergie de la batterie (7) sont donnés par la solution analytique du problème d'optimisation par (8).

$$SoE = 100\left(\frac{\varepsilon}{\varepsilon_{max}}\right);\quad \varepsilon = \int P_{batt}dt \tag{7}$$

$$P_{batt}^*(t) = \frac{\lambda + (2a_1(P_{vehicule}(t)) + a_2)}{2a_1} \tag{8}$$

Cette solution est une forme analytique dépendant du co-état $\lambda$, qui ne possède pas de valeur initialement connue. Cette problématique du choix de $\lambda$ sera traitée dans les sections suivantes.

# Dimensionnement optimale du véhicule hybride à pile à combustible

Le but de cette section est de présenter la méthodologie proposée pour le dimensionnement d'un VHPAC. La méthode est basée sur utilisation des différents critères comme par exemple un cahier des charges se référant aux spécifications techniques du véhicule. Néanmoins, pour définir ce cahier de charges, il faut établir les fonctionnalités et la plateforme du véhicule.

Comme dans ce travail le mode "full hybrid" est adopté, certaines contraintes sont intégrées au cahier des charges. La condition $SoE(0) = SoE(t_f)$ et le mode de traction utilisant seulement le système pile (110 km/h à 5 % de pente) sont des exemples de contraintes spécifiques à l'application. Les autres spécifications du cahier des charges sont obtenues à partir des performances typiques du véhicule de référence et des indications données par des organismes spécialisés de l'usage automobile. Le véhicule de référence de ce travail est la Renault Clio II 1.5L DCi, tandis que l'organisme spécialisé est le PNGV (Partnership for a New Generation Vehicles, Moore and Lovins [90]). Le cahier des charges du véhicule est présenté dans le tableau (0.1).

| Contraintes | Description |
|---|---|
| Temps d'accélération | 0–100 km/h $\leqslant$ 13 s<br>80–120 km/h $\leqslant$ 20 s<br>30–60 km/h $\leqslant$ 6 s |
| Démarrage en pente | 0-10 km/h dans 2s avec 20% pente<br>et SoE entre 20–70 % |
| Vitesse maximale (véhicule) | $\geqslant$ 145 km/h |
| Vitesse maximale (mode système PAC) | $\geqslant$ 110 km/h avec 5% de pente |

**Table 0.1**: Performances désirées pour le VHPAC

Combinant le cahier de charges du tableau (0.1) avec l'optimisation global, l'analyse de statistique de mobilité et l'analyse de la viabilité économique, la méthodologie complète de dimensionnement peut être représentée par le schéma de la figure (0.5).

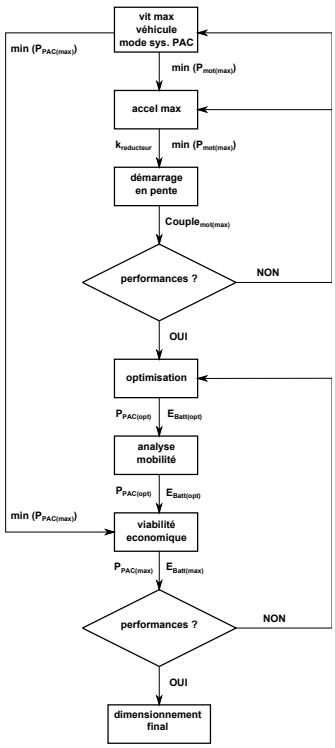


**Figure 0.5**: Méthodologie de dimensionnement du VHPAC

**Dimensionnement de la chaîne de traction** La chaîne de traction est dimensionnée en utilisant les spécifications techniques . Les critères de vitesse maximale et accélération maximale permettent de trouver le dimensionnement de la puissance maximale du moteur

$P_{mot(max)}$ et le rapport de réduction $k_{reducteur}$. Dans ce processus, le modèle du moteur consiste en une inertie pure et une cartographie possèdant une région de couple maximale et une région d'iso-puissance maximale (fig. (0.6)).

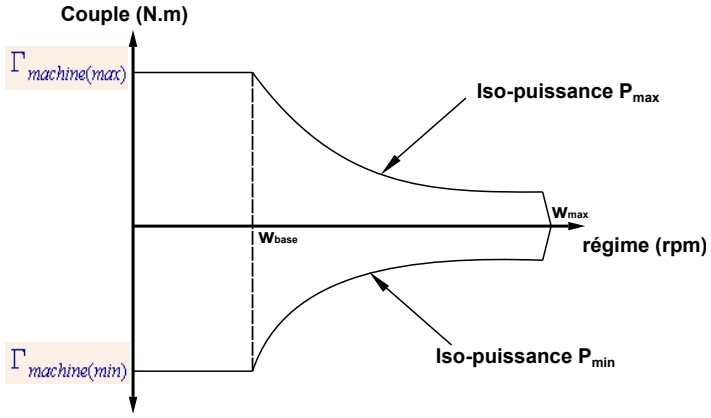


**Figure 0.6:** Cartographie idéale du moteur électrique

Pour la résolution liée à la vitesse maximale, il est considéré que le véhicule est en régime stationnaire ($\frac{dv}{dt} = 0$) et le fonctionnement du moteur se place sur la courbe d'iso-puissance. Ainsi, à partir de l'équation (9), la puissance maximale peut être obtenue par une résolution analytique.

$$M\frac{dv\,(t)}{dt} = F_{traction} - F_{resistance} = 0;\ F_{traction} = \frac{P_{traction}}{v\,(t)} \tag{9}$$

Les mêmes considérations ne peuvent pas être faites pour le critère d'accélération maximale. Donc, l'équation dynamique complète du véhicule (10) est résolue de façon numérique.

$$M\frac{dv(t)}{dt} = F_{traction} - F_{resistance}$$

$$\begin{cases} F_{traction} = \frac{k_{red}.\Gamma_{traction\,max}}{R_{wheel}}\ (région\,couple\,max) \\ \\ F_{traction} = \frac{P_{traction}}{v(t)}\ (région\,puissance\,max) \end{cases} \tag{10}$$

Le couple maximal du moteur est obtenu à partir de la spécification liée au démarrage en pente et grâce à la résolution numérique de l'équation dynamique du véhicule et de la chaine de traction (10).

A la fin de cette étape, le dimensionnement de la chaîne de traction obtenu est vérifié par rapport aux performances fixées par le cahier des charges.

**Dimensionnement système PAC et batterie** L'étape suivante consiste à définitir le taux d'hybridation. En utilisant la programmation dynamique comme méthode d'optimisation, en fonction de différents cycles de conduite et du dimensionnement de la chaîne de traction obtenu, une étude paramétrique vérifie la consommation optimale d'hydrogène pour chaque combinaison de système PAC et batterie. Ainsi, pour chaque type de cycle, un taux d'hybridation optimal est trouvé. Cette étude tient également en compte des effets de changement de masse et de consommation électrique des auxiliaires en fonction des capacités de puissance et d'énergie du système PAC et de la batterie.

Dans un deuxième temps, l'ensemble des résultats est soumis à l'analyse statistique des mobilités des véhicules particuliers et de la viabilité économique de la solution. A partir des données de l'enquête nationale de déplacement en France [4], une capacité utile minimale de la batterie est définie suivant des critères d'usage du véhicule. L'analyse de la distance parcourue par les conducteurs et des types de parcours ($15\,km$ avec cycle urbain/extra-urban) permettent de connaitre l'énergie minimale que la batterie doit avoir pour que le véhicule effectue ce parcours uniquement sur l'énergie de la batterie. Les résultats caractérisent une nouvelle contrainte d'énergie minimale de la batterie $min\left(\varepsilon_{batt(max)}\right)$.

Les résultats de l'optimisation, de la vitesse maximale en mode système PAC et de l'étape d'analyse de mobilité ($min\left(\varepsilon_{batt(max)}\right)$) sont soumis à une analyse de viabilité économique des solutions de dimensionnement. Dans cette analyse, le gain en performance (réduction de consommation d'hydrogène) entre les configurations limites ($min\left(P_{PAC(max)}\right)$ et $min\left(\varepsilon_{batt(max)}\right)$) et les réponses optimales obtenues sont comparées en fonction du coût.

Finalement, le véhicule avec la configuration finale est soumis à une vérification des performances pour valider que les dimensionnements du système PAC et batterie afin de ne pas dégrader les performances désirées pour le véhicule.

## Gestion d'énergie optimale intégrant la dynamique du système PAC

Dans cette section, la gestion d'énergie du VHPAC est définie de manière à résoudre en temps réel le problème d'optimisation incluant la dynamique du système pile à combustible. La dynamique du système PAC est définie et contrôlée, puis l'algorithme de gestion d'énergie est proposé.

Etant un système complexe composé des divers éléments et sous systèmes, le système

pile a combustible possède une réponse dynamique dépendant des interactions entre les sous-systèmes. Les différentes de dynamique entre les sous-systèmes sont les causes principales de mécanismes de dégradations réversibles et irréversibles dans l'opération d'une pile à combustible. Ainsi, pour représenter la dynamique du système PAC dans la gestion d'énergie, nous avons retenu la dynamique la plus contraignante est retenue. Divers auteurs [121, 65, 109] ont indiqué que le circuit d'air dans le système PAC peut impacter fortement le fonctionnement en termes de perte de performance et de dégradations irréversibles. La présence d'éléments de dynamique lente comme le compresseur et les non-linéarités du circuit complet rendent complexe la régulation des variables d'état afin d'assurer le point de fonctionnement optimal. Par conséquent, dans ce travail, la dynamique du sous système d'air est choisie pour représenter la dynamique principale du système PAC. Cette dynamique peut être représentée par un système d'équations composé par les dynamiques du compresseur, de la cathode et de la vanne de régulation de pression (11). Les trois variables d'état de ce système sont la vitesse de rotation du moteur du compresseur, la pression à la sortie de la cathode et le déplacement du clapet de la vanne. Dans (11) la pression aval du compresseur $p_{sm}$ et amont de la vanne peut être rapporée à la pression aval de la cathode $p_{cath(out)}$ en tenant compte des pertes de charges à l'intérieur de la cathode et de l'humidificateur. De plus, les débits d'oxygène $q_{O_2}$ et d'eau $q_{H_2O}$ dépendent directement du courant fourni par la pile. Par contre le modèle ne prend pas compte l'échange de matière à travers la membrane entre le compartiment cathodique et anodique.

$$\begin{cases} \frac{d\omega}{dt} = \frac{1}{J}\left(\alpha.u_{mot} - \frac{C_p T_{atm}}{\omega \eta_{cp}}\left[\left(\frac{p_{sm}}{p_{atm}}\right)^{\frac{\gamma-1}{\gamma}} - 1\right] q_{cp}\left(\omega, p_{sm}\right) - \varphi\omega\right) \\ \frac{dp_{cath(out)}}{dt} = \frac{RT_{cath}}{V_{cath} m_{molar}}\left(q_{cp}\left(\omega, p_{sm}\right) - q_{O_2} + q_{H_2O} - q_{vanne}\left(p_{vanne(in)}\right)\right) \\ \dot{x}_{vanne} = \frac{1}{\tau_{vanne}}\left(-x_{vanne} + k_{vanne} u_{vanne}\right) \end{cases} \tag{11}$$

La dynamique est donc non-linéaire, et son intégration dans le problème d'optimisation rend difficile le développement d'une loi de gestion d'énergie optimale pour des applications en temps réel.

Pour surmonter cette difficulté, une commande non-linéaire est appliquée à ce circuit avec un double objectif: la stabilisation et la linéarisation des dynamiques. La technique de commande choisie ici est la commande plate [58, 59]. Dans son implémentation, les sorties plates doivent être choisies pour rendre le système plat.

Un système est dit plat si ses commandes et ses états peuvent être représentés en fonction de sorties plates et leurs dérivées successives. Cependant, le choix de ses sorties n'est pas évidente sur un système non-linéaire car il n'existe pas de méthodes systématiques pour trouver les sorties plates. Dans notre cas, les deux sorties plates $y_1$ et $y_2$ ont étés choisies respectivement comme les états $\omega$ et $p_{cath(out)}$. A travers de ce choix on arrive facilement à montrer que le troisième état $x_{vanne}$ est aussi dépendant des sorties plates et de leurs dérivées (12). Il en est le même pour les commandes $u_{mot}$ (13) et $u_{vanne}$ (14).

$$x_{vanne} = \frac{\dot{y}_2 - f_4\left(y_1, y_2, q_{O_2}, q_{H_2O}\right) - f_6\left(y_2\right)}{f_9\left(y_2\right)} \tag{12}$$

$$u_{mot} = \frac{W_1 + c_2 \frac{1}{y_1^d}\left[\left(\frac{y_2^d + f_1\left(y_1^d, y_2^d\right)(c_3)}{p_{atm}}\right)^{\frac{\gamma-1}{\gamma}} - 1\right] f_{comp}\left(y_1^d, y_2^d\right) + c_4 y_1^d}{c_1} \tag{13}$$

$$u_{vanne} = \frac{f_{x\,vanne}}{c_7} + \left\{ \frac{\frac{1}{c_5} W_2 - \dot{f}_{comp} + \dot{q}_{O_2} - \dot{q}_{H_2O}}{k_{hu}\zeta_1\left(\zeta_1 f_{x\,vanne} + \zeta_2\right) - \frac{\left[k_{hu}^2 \zeta_1 (\zeta_1 f_{x\,vanne} + \zeta_2)^3 + \zeta_1\left(y_2^d - p_{atm}\right)\right]}{\sqrt{k_{hu}^2 (\zeta_1 f_{x\,vanne} + \zeta_2)^4 - 4\left[(\zeta_1 f_{x\,vanne} + \zeta_2)^2\left(y_2^d - p_{atm}\right)\right]}}} \right\} \tag{14}$$

Dans ces deux commandes $W_i$ sont les nouvelles commandes, $y_i^d$ sont les trajectoires désirées de sorties et les débit $q_{O_2}$et $q_{H_2O}$ sont considérés comme des perturbations connues. La fonction $f_{x\,vanne}$ dépend donc des sorties plates, de leaurs dérivées et des perturbations connues.

L'application de ces commandes du système permet de transformer la dynamique en (11) dans un équivalent linéaire constitué d'une chaîne d'intégrateur comme en (15). Des commandes linéaires simples comme un retour d'état peuvent être alors utilisées pour rendre le système stable et robuste.

$$\begin{cases} \dot{Z}_1^d = W_1 \\ \dot{Z}_2^d = Z_3^d \\ \dot{Z}_3^d = W_2 \end{cases} \tag{15}$$

En conséquence, la nouvelle dynamique équivalente du système PAC est intégrée au problème d'optimisation et sa résolution est fait premièrement par l'application du Principe du Maximum de Pontryaguine, qui donne un résultat très simple (16):

$$P^*_{batt}(t) = \frac{\lambda_1 - (2a_1(P_{vehicule}(t)) + a_2)}{2a_1}$$

$$\frac{\partial \mathcal{H}}{\partial W_1} = 0 = \lambda_2 \tag{16}$$

$$\frac{\partial \mathcal{H}}{\partial W_2} = 0 = \lambda_3$$

A partir de cette formulation, on peut noter que la commande appliquée a simplifiée la résolution du problème. Néanmoins, le co-état $\lambda_1$ reste indéterminé. De façon à surmonter cette difficulté, une approche prédictive est proposée dans ce travail. Considérant que $\lambda_1$ est constant et faisant l'hypothèse que la distribution de puissance demandée par le véhicule dans une fenêtre de temps $t_h$ du passé est équivalente à la distribution du futur [21, 75, 77], la valeur de $\lambda_1$ peut être calculée par (17).

$$\lambda_1 = \frac{2a_1\left(\left(\sum_{j=t}^{t+t_h}\left(P_{batt}(j)\right)\right) - \sum_{j=t}^{t+t_h} P_{vehtot}(j)\right)}{\left(\frac{t_h}{\Delta t}\right)} + a_2 \tag{17}$$

Avec un changement de variable sur la somme $\left(\sum_{j=t}^{t+t_h}\left(P_{batt}(j)\right)\right)$, le $SoE$ apparaît dans le calcul de $\lambda_1$ (18).

$$\lambda_1 = \frac{2a_1\left(\frac{\Delta SoE_{desire}\cdot\varepsilon_{max}}{\Delta t} - \sum_{i=t-t_h}^{t-1} P_{vehicule}(i)\right)}{\left(\frac{t_h}{\Delta t}\right)} + a_2 \tag{18}$$

$\Delta SoE_{desire}$ indique la différence entre la valeur actuelle et la valeur de référence du $SOE$ et cette que cette différence doit être nulle à la fin de la fenêtre de temps. Afin de profiter au maximum de la récupération au freinage, la référence du $SoE$ s'adapte en fonction de l'état d'énergie cinétique et potentielle du véhicule. L'idée principale vient du fait que quand le véhicule a une vitesse différente de zéro, une partie de l'énergie cinétique peut être récupérée dans les phases de freinage. Par conséquent, dans cette situation le véhicule peut optimiser la récupération en augmentant le domaine du $SoE$ à partir de la réduction de la référence $SoE_{ref}$. Il en est de même concernant l'énergie potentielle (en fonction de l'altitude $h$). L'équations dans (19) et (20) montrent les contribution des énergies cinétiques et potentielles au calcul du $SoE_{ref}$ , où $\eta_{chaine\,freinage}$ est le rendement moyen de la chaîne de traction pendant les phases génératives (moteur en mode générateur).

$$SoE_{cinetique} = (SoE_{max} - SoE_{min})\,\eta_{chaine\,freinage}\frac{Energie\,cinetique(v(t))}{Energie\,cinetique(v_{max})} \tag{19}$$

$$SoE_{Potentielle} = (SoE_{max} - SoE_{min})\,\eta_{chaine\,freinage}\frac{Energie\,Potentielle\big(h(t)-h_{ref}\big)}{Energie\,Potentielle(h_{max}-h_{min})}$$

$$SoE_{ref} = SoE_0 - SoE_{cinetique} - SoE_{potentielle} \tag{20}$$

Où $SoE_0$ est la valeur de référence à altitude et vitesse nulle fixée à 60 %.

Ce développement a permis de créer une architecture de contrôle pour la gestion d'énergie (fig. 0.7) qui permet d'intégrer facilement des autres contraintes, comme nous le montrerons dans la suite avec l'intrégration de la durabilité de la PAC dans la commande optimale.

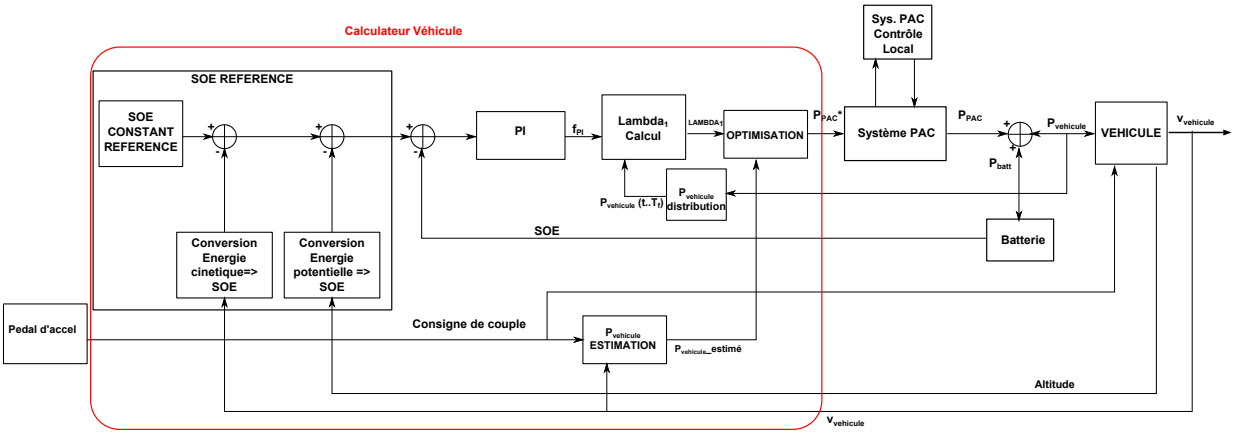


**Figure 0.7**: Schéma block d'optimisation

# Gestion d'énergie intégrant la durabilité de la PAC

La troisième contribution de ce travail est l'introduction de la durabilité de la pile à combustible dans la gestion d'énergie du véhicule. L'objectif de cette implémentation est de contrôler le taux de dégradation de la PAC pendant les différents modes opératoires d'un VHPAC, et en conséquence de maximiser sa durabilité pour atteindre l'objectif établi par le DOE (5000 $hrs$ de durée de vie pour le système PAC). Les grandeurs liées à la durabilité doivent tout d'abord être définies. Parmi ces grandeurs, le critère de fin de vie peut être caractérisée en fonction de la performance de la PAC, ainsi on peut définir un niveau de performance minimal permettant d'assurer les conditions de fonctionnement minimales dans le contexte des applications automobiles. Pei et al. 95 ont définit que le critère d'observation est la tension de la PAC lorsqu'elle fournie sa puissance maximale

(déterminée selon les exigences de l'application, $30\,kW$ en mode stationnaire par exemple ). Ainsi, les dégradations irréversibles sont observés par le changement de la réponse en tension de la PAC. Donc, pour fournir une même puissance, la densité de courant pour fournir une puissance donnée sera différente pour une PAC en début de vie et qu'une PAC en fin de vie (fig. (0.8) [64]). Une conséquence est une perte de rendement et donc une consommation d'hydrogène différent (la PAC dégradée consomme plus d'hydrogène pour fournir la même puissance). A partir de cette analyse, il est possible de définir la fin de vie d'une PAC lorsque sa tension à puissance nominale est 10 % inférieure à celle observée en début de vie [95].

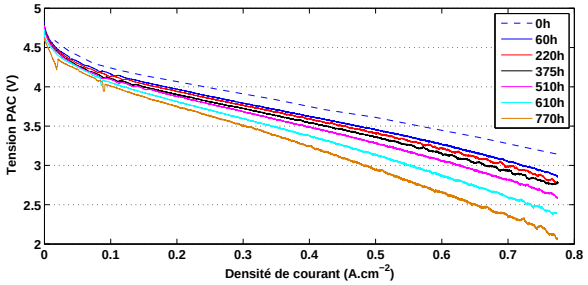


**Figure 0.8:** Réponses en tension pour une PAC (5 cellules) à différents temps de durée d'utilisation [64]

Les dégradations de la PAC reduisent la durée de vie de la PAC sont fortement liées aux conditions de fonctionnement imposées. Chaque mode de fonctionnement contribue à la dégradation de la PAC avec un taux spécifique. Par exemple, des démarrages à froid ($< 0°C$) amènent certains phénomènes de dégradations irréversibles à l'intérieur de la PAC, modifiant ses performances et sa réponse en tension. Cela indique que la contribution à la dégradation de chaque mode de fonctionnement est une information importante pour estimer l'état de santé de la PAC ($SoH$ - State of Health). Pei et al. [95] ont obtenu des valeurs expérimentalement en mesurant les taux de dégradations pour chaque mode de fonctionnement (arrêt-démarrage, veille, puissance max, etc.). Ce type d'analyse expérimentale n'est pas pris en compte dans la démarche de ce travail. En effet la méthode proposée est basée sur les modèles physiques pour extraire les taux de dégradation de la PAC. A partir du travail réalisé au sein du CEA par Robin et al. [102] montrant qualitativement la dégradation d'une PAC soumise à des conditions automobiles en utilisant des modèles à des échelles différentes (système et réactions), l'observation de la surface active équivalente de la cathode ($S$) permet de donner le taux de dégradation de la PAC en fonction du taux de perte en surface active équivalente. La perte de surface active est due à la dissolution du catalyseur et est fonction des conditions locales de

focntionnement de la couche active cathodique (pression, température, stoechiométries, humidité et courant) [102].

A partir de cette étude, il a été possible de définir le calcul de l'indicateur $SoH$ en (21) et la dynamique de dégradation de la surface active équivalente en fonction de la puissance fournie par le système PAC (6.1) (fig. (0.9)).

$$SoH\,(\%) = 100.\frac{S}{S_{tot}}\;;S_{tot} = surface\,totale\,initiale \tag{21}$$

$$\dot{S} = f_{degradation}\,(P_{PAC}) = b_1 P_{PAC}^2 + b_2 P_{PAC} + b_3 \tag{22}$$

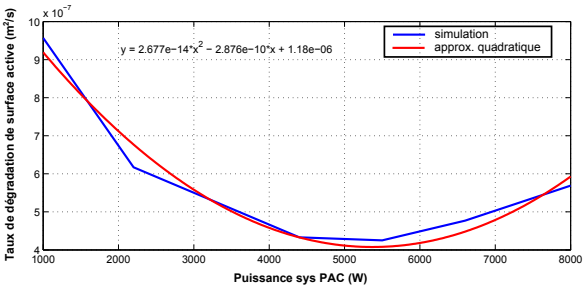


**Figure 0.9:** Taux de dégradation de surface active x Puissance fourni système PAC

A partir de l'intégration du $SoH$ et de la dynamique de dégradation comme contraintes dans les exigeances imposées à la gestion d'énergie, un nouveau problème d'optimisation est défini. La fin de vie de la PAC est introduit dans le problème d'optimisation par le niveau minimum du $SoH$ admissible en fin de vie ($5000\,hrs$). Par conséquent, la limite de performance en tension est traduite en fonction de la surface active équivalente, résultant d'une réduction de $20\,\%$ du $SoH$ en fin de vie d'une PAC.

Comme cette contrainte de $SoH$ ne définit que la valeur en fin de vie, un profil de $SoH$ limite également est intégré au problème. En adoptant une caractéristique linéaire. Le $SoH_{limite}$ indique la région autorisée (au dessus de la limite) pour que la PAC arrive à son objectif final de durabilité (fig. (0.10)).

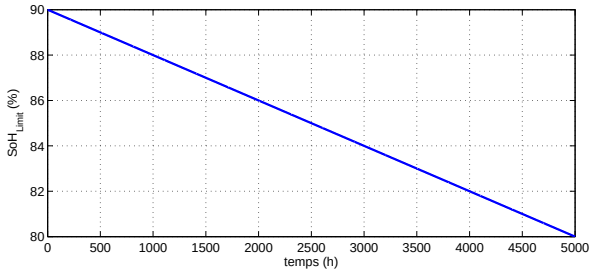


**Figure 0.10**: Profil de $SoH_{limit}$ proposé

La résolution du problème d'optimisation, se base sur le même approche que précédement. On obtient alors:

$$\Rightarrow P^*_{batt}(t) = \frac{\lambda_1+(2(a_1+\lambda_4 b_1)(P_{vehicule}(t))+(a_2+\lambda_4 b_2))}{2(a_1+\lambda_4 b_1)}$$

$$\frac{\partial \mathcal{H}}{\partial W_1} = 0 = \lambda_2 \tag{23}$$

$$\frac{\partial \mathcal{H}}{\partial W_2} = 0 = \lambda_3$$

Ici, le co-état $\lambda_4$ est lié à la contrainte sur le $SoH$, qui est respectéé à l'aide d'un contrôle par retour d'état. Dans ce travail, les méthodes de mésure du $SoH$ ne sont pas développées, mais la valeur du $SoH$ est considérée comme disponible à tout instant. Ainsi, $\lambda_4$ est calculé par l'équation (24), où $f_{durabilité}$ est une fonction qui évite le rapprochement du $SoH$ de sa trajectoire limite $SOH_{limite}$ (fig. (0.11)).

$$\lambda_4 = f_{durabilité}(SoH - SoH_{limite}) = \frac{k_1}{e^{k2(\triangle SoH(t))} - 1} \tag{24}$$

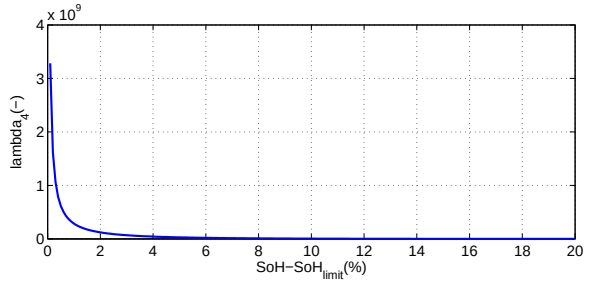


**Figure 0.11**: $\lambda_4$ en fonction du $\triangle SoH(t)$

En intégrant le contrôle du $SoH$, la gestion d'énergie détermine un compromis entre la consommation et la durabilité. En outre la solution du problème d'optimisation fait apparaître trois échelles de temps liées au critère (consommation instantanée), au $SoE$

($\Delta SoE = 0$ pour un cycle de conduite) et au $SoH$ (temps de vie de la pile à combustible) (fig. 0.12).

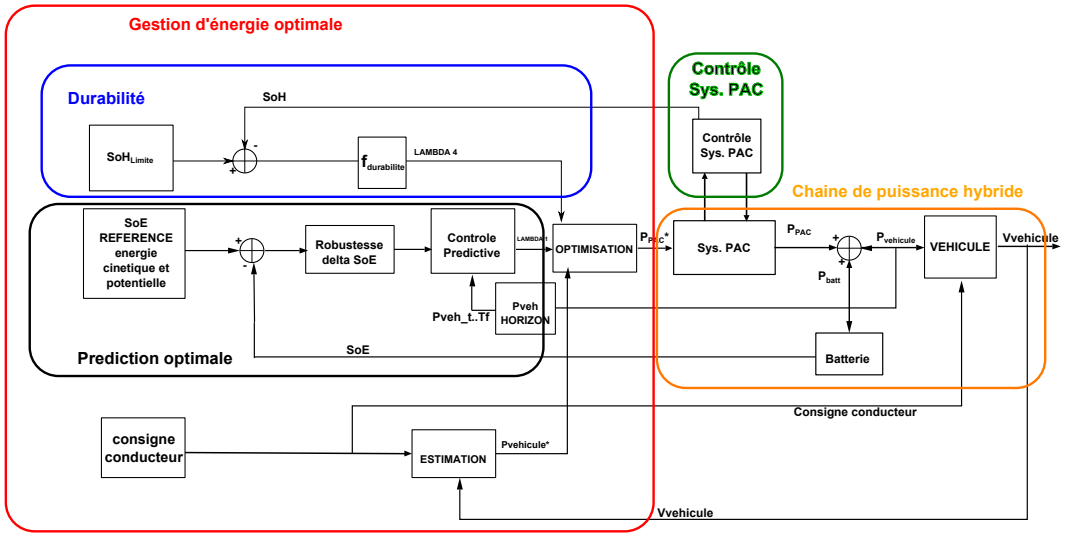


**Figure 0.12:** Nouvelle structure d'optimisation avec l'inclusion du contrôle du $SoH$

# Conclusions

Dans le contexte de nouvelles options d'énergie pour le secteur de transport, ce travail se concentre à l'utilisation de l'hydrogène à partir de l'utilisation des véhicules à pile à combustible. Plus précisément, nous nous proposons de traiter des certaines limitation technologiques des véhicules à pile à combustible. Trois sujets définissent les objectifs établis:

- Le dimensionnement optimal des éléments de la chaine énergétique présents dans un véhicule hybride à pile à combustible.
- La gestion d'énergie optimale pour les applications en temps réel et intégrant les contraintes dynamiques du système PAC.
- La prise en compte de la durabilité de la pile à combustible dans la gestion d'énergie du véhicule.

Ces thèmes ont été traités en utilisant de la modélisation et commande des systèmes présentes, ainsi que des méthodes d'optimisation. Les solutions proposés ont été testées et validés premièrement sur modèles représentant la réponse des systèmes réels et après sur des systèmes réels qui représentent les comportements d'un véhicule en échelle.

Finalement, les résultats obtenus permettent de tracer des perspectives comme la validation des méthodes proposés en utilisant un vrai véhicule à pile à combustible. En plus, l'approche de durabilité du SPAC peut être mieux développée pour intégrer d'autres variables et commandes.

# Table of Contents

**Table of Contents** **xxxv**

**1 General Introduction** **1**

1.1 Context . . . 1
1.2 Hydrogen economy in the transportation context . . . 3
1.3 Fuel Cell Vehicle: advantages, challenges and motivations . . . 4
1.4 Objectives . . . 5
1.5 Overview of the chapters . . . 6
1.6 Summary of the contributions . . . 8

**2 Fuel Cell Electric Vehicles** **11**

2.1 Fuel cell electric vehicles: State of the Art . . . 11
2.2 Vehicle architectures . . . 19
2.2.1 Main architectures . . . 20
2.2.2 Architecture for a fuel cell vehicle . . . 22
2.2.3 Hybrid functionalities . . . 23
2.3 Elements of the FCEV . . . 24
2.3.1 Vehicle . . . 24
2.3.2 Drive train . . . 26
2.3.3 Battery . . . 27
2.3.3.1 Li ion batteries . . . 28
2.3.4 Fuel cell system . . . 31
2.3.4.1 Fuel cell . . . 32
2.3.4.2 PEMFC . . . 33
2.3.4.3 Description of a fuel cell system . . . 38
2.4 Conclusion of the chapter . . . 45

**3 Models and optimization tools** **47**

3.1 Introduction . . . 47
3.2 Modeling and energy management strategy for FCHEV . . . 48
3.2.1 Modeling tools and concepts . . . 48
3.2.2 Energy management strategy: concepts and state of the art . . . 52
3.2.2.1 State of the art: Energy management . . . 52
3.2.3 Optimization problem . . . 55
3.2.4 Conclusion about the modeling and EMS concepts . . . 56
3.3 Models and optimization methods for the optimal sizing . . . 57
3.3.1 Drive train sizing . . . 58
3.3.2 Fuel cell system and battery sizing . . . 59
3.3.2.1 Global optimization method: Dynamic Programming . . . 60
3.3.2.2 Models for the optimization process . . . 62
3.3.3 Validation of the sizing . . . 65
3.3.4 Conclusion about the tools related to the optimal sizing objective 65
3.4 Models and optimization methods for the design of online energy management strategy . . . 66
3.4.1 Dynamic fuel cell system model for the validation of a control law 67
3.4.1.1 Air supply subsystem . . . 68
3.4.1.2 Hydrogen subsystem . . . 69
3.4.1.3 Cooling subsystem . . . 69
3.4.1.4 Electric subsystem . . . 70
3.4.1.5 Fuel cell . . . 70
3.4.2 Fuel cell system dynamic model and PROSPAC prototype in the control context . . . 71
3.4.3 Models and optimization algorithm for the conception of the online energy management strategy . . . 72
3.4.3.1 Drive train model . . . 72
3.4.3.2 Battery model . . . 72
3.4.3.3 Fuel cell system consumption model . . . 72
3.4.3.4 Optimization method . . . 73
3.5 Conclusion of the chapter . . . 75

**4 Fuel Cell Hybrid Electric Vehicle Sizing 77**
4.1 Introduction . . . 77
4.2 FCHEV Sizing methods: state of art, concepts and basic requirements . . . 78
4.2.1 State of art . . . 78

4.2.2 Sizing requirements related to the hybrid functionalities . . . . . 80
4.2.3 Reference Vehicle . . . . . 81
4.2.4 Technical Specifications . . . . . 83
4.3 Sizing Methodology . . . . . 85
4.3.1 Maximum Power Step . . . . . 87
4.3.1.1 Methodology to obtain the maximum power . . . . . 88
4.3.2 Maximum Torque Step . . . . . 92
4.3.3 Drive train validation step . . . . . 92
4.3.4 Conclusions about the drive train sizing . . . . . 92
4.3.5 Optimization step . . . . . 93
4.3.5.1 Optimization process . . . . . 94
4.3.5.2 Optimization conditions and results . . . . . 96
4.3.6 Mobility statistical step . . . . . 104
4.3.7 Economic feasibility step . . . . . 105
4.3.8 Validation of the sizing . . . . . 107
4.4 Conclusions of the chapter . . . . . 107

**5 Online energy management strategy 109**
5.1 Introduction . . . . . 109
5.2 Fuel Cell System Dynamics . . . . . 110
5.3 Air circuit control . . . . . 112
5.3.1 Control Model . . . . . 113
5.3.2 Proposed Control Strategy . . . . . 114
5.3.2.1 Differential flatness theory . . . . . 114
5.3.2.2 Implementation of the differential flatness control strategy 115
5.3.2.3 New Dynamics of the System . . . . . 120
5.3.2.4 Control Structure . . . . . 121
5.3.3 Simulation Results . . . . . 121
5.3.4 Results in Real Fuel Cell System . . . . . 125
5.3.5 Conclusion on the air supply subsystem control . . . . . 128
5.4 New Optimization problem and predictive online energy management strategy . . . . . 129
5.4.1 Optimization problem . . . . . 129
5.4.2 Online predictive energy management method . . . . . 130
5.4.2.1 Predictive approach . . . . . 131
5.5 Optimization Results . . . . . 135

5.5.1 Results from the optimization applied in the model . . . . . 135
5.5.2 Experimental tests of the optimization algorithm . . . . . 139
5.5.2.1 Experimental structure . . . . . 139
5.5.2.2 Developed tests . . . . . 140
5.6 Conclusions of the chapter . . . . . 142

**6 Optimal energy management strategy including fuel cell durability constraint 145**
6.1 Introduction . . . . . 145
6.2 Important concepts and requirements about durability in a FCHEV . . . 146
6.3 Degradation of FC in a FCHEV: Operation modes, degradation mechanisms and diagnostic methods . . . . . 149
6.3.1 Vehicle operating modes and their degradation mechanisms . . . . 149
6.3.2 Diagnostic methods for the fuel cell stack durability . . . . . 151
6.4 Fuel cell stack degradation dynamic model and optimization problem for EMS application . . . . . 154
6.4.1 Degradation dynamic model . . . . . 154
6.4.2 Optimization problem with durability constraint . . . . . 159
6.4.3 *SoH* limits for the optimization problem . . . . . 160
6.5 Optimal energy management strategy with durability constraints . . . . . 162
6.6 Optimization results . . . . . 167
6.7 Conclusion of the chapter . . . . . 169

**7 General Conclusion 171**

**Bibliography 179**

**A Drive Cycles I**

**B PROSPAC Prototype V**

**C Parameters of the air supply subsystem IX**

# Chapter 1

# General Introduction

## 1.1 Context

During long time petroleum has been considered an abundant raw material and low cost. However, the dramatic spread of transport throughout in the twentieth century has resulted in increased oil consumption. This trend may not be sustainable in the medium and long term. On the one hand, fossil fuels need million of years to replenish stocks: their production is limited by the physical provision of the planet as well as the possibility of extraction according to technical and economic conditions. On the other hand, the burning of fossil fuels releases large quantities of polluting gases that reinforce the problem of climate change (eg carbon dioxide) or increase the pollution of atmospheric air (eg oxide nitrogen, carbon monoxide).

In terms of energy security, a fossil fuel economy presents weaknesses, such as the instability that has been a feature of the oil industry from its inception [20]. In fact, the competition between producers to recover the largest possible amount of oil and the arrival of new producers on the market did not allow optimum rate of production, resulting in overproduction crises. A direct effect of this instability in production are the occurrence of sharp increases in the price of petroleum [67], which are explained by the combined effect of the increase in consumption and supply constraints, and amplified by the action of speculation. Besides, the production becomes more expensive when new fields, where production is more expensive, replace the old ones that arrived at the end-of-life.

As reservoirs of petroleum are increasingly rare and concentrated in some geographic regions, a situation of dependency is created [93]. Hence, the consumer countries are in a socio-political vulnerable position in relation to the producer countries, possibly causing geopolitical tensions at international level.

Addressing the fossil fuel economy to the application level, in particular to the transport sector, it can be considered the largest consumer of petroleum products. In terms of energy it accounts 27 % of global energy demand, of which almost all is derived from fossil fuels [67]. So, if nothing is done to counteract this trend, the growth in transport demand would necessarily lead to increased oil imports and emissions. Meanwhile, global demand for automotives should be tripled by 2050 due to the increase in developing countries [63, 20]. The continuation of this trend may not be sustainable given the existing resources and environmental impacts. Thus, it is essential that the inevitable increase in the global car fleet is offset by a sharp decline in consumption and vehicle emissions.

To deal with the energy demanded and reduction of emissions of greenhouse gases, major technological innovations in vehicles are needed (conception, engine, structure, etc.). Low improvements in the actual technology (ICE vehicles) are not sufficient to meet the emissions objectives and to deal with the demand of energy created by the increasing number of vehicles [86]. Technological changes are necessary to deal with this context and among the existing alternatives three appear more adapted: electricity, biofuels and hydrogen [20].

Technologies as the biofuel for the vehicular applications represent a valid option in the task of fossil fuel replacement, as verified in some parts of the world [29, 20]. However, since there is an uncertainty if the production of biofuels will be available for passenger cars, given the potential demand from other sectors, such as aviation, marine, and heavy industry, it is vital to develop a range of sustainable mobility technologies over the long term.

Nowadays, the battery electric vehicles become a reality in terms of the replacement of the conventional power train using internal combustion engine (ICE). The electrification of the vehicles is considered the simplest solution to achieve the emissions goals [93]. Moreover, compared with the conventional power train, it presents an outstanding weaknesses [34]. Major shortcomings of this alternative are attributed to the energy storage: low capacity, high cost, long charging time, small operating temperature range and low cycling stability [33]. These drawbacks limited their wider use for propulsion of passenger vehicles.

Hydrogen is considered as a well adapted solution to the energetic and environmental challenges. As the electricity, the hydrogen is an energetic vector, which offers multiple advantages when compared to primary energy sources, such as the petrol. The hydrogen has a technical potential to compete with the fossil energy solutions in different applications (transport, stationnary applications, power grid storage); however, it is in the transport domain that this energy vector can provide better results, especially when it is

part of a competitive of hydrogen economy concept.

## 1.2 Hydrogen economy in the transportation context

Defined first by the electrochemist John Bockris [20], the hydrogen economy concept has been continuously developed by different authors in order to present an possible context of massive hydrogen adoption.

Since its inception, such idea was always related to the sustainable and non-polluting objectives. Therefore, even if the fossil fuels can be used to produce hydrogen, renewable energies have a main role in the hydrogen economy.

The ideal representation of the hydrogen economy is illustrated in fig. 1.1. As can be noticed, the hydrogen and electricity are carriers operating between the energy sources and applications. On the other side, this energy transportation produces non-harmful effects in the environment by the consumption and production of oxygen and water. Differently from a typical combustion application, there is a presence of sustainable cyclic exchange without pollutant emissions. In this way, the hydrogen participates to the decarbonization process of the energetic system, meaning a reduction of carbon emissions per energy unit.

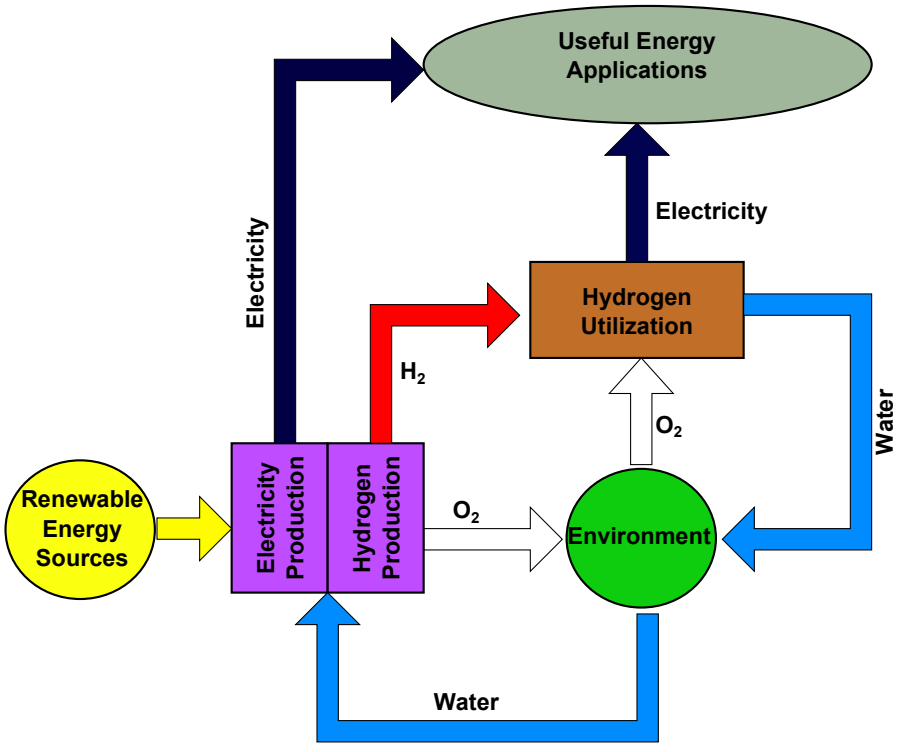


**Figure 1.1**: Hydrogen economy scheme

In the particular case of the transport sector, the hydrogen and electricity association illustrated in fig. 1.1 is performed by the adoption of fuel cells (FC) embedded in the vehicles. Despite the not yet achieved requirements of technical and economical structure for hydrogen production and distribution, such fuel cell vehicle has been considered one of the best options to reach the assigned decarbonization targets [86, 124].

## 1.3 Fuel Cell Vehicle: advantages, challenges and motivations

Compared with ICE vehicles, a power train powered by a fuel cell stack offers many advantages related to its energy efficiency, clean and fuel flexible characteristics. An efficiency peak of 60 % can be reached by FC with a conversion of hydrogen in traction power and producing only water [53, 70]. Besides, as aforementioned, the hydrogen used can be produced from a variety of sources including fossil fuels such as natural gas, renewable such as solar and wind power, biomass and nuclear energy [71].

Despite all the encouraging reasons, the fuel cell vehicle technology still faces some limitations. Out of all the limiting factors, cost, hydrogen storage technology, fuel cell system dynamics and durability are considered by the automotive constructors as the most challenging factors.

These challenges should be overcome to render the hydrogen fuel cell vehicle a competitive option in the market. Cost and hydrogen storage has been subjected to continuous developments and presented significant progress towards commercialization target values [92]. Nevertheless, there is a consensus that the slow dynamics and durability require a special attention in order to reach the stated objectives. Hence, these drawbacks have been dealt using different approaches such as technological developments in the elements constructions or in their integration procedure.

The hybridization approach applied to the ICE vehicles is another frequent solution proposed. Such hybridization using batteries would permits to compensate the slow dynamics of the fuel cell system, reduce the degradation effects and aggregate the possibility to obtain a reduction in energy consumption. Even though the extra degree of freedom brings advantages to the fuel cell vehicle, the hybrid configuration demands a more elaborated control strategy regarding all these criteria and an optimum sizing of the hybridization rate.

Represented by an energy management strategy, the power split between the fuel cell system and the energy storage elements (batteries) could be designed using several

methods and choosing different objectives. Although it exist different methods proposed, the energy management strategy is considered as an open subject yet.

Believing that it is a coherent alternative and very well adapted to the needs of the transportation sector, this work is developed around the hydrogen energetic alternative through the adoption of the fuel cell vehicles and dealing with their main technical challenges.

## 1.4 Objectives

Being motivated by the aforementioned limitations, this work intends to make a research contribution in order to find out a solution for each challenge. Specifically, this work aims to include the fuel cell system dynamics and durability aspects in an energy management strategy. It requires an approach that deals with phenomena and features presented in reaction, system and vehicle levels. In order to achieve this objective, control strategies allied with models of different scales should be developed and applied. Moreover, this thesis considers that the fuel cell vehicle sizing is also related to the mentioned challenging requirements; therefore, the development of a sizing procedure adapted to the needs composes as well the proposed objectives. Figure 1.2 illustrates these objectives and the outline adopted to meet them.

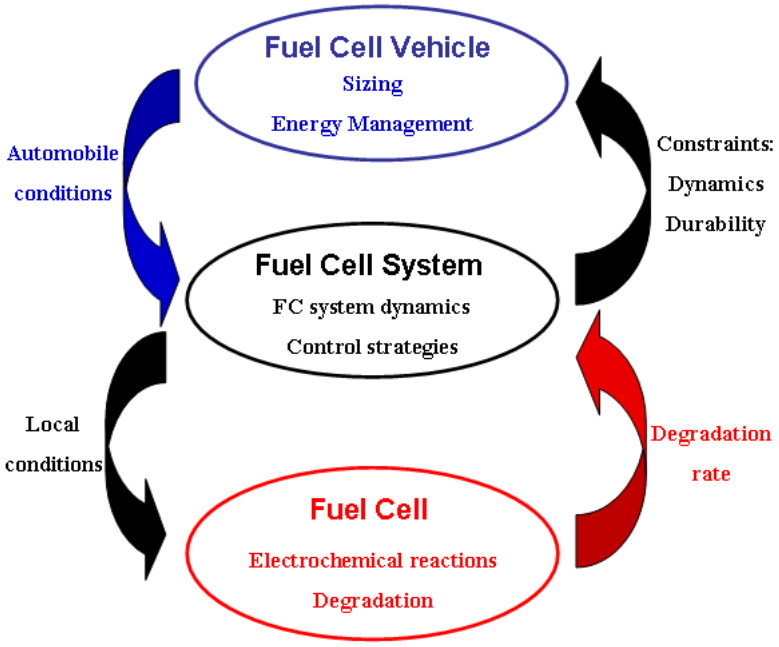


**Figure 1.2**: Approach structure

The developments are based in three levels associated to the vehicle, fuel cell system and fuel cell, where each one is responsible for a set of specific tasks:

- Vehicle level: sizing and energy management strategy of the vehicle.
- Fuel cell system level: definition of the dynamics and the control laws to regulate the system.
- Fuel cell level: definition of the degradation dynamics analyzing the phenomena at the electrochemical reaction scale.

An information chain allows to transport the information from the vehicle level down to the fuel cell level and feedback. It starts with the assignment of the automobile conditions to the fuel cell system, which results in the definition of the fuel cell dynamics and the local conditions within the fuel cell. These local conditions are imposed to the fuel cell level, returning the degradation rate that combined with the FC system dynamics. They compose the constraints of the energy management strategy. In this manner, the different application levels are brought to the vehicle level in order to solve the energy management strategy problem.

The developments and background knowledge present in this process are described through five main chapters.

## 1.5 Overview of the chapters

**Chapter 2: Fuel Cell Electric Vehicles** The first chapter presents the hybrid fuel cell vehicles and its characteristics. Initially, a state of art is introduced to clarify the advances in the technologies, the commercialization requirements and the remaining issues to be overcome. Thereafter, possible architectures are described and discussed aiming to define the one to be adopted. In sequel, the basic vehicle modeling concepts are presented, comprising the losses and its longitudinal dynamics. This chapter also presents a brief state of art about the battery technologies and the most adopted types of models for this work. The fuel cell and its system are firstly introduced by a description of its operating principles, emphasizing the interactions among the fuel cell and the other elements composing the system. Due to the importance of these interactions, the main characteristics of each subsystem are described briefly with a focus on the effects of their state variables in the fuel cell stack behavior.

**Chapter 3: Models and Optimization tools** The second chapter is related to the description of the tools used in this work. Due to the presence of several elements and different application levels (vehicle, system and reactions), a set of different models are necessary to study and observe the important phenomena involved in the objectives of this work. Therefore, the first part of the chapter is devoted to the definition of the modeling tools and the models used. Each model is presented according to its desired application, which means that the link concerning models features and applications is highlighted. The other part of this chapter is about the optimization tools used in the energy management development and the optimum sizing. A state of art about this subject aims to show an overview of the methods used so far. Among the presented methods, some of them are chosen to be used in this work; thereby, they are described by their main characteristics and assigned as the reference tools for the energy management task.

**Chapter 4: Fuel Cell Hybrid Electric Sizing** The third chapter deals with the sizing of the Fuel Cell Hybrid Electric Vehicle (FCHEV). Intending to obtain an optimal sizing, a systematic sizing procedure is built to define the dimensions of the main elements in the powertrain and in the hybrid configuration. Initially, a reference vehicle is chosen and it's functional and performance characteristics are assigned. Combining adapted technical specifications, optimization approach, population mobility aspects and economical study, the dimension of the vehicle's elements are obtained, providing a commitment between different criterions, such as consumption, performance and cost.

**Chapter 5: Online energy management strategy** In this chapter is proposed an optimal energy management strategy oriented for online applications. Prior to the developing of such strategy, the dynamics of the fuel cell system is discussed in order to prepare its inclusion in the optimization problem. A control strategy is applied to the defined dynamics, leading to a regulation of the state variables and a simplification of the dynamics structure. Afterwards, the online energy management strategy is defined using the optimal theory and concepts such as the predictive control to overcome some typical drawbacks presented in this task. The proposed energy management strategy is validated by simulations using dynamic models and experimental tests using real systems (fuel cell system and battery), electric motor and a motor test bench.

**Chapter 6: Fuel cell durability** The study of the fuel cell durability, in the context of the FCV energy management, is presented in this chapter. Through a definition

of the fuel cell end of life and a state of art about the degradation mechanism and diagnostics methods, the chapter introduces the necessary background to implement the durability in the optimal power split strategy. In the sequence of the chapter, a durability simplified model is presented with the assumptions made and the main characteristics, which renders it adapted to the optimization task. Such model determines the degradation dynamics to be used as a constraint of the optimization problem. The strategy proposed in chapter 4 is adapted to include the durability aspects in the optimization process. Simulation results are also presented.

## 1.6 Summary of the contributions

Motivated by the challenges presented above, the work can yield interesting results for the advancement in the technology of the fuel cell vehicles. Indirectly, models and tools that are created in this work enabled the development of techniques and the understanding of phenomena and characteristics related to different parts of the vehicle and the fuel cell system. Meanwhile, the direct contributions resulting from this work concentrate their efforts on the three main topics contained in the established objectives:

- Optimal sizing
- Optimal energy management
- Fuel cell system durability

The chapters dealing with the respective subjects (chapters 4, 5 and 6) describe, in a different manner, the contributions that were also presented through publications in scientific journals and conferences.

Regarding the sizing of the fuel cell vehicle, the systematic approach and especially the optimization feature embedded in the process constituted the content of a national communication [40]. Specifically, the definition of the optimal hybridization rate between the fuel cell system and battery represented the major contribution of this publication. The basis in terms of development and knowledge brought by the optimization tools and models were of fundamental importance in this task.

As the central objective of this work, the energy management was addressed in several ways and at different stages. Initially, a energy management strategy based on the responses from global optimization methods was the subject of a scientific paper [43], which was presented at the SAE world conference exhibition. This strategy combined the

optimal characteristics of the off-line optimization methods results to a complementary aspect that added an expert content (rule based) to the solution.

Despite the discovery of this strategy, the solution of the energy management problem converged in direction to the development of a method that allowed online applications with low computation time, with a performance close to the global optimization methods and integrating the dynamic response of the fuel cell system. This evolution is evidenced by a set of publications and a patent filed.

The scientific articles [44, 45] dealt with a necessary stage in the optimization process that is the control of the fuel cell system dynamics. The application of a nonlinear control method leads to a stabilization of the system dynamic behavior (verified by simulation and by tests in real platforms) and simplify its inclusion in the energy management strategy.

Subsequently, the conception of an energy management strategy adapted to be implemented in fuel cell vehicles was performed and tested. Given the innovative character of the solution, its content was protected through the elaboration of a patent that has already been accepted. Such protection created for the patent initially limited the possible communications, but part of its content has already been published [41] in an international conference and must produce some future publications and scientific articles.

Finally, the aim to include the information of durability of the fuel cell system in the energy management task generated the synthesis of a new energy management strategy. Their results constituted the basis for the elaboration of a communication [42] presented at international conference and still allow the development of another article.

# Chapter 2

# Fuel Cell Electric Vehicles

**Abstract**

This first chapter is devoted to the definition of the fuel cell electric vehicles, addressing the context in which it is inserted and the state of art. Over the functional aspect, the chapter presents the definition of existing hybrid architectures and description of the elements that compose the fuel cell electric vehicle, with emphasis on their technology and functional characteristics.

## 2.1 Fuel cell electric vehicles: State of the Art

As electric cars try to forge more than just a niche in the market, the automotive industry is already looking to another form of clean technology that could overtake today's battery-powered vehicles.

Commitments by automobile manufactures and various government agencies to develop hydrogen fuel-cell cars have surged in recent times. Applications in which these vehicles are involved include personal vehicles, fleet vehicles (for municipal and commercial use), transit buses, short-haul trucks (such as delivery trucks and drayage trucks for port facilities), and others [37, 71, 31, 70]. In the case of light-duty vehicles auto makers like Ford, Hyundai, Daimler and others had already announced plans to build vehicles and prototypes that run on hydrogen. As an example, Ford, Daimler and the Renault-Nissan Alliance sign an agreement to accelerate the development of fuel-cell electric-vehicle technology with a goal of launching the world's first affordable mass-market FCEV as early as 2017.

Ford already presented some years ago (2007) its HySeries Drive concept that associates batteries and fuel cells in a hybrid configuration to be used in its Edge hydrogen

version (figure 2.1). This prototype represented a solution where the fuel cell has the function recharge the battery pack (range extender), not effecting the delivery of power directly to the load (power train). The combined autonomy (battery + hydrogen) allows to reach up to 490 km with a speed up to 135 km/h [6].

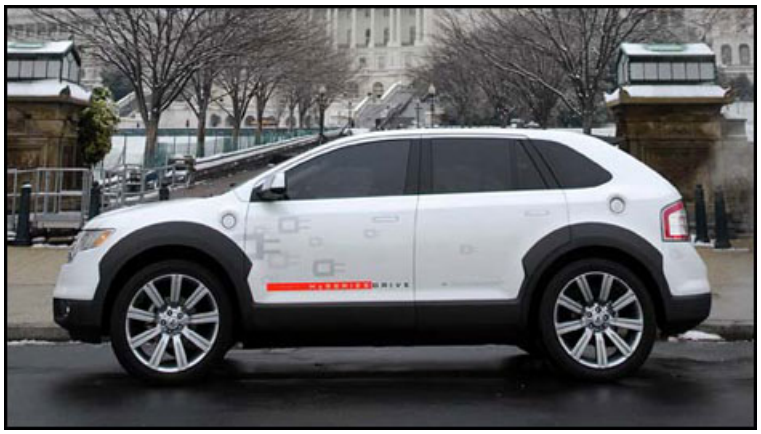

**Figure 2.1**: Ford Edge FCEV

General motors first built a FCEV prototype based in a futuristic design (figure 2.2) 2007 using the hybridization of battery and fuel cell as well. In the configuration proposed the fuel cell can charge the battery and deliver the electric power to the traction, differently from the Ford approach. This prototype presented a range of 480 km of electric driving between refills [7] and was useful as a base to the conception of its future commercial model, the Equinox FCEV.

**Figure 2.2**: GM Chevy Volt FCEV

Despite the technology involved in hydrogen mobility did not have reach a stable state, some builders are experiencing to pass from the prototyping in direction to a initial

production (1000 cars by Daimler/Ford/Nissan) [92, 53]. The move within the automotive industry to establish plans to mass produce fuel-cell cars appears to be gaining traction due to the positive perspectives in terms of the acceptation of this technology [19]. Figure 2.3 shows the trend for the UK market [68]. As the structure of hydrogen refueling stations (HRS) and the fuel cell technology increases in maturity level, the market tends to absorb more of this technology as an available option to the conventional ICE vehicles.

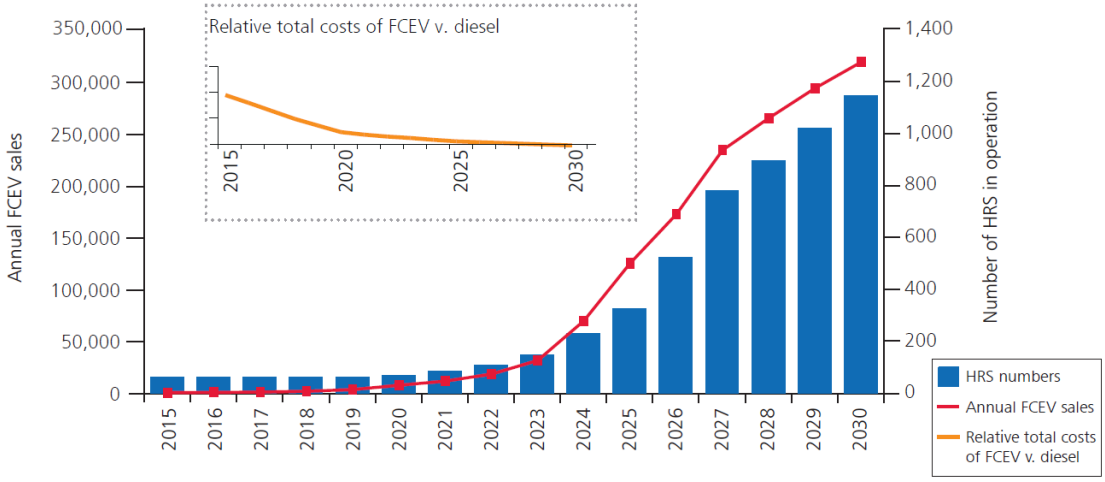


**Figure 2.3:** FCEV perspective sales at UK market [68]

Relying on this trend, some constructors are closer to the production level. Hyundai has announced that it will offer a fuel-cell version of its ix35 sport utility vehicle (figure 2.4) on lease by the end of this year. Announcing a range of 588 km between charges and performance consistent with the conventional model, it plans to make up to 1,000 fuel-cell cars by 2015 and thereafter 10,000 fuel-cell cars per year [9, 8].


**Figure 2.4:** Hyundai ix35 FCEV

Among automotive manufacturers Daimler-Mercedes Benz is considered in more advanced stage of commercialization purposes, despite the important advances and efforts shown by Hyundai and others auto makers. With the proposal of a Class B hydrogen-powered (figure 2.5) [2], capable of a range of 400 km between refills and a technology state that has allowed to reach 30000 km in a continuous worldwide drive campaign [3], this constructor already started the diffusion of this vehicle in a leasing out program in some regions in the world and announces commercialization goals to 2015 that are allied to the necessary structure to the new fuel cell vehicle fleet.


**Figure 2.5:** Daimler-Mercedes Benz [2]

The established starting date of commercialization reflects the evolution of the vehicles technology, which means that many advances have already been made since the early versions, but there are remaining challenges to be overcome until the estimated time.

The Department of Energy of the United States (DOE) [92] lists the main challenges to the adoption of hydrogen mobility as the following categories:

- Technology
  - ⋆ Hydrogen cost
  - ⋆ Hydrogen storage, capacity and cost
  - ⋆ Fuel cell cost, durability and performance
- Economic and Institutional
  - ⋆ Safety codes and standards
  - ⋆ Hydrogen supply and delivery structure

⋆ Manufacturing cost and supplier base

⋆ Public awareness and acceptance

Since the context of this work is focused on technological aspects, economical and institutional aspects will not be presented.

**Hydrogen cost** The cost of hydrogen is defined by the form of production and delivery. The production of hydrogen can be done in different ways; obviously the main objective at long term is to make the production based on the use of renewable or low carbon resources.

Currently, the production source that proves to be more competitive in relation to petrol is through the natural gas reforming method [31, 92]. Adopting this method, projections of high production indicates a possible cost near to $ 3 per gallon of gasoline equivalent (gge, roughly equal to 1 kg of hydrogen), representing a competitive value in the market.

However, the obtaining of competitive costs using renewable sources without carbon emission is still an open problem. Projections of high productions presents a cost of $4.90–5.70/kg at the refueling site when using water electrolysis method [71, 92]. The cost of production using wind-powered water electrolysis at a centralized plant is $2.70–3.50/kg, but the costs associated to the delivery are not included.

Concerning the technologies for delivering, the current advances in technology allow to obtain a projection of a value approximately $2 to $3 per gge (delivering hydrogen from a central production facility to a fueling station 60 miles away) [92]. These values are subject to necessary infrastructures, resulting in investments and maintenance costs.

Figure 2.6 shows the status of production and delivery cost for different methods.

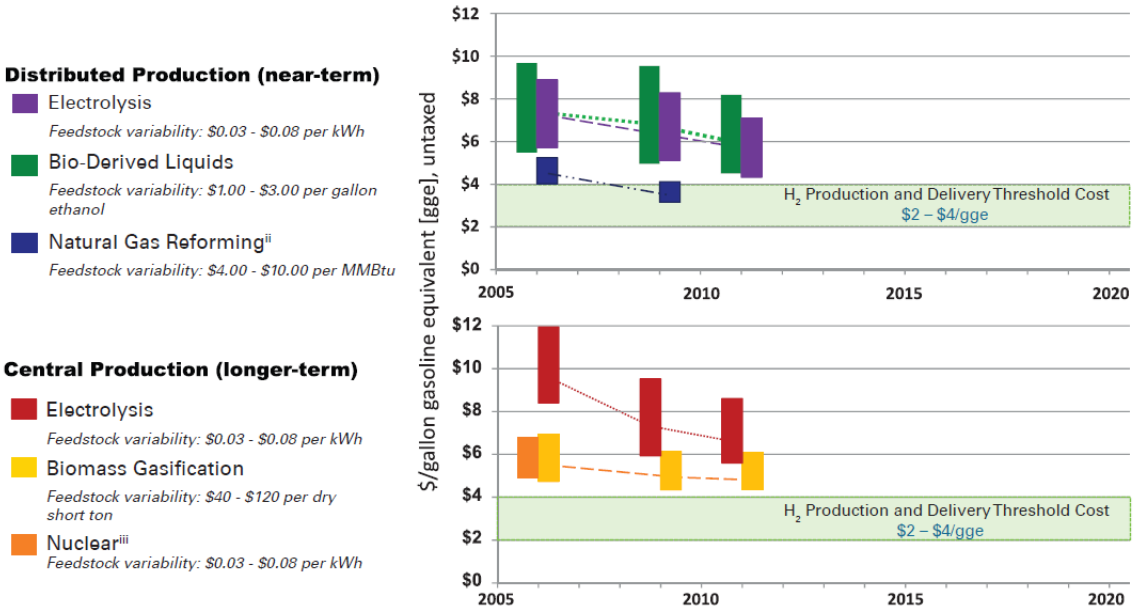


**Figure 2.6:** Hydrogen production and delivery cost status [92]

**Hydrogen storage, capacity and cost** One of the biggest challenges for hydrogen FCEV technology is to store a sufficient amount of hydrogen on board the vehicle for an acceptable range in a practical amount of space. There are different technologies for hydrogen storage: modest-pressure gas ($350\,bar$), high-pressure gas ($700\,bar$), cryo-compressed hydrogen (CcH2), and material-based storage elements [94].

Since possible leaks by diffusion are controlled (that is already achieved with current technology), the procedure to store hydrogen under pressure allows to deal with the inconvenient low volumetric energy density of hydrogen. In this process, the increased pressure leads to a gain in energy density, to the detriment of energy consumption due to compression.

Cryo-compressed hydrogen storage refers to the storage of hydrogen at cryogenic temperatures in a vessel that can be pressurized (nominally to 250-350 $atm$), in contrast to current cryogenic vessels that store liquid hydrogen at near-ambient pressures. Cryo-compressed hydrogen storage can include liquid hydrogen, cold compressed hydrogen, or hydrogen in a two-phase region (saturated liquid and vapor). Even having achieved a technological advancement state consistent with the needs of the process, the manufactured system costs is a barrier to be overcome [50]. State of current technology shows a cost twice that required for the purpose of commercialization, even assuming a large-scale production.

Materials-based approaches using ammonia borane, hydrides, amides, composite ma-

terials, metal-organic frameworks, organic molecules, etc. are being explored extensively. The hydrogen is included in these materials and by different processes it is possible to separate it from its carrier. Materials-based approaches are divided in three classes [94]:

- The compounds of with high specific surface
- Reversible chemical hydrides
- The rechargeable metallic or intermetallic hydrides

The metallic hydride approach is the most advanced one, allowing to store from $10\,kg$ to $70\,kg$ of hydrogen in $1\,kg$ of metallic hydride, corresponding from $0.3\,kWh/kg$ to $2.1\,kWh/kg$ of mass density and $1.3\,kWh/L$ of volumetric capacity [117]. Compared with the DOE ultimate targets [92] ($2.5\,kWh/kg$ and $2.3\,kWh/L$) there are still improvements to be made by 2015 (date set by DOE).

Among the mentioned storage ways, high-pressure tanks (700 bar) are the most adopted so far. This storage method has been submitted to some improvements beyond the materials level to get the acceptance of the auto makers. By the system optimization, it could be increased the onboard storage capacity of hydrogen, which allowed to some demonstration and prototype vehicles achieve driving ranges as high as 690 km on a single fill, representing more than the DOE goal ($500\,km$). Despite the goal has been already achieved, it must be applicable for different vehicle platforms, without compromising space and performance, and at a competitive cost, which leaves open the problem.

**Fuel cell cost, durability and performance** Since the first major application in the U.S. spatial program in the sixties, the fuel cell technology had a remarkable evolution. Specifically in the application of vehicles, the use of this power converter element opened the prospects to a transport that is efficient, clean, accessible and adapted to current personal uses.

The state of development achieved by the fuel cells embedded in the vehicles has reached a level of improvement that allows to obtain efficiencies of up to 60%, accounting more than twice of the maximum efficiency of a current internal combustion engine. Nevertheless, in order to be ready for commercialization, the efficiency presented must be followed with a cost, durability and performance of the vehicle consistent with the constrains of the transport sector.

**Cost** In the mainstream transportation sector, internal combustion engines represent the reference in terms of cost. Costs of ICEs for automobiles are much lower than for other

applications, due to the very high manufacturing volumes and the associated economies of scale, as well as the efficiencies of well-established supplier bases and distribution networks. Current costs of conventional ICE are about \$30/kW for light-duty vehicles [92, 86].

Despite the reduction in cost of more than 80% since 2002 (figure 2.7), fuel cells will have to be less expensive than they are today (\$49/kW) in order to be competitive in transport sector and meet consumer requirements. According to the prospects and evolution of the technology, the target cost established by DOE (\$30/kW) can be reached by 2017. Meanwhile, advances in the development of the fuel cell and its system should continue, particularly with regard to the development and adoption of equipment in the system with lower cost of production and maintenance. For the fuel cell the advances should be done by replacing expensive noble materials such as platinum by other materials with same performance and lower cost.

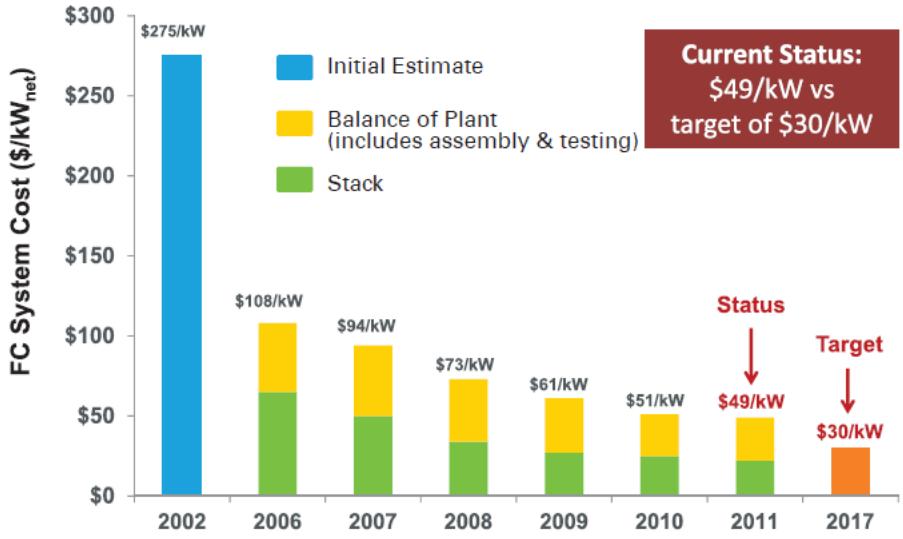


**Figure 2.7:** Projected transportation fuel cell system cost - projected to high-volume (500,000 units per year) an for $80\,kW$ fuel cell systems [92]

**Durability** In order to be adapted to the current needs of consumers, a fuel cell vehicle must have a lifetime consistent with current technologies on the market. According to what was established by DOE [92], a minimum of 5000 hours (equivalent to 150,000 miles) of operation shall be provided before the end of its useful life, defined through a degradation value of 10 % in the efficiency.

Even if the criterion of end of life is not clear to dynamic applications, the current status of durability presents only half the stated goal (2500 hours, 75,000 miles). Despite

this difference, there has been a significant evolution in the direction of the DOE goal. Due to investment in research of new materials and diagnosis, it could achieve a level of durability that validates the first phase of the DOE goals (2000 hours). Therefore, in order to overcome the 50% remaining difference, efforts should be continued in the fuel cell conception and optimal management of system.

**Performance** Despite the good efficiency aforementioned, fuel cells still present some performance limitations when it is submitted to some particular operational conditions presented in the transport domain. Cold start operations, environmental condition that impose temperatures of -40°C Ahluwalia and Wang [11] to 50°C or dynamical responses required by the vehicle are clear examples of situations where the performance of the fuel cell is limited. As an element that is inserted in a system, the coordination of the subsystems should be well conducted to not result in an acceleration of the degradation status, when such situations happen.

Besides, despite the fairly homogeneous behavior in terms of efficiency, it is not possible to ensure such good efficiency during an automobile application. If subjected to a demand that it imposes a point of low operating efficiency (very low power and high power), the advantages compared to a conventional vehicle are reduced. Therefore, a hybrid character is usually inserted into the conception of the fuel cell vehicle. Using an element of energy storage it is possible to select the operating points of the stack to ensure good efficiency and at the same time the dynamical demands of an automotive application [33, 53], compensating the slow dynamics of the fuel cell system.

The inclusion of a new element in the energetic chain of the vehicle implies the need for an adoption of hybrid architecture. This topic is the subject of the next section.

## 2.2 Vehicle architectures

The demand for new types of powertrains that are more efficient and reduce the emission of pollutants of vehicles caused an evolution in the technology of electric motors. This technological evolution has led to obtain models that feature all the dynamic performances of a conventional engine coupled to a much higher efficiency, which drove the acceptance of electric vehicles in the market. However, due to autonomy limitations of pure electrical vehicle, solutions hybridizing conventional engine (ICE) and electrical motors were necessary to fill this gap. Although of the real gains in terms of fuel economy and emissions reduction presented by this type of hybridization, the long-term goal for new technologies is to completely eliminate local emissions or reducing them to values

near zero [93, 92, 31], qualifying this type of solution as intermediate. This not definitive character will allow the transition from the conventional form of transportation (based on the use of petroleum) to a transportation that adopts energy coming from renewable sources. Hydrogen fuel cell vehicles make part of the sustainable solutions group.

This session will present the most adopted architectures, the definition of the chosen architecture and the classification of hybridization functionalities.

### 2.2.1 Main architectures

The following topologies represent the most adopted technologies [52, 60, 89]:

- Electric vehicle architecture
- Series hybrid architecture
- Parallel hybrid architecture
- Series-parallel hybrid architecture (power split)

Such architectures are presented in figure 2.8.

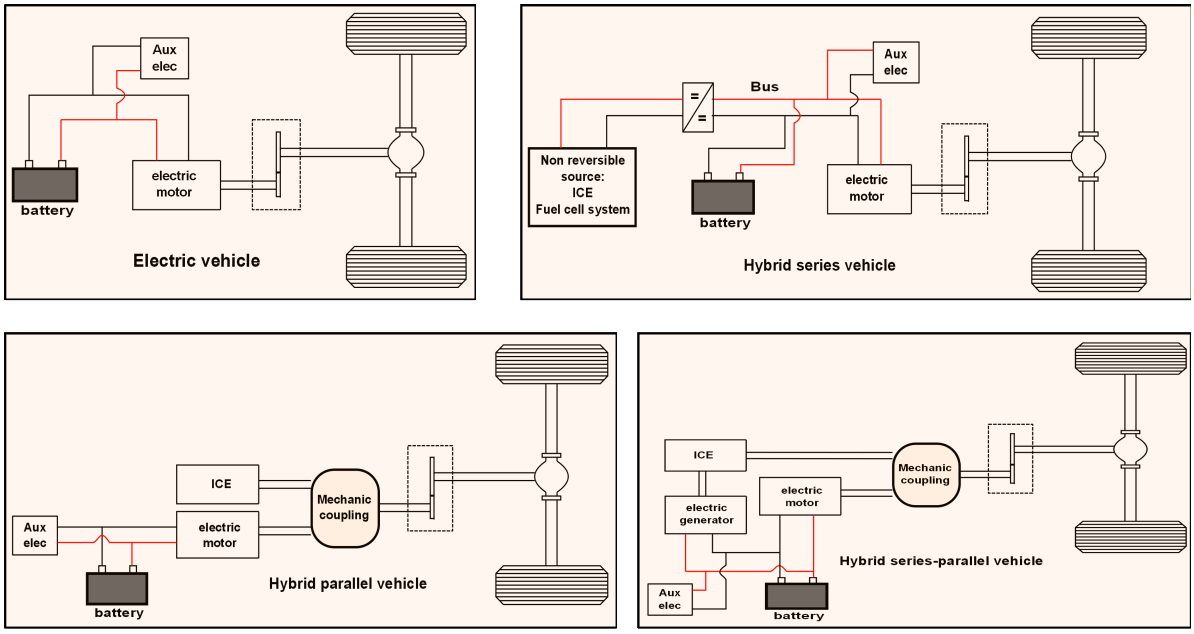


**Figure 2.8:** Vehicles architectures

**Electric vehicle architecture** The electric vehicle architecture has a simple topology like a conventional vehicle, where the powertrain and energy source have electrical

characteristics (electric powertrain and batteries). In addition to the good efficiency in the powertrain compared to a conventional vehicle, an electric vehicle has the advantage of its reversibility in terms of the electric motor. This allows energy recovering during braking processes, which will be stored in the battery and can be used later, increasing the energy efficiency of the vehicle.

Such energy recovering functionality is desired for other type of vehicles. Therefore, hybrid architectures seek to add this functionality to vehicles through the insertion of energy storage elements and energy conversion elements that are reversibles, such as electric motors and batteries.

**Series hybrid architecture** In series hybrid architecture only one traction element is commonly used. During the braking phase, the mechanical power for braking is converted to electrical power through the electric motor and then absorbed by the battery. During the traction, the demanded electrical power can come from the not reversible source and/or from the energy storage element (batteries). This power split should be done dynamically in order to take advantage of the best efficiency region of the non reversible source. Thus, this architecture allows a decoupling between the dynamic behavior imposed by the vehicle dynamics and the dynamics of the not reversible source, which is done through the energy storage elements. This decoupling allows the irreversible source to have a stabilized behavior around its best efficiency point while the battery is responsible for ensuring the power dynamics of the vehicle.

When many energy conversion elements are present in the powertrain, this architecture has the disadvantage of putting in series their efficiencies, reducing the overall efficiency of the vehicle. In the case of a series hybrid vehicle using the internal combustion engine and batteries, successive conversions between mechanical and electrical power degrade the efficiency of the vehicle.

**Parallel hybrid architecture** In parallel configuration, two motors with different features are used and connected directly to the transmission. They can participate together of the vehicle traction, acting directly on the wheels. In order to perform this, a system of transmission and gearbox are necessary for the power transmission. For a same hybrid application using a combustion engine, this architecture presents an overall efficiency greater than the series architecture. However, parallel configuration presents major disadvantages, such as the complexity of control and rigid connection between the combustion engine and the wheels.

**Series-parallel architecture** Also referred as power split, this configuration combines the advantages of series and parallel configurations. Through an effective control, the regime of operation of the combustion engine is regulated in order to make it work at its best efficiency point. The power generated is split between traction and recharge of the storage element. Since this architecture has more elements, the system control and command becomes more complex.

### 2.2.2 Architecture for a fuel cell vehicle

In current applications of fuel cell vehicles the series architecture is usually adopted. The good performance of this conversion element allows to deal with the inconvenience of the efficiency serialization without compromising too much the overall efficiency of the vehicle. Allied to this, the simple control necessary for this architecture enables a definition of power split that favors the good performance of the fuel cell.

Regarding the possible degrees of freedom to control the power split, the topology used can contain zero, one or two electric DC/DC converters. Being a system with not reversible characteristics, the fuel cell system generally needs an irreversible interface to perform its conditioning and security. However, the energy storage system should have reversible characteristics and consequently may or may not be interfaced with the electric bus through DC/DC converters. The absence of this element would impose a floating voltage level on the bus. Therefore, depending on the chosen storing element, the bus and the elements connected to it may be subject to voltage fluctuations.

Adopting batteries used in the new electric vehicles as the storage element, the voltage fluctuations are tolerated by equipment connected to the bus (motors and auxiliary elements of the vehicle). From the point of view of efficiency gains and control, the inclusion of another degree of freedom (as a battery interface) do not presents enough advantages to justify its adoption, according to Trischiler et al.[117].

In this work, series hybrid architecture will be adopted for an electric fuel cell vehicle, where there will be only one DC/DC converter for interface and security of the stack. Figure 2.9 shows the architecture adopted in this work.

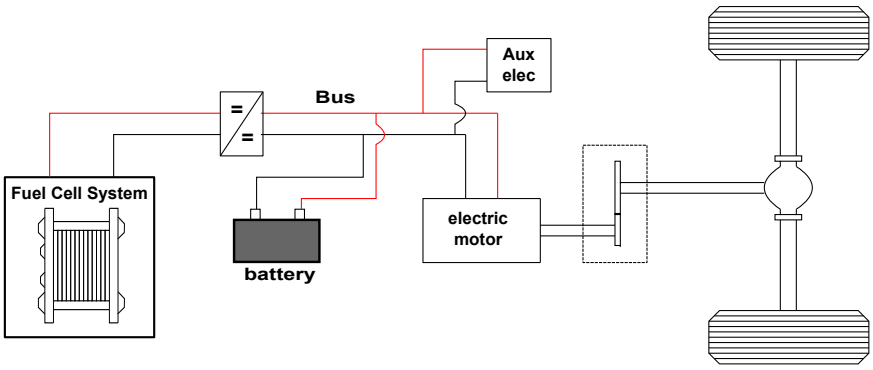


**Figure 2.9:** Fuel cell vehicle architecture

### 2.2.3 Hybrid functionalities

The hybridization has different levels of functionality. According to Chan et al. [35], they can be classified as a function of the relation between the power of the non reversible source and the energy storage element, which are respectively the fuel cell system and batteries for this application.

1. Micro Hybrid: The fuel cell system is responsible for the propulsion power while batteries have an auxiliary function in startup operations and stop-and-go, preventing the fuel cell to be subject to unfavorable conditions during starting procedure and allowing its stop during standstill situations.

2. Mild Hybrid: Adds the power boost mode to the stop-and-go function. The battery provides power during peak power because of the fuel cell system delay. Besides, in this hybrid level, during braking the vehicle's kinetic energy can be converted into electric used to recharge the battery. However, the battery is not authorized to deliver alone the power to propel the vehicle.

3. Full Hybrid: In this case, beyond the features of the other modes, the battery is able and authorized to provide alone the power for propulsion of the vehicle. Nevertheless, the battery can not be recharged externally and hydrogen used in the fuel cell should represent the total energy expended by vehicle in its mission. This means that, although it can provide power for propulsion, the battery has function of electric assistance. Therefore, at the end of its mission the state of charge should be near to its initial value. This characteristic configures a mode called charge sustaining. Performing a good strategy for the power split between fuel cell and battery, it is possible to obtain important reductions in consumption.

4. Plug-in Hybrid: This mode is present when the battery can be recharged through the electric grid. In the vehicle, the battery assumes the source function and not only reversible storage element. The energy management strategy changes in order to permits the battery to reach the end of the mission with depleted state, defining the charge depleting mode. This hybridization mode enables to adopt a strategy close to an electric vehicle behavior (with a range extender) or more elaborated ones that associates the two sources with more complex objectives.

In order to be able to propose more elaborated energy management strategies, only the full hybrid and plug-in hybrid modes will be tackled.

## 2.3 Elements of the FCEV

This session will be destined to the description of the main elements that compose the selected architecture:

1. Vehicle
2. Drive train
3. Battery
4. Fuel cell system

### 2.3.1 Vehicle

For the analysis of energy consumption purposes, the vehicle may be considered through its longitudinal kinematics and dynamics [116, 77, 60]. The movement of the vehicle is obtained as a result of forces acting on it. Figure 2.10 illustrates the forces acting on the vehicle.

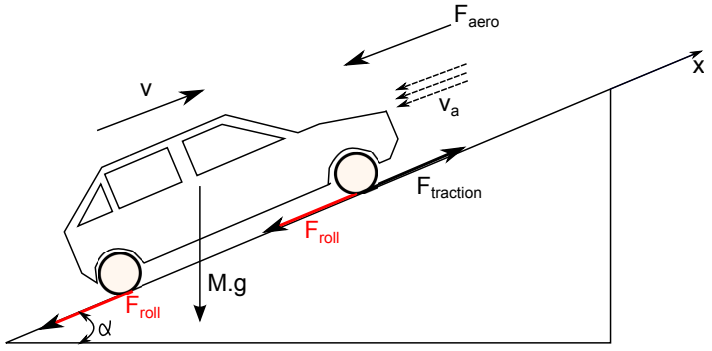


**Figure 2.10**: Vehicle dynamics

$F_{traction}(t)$ is the traction force resulted from the torque imposed by the traction train $\Gamma_{wheel}(t)$ through the wheels. Considering that the losses in slippering are negligible, this transformation is represented by the equation 2.1 ($R_{wheel}$ is the wheel radius). In terms of kinematic variables, equation 2.2 shows the transformation of the angular speed of the wheels $\omega_{wheel}(t)$ in linear speed $v(t)$.

$$F_{traction}(t) = \frac{\Gamma_{wheel}(t)}{R_{wheel}} \tag{2.1}$$

$$v(t) = \frac{\omega_{wheel}(t)}{R_{wheel}} \tag{2.2}$$

Performing the balance between traction force and the movement resistance resultant $F_{resistance}$, it is obtained the acceleration of the vehicle via the fundamental principle of dynamics (equation 2.3). Where $M$ is the total mass of the vehicle.

$$\frac{dv}{dt} = \frac{F_{traction} - F_{resistance}}{M} \tag{2.3}$$

The resistive force $F_{resistance}$ is mainly composed of three components (equation 2.4): aerodynamic resistance $F_{aero}$, rolling resistance $F_{roll}$ and resistance due to the route profile $F_{slope}$ (slope profile).

$$F_{resistance} = F_{aero} + F_{roll} + F_{slope} \tag{2.4}$$

**Aerodynamic resistance** $F_{aero}$ It is the force exerted by the wind according to the vehicle axis of movement. It is dependent on air density $\rho_{air}$, front surface $S$, air penetration coefficient of the vehicle $C_x$ and the sum of the square of the speed of the vehicle $v$ and the relative velocity of the air $v_{air}$. The equation 2.5 defines $F_{aero}$.

$$F_{aero} = \frac{1}{2}.\rho_{air}.S.C_x.(v + v_{air})^2 \tag{2.5}$$

**Rolling resistance** $F_{roll}$ It represents the resistant effort due to the contact between the tire and the surface bearings. It is proportional to the mass of the vehicle $M$, gravitational acceleration $g$, the rolling resistance coefficient $\mu$ and to the slope $\alpha$. Mathematically it is represented by the equation 2.6.

$$F_{roll} = M.g.\mu.cos(\alpha) \tag{2.6}$$

**Slope profile resistance** $F_{slope}$ Represents the resistive effort to carry out a movement on a surface with inclination $\alpha$ (equation 2.7).

$$F_{slope} = M.g.sin\left(\alpha\right) \tag{2.7}$$

The mathematical representation of the longitudinal dynamics of a vehicle is given by the equation 3.2.

$$\frac{dv}{dt} = \frac{\frac{\Gamma_{wheel}(t)}{R_{wheel}} - \left[\left(\frac{1}{2}.\rho_{air}.S.C_x.\left(v\left(t\right) + v_{air}\left(t\right)\right)^2\right) + M.g.\mu.cos\left(\alpha\right) + M.g.sin\left(\alpha\right)\right]}{M} \tag{2.8}$$

### 2.3.2 Drive train

Composed mainly by electric powertrain (electric machine) and gear reducer, the drive train provides the torque that will be applied to the wheels $\Gamma_{wheel}$.

**Gear reducer** The reducer has the function of adjusting torque and speed of the electric machine to the wheels. Ideally, this element allows a total transmission of power. However, due to losses such as friction losses, the gear reducer has an efficiency dependent on the turning speed.

Assuming a constant efficiency $\eta_{red}$ and a transformation gain $k_{red}$, the gear reducer is represented by the system of equations 3.3.

$$\begin{cases} \Gamma_{machine}\left(t\right) = \frac{\Gamma_{wheel}(t)}{\eta_{red}k_{red}} \\ \\ \Omega_{machine}\left(t\right) = \Omega_{wheel}\left(t\right)k_{red} \end{cases} \tag{2.9}$$

**Electrical machine** An electrical machine can be regarded as a controllable power converter. This means that the electrical power provided to the machine is transformed into mechanical power that is provided to the vehicle. Being a reversible element, it can act in motor mode (as described above) or in generator mode where mechanical power is converted into electricity, case of braking in vehicles with electric power train.

In general, the electrical machines have good efficiency when compared to internal combustion engines, reaching values higher than 90% [85, 62]. The construction technology defines the characteristics of performance and operation. For applications in electric traction, three types of electrical machines are commonly used:

- Direct current machine

- Synchronous machine
- Asynchronous machine

The asynchronous machine, specifically with permanent magnet, is the most adopted for applications in vehicles having electric traction. This is due to its good efficiency, reliability and performance in terms of maximum engine speed [60].

For purposes of energy analysis, an electrical machine can be represented by its mechanical inertia and its static response in terms of torque and speed. Thus, by requiring to the machine a given amount of torque at a given speed, it is necessary an electrical power $P_{elec}$ equivalent to the required mechanical power (torque x speed), adding to it the intrinsic losses to operate this machine.

Figure 2.11 illustrates a basic profile of this relationship torque vs speed. The torque signal indicates that the machine operates in motor mode (positive torque), or generator mode (negative torque). The operating limits indicate a region of maximum torque (or minimum in the case of generator) and a region of iso-power. Inside, the different zones of efficiency are present.

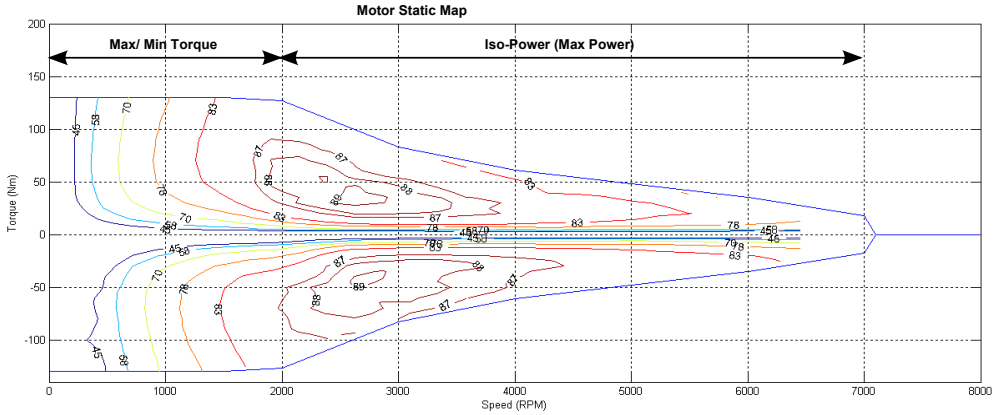


**Figure 2.11:** Electrical machine static representation

### 2.3.3 Battery

The batteries act as an essential element in a fuel cell vehicle. For this particular application there are different types of batteries. The choice of the most suitable technology must take into account a range of factors such as [117]:

1. Energy density
2. Power density

3. Durability
4. Operation temperature
5. Cell nominal voltage
6. Cost
7. Cyclability

Table 2.1 presents functional characteristics of the main battery technologies intended for hybrid vehicle applications.

| | Ni/Cd | Ni/MH | Li ion | Li ion $FePO_4$ | Li polimero |
|---|---|---|---|---|---|
| 1- [Wh/kg] | 45-80 | 60-110 | 150-190 | 120-140 | 150-190 |
| 2- [W/kg] | 200 | 220 | 220-330 | 200 | 220-330 |
| 3- n° cycles | 2000 | 1500 | 500-1000 | >2000 | 200-300 |
| 4- (°C) | -40 à 60 | -20 à 60 | -20 à 60 | -20 à 60 | 0 à 60 |
| 5- (V) | 1.2 | 1.2 | 3.9 | 3.2 | 3.7 |
| 6- Euros/kWh | 600 | 1500 à 2000 | 2000 | 1000 à 1800 | 1500 à 2000 |

**Table 2.1**: Features of different technologies of batteries

Historically, technologies Ni/Cd and Ni/MH were the first to be adopted for hybrid vehicular applications. With the increasing development of technology based on Li ion, the automotive applications directed their expectations on this technology. Despite the high price, the automotive constructors adopted it for electric and hybrid vehicles due to its high energy and power density.

#### 2.3.3.1 Li ion batteries

From the point of view of its construction, a cell of a Li ion battery consists of an electrolyte and two electrodes (figure 2.12): a negative electrode based on graphite ($Li_xC_6$) and a positive electrode based on lithium metallic oxide ($LiMeO_2$), where $Me$ can be $Co$, $Ni$, etc [49].

As the cathode has a higher potential, in discharge mode the electrons comes from the external circuit in its direction such the current flows from the cathode to the anode. Inside the cell, the cations $Li^+$are transferred between the cathode and the anode through the electrolyte and a separator. Each atom of Lithium is liberated from the anode and releases an electron to circulate through the external circuit in the cathode direction.

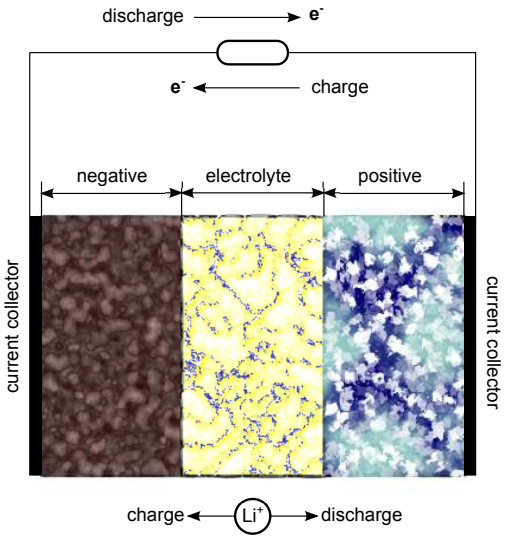


**Figure 2.12:** Functioning of a Li ion battery cell

Meanwhile, the cation $Li^+$ migrates in the cathode direction through the electrolyte and reach the cathode, binding to an electron. In charge mode, the motion of electrons and cations is done in reverse. Figure 2.12 illustrates this process. Electrochemically, this whole process is represented by oxido-reduction reactions.

Regarding the type of application, a battery may have predominant characteristics that favor higher energy density or higher power density. For electric vehicles, energy batteries are the most suitable because they should ensure greater autonomy of the vehicle. In the case of full hybrid fuel cell vehicles, battery has function of electric assistance by providing power. Then power batteries are the most indicated.

In order to obtain these different behaviors, the two types of cells have different constructive aspects. Adopting the same mass, a cell intended for power will present a larger electrode surface leading to a lower impedance, while an energy cell possess larger capacity and a higher impedance. The result of these structural differences lead to a kinetic limitation with lower currents for energy cells than for power ones [26].

Whatever the type (power or energy), a battery can be represented mathematically with a higher or lower level of detail. Normally for purposes of energy consumption analysis, a model using equivalent electrical circuits is used. These models can go from simple representations where the battery acts as a perfect voltage source in series with a resistance (fig. a 2.13) [32, 77], up to more complex representations where the dynamic evolution of states is considered.

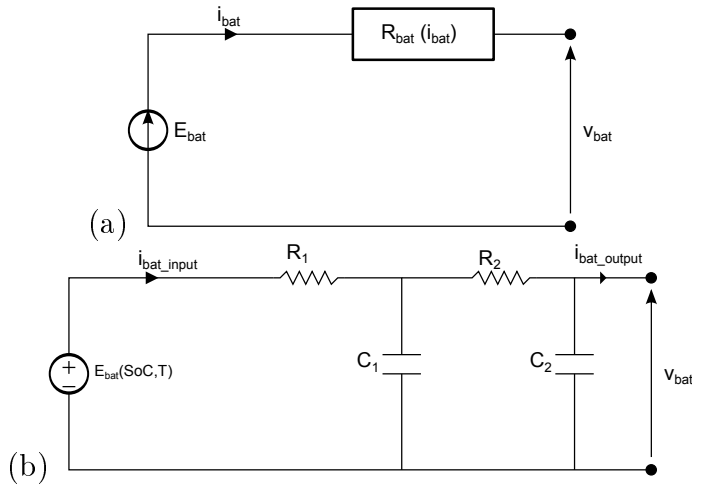


**Figure 2.13:** Electric circuit battery representation- (a) perfect source+ internal resistance, (b) dynamic model

In order to incorporate dynamic effects and storage capacity, more complex equivalent circuit models are adopted. In these models the internal resistance is replaced by an impedance output resulting from the association of non linear resistances and capacitances. This imposes the dynamic response of the cell (fig. b 2.13). The open circuit voltage becomes dependent on the state of charge of the battery and operating temperature, which is valid as well for the resistances and capacitances. The equation 2.10 represents the voltage response of a cell.

$$v_{bat}(t) = E_{bat}(SoC(t), T(t)) - Z_{bat}(i_{bat}, SoC(t), T(t)).i_{bat}(t) \tag{2.10}$$

In this equation, $E_{bat}$ is the open circuit voltage, $SoC$ is the state of charge, $T$ is the temperature and $i_{bat}$ is the current that can be absorbed or delivered. The impedance $Z_{bat}$ is dependent to the mode which the battery is submitted to. This means that the cell has different impedances for charge ($i_{bat} < 0$) and for discharge ($i_{bat} > 0$).

The state of charge of the battery ($SoC$) is calculated through the integral of the current of the battery $i_{bat}$ and using the relation between the actual electrical charge stored $Q(t)$ and the maximal charge that can be stored in the element $Q_{tot}$ (equation 2.11).

$$SoC(t) = \frac{Q(t)}{Q_{tot}}.100\,[\%];\ Q(t) = \int i_{batt}(t)\,dt \tag{2.11}$$

Due to the influence of $SoC$ in the durability of the batteries during storage and used conditions [89, 49], its operating region may be limited in order to achieve a compromise between storage capacity and durability. For applications in hybrid vehicles, some studies

[26, 104] show that the operation between 40 % and 80 % $SoC$ do not lead to life time reduction by degrading effects, but the type of cycle may have an influence on it.

The maximum capacity is also used in the definition of the maximum current of the battery. The maximum current (for discharge mode or minimum in charge mode) is done using a $C$ rate to normalize relation with the maximum capacity. The $C$ rate is a measure of the rate which the battery is discharged in relation to its maximum capacity. A rate of $1C$ indicates the current that will discharge the battery in one hour. For a battery $100\,Ah$, this equates to a discharge current of $100\,A$ and for a $5C$ rate the current would be $500\,A$.

For the objectives considered in this work (sizing and energy management), a quasi-static map, obtained experimentally, is used to represent the behavior of the battery. The voltage response is function of the $SoC$ and current (equation 2.12). Besides, the battery voltage has a dynamic component represented by a first order transfer function with a time constant $\tau_{batt}$ about $0.1\,s$.

$$v_{batt} = \frac{k}{\tau_{batt}s + 1} f\left(SoC, I_{batt}\right) \tag{2.12}$$

Normally presented in a real battery system, a BMS (Battery Management System) provides indicators and observation of important measurements that are used by the vehicle control unit. One of the calculated variables is the state of energy of the battery $SoE$.

In spite of the similarities with the $SoC$ information, some studies already have shown that the $SoE$ represents a valid and reliable information in terms of autonomy and capacity [49]. Equation 2.13 gives the $SoE$ calculation, where $\varepsilon_{max}$ is the maximum energetic capacity of the battery and $\varepsilon$ is the actual energy in the battery and $P_{batt}$ the power supplied by the battery.

$$SoE\,(\%) = 100.\left(\frac{\varepsilon}{\varepsilon_{max}}\right); \quad \varepsilon = -\int P_{batt}dt \tag{2.13}$$

Finally, the battery pack is a series and parallel association of cell to meet a voltage level (resulting from an association in series) and a level of storage capacity (resulting from the association in parallel).

### 2.3.4 Fuel cell system

In this part of the chapter will be described the characteristics of a fuel cell system. First, will be presented the available fuel cell technologies, with emphasis on applications in the

transportation field. Then, the system will be described from their groups and elements.

#### 2.3.4.1 Fuel cell

Although the principle of reverse electrolysis (to obtain electricity by reacting hydrogen and oxygen) was discovered in 1802 by Sir David Henry, only through the technological requirements imposed by space programs on the 60s and 70s that this operating principle gained the status of technological application. Since then, the fuel cell has undergone a significant evolution up to the current level of development.

Just as an electrochemical battery, the operating principle of a fuel cell is based on an oxido-reduction reaction. The oxidation happens at the negative electrode, while the reduction happens at the positive electrode. In order to minimize the entropy of the chemical reaction and thus reduce the heat built, the chemical reaction must occur in an orderly manner and without direct contact between the reactant gases. An electrolyte is used to achieve this orderly procedure. The electrons pass through the external circuit while only the cations pass through the electrolyte to reach the electrode. The semi-reactions in 2.14 represent this process.

$$\begin{aligned} Anode: \quad & H_2 \longleftrightarrow 2H^+ + 2e^- \\ Cathode: \quad & \tfrac{1}{2}O_2 + 2H^+ + 2e^- \longleftrightarrow H_2O \\ & \cdots\cdots\cdots\cdots\cdots\cdots\cdots\cdots\cdots\cdots\cdots\cdots \\ & H_2 + \tfrac{1}{2}O_2 \longleftrightarrow H_2O \end{aligned} \tag{2.14}$$

**Fuel cell technologies** The electrolyte and the operating temperature define the types of technologies for fuel cells. Table 2.2 presents the existing fuel cell technologies and its main features.

| Acronym | Name | Temperature | Electrolyte |
|---|---|---|---|
| PEMFC | Polymer Electrode Membrane Fuel Cell | 50°C - 80°C | Polymer |
| MT-PEMFC | Medium Temperature PEMFC | 90°C - 120°C | Polymer |
| HT-PEMFC | High Temperature PEMFC | 120°C - 180°C | Polymer |
| DMFC | Direct Methanol Fuel Cell | 25°C - 50°C | Polymer |
| DEFC | Direct Ethanol Fuel Cell | 25°C - 50°C | Polymer |
| SOFC | Solid Oxide Fuel Cell | 700°C - 1000°C | Ceramic |
| MCFC | Molten Carbonate Fuel Cell | 650°C | Liquid |
| PAFC | Phosforic Acid Fuel Cell | 150°C - 200°C | Liquid |
| AFC | Alkaline Fuel Cell | 60°C - 120°C | Liquid |

**Table 2.2:** Fuel cell technologies [117]

These technologies should not be considered as competitors. Each type has a favored niche of application to which its advantages and disadvantages fits.

The high temperature fuel cells have the advantage of being able to use directly hydrogenated compounds as fuel; however, it requires the adoption of high temperature materials and needs a significant time for heating up to the operating temperature.

The low-temperature fuel cells do not have the warming up problem, but the lack of activation energy for the reaction requires the use of catalysts, which are made from precious metals increasing the cost and make them more sensitive to poisoning by pollutants such as carbon monoxide and some sulfur compounds [28].

SOFC and PEMFC represent respectively the two types of cells mentioned. They are considered the most promising technologies, showing a level of maturity able to lead them to be implemented in market applications.

For applications in transport domain PEMFC is considered the most suitable due to its operating temperature, compactness, power density and good efficiency [92, 19]. Consequently, this technology will be emphasized and used in this work.

#### 2.3.4.2 PEMFC

Each cell in a PEMFC stack comprises a pair of bipolar plates, positive electrode (cathode), negative electrode (anode) and electrolyte (membrane) (figure 2.14).

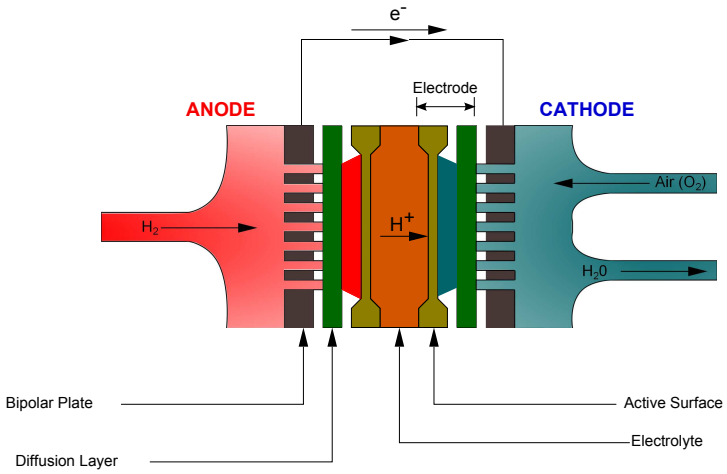


**Figure 2.14:** Cell structure

**Bipolar plates** The bipolar plates have the function of gas transportation towards the electrodes (hydrogen to the anode and oxygen to the cathode). These plates also allow to gathering of current, add mechanical stiff and separate the reactive of two cells. When located at the ends of the stack, they are called monopolar or end plates. The geometry of the channels contained within these plates should not only allow the transport of gases in direction to the electrodes, but should also allow to evacuate the results of the reaction, not consumed gas and facilitate the transfer of heat in order to regulate the cell temperature.

**Electrodes** The electrodes (anode and cathode) must have a large contact surface with the gas. They are composed of a diffusion layer (GDL and MP) and an active surface. The diffusion layer is on the side of the bipolar plate and serves to obtain a uniform distribution of gases over the active surface. This active surface is composed of a suppport carbon base where the catalyst (for example platinum or alloys) is deposited, with impregnated polymer Nafion$^{(R)}$. It corresponds to a coupling zone between electrical, chemical and mass transfer. It must provide the diffusive transport of species dissolved in solution, the migration of protons and electron transfer through the carbon.

**Electrolyte** For the PEMFC technology, the electrolyte corresponds to a membrane. It lies between the two active layers of the electrodes. Its function is to ensure the passage of protons $H^+$ from the anode to the cathode. It presents transport phenomena, such as the transport of water that governed by two mechanisms [96]:

- Electro-osmose: the formation of water molecules by passing of ions $H^+$ from the anode to the cathode.
- Diffusion: transport of the water from the cathode to the anode due the presence of a concentration gradient.

These transport phenomena must be taken into consideration in the construction and operation of the fuel cell, since to ensure good proton conductivity it is necessary a good state of membrane hydration.

**MEA (Membrane Electrode Assembly) and the stack** The association of the electrodes and the membrane define the core of each cell (MEA). With the assistance of bipolar and terminal plates, the MEA stacking configures the fuel cell stack, which operates as an association in series of cells. Thus, the output voltage of the stack is the sum of each individual cell voltage and the current required to stack is the current that will be passed through each cell. The gas transport (H2 and air) is achemined in parallel in each cell. The figure 6.5 shows a stack for automotive applications.

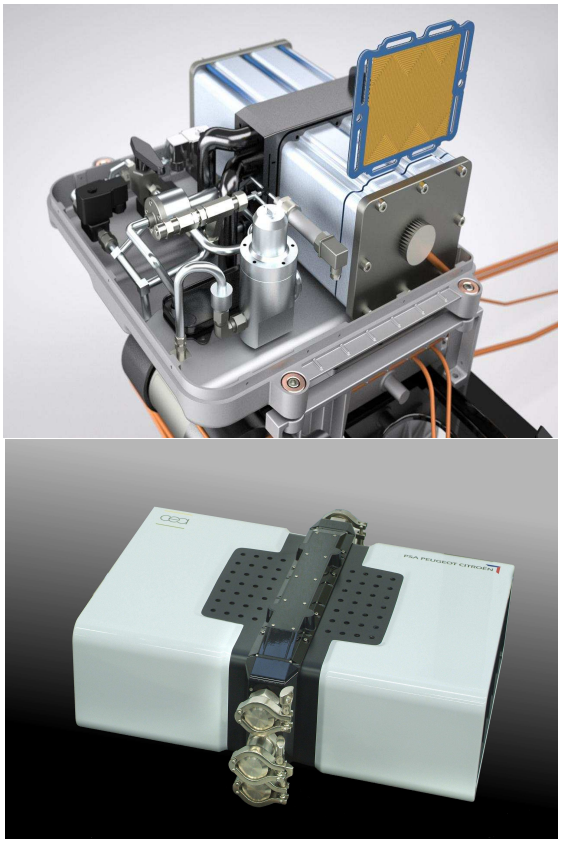

**Figure 2.15**: Fuel cell stack for automotive applications [64]

**PEMFC electric response** The variation of the global reversible energy of the overall reaction is obtained as a function of the Gibbs free energy [28, 96]. Neglecting irreversible losses within the cell, this energy $\triangle G$ is given by the equation 2.15. Where $n$ is the number of electrons involved in the reaction, $F$ is Faraday's constant and $E_{max}$ the maximum voltage of the cell in open circuit.

$$\triangle G = -nFE_{max} \tag{2.15}$$

Through this equation and using the relationship of equation 2.16, one can estimate the thermodynamic potential of equilibrium at a temperature $T$. As the entropy $\triangle S$ is dependent on temperature and pressure, the expression of the reversible voltage $E_{rev}$ is a function of the partial pressures and the temperature. It is obtained through the Nerst equation (equation 2.17) [28].

$$\triangle G = \triangle H - T\triangle S \tag{2.16}$$

$$E_{rev} = E_{max} - \frac{RT}{nF} ln\left(\frac{P_{H_2}}{P_{atm}}\sqrt{\frac{P_{O_2}}{P_{atm}}}\right) \tag{2.17}$$

Where $P_{H_2}$ and $P_{O_2}$ are the partial pressures of hydrogen and oxygen respectively, $R$ is the perfect gas law constant and $P_{atm}$ is the atmospheric pressure.

The reversible voltage $E_{rev}$ is equal to 1.23 V for the water production in liquid state, while its value is 1.18 for the water production in steam state. Nevertheless, when the cell delivers a current $i_{fc}$, the value of its voltage $U_{cell}$ becomes different from $E_{rev}$ due to the irreversible losses. The main losses are: activation $\eta_{act}$, ohmic $\eta_{ohm}$ and concentration losses $\eta_{conc}$ [117, 28, 96]. Equation 2.18 presents the cell voltage $U_{cell}$ as a function of these different variables.

$$U_{cell} = E_{rev}\left(T, P_{H_2}, P_{O_2}\right) - \eta_{act}\left(i_{fc}, H_r, T\right) - \eta_{ohm}\left(i_{fc}, H_r, T\right) - \eta_{conc}\left(i_{fc}\right) \tag{2.18}$$

Figure 2.16 shows the characteristic curve voltage vs current density for a cell (polarization curve), where can be seen the operating region of each specific loss.

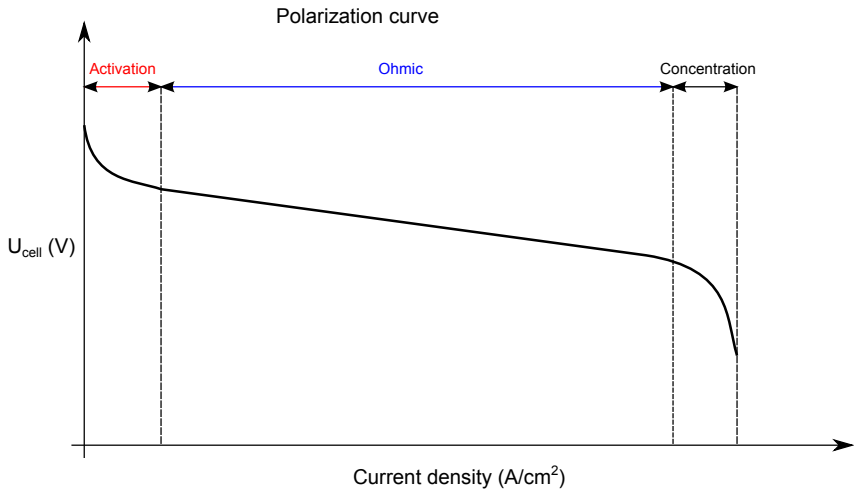


**Figure 2.16:** Polarization curve

A mathematical representation of this voltage response was proposed in [96] as the equation (3.7), where the coefficients $\beta_i$ are fitted using experimental results.

$$U_{cell} = \beta_1 + \beta_2 T_{FC} + \beta_3 T_{FC} ln\left(p_{cath} - \beta_5 \frac{i_{FC}}{\beta_6}\right) + \ldots$$
$$\ldots + \beta_7 T_{FC} ln\left(p_{an}\right) + \beta_8 \frac{i_{FC}}{e^{-\frac{1268}{T_{FC}}}} + \beta_9 ln\left(H_r\right) \tag{2.19}$$

The voltage response of the complete stack is given by the sum of the individual cells response ($U_{stack} = U_{cell}.N_{cell}$).

The amount of oxygen and hydrogen required for reaction, and the amount of water created are directly dependent on the current required to stack. Equations 2.20, 2.21 e 2.22 present these relations.

$$q_{O_2(FC)} = \frac{N_{cell} i_{FC}}{4F} \tag{2.20}$$

$$q_{H_2(FC)} = \frac{N_{cell} i_{FC}}{2F} \tag{2.21}$$

$$q_{H_2O(FC)} = \frac{N_{cell} i_{FC}}{2F} \tag{2.22}$$

As a result of the reaction, the heat created is obtained from the electric losses that are converted to heat flow $Q_{FC}$.

Even though the fuel cell has a static response, a dynamic content is imposed to this response by the dynamics of each subsystem. This is achieved through the influence of subsystems state variables ($p_{cath}$, $T_{FC}$, $p_{an}$, $H_r$ and $i_{FC}$) on the cell voltage response (equation 3.7).

#### 2.3.4.3 Description of a fuel cell system

Equation 2.18 indicates that to obtain a good response of a fuel cell stack, a good conditioning of the system state variables, such as current, pressures, temperatures and hygrometry is required. For this reason, a system that regulates these variables close to an operating point is needed in order to garanty the best response of the fuel cell stack. Figure 2.17 illustrates all the components required in a possible PEMFC system for vehicular applications.

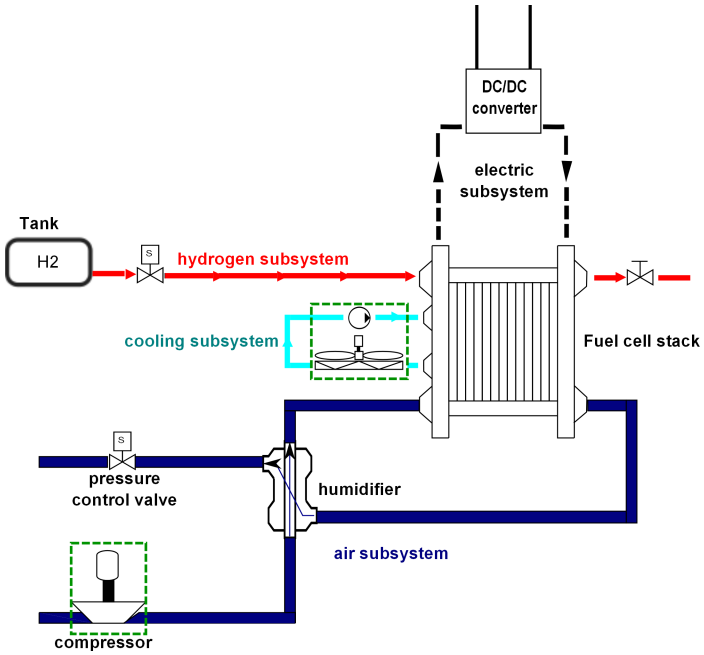


**Figure 2.17**: Example of a fuel cell system

It contains four subsystems:

- Hydrogen subsystem
- Air/ oxygen subsystem
- Cooling subsystem
- Electric subsystem

**Hydrogen subsystem** The main objective of this circuit is to control and regulate the flow and pressure of hydrogen within the fuel cell. This is accomplished through a coordinated control between the two valves present in the circuit (figure 2.17). The inlet valve allows the passage of the hydrogen flow from the tank in direction to the

anode chamber of the cell. Normally this valve controls the pressure at the anode side. Thus, when the pressure in the anode is lower than the desired value the valve opens proportionally to this pressure difference. This ensures the pressure regulation and the amount of hydrogen inside the anode chamber. However, the presences of transport phenomena through the membrane cause the passage of water and nitrogen from the cathode side to the anode, thereby reducing the fraction of hydrogen in the anode and the cell performance. In order to overcome this problem, a purge procedure is necessary. This procedure is performed by opening the outlet valve for a short time. The difference in pressure between the anode and the environment causes a strong flow that allows to dispel water and nitrogen accumulated at anode. Beside, there is a depressurization at anode, which causes the filling of the anode chamber with hydrogen by opening the inlet valve. Equation (2.23) can be used to represent the anode chamber pressure ($p_{an}$) behavior, when it is considered as a unique volume. Where $q_{purge}$ is the outlet flow of the purge valve, $q_{H_2(input)}$ is the hydrogen inlet flow.

$$\frac{dp_{an}}{dt} = \frac{RT_{an}}{V_{an}} \left( q_{H_2(input)} - q_{H_2(FC)} - q_{purge} \right) \tag{2.23}$$

The circuit configuration illustrated in figure 2.17 represents an operating mode called dead-end. To operate with higher stoichiometries (between 1.2 and 1.5), an hydrogen recirculation is applied from the anode outlet to its inlet. This recirculation mode is accomplished through the use of a pump (active system) or through an ejector system (passive system) [64].

Even if the recirculation mode presents a better flow of hydrogen, in this work the dead-end configuration has been adopted.

Despite the improvement obtained in terms of the stack performance, the depressurization and especially the amount of hydrogen eliminated from the anode during the purge procedure require the definition of a strategy that adapts well the demands of the stack. Nowadays, a periodic purge strategy is the most used. The frequency and duration of the outlet valve opening are dependent on the current required by the stack.

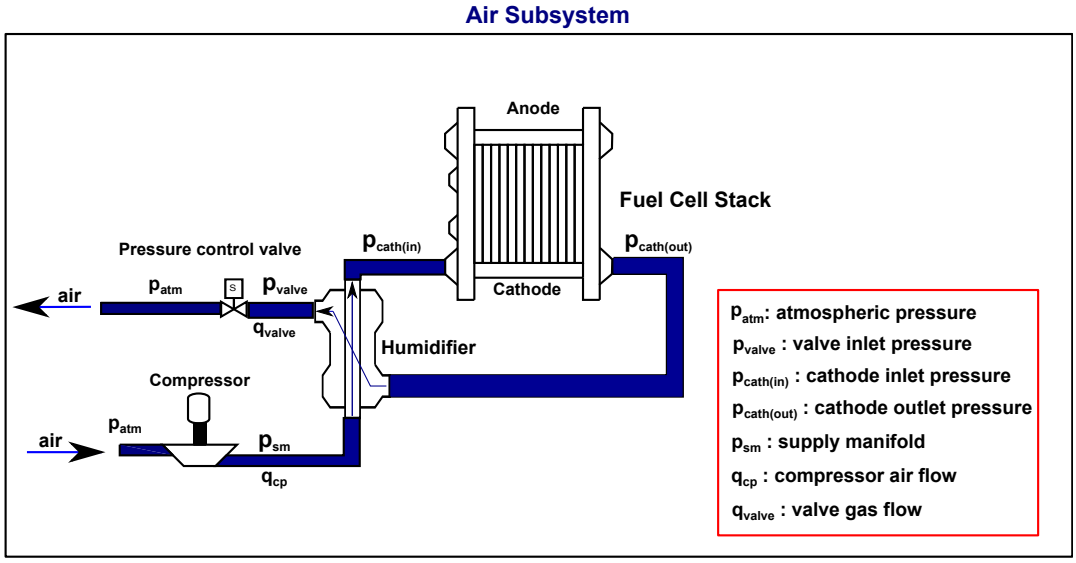


**Figure 2.18:** Fuel cell air supply subsystem

**Air/oxygen subsystem** As in the case of the hydrogen subsystem, the air/oxygen subsystem has the function to control the pressure and oxygen flow inside the cathode chamber.

Concerning the cathode pressure ($p_{cath}$), it can be calculated using the ideal gas law (2.24) as in the anode case, considering it as an unique volume without pressure drop and mass transfer across the membrane (O2, N2 or H2 crossover). In (2.24), $q_{cp}$ is the air flow delivered to the stack, $q_{valve}$ is the gas flow through the control pressure valve towards to the environment, $R$ is the ideal gas constant and $T_{cath}$ is the cathode temperature.

$$\frac{dp_{cath}}{dt} = \frac{RT_{cath}}{V_{cath}} \left(q_{cp} - q_{O_2(FC)} + q_{H_2O(FC)} - q_{valve}\right) \tag{2.24}$$

Typically the oxygen is delivered in the form of air rather than through reservoirs, as in the case of hydrogen. This requires an air compressor which has effects on the temperature and humidification of the supplied air. Thus, this circuit has also to ensure the conditioning in temperature and humidity of the air delivered to the stack.

Basically, it consists of three elements (figure 2.18): air compressor, humidifier and control pressure valve.

**Air compressor** For powers above 1 kW, it is necessary to use air compressors to ensure the flow into the stack. Typically for this type of application, it is required a capacity to deliver large air flow with a relatively low compression ratio. Among the compressors adapted for FC applications, the following models are the most used [64, 24]:

- Scroll compressors
- Claw compressors
- Turbochargers (centrifugal compressors)

To choose the type of compressor, it should take into account the fact that the presence of this element leads to an increase of energy consumption and a reduction of the dynamic response of the stack. According to different authors [119, 120], the turbochargers are best adapted for fuel cell in vehicle applications. They have a good dynamic response, low power consumption and compactness, but they have a drawback in terms of control. Compared to other technologies, the centrifugal compressor has a highly nonlinear dynamic response.

In our work, a compressor of this type is an association of an electric motor and a compression stage. In the compression stage, the outlet air flow $q_{cp}$ is calculated in 2.25 by an experimental static map and highlights its strong dependence on the rotational speed of the motor $\omega$ and the compression ratio ($\Pi_{compression} = \frac{p_{sm}}{p_{atm}}$). $\omega$ is function of the applied control $u_{mot}$ and the resistive torque $C_r$ (eq. 2.27), which is dependent on $\omega$, $q_{cp}$ and $\Pi_{compression}$. Equations 2.26 [119] represents the dynamics of the motor-compressor system.

$$q_{cp} = f_{comp}\left(\omega, \Pi_{compression}\right) \tag{2.25}$$

$$\frac{d\omega}{dt} = \frac{1}{J}\left(\alpha.u_{mot} - C_r - \varphi\omega\right) \tag{2.26}$$

$$C_r = \frac{C_p T_{atm}}{\omega \eta_{cp}}\left[\left(\Pi_{compression}\right)^{\frac{\gamma-1}{\gamma}} - 1\right] q_{cp} \tag{2.27}$$

Where $J$ is the motor inertia, $\alpha$ is the torque constant amplifier and $\varphi$ is the viscous friction coefficient, $C_p$ is the air specific heat capacity, $T_{amb}$ is the ambient temperature, $\eta_{cp}$ is the compressor efficiency, $p_{sm}$ is the outlet pressure, $p_{atm}$ the atmospheric pressure and $\gamma$ is the air specific heat ratio ($\gamma = 1.4$).

As pointed out by Venturi et al. [120], a small change in pressure leads to a large change in flow for this type of compressor. Therefore, a control scheme that couples rotation speed and pressure must be used in order to make a good flow regulation.

**Humidifier** In order to ensure a humidity level that is consistent to the operating conditions of the stack, it is necessary to have the presence of a humidifier in the air circuit to prevent the drying of the fuel cell membrane.

Humidifiers can be either passive or active [66]. In the case of this study, the passive option is chosen because it meets the needs of the system and does not consume energy. This type of humidifier is also known as the membrane humidifier. It has two chambers separated by a membrane. Inside one passing inlet dry air and humidified oulet air into the other. Transport of water and heat is performed by the membrane.

In order to take advantage of the water inside the cathode (created by the reaction), the other edge of the humidifier is connected to cathode outlet, so there is a transport of the humidity from the outlet reacted gas to the inlet air (figure 2.18).

Considering as a constant control volume where a heat flow and mass balance is done, this component has its heat transfer behavior given by the Fourier equation in (2.28), where $\mu$ is the overall heat transfer coefficient, $S$ is the contact surface and $\Delta T_{mem}$ is the difference of temperature across the membrane.

$$\frac{dQ}{dt} = \mu.S.\Delta T_{mem} \tag{2.28}$$

The vapor mass transfer in the humidifier is driven by a concentration gradient of the humidity at the boundary of the membrane. Linked to the different transport phenomena through the membrane, the vapor mass transfer defines a dynamic pressure behavior inside the humidifier, modeled by (2.29). $V_{hu}$ is the volume of each chamber of the humidifier, $p_{hu}$ is the pressure in the chamber, $R$ is the ideal gas constant, $T_{hu}$ is the temperature in the humidifier, $m_{molar}$ is the molar mass of the gas (air). The flows variables $q_i$ represents the input, and output flows and the transport phenomena.

$$V_{hu}\frac{dp_{hu}}{dt} = \frac{RT_{hu}}{m_{molar}}\sum_i q_i \tag{2.29}$$

The volume of the humidifier chamber, defines the pressure dynamic of the humidifier. Moreover, the flows and the geometry of the component create a pressure drop between the compressor outlet and the cathode inlet, as well as between the cathode outlet and the pressure valve inlet.

**Control pressure valve** The valve on the outlet of the humidifier (figure 2.18) is responsible of the pressure control inside the cathode by regulating the output flow. Typically, this element has a dynamic behavior where the output flow $q_{valve}$ is dependent on the pressure difference between its extremities $\triangle p_{valve}$ and the aperture surface of the orifice valve $S_{valve}$.

This relationship can be represented by a non-linear equation such as 2.30, where the air flow dynamics in the valve is neglected. The parameters $\zeta_i$ are defined by the

constructor data and $\triangle p_{valve}$ is the pressure difference across the valve. In this equation, the fluid is considered very slightly compressible due to the small operational value of $\Delta p_{valve}$. This mass flow response $q_{valve}$ is linked to $S_{valve}$ by the opening and closing of the mechanical part of the valve, where $x_{valve}$ is the displacement of the valve operating mechanism.

In terms of dynamic response, the transfer function between the mechanic displacement of the valve $x_{valve}$ and the control input of the valve $u_{valve}$ can be represented by a first order in (2.31). This dynamic is assumed to be identical on both directions (opening and closing) with a time constant $\tau_{valve}$ and a gain $k_{valve}$.

$$q_{valve} = (\zeta_1 x_{valve} + \zeta_2)\sqrt{(\triangle p_{valve})} \tag{2.30}$$

$$\dot{x}_{valve} = \frac{1}{\tau_{valve}}(-x_{valve} + k_{valve} u_{valve}) \tag{2.31}$$

Allied to this dynamic behavior, characteristics of discontinuities such as death zone, hysteresis, etc. may be present, which complicates the pressure regulation.

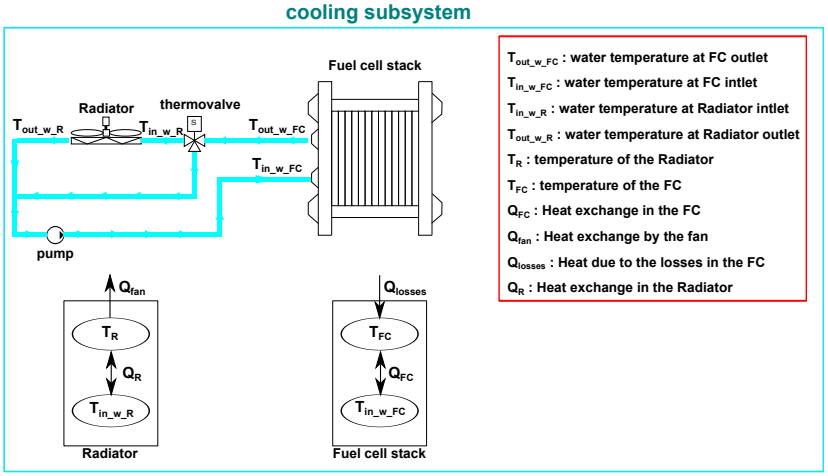


**Figure 2.19:** Cooling subsystem

**Cooling subsystem** Since the fuel cell reaction is an exothermic reaction, it is necessary to evacuate the heat produced. The temperature of the fuel cell stack should be regulated within the acceptable region of operation and as close as possible of its optimal value (table 2.2). Temperature regulation allows the performance of the fuel cell stack to be improved and avoids its degradation. Cooling systems are used for this purpose. For stacks with significant power (case of automotive applications), the cooling is made by

heat exchange using passing fluid. A cooling circuit passes through the cell and through a heat exchanger (radiator), in which heat is exchanged in a natural way or by forced convection using fans. The liquid circulates in the circuit with the help of a pump (figure 2.17).

The cooling circuit can be composed by a radiator, a thermovalve and a pump (fig. (2.19)). In the cooling process, the thermal capacities are used to calculate the temperature at different places of the circuit. The most important thermal capacities are:

- Fuel cell stack heat capacity
- Water inside the fuel cell heat capacity
- Radiator heat capacity
- Water inside the radiator heat capacity

The temperature of the fuel cell stack and the radiator are calculated by the equation 2.32. For each element $i$ (stack or radiator), $T_i$ is the temperature, $m_i$ is the mass, $C_{p_i}$ is the heat capacity and $Q_j$ are the heat flows involved.

$$\frac{dT_i}{dt} = \frac{1}{m_i C_{p_i}} \sum Q_j \tag{2.32}$$

At the outlet of the two mentioned elements is calculated the temperature of the cooling liquid $T_{out}$, which depends on the liquid flow $q_{water}$, the temperature differences, the convection coefficient $h_i$ and the thermal exchange surface $S$.

$$\frac{dT_{out}}{dt} = \frac{1}{m_{water} C_{p_{water}}} \left[ q_{water} \left( T_{in} - T_{out} \right) + h_i S \left( T_i - T_{in} \right) \right] \tag{2.33}$$

In order to control the temperature of the stack, the thermovalve acts passively to pass the liquid either through a by pass or through the radiator. If more heat exchange is necessary to reduce the temperature of the stack, a control is applied on the fan that is placed on the radiator.

**Electric subsystem** The electric subsystem performs the interface between the electric bus and the fuel cell stack. This interface transports the power from the stack to the electric bus, converting the voltage and current levels. A static DC/DC converter is used as interface. As the fuel cell does not act as reversible element, the DC/DC converter must be irreversible to protect the stack in case of a reverse current.

In the case of series hybrid applications, the converter has an important function in controlling the power output of the fuel cell stack system. Specifically for the architecture

used in this work (with just one converter), the energy management is controlled by the DC/DC converter.

The converters can be step-up (boost), step-down (buck) or both (buck-boost). They are chosen according to the nominal voltage of the stack and the desired bus voltage and the DC bus. When it exceeds the voltage of the electric bus, a buck converter should be used. In case of a stack nominal voltage below the bus voltage, the converter must be of boost type. Finally, a buck-boost converter is adopted when the operating voltage of the stack can be higher or lower than the bus voltage.

For our application, a buck DC/DC converter is used to represent this subsystem. Equation 2.34 is used, such that the current $i_{FC}$ is imposed to the fuel cell stack while it replies with the voltage $U_{FC}$. Where $L$ is the inductance and $U_{FC}$ is the fuel cell stack voltage

$$L\frac{di_{FC}}{dt} = U_{FC} - \alpha_{buck}U_{bus} \tag{2.34}$$

A control strategy is implemented in order to regulate the output current. The voltages of the fuel cell and the electric bus $U_{bus}$ are considered as measurements in order to calculate the value of the duty cycle $\alpha_{buck}$.

## 2.4 Conclusion of the chapter

The aim of this chapter was to present briefly the features of hybrid fuel cell vehicles in order to identify the issues involved. Among them there are the objectives of this thesis.

In the first part was presented a state of art about the fuel cell vehicles. This state of art has show the positive trend to the advancement of this technology and the challenges that remain for its full consolidation as a viable transportation alternative.

The architectures available today were presented and analyzed in order to extract their main features. We could then define the hybrid series architecture as the most suited to fuel cell vehicle applications. In this architecture, the non reversible source is the fuel cell stack and the battery is the reversible energy storage element. This combination of elements allows the elaboration of energy management strategies that optimize energy consumption, compensate the dynamic constraints of the fuel cell stack system and act against the cell degradation.

According to our specific application, a description of the main characteristics of each element of the architecture was made. This allows to understand the general operation principle of the elements and how they act on the vehicle in terms of dynamic and energy response. The technologies involved show that there are operational conditions that

should be targeted. Specifically for the fuel cell system, it can be seen that it is a complex system which requires the control of state variables to obtain a proper functioning of the cell.

In order to obtain the optimal sizing of the vehicle and the optimal energy management including the dynamics and durability aspects, it is important the prior knowledge about the main characteristics of the vehicle components. Therefore, in the next chapter modeling for sizing and optimization will be done based on the information presented in here. It will present the mathematical models developed in accordance with the technologies presented and the most indicated optimization tools for the problem involving the chosen architecture.

# Chapter 3

# Models and optimization tools

**Abstract**

This chapter has the role to present the tools that will be useful to reach the objectives of this thesis. These tools represent the modeling tools, the models and the energy management algorithms related to the fuel cell hybrid electric vehicle. In order to clarify the choices made about the models and algorithms, some important concepts and theories are introduced as well.

## 3.1 Introduction

Even if the fuel cell vehicle is considered as an important option to compose the set of transport solutions, the technology involved has not achieved yet a desired maturity level, requiring more efforts in research and developments.

Having the objectives to propose new methodologies to overcome some remaining technical limitations, the scope of this work is essentially focused essentially on two key topics:

1. Optimal sizing methodology
2. Optimal energy management strategy, integrating the aspects of dynamics and durability of the fuel cell system.

These subjects demand studies that combine multiple disciplines as mechanics, electrics, chemistry, automatic control, etc. Furthermore, to reach all the goals, it is also required a basic structure adapted and defined in introduction to each of these topics. Therefore, this chapter is oriented to present the tools that will be necessary to reach the objectives. Such tools are:

- Models (forward/backward, simulation, control)
- Optimization tools for the energy management

This chapter presents two main parts that are related to the previously established objectives. However, important concepts about modeling and optimization are introduced before the description of the required structure. Besides, the initial part of the chapter includes also a state of the art about the energy management for hybrid applications and a presentation of the modeling tool that is used in these works.

In the sequence, the structure needed to perform the optimal sizing task is described through the different models adopted and the optimization tool selected to compose the sizing process. An outline in accordance to the steps of the sizing procedure establishes the order to present the models and the optimization method.

The final part of the chapter deals with the description of the models and optimization tools that are used to the design of an energy management strategy (EMS). The constraints brought by the inclusion of the fuel cell dynamics in the EMS require an optimization method capable to perform this inclusion. Moreover, to obtain the fuel cell system dynamics, it is necessary a model that has the ability to represent it. In this part of the chapter, the FC system dynamic model and the chosen optimization method are presented.

## 3.2 Modeling and energy management strategy for FCHEV

In this section, the modeling and EMS for hybrid architectures, in particular for the FCHEV, are approached by the presentation of important concepts, state of the art and the tools related to their developments.

### 3.2.1 Modeling tools and concepts

The models of the FCHEV for this work are constructed using the modeling environment VEHLIB [116] developed by IFSTTAR in Matlab-Simulink$^{(c)}$. The VEHLIB is a library that contains models of vehicles and elements that compose them. Figure (3.1) presents this library.

The elements of the library were built using quasi-static models based on the mapping of components originated from experimental results. This allows to obtain a reasonable calculation time, keeping the coherence in terms of the energy consumption.

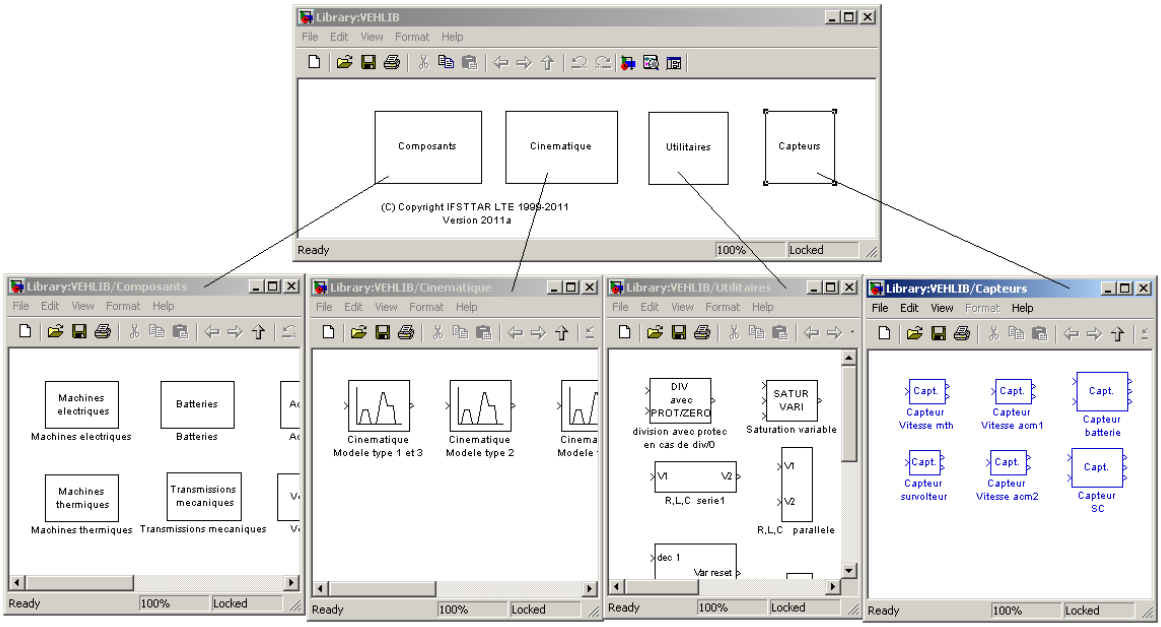


**Figure 3.1**: VEHLIB

The modeling tool has a library of drive cycles that are used for the simulations of the driving conditions. They are imposed to the vehicle by a close loop model of the driver, who is represented as a PID controller approach.

Normalized cycles and cycles recorded during real driven test campaigns are examples of cycles contained in the library. In this work, the real cycles HYZEM Urban, HYZEM Route, HYZEM Autoroute and Mountain cycle [14, 15] are the most adopted to analyze the behavior of the models. Figure 3.2 illustrates the extra-urban drive cycle, while the other cycles are present in the appendix 1.

Using VEHLIB, causal models can be created with a formalism based on the Bond-Graph theory [23, 107].

The models may have two different representations that can be called behavior models and design models, depending on the objectives and the type of problems to solve [88]. Such type of problems are known as forward and backward, and they are identified using the principle of causality. This cause and effect relationship indicates that the method to solve a forward problem, which means calculation from the source (cause) to the effect, should be different from the method to solve a backward problem (from the effect to the cause). Therefore, the behavior and design models, called as well as forward and backward models, are mainly differentiated by the sense and type of calculations used to solve the model's equations [51]:

- Forward models: The starting point is the setpoint (cause) of the closed loop system,

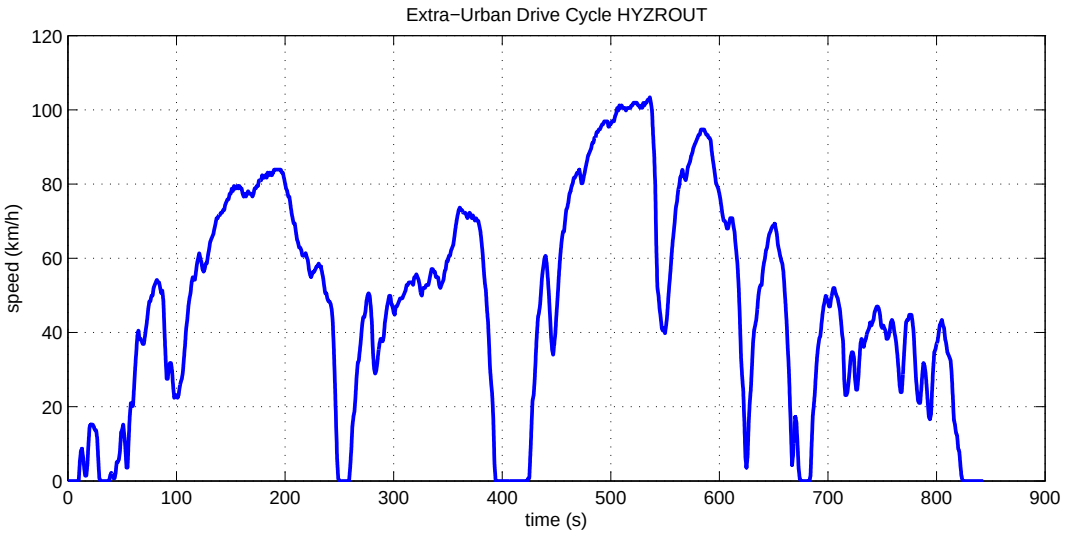


**Figure 3.2:** Extra-Urban Cycle HYZROUT

and the aim of the calculation is to calculate the system response (effect) to follow this setpoint. In the case of the vehicle, the effect is the speed of the vehicle and the setpoint is the driver speed requirements. This modeling is the most accurate to the reality and can be adapted to the control of real time systems without too much implementation efforts.

- Backward models: The starting point is the effect of the forward model. Considering the vehicle, this starting point is the speed. From this speed, it is possible to calculate the other variables up to the traction power necessary to meet the assigned speed. This type of modeling does not represent the reality as the forward one, but it allows to simplify the decision about the command to be applied.

Figure 3.3 illustrates these two types of models for the same electric powertrain.

They will be used to represent the behavior of the vehicle (components) and to the design of control laws and energy management strategies in order to achieve the stated objectives of this work.

Figure 3.4 illustrates a fuel cell hybrid electric forward model created using VEHLIB.

After the overview about the modeling aspects, concepts and tools, the sequence of this section introduces a general study of the energy management strategy.

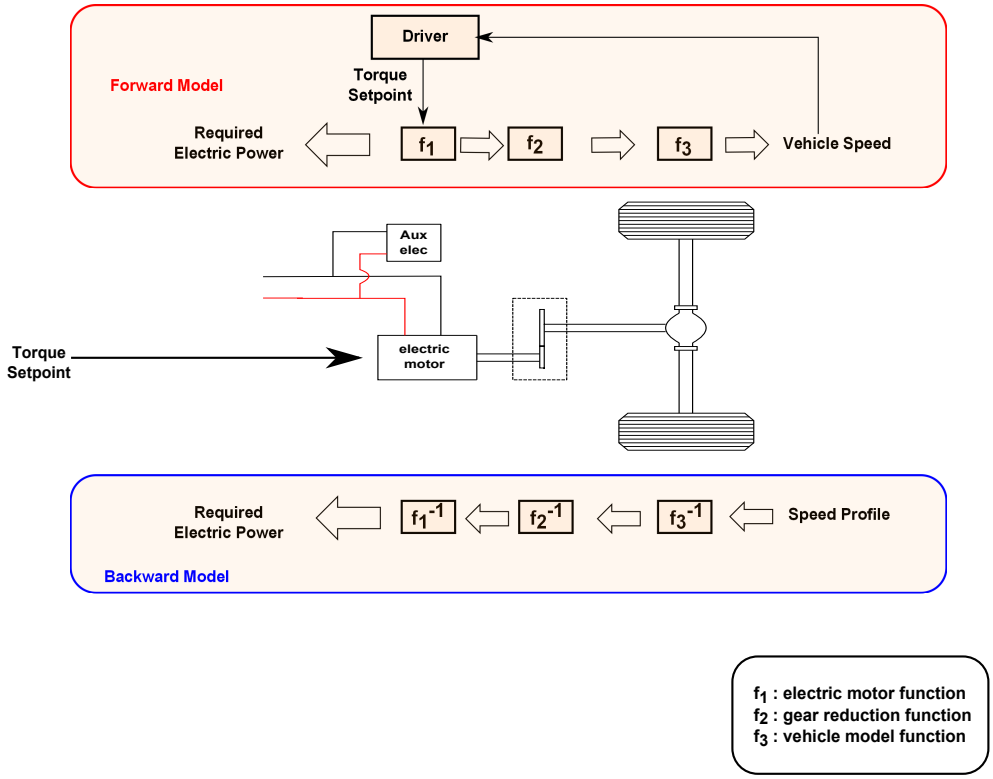


**Figure 3.3:** Forward and backward modeling

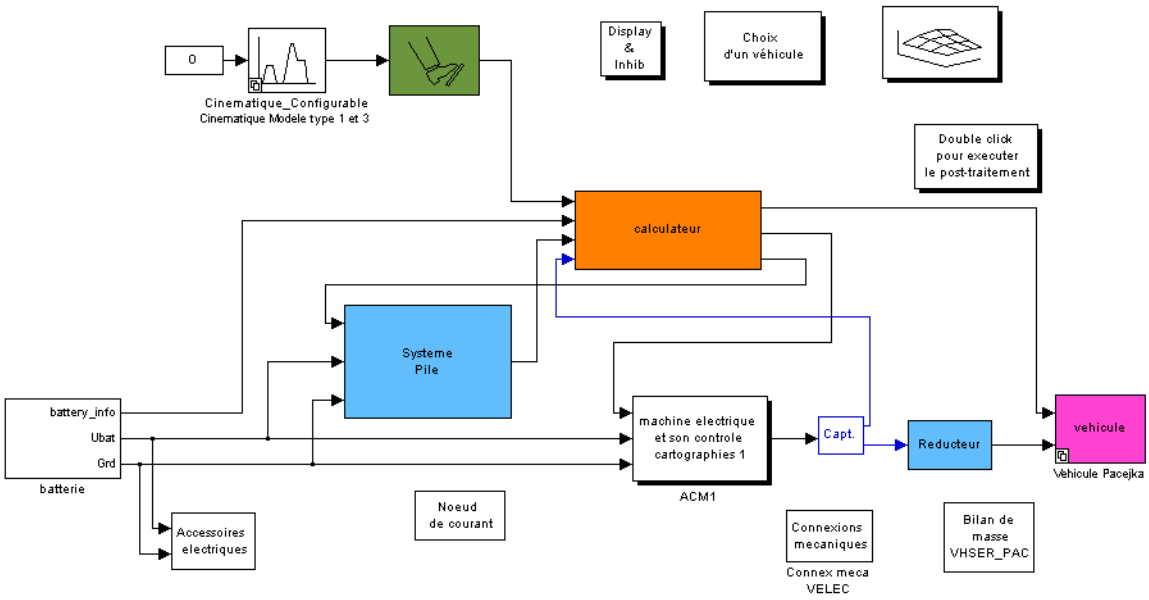


**Figure 3.4:** Fuel cell hybrid electric vehicle model in VEHLIB

### 3.2.2 Energy management strategy: concepts and state of the art

As already mentioned, a full hybrid architecture, such as the adopted in this work, offers an extra degree of freedom that can be used to optimize the power sharing between battery and fuel cell system. Nevertheless, the energy management involved in this power split should tackle with the following operating modes:

- Fuel cell system traction mode: traction power delivered by the fuel cell system
- Battery traction mode: traction power delivered by the battery
- Hybrid traction mode: traction power delivered by the fuel cell system and battery at the same time
- Energy recovery mode: recovery power during braking procedures is stored in the batteries

The aim of a good energy management strategy is to appropriate all these modes during the mission and to find the battery and fuel cell system power profiles that represent the minimum of hydrogen consumption to accomplish the mission. Such minimization is not only used to design the FCHEV energy management strategy, but also can be applied in the scope of sizing procedure, defining the most adapted dimensions of FC system and battery in terms of hydrogen consumption.

The EMS can be performed using different methods, as presented in the sequence.

#### 3.2.2.1 State of the art: Energy management

For a better understanding of the energy management strategies for hybrid vehicles with multiple on-board power sources, numerous studies were performed by various authors can be found in the literature. The mainly adopted approaches are grouped according to their characteristics in terms of methodology and implementation.

**Intelligent based strategies** There exist many studies using artificial intelligence-based energy management strategy such as fuzzy logic and neural networks for use in PEMFC powered systems. Among them, fuzzy logic based controllers (FLC) have a predominant position due to its independence of a full mathematical plant model and training procedure. Fuzzy logic incorporates an alternative way of thinking, which allows modeling complex systems using higher level of abstraction originating from our knowledge and experience. However, this knowledge represents a drawback due to the

dependence of a certain level of expertise embedded in the strategy. This means that some strong assumptions can be made according to a definition of expertise, which is dependent on the designer's knowledge about the problem.

Many researchers focused on fuzzy logic approach and applied it to hybrid systems with PEMFC for different applications. Among them, Gao et al. [61] have proposed a management algorithm for the power split in a hydrogen powered hybrid heavy vehicle (bus) composed of PEMFC, as the main power source, and a battery/UC (ultra capacitor) combination as the reversible converter/storage unit. Caux et al. [30], regulated the energy management in PEMFC/Battery powered hybrid light vehicular systems using fuzzy logic. As a contribution to the mentioned studies, Erdinc et al. [54, 55], Li and Liu [83] and Eren et al. [56] inserted the control of internal dynamics of PEMFC system in the fuzzy logic based energy management approach in order to better provide a safe and efficient operation of PEMFC. Eren et al. controlled both the power distribution in the hybrid structure and the oxygen stoechiometry of PEMFC as the outputs of the FLC.

Another artificial intelligence method used for the control of hybrids system is the neural network approach. Neural network models are computer programs that are designed to emulate human information processing capabilities. The ability of neural network system to spontaneously learn from examples and to provide adequate and fast responses to new information, which are not previously stored in memory, has generated increasing acceptance for this technology in various engineering fields. The drawbacks of this approach are about the need of training process using a large database obtained experimentally and the lack of stability proof.

Some studies using the neural network approach for energy management can be found in the literature. Ates et al. [18] provided a neural network supervisory controller using Adaptive Linear Neural Network (ADALINE) that is combined with a multi-level Haar wavelet transform to define the power delivered by the fuel cell system in a FCHEV. Askarzadeh et al. [16] and Prokhorov [97] also used the same neural network type, but combined with fuzzy logic in order to be adapted to different drivers.

To summarize, these methods represent a "black box" approach, which simplifies the modeling requirements, especially in the case of complex systems, however, they can not guarantee the global optimization either the stability of the solution. Besides, they are strongly dependent to the designer knowledge and the database used.

**Frequency decoupling strategies** In vehicular FC systems, transient changes in load demand may often occur. This can cause a dynamic stress into the fuel cell membrane due to pressure oscillation and possible oxygen starvation, reducing the lifetime of the

fuel cell [125]. Therefore, frequency decoupling techniques have been applied to prevent the fuel cell system from load changes at high frequencies.

The most basic approach is using a transfer function for a delay with a suitable time constant, such as a first order low pass filter. Liu et al. [84] applied this concept to PEMFC hybrid system. These filters decouple the main signal with a pre-defined cut-off frequency, preventing the FC from transient variations. However, the loss of important edge information is a significant phenomenon in conventional filtering techniques.

In order to deal with this drawback, wavelet transform based decoupling strategy for PEMFC has been applied by some authors such as Uznoglu and Alam [118], Zhang et al. [133] and Ates et al [18]. The advantage of this type of analysis is that the wavelet transform decomposes a signal into a series of short duration waves or local basis functions (wavelets) on the time axis which allows the analysis of the local phenomena in signal consisting of many transients.

This kind of strategy allows a real-time application, but it presents a difficulty to deal with the durability, dynamic aspects and the consumption at the same time.

**Optimization based strategy** In these types of energy management approaches, the optimal reference power signals for the on board power sources are calculated by minimization of a cost function. This cost function generally represents the fuel consumption or emissions especially for vehicular applications. If the optimization is performed over a fixed drive cycle, a global optimum solution can be found. Many approaches such as optimal control theory, linear programming, dynamic or stochastic programming and non-linear model predictive are used for solving the global optimization problem. In fact, the global optimal solution is non-causal because it finds the minimization of the cost function based on the knowledge of the future and past power demands. Therefore, for on-line application these approaches are not indicated. Nevertheless, they might be a basis of designing rules for online implementation or comparison for evaluating the quality of other control strategies. Moreover, an on-line optimization-based control strategy can be found by using the definition of an instantaneous cost function. Such cost function should include an equivalent fuel consumption to guarantee the self-sustainability of the electrical path. Even if the solution of this problem is not globally optimal, it can be used for online application.

In terms of global optimization, the Dynamic Programming (DP) and the Pontryaguin's Maximum Principle (PMP) [39] are often used in vehicle energy management and optimal sizing. Scordia et al. [106] adopted the dynamic programming coupled with neural networks to design a power split strategy for hybrid vehicles. Vinot et al. [122]

studied the two approaches for a hybrid electric vehicle battery/UC. As done by Vinot et al., Delprat et al. [46] used the PMP and an iterative method to design a energy management strategy for conventional hybrid vehicles (ICE/batteries).

For on-line applications, some authors have based their energy management controllers on these optimization methods (DP and PMP). Rodatz et al. [103] presented an equivalent fuel consumption minimization strategy (ECMS) in order to minimize the amount of hydrogen in a PEMFC/UC hybrid vehicle. A similar approach is used by Xu et al. [127] for a fuel cell/ battery hybrid bus and by Trischler [117] for a PEMFC/battery tractor. Bernard et al. [75] have proposed to complete the previous controls with a predictive approach in the ECMS for a PEMFC/battery vehicle.

Each of the abovementioned approaches provided an important contribution to the energy management issue of PEMFC powered hybrid systems, ensuring the stability of the response. Despite the advances obtained with these methods, it is still necessary to develop a more computationally efficient solution that approaches the local optimization to the global optimization, but taking into account the operating constraints.

An optimization based strategy is adopted to perform the energy management strategy in this work. The knowledge of the dynamics and the consumptions aspects allow to represent the energy management issue in a optimization problem, that can be solved by the DP, PMP, and methods based on these approaches and theories.

### 3.2.3 Optimization problem

The objective of the energy management is to define the power split that minimize the cost function $g\left(P_{FC}\left(t\right)\right)$ (hydrogen consumption according to the power supplied by the fuel cell system), while respecting the constraints and boundary conditions. This can be summarized in an optimization problem defined in (5.29). The trajectory of $P_{FC}^{*}$ is the control trajectory input that minimizes the function **J** in a drive cycle. Moreover, $P_{FC}^{*}$ must be well adapted to the dynamics of the system (fuel cell system and battery).

$$\begin{cases} Cost\,Minimization: \\ \mathbf{J}\left(P_{FC}^{*}\right) = min_{P_{FC}^{*}} \int_{0}^{t_f} g\left(P_{FC}\left(t\right)\right).dt \\ P_{FC}^{*} = argmin\mathbf{J}\left(P_{FC}\left(t\right)\right) \\ \hline Constraints: \\ P_{batt\,min}\left(-3C\right) \leq P_{batt} \leq P_{batt\,max}\left(10C\right) \\ P_{FC\,min} \leq P_{FC} \leq P_{FC\,max} \\ SoE_{min}\left(40\%\right) \leq SoE \leq SoE_{max}\left(80\%\right) \\ Boundary\,condition: \\ SoE\left(0\right) = SoE\left(t_f\right) \end{cases} \tag{3.1}$$

### 3.2.4 Conclusion about the modeling and EMS concepts

The concepts and study peformed in this section will be used as a knowledge basis to describe the elements adopted to accomplish the objectives. Forward and backward models are be adopted for different applications. Concerning the energy management strategy, optimization based methods were selected to solve the optimization problem in order to find the power split that minimizes the hydrogen consumption.

In the sequence, the optimal sizing objective has its models and optimization method described according to the stages that compose it. Thereafter, is the turn to describe the elements (models and optimization methods) related to the objective about the conception of an online energy management strategy.

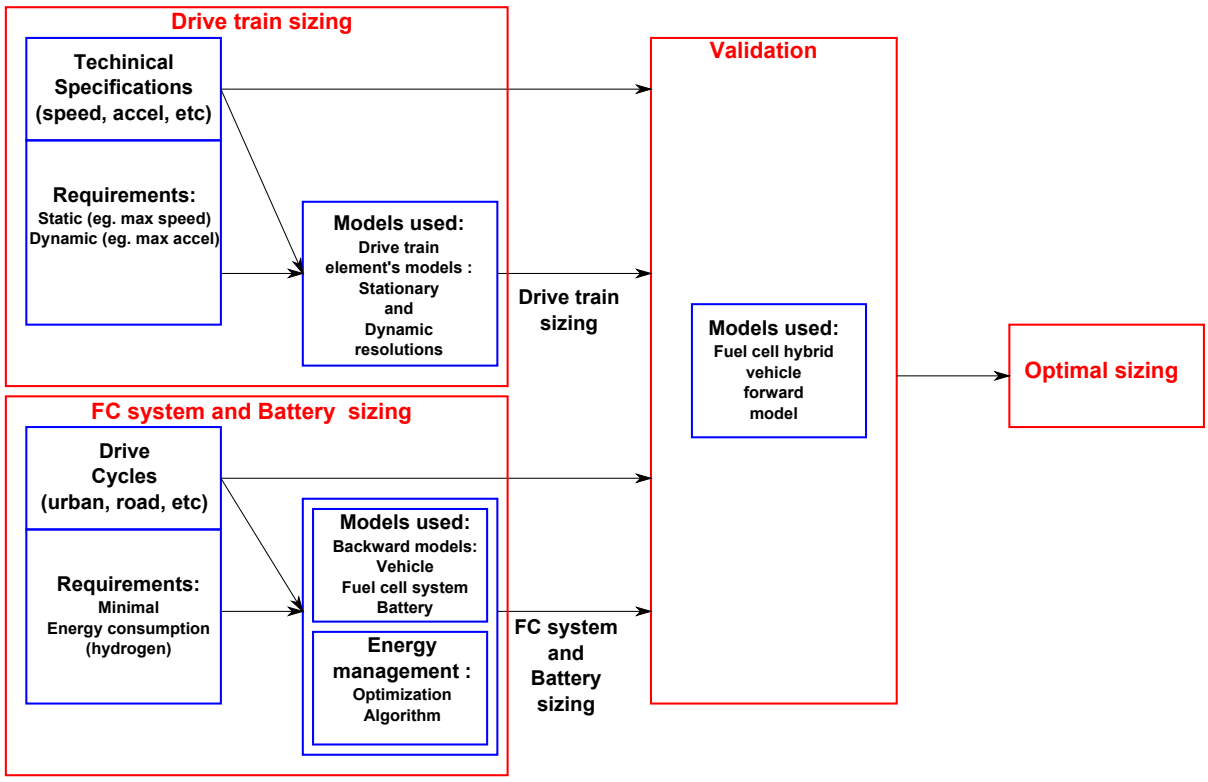


**Figure 3.5**: Structure to perform the optimal sizing procedure

## 3.3 Models and optimization methods for the optimal sizing

The sizing of a hybrid vehicle can be performed using different methodologies, technical specifications and sizing criteria (cost, consumption, etc.). According to the choice made, it would be necessary a set of tools that will be involved in each element's sizing stage and validation. Besides, the optimization included in the process aggregates optimal algorithms used for the sizing purpose. Victor Mester [88] structured the optimal sizing process by the requirements, models and tools used at each step. Figure (3.5) summarizes this idea for our particular case.

In the drive train sizing, depending on the type of the technical specification, a static or a dynamic requirement is imposed to the sizing procedure, which demands either stationary or dynamic models of the drive train elements.

In the case of the fuel cell system and battery, the optimization requirement (reduction of hydrogen consumption) leads to the adoption of backward models to discover the electric power that must be shared between these elements. In order to solve the optimization problem, the algorithm used needs the information about the energy con-

sumption during the drive cycle. Therefore, the models of these elements should be simple, but must keep the energy content information.

Both the drive train dimension and the FC system and battery sizes are validated using the technical specifications and the drive cycles. To perform such validation, a complete model of the vehicle is used. As the objective of this task is to analyze the behavior of the vehicle and its elements, a forward model is adopted.

In the sequel of this section, the models and optimization algorithms chosen for these sizing steps are described, initiating by the drive train.

### 3.3.1 Drive train sizing

As illustrated in (3.5), the technical specifications imposed to the vehicle are responsible for the sizing of drive train elements. They are mainly related to the performances of the vehicle such as maximal acceleration and speed or even the ability to take-off with a high slope. The models and the calculations used to define the sizing of the elements are depending on the type of these performance requirements. This means that a stationary performance index, like maximum speed, only requires an analytical solution of the model, while dynamic performance index, such as maximum acceleration, needs a solution of the dynamic equations related.

The elements present in this part of the vehicle include the vehicle itself (dynamic behavior), the gear reducer and electrical motor. The models of these elements used for the sizing procedure are:

**Vehicle model:**

$$\frac{dv}{dt} = \frac{\frac{\Gamma_{2x\,wheel}(t)}{R_{wheel}} - \left[\left(\frac{1}{2}.\rho_{air}.S.C_x.\left(v\left(t\right)+v_{air}\left(t\right)\right)^2\right) + M.g.\mu.cos\left(\alpha_{slope}\right) + M.g.sin\left(\alpha_{slope}\right)\right]}{M} \tag{3.2}$$

By this equation, the force balance in the vehicle allows to calculate its speed and the acceleration Through the traction torque applied.

**Gear reducer:**

$$\begin{cases} \Gamma_{machine}\left(t\right) = \frac{\Gamma_{2x\,wheel}(t)}{\eta_{red} k_{red}} \\ \\ \Omega_{motor}\left(t\right) = \Omega_{2x\,wheel}\left(t\right) k_{red} \end{cases} \tag{3.3}$$

As a static element, the calculation of the torque or the speed in the gear reducer is performed analytically, no matter the required performance index. In this model (3.3),

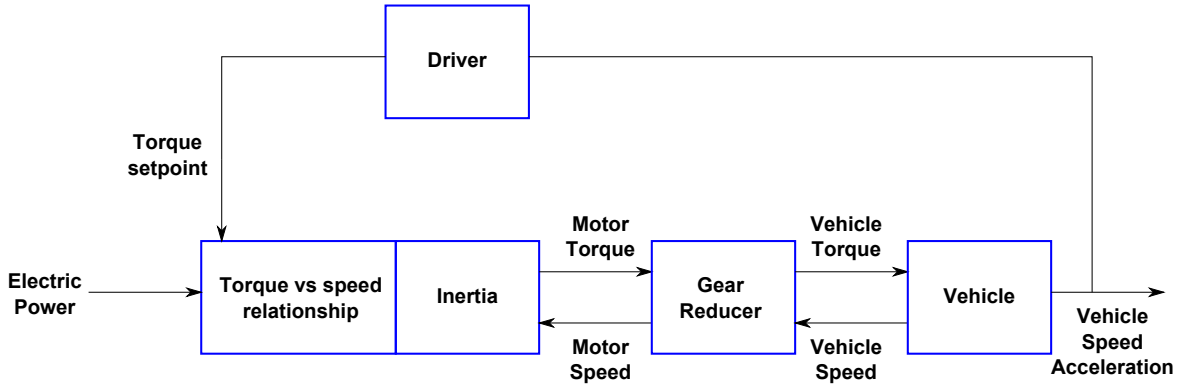


**Figure 3.6**: Structure of the models for the drive train sizing procedure

the gain $k_{red}$ is the parameter that should be find by the sizing method. Such parameter is related to performance indexes such as take-off with high slope and maximum accelerations.

**Electric motor:** The model of the electric motor and its power electronics are represented by an association of a torque $\Gamma_{motor}$ vs speed $\Omega_{motor}$ static map and an inertia component. Through the static map is possible to calculate the losses in the motor and to include them in the electric power required to provide the demanded mechanical power. In terms of sizing procedure, the maximum power and maximum torque presented in the motor static map are linked to several performance indexes such as maximum acceleration and maximum speed.

**Drive train model structure:** Allying these three models, it is possible to achieve the drive train sizing objectives. Figure (3.6) illustrates the drive train structure that will be used in its respective sizing procedure.

Being defined the models involved in the sizing of the drive train elements, the sequence deals with the fuel cell system and battery dimensions, which requires the definition of an optimization method and models adapted to it.

### 3.3.2 Fuel cell system and battery sizing

As pointed out in fig. (3.5), the dimensioning of FC system and battery are obtained by the application of an optimization method that minimizes the hydrogen consumption. This method should solve the optimization problem stated in (5.29), ensuring the global minimization of the criterium. However, the implementation of this type of optimization

method requires the knowledge of the drive cycle and models of the vehicle elements (vehicle, drive train, FC system and battery) that are dedicated for this task.

The global optimization method and the models used in this part of the sizing process are described in the sequence.

#### 3.3.2.1 Global optimization method: Dynamic Programming

Among the existing global optimization methods, the Dynamic Programming (DP) was chosen as optimization tool due to the fact that it presents all the characteristics necessary to solve the optimization problem.

Dynamic programming is a method that uses the graph theory to transport a system governed by a state equation described in discrete time $x(t+1) = f(x(t), u(t), t)$ from a state A to state B regarding some constraints [106]. Therefore, at each time $t$, it is possible to choose $u(t)$ among all eligible values in order to move the system from initial state to final state. The main idea is to choose a sequence of commands $u(t)$ to minimize the cost criterion in (3.4).

$$\mathbf{J}(u^*) = min_{u(0),\ldots,u(t_f-1)} \sum_{t=0}^{t_f} g(x(t), u(t), t) \tag{3.4}$$

By knowing the initial state, the dynamics of the system, all possible commands and mission, the set of possible states are determined. With all possible commands and states, it is possible to find the optimal control sequence $u* = u_1, u_2 ... u_t, ..., u_{t_f}$ that minimize the criterion. The Hamilton-Jacobi-Bellman equation is applied to find this sequence. Belleman optimality principle is the basis of the equation of Hamilton-Jacobi-Belleman. It states that "A series of decision is optimal if and only if, whatever the state and instant considered, the following decisions constitute an optimal decision series for the sub problem which has this state and this instant has initial consitions" [39].

Specifically for the DP method applied on the fuel cell hybrid electric vehicle, the FC dynamics is neglected in order to simplify the optimization process. This leads to build a 2D graph to solve the optimization problem (figure 3.7). The two dimensions in the graph are the time and the energy of battery ($\varepsilon$), which is replaced, for practical applications, by the $SoE$ information.

Therefore, the graph implementation depends on the calculation of the feasible area. The construction of the graph begins with the definition of the $SoE$ grid, which is made using the $SoE$ bounds and discretization ($\triangle SoE$). Thereafter, the edges are built using the possible range of the control input $P_{FC}$ and the battery power $P_{batt}$. They have a discretization given by $\triangle P_{FC}$ and $\triangle P_{batt}$. The operating range of the battery is reduced

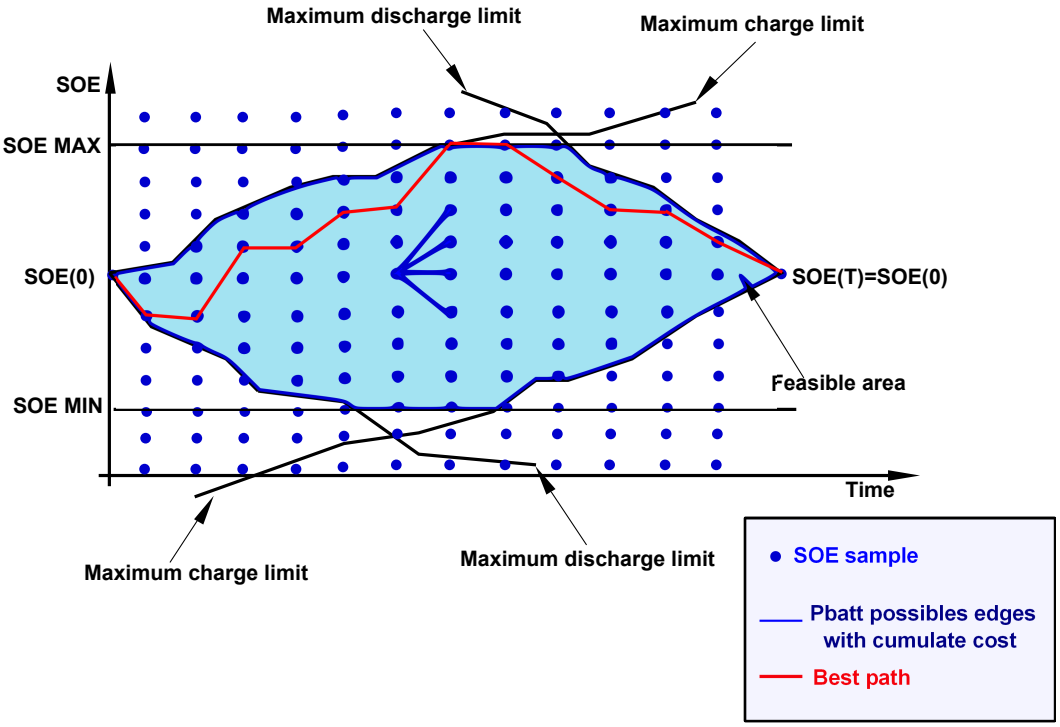


**Figure 3.7:** Dynamic programming diagram

further by considering only those trajectories that are possible between an initial energy level of the battery $SoE\,(0)$ and a desired end state $SoE\,(t_f)$ . Finally, the feasible area for the driving cycle is restricted by the eight individual constraints, i.e., $P_{batt}$ upper and lower bound, $P_{FC}$ upper and lower bound, the upper and lower bound on $SoE$, the initial state $(SoE\,(0))$ , and the final state $(SoE\,(t_f))$. The figure 3.7 presents an example of this feasible area, normally in diamond shape.

The solving procedure of the DP is achieved by a step by step time resolution and consists of the following algorithm [79]:

- Calculate the hydrogen cost for all the feasible edges.
- For each edge of the graph, store the minimal hydrogen consumption (best efficient) to go from the starting point of the cycle until the current edge, and store the best path to go from the preceding point to the current one.
- At the end of the evaluation process, recalculate the best path fo the entire graph: The sequence of $P_{batt}$ that achieves minimum hydrogen consumption is obtained, and thus the control trajectory $P^*_{FC}$ in known.

As can be noticed, the DP method is not well adapted for online application due to its non causal characteristic. Moreover, it presents a computation time and a memory

allocation that can increase fast according to the drive cycle, battery size and precision of the graph. However, the mentioned drawbacks do not represent impediments for design and sizing applications. They can be overcome by the utilization of powerful calculation platforms, with enough memory and applying typical drive cycles. Besides, at a given discretization, the DP provides global optimization responses that can be used as as benchmark to evaluate other optimization methods.

In order to be developed and implemented, the DP requires models to represent the hydrogen consumption of the FC system, the battery behavior and the electric power related to the drive cycle.

In the following, the models used in this optimization process are presented.

#### 3.3.2.2 Models for the optimization process

**Drive train model for the dynamic programming optimization** A backward modeling approach is used to obtain the electrical power profile demanded by the vehicle to follow a speed profile. Therefore, it must be effectuate an inversion of the drive train model. Consequently a speed profile is imposed as an input to the vehicle model that replies with the traction torque to be applied on the wheels. Equation (3.5) shows this inversion, presenting the speed as the input and the torque as the output.

$$\begin{aligned}\Gamma_{2x\,wheel}(t) = R_{wheel}\left\{M.\tfrac{dv}{dt} + \left[\left(\tfrac{1}{2}.\rho_{air}.S.C_x.\left(v(t) + v_{air}(t)\right)^2\right)\cdots\right.\right. \\ \left.\left.\cdots + M.g.\mu.cos\left(\alpha_{slope}\right) + M.g.sin\left(\alpha_{slope}\right)\right]\right\}\end{aligned} \tag{3.5}$$

This torque is transformed by the gear reducer (3.3) to represent the torque that the electric motor must deliver.

The angular speed on the wheels are obtained by (3.6) and is transported to the motor level ($\Omega_{motor}$) using the gear reducer equation (3.3).

$$\Omega_{wheel}(t) = R_{wheel}.v(t) \tag{3.6}$$

For this optimization purpose the inertia of the motor is ignored, so $\Omega_{motor}$ and $\Gamma_{motor}$ define together the mechanical power necessary to the traction. The losses in the electric motor (obtained from its static map) are added to this power, resulting in the electrical power necessary to follow the cycle. This inversion process is illustrated in fig. (3.8).

The electric power obtained from this inversion is shared between the FC system and battery by the DP. Therefore, the characteristics of these elements must to be integrated in the DP method. According to (5.29), it is required a fuel cell system hydrogen consumption model to represent the criterion to be minimized, while the battery model

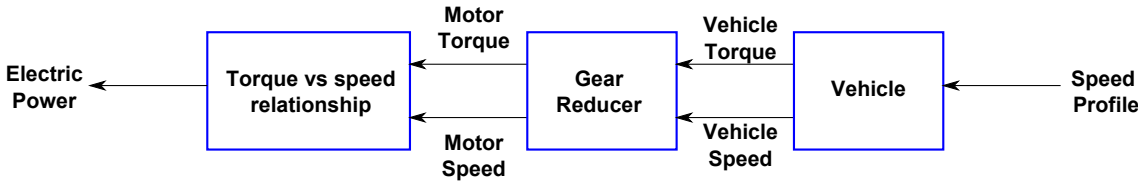


**Figure 3.8:** Invesion of the drivetrain

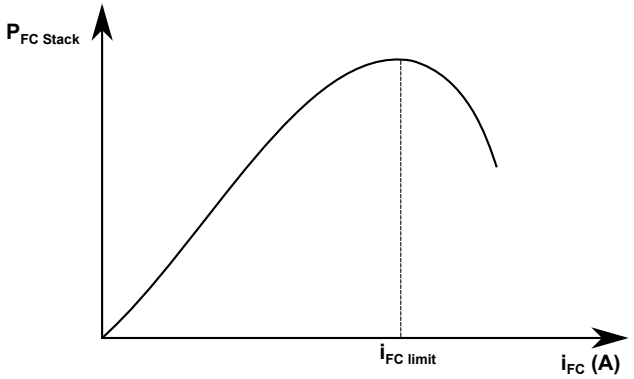


**Figure 3.9:** Typical FC Stack power vs current

should present the $SoE$ information. Thus, simplified models were created to represent these elements.

**Fuel cell system simplified model for the dynamic programming optimization**
The fuel cell voltage response is given by (3.7), where the state variables $T_{FC}$, $p_{an}$, $p_{cath}$ and $H_r$ are assumed constant on their best operation points.

$$\begin{aligned} U_{cell} = \beta_1 + \beta_2 T_{FC} + \beta_3 T_{FC} ln\left(p_{cath} - \beta_5 \frac{i_{FC}}{\beta_6}\right) + \ldots \\ \ldots + \beta_7 T_{FC} ln\left(p_{an}\right) + \beta_8 \frac{i_{FC}}{e^{-\frac{1268}{T_{FC}}}} + \beta_9 ln\left(H_r\right) \end{aligned} \tag{3.7}$$

The fuel cell stack power is given by (3.8) and presents a parabolic profile when it is ploted in function of $i_{FC}$ [82] (fig. (3.9)). For the optimization purpose, the current is limited to avoid the falling part of the power profile.

$$P_{FC\,stack} = N_{cell}.U_{cell}.i_{FC} \tag{3.8}$$

A DC/DC converter, used to link the fuel cell stack to the electric bus, is represented by a constant efficiency of 90 % (eq. (3.9)) This allows to determine the power to be supplied by the fuel cell stack.

$$P_{FC\,bus} = \eta_{DC/DC}.P_{FC\,stack} \tag{3.9}$$

As the fuel cell system is composed by auxiliaries, an energy consumption model was created to represent these elements, even if they are not directly powered by the fuel cell stack (they are linked to the electric bus). Some of them have a continuous operation, such as the pump in the cooling subsystem, and these elements are represented by a power consumption that depends only on the size of the stack ($N_{cell}$). Other elements present behavior that follows the fuel cell stack operation. The air compressor is an example and its electric consumption is related to the current delivered by fuel cell stack (air supplied proportional to the FC current). The auxiliary power consumption modeling is defined by the equation (3.10).

$$P_{FC\,auxiliary} = N_{cell}\left(k_{aux1}i_{FC} + k_{aux2}\right) \tag{3.10}$$

Where $k_{aux1}$ is the gain to transform the current demanded to the stack in the power consumed by the compressor to make the cathode conditioning and $k_2$ is the power due to the other elements with constant operation.

This notion of the stack size in the auxiliary consumption is useful in the optimal sizing procedure, which means that a bigger stack will need a more powerful conditioning and consequently they will consume more energy.

To integrate this consumption model in the optimization algorithm, it is necessary to transform the electric power of the stack and fuel cell system auxiliaries in hydrogen consumption rate ($g_{H_2}/s$). Disregarding the losses in hydrogen due to the purge procedure, the hydrogen consumption rate is directly depend on $i_{FC}$, as presented in (3.11).

$$q_{H_2(FC)} = \frac{N_{cell}i_{FC}}{2F} \tag{3.11}$$

In order to calculate $q_{H_2(FC)}$ in terms of the power delivered by the stack ($P_{FC\,stack}$) and consumed by the auxiliaries ($P_{FC\,auxiliary}$), a sequence of calculation and interpolation is needed. Figure (3.10) shows this sequence.

In the Fuel Cell Stack block, the current and voltage are obtained from the power input by interpolation. This can be effectuated due to the limitation of the power profile in (3.9), permitting to consider only the bijective part defined by the current range between zero and $i_{FC\,limit.}$.

**Battery pack simplified model for dynamic programming optimization** The battery voltage model adopted for this task uses a static map obtained experimentally,

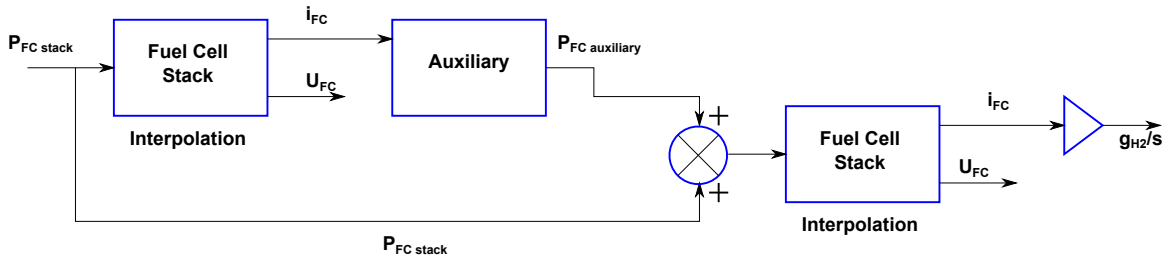


**Figure 3.10:** Hydrogen consumption calculation

where the voltage depends on the $SoE$ and $i_{batt}$ (3.12). Differently from the model presented in the last chapter, the dynamics related to the voltage response was excluded to simplify the calculations, while the $SoE$ is still calculated by (3.13).

$$U_{batt} = f\left(SoE, i_{batt}\right) \tag{3.12}$$

$$SoE = 100\left(\frac{\varepsilon}{\varepsilon_{max}}\right); \quad \varepsilon = \int P_{batt} dt \tag{3.13}$$

Optimization process permits to define the optimal dimensions of the fuel cell system and battery, which completes the sizing of the vehicle elements. However, a validation step has to be done to ensure that the obtained dimensioning is still capable to accomplish the drive cycles and to meet the performance index. To verify this, a vehicle behavioral model is used.

### 3.3.3 Validation of the sizing

The tools used in this part of the sizing process are the models of each part of the vehicle. As the objective of this step is to verify if the response of the obtained dimension is compatible to meet the specification requirements and to perform the drive cycles, a dynamical forward model of the vehicle is indicated.

Such model is built using the equations of all the elements in the vehicle presented in the chapter 2, including the models of the fuel cell subsystems.

### 3.3.4 Conclusion about the tools related to the optimal sizing objective

The sizing of a hybrid fuel cell vehicle requires the development of several tools to be used in different steps that compose this procedure. The set of tools (presented in this section) is composed by models with different approaches (forward and backward) and

a optimization tool (dynamic programming) to define, through the energy management, the size of fuel cell system and battery that minimize the hydrogen consumption.

In the next section the energy management objective is again approached in terms of structure necessary to execute it, but with a different scope that will demand other models and optimization tools.

## 3.4 Models and optimization methods for the design of online energy management strategy

The second objective of this work is to develop an optimal energy management strategy capable to be integrated in an FCHEV. To embed such strategy in a real time system as the FCHEV, some important requirements should be regarded in the conception of the optimization algorithm. Differently from the optimization that is indicated to the optimal sizing procedure, the drawbacks about computation efforts, memory used and knowledge in advance of the entire drive cycle must be overcome to be available for embedded applications. Therefore, this work proposes to develop an optimization algorithm adapted to online embedded applications (without the mentioned drawbacks) that includes the dynamic of the fuel cell system.

Normally, the inclusion of such dynamic is not adapted to global optimization methods, such as the dynamic programming used in the sizing approach. Thus, it requires the adoption of another optimization method and a representation of the fuel cell system dynamic. A special attention should be given to the FC system dynamic in order to simplify its inclusion in the optimization algorithm. Our work proposes a control law for this purpose and to provide a gain in performance and stabilization to the fuel cell system. Nevertheless, to perform the conception and validation of the the control law, it is necessary the development of a dynamic model of the fuel cell system.

Consequently, this section presents the optimization method to be used in the develop of an online energy management strategy and that can easily include extra dynamics constraints such as the fuel cell system dynamic. Besides, the models used to perfom the optimization procedure and to design the control of the fuel cell system dynamic are also described in this section. The structure in (3.11) presents the outline of the development stages and the tools necessary to reach the objective.

In this structure, the first element to be developed is the fuel cell system dynamic model to be used in the validation of the control law. Afterwards, hydrogen consumption model, battery dynamic model and the vehicle backward model (used to define the

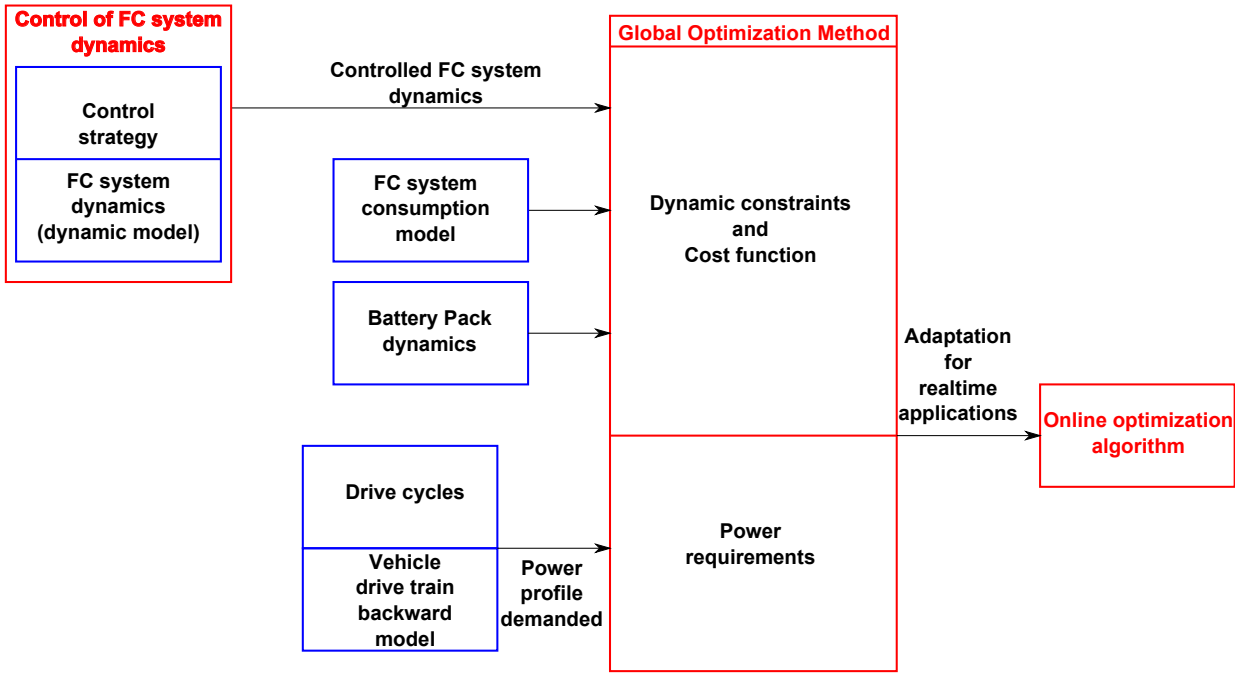


**Figure 3.11:** Structure for the development of the online energy management strategy

demanded power profile) are introduced before the description of the global optimization method adopted to create the online energy management strategy.

### 3.4.1 Dynamic fuel cell system model for the validation of a control law

In the chapter 2 it was shown that the fuel cell stack response is highly dependent on its subsystems state variables. Due to this reason, the fuel cell system model used to validate the control law has its subsystems modeled using dynamic equations that enable to observe the behavior of the main state variables. In our work, this model represents a $5\,kW$ $(90\,cells)$ real fuel cell system that is integrated in a prototype called PROSPAC (appendix 2).

Adopting the same 2D base model as used by Gerard in [64], the constructed fuel cell system model is able to describe some phenomena and properties such as mass transport, electrochemical reaction, heat transport, proton conduction and mass conservation by the adoption of physical laws. The parameters of the used functions are fitted and verified using experimental data. Local conditions (membrane hydration, current density distribution, temperature distribution, liquid water distribution, etc.) can be also observed in the model.

In the following, the fuel cell system has its element's models presented by their equations and hypotheses made.

#### 3.4.1.1 Air supply subsystem

**Cathode model:** To calculate the outlet cathode pressure, its capacity is considered as an unique volume. The state variable ($p_{cath\,outlet}$) is dependent on the average temperature in the cathode and the gas flow balance (eq. 3.14).

$$\frac{dp_{cath\,outlet}}{dt} = \frac{RT_{cath}}{V_{cath}} \left(q_{cp} - q_{O_2(FC)} + q_{H_2O(FC)} - q_{valve}\right) \tag{3.14}$$

The cathode presents as well a pressure drop between the inlet and outlet. It is dependent on the flow that the crosses the cathode $q_{cath}$, which is considered laminar. Such relation is presented in (3.15).

$$\Delta p_{cath} = p_{cath\,inlet} - p_{cath\,outlet} = k_{cath}.q_{cath}^2 \tag{3.15}$$

Where the parameter $k_{cath}$ is obtained from experimental data.

**Compressor model:** The compressor model represents the centrifugal air compressor present in PROSPAC system. This element is composed by a brushless dc motor and a compressor stage. Concerning the dc motor, it was considered that the electrical dynamic is much faster than the mechanical one, which enables to neglect it. Equations (3.17) and (3.18) represent the motor speed and resistive torque imposed to it Vahidi et al. [119], while (3.16) is an experimental static map that defines the air flow delivered as in the real compressor.

$$q_{cp} = f_{comp}\left(\omega, \Pi_{compression}\right) \tag{3.16}$$

$$\frac{d\omega}{dt} = \frac{1}{J}\left(\alpha.u_{mot} - C_r - \varphi\omega\right) \tag{3.17}$$

$$C_r = \frac{C_p T_{atm}}{\omega \eta_{cp}} \left[\left(\Pi_{compression}\right)^{\frac{\gamma-1}{\gamma}} - 1\right] q_{cp} \tag{3.18}$$

**Humidifier:** As in the case of the cathode model, the humidifier is considered as a single volume with an iso-temperature characteristic. This allows to calculate the pressure at its outlet by (3.20) and the heat transfer inside it by (3.19). Besides, the model of this component has the same type of pressure drop as in the cathode (3.21).

$$\frac{dQ}{dt} = \mu.S.\Delta T_{mem} \tag{3.19}$$

$$V_{hu}\frac{dp_{hu\,outlet}}{dt} = \frac{RT_{hu}}{m_{molar}}\sum_i q_i \tag{3.20}$$

$$\Delta p_{hu} = p_{hu\,inlet} - p_{hu\,outlet} = k_{hu}.q_{hu}^2 \tag{3.21}$$

**Control pressure valve:** This element is modeled by the flow and displacement equations in (3.22) and (3.23) respectively. In (3.22) it was considered a laminar resultant flow, while in the displacement equation the influence of temperature is neglected due to the lack of information and for the sake of simplicity.

$$q_{valve} = (\zeta_1 x_{valve} + \zeta_2)\sqrt{(\triangle p_{valve})} \tag{3.22}$$

$$\dot{x}_{valve} = \frac{1}{\tau_{valve}}(-x_{valve} + k_{valve}u_{valve}) \tag{3.23}$$

#### 3.4.1.2 Hydrogen subsystem

This subsystem is mainly represented by the pressure dynamic equation (3.24). The same assumptions of the cathode pressure calculation were made here. The anode also presents a pressure drop between the inlet and outlet (3.25).

$$\frac{dp_{an\,outlet}}{dt} = \frac{RT_{an}}{V_{an}}\left(q_{H_2(input)} - q_{H_2(FC)} - q_{purge}\right) \tag{3.24}$$

$$\Delta p_{an} = p_{an\,inlet} - p_{an\,outlet} = k_{an}.q_{an}^2 \tag{3.25}$$

The model integrates the purge strategy designed for the PROSPAC prototype, with constant purge frequence and opening time of the purge valve.

#### 3.4.1.3 Cooling subsystem

The temperatures in the thermal capacities are calculated by (3.26), considering that the capacities are unique volumes and the parameters do not change according to the temperature and other state variables. The heat transfer phenomena adopted are the convection and conduction.

$$\frac{dT_i}{dt} = \frac{1}{m_i C_{p_i}}\sum Q_j \tag{3.26}$$

Temperature of the cooling liquid at the outlet of each thermal capacity is calculated by (3.27). In this computation, the water (cooling liquid) flow is assumed constant due to the constant pump cadence. It is also assumed that there are no losses of cooling liquid in the circuit and, as in the previous equation, there are no changes of the parameters values according to the temperature and other state variables.

$$\frac{dT_{out}}{dt} = \frac{1}{m_{water}C_{p_{water}}}\left[q_{water}\left(T_{in} - T_{out}\right) + h_i S\left(T_i - T_{in}\right)\right] \tag{3.27}$$

#### 3.4.1.4 Electric subsystem

Buck converter model in (3.28) is adopted to integrate the fuel cell system model. As can be noticed, this equation do not takes into account the losses in switching and the changes in the parameters due to the temperature effects. Such informations were not available to integrate in the model, but for the assigned purposes the model is enough detailed.

$$L\frac{di_{FC}}{dt} = U_{FC} - \alpha_{buck}U_{bus} \tag{3.28}$$

#### 3.4.1.5 Fuel cell

In order to better observe the dynamic phenomena inside the fuel cell, a different approach is made in the fuel cell model structure. Instead of considering the cell as a single element (voltage response for the entire cell), a spatial discretization is applied on it. The meshed cell is constituted of the bipolar plate channels and the MEA (Membrane Electrode Assembly) as presented in figure (3.12).

Reactant channels are meshed such that the behavior of each mesh element is represented by a capacity ($\boldsymbol{C}$) that performs the gas flow balance in the mesh. The interactions between the mesh elements are represented by resistive elements ($\boldsymbol{R}$) to indicate the losses in the interfaces of the meshes (pressure drop).

In the MEA, the membrane is modeled using a $\boldsymbol{R}$-$\boldsymbol{C}$-$\boldsymbol{R}$ association in order to deal with multiple types of variables involved in the fuel cell reactions. The multiport $\boldsymbol{C}$ elements use the balance of the flow variables (current, gas and heat flow) to calculate the effort ones (voltage, pressures and temperature). $\boldsymbol{R}$ elements perform the losses in the interfaces between the membrane and the two chambers (cathode and anode). Another effect dealt in the membrane is the water transport, which is resulted from the combination of two mass transfer processes: electro-osmosis and diffusion [96].

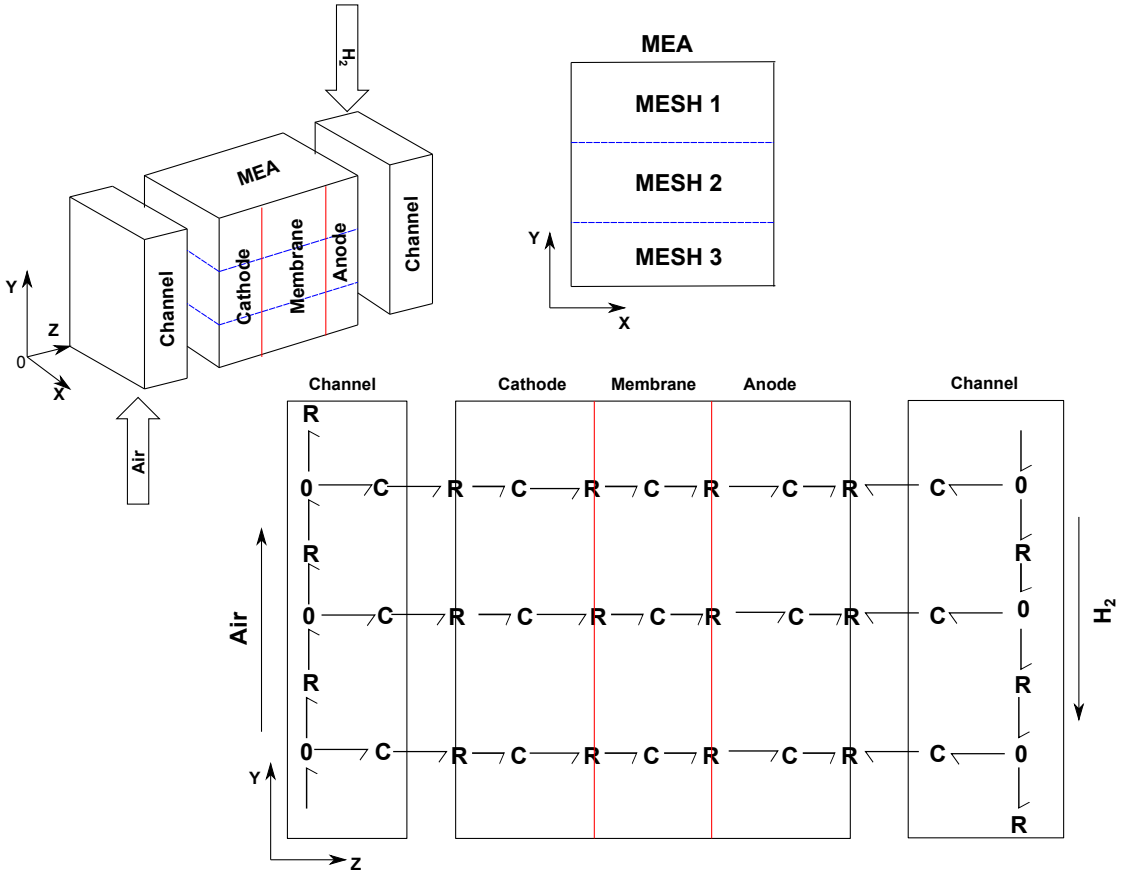


**Figure 3.12:** Cell meshed scheme

The electrochemical response of the mesh elements is given by the same equation of the cell model used for the sizing procedures (3.7), but with different local conditions.

### 3.4.2 Fuel cell system dynamic model and PROSPAC prototype in the control context

The adoption of the dynamic model aids in the validation of the control law and also in its conception. The synthesis of the control strategy will need a definition of a model oriented to the control. Such model is derived from the presented fuel cell system model with simplification hypotheses. Thus, the control strategy based on a simplified model is validated in the complex model to verify its robustness. Afterwards, the control law is verified in the real system, testing the conditions that were not inserted in the validation model, such as unknown non linearities of the elements.

When the control law is completely validated, the resulted dynamics is ready to compose the set of requirements to develop the online energy management strategy.

### 3.4.3 Models and optimization algorithm for the conception of the online energy management strategy

As illustrated in fig. (3.11), models of vehicle's drive train, battery and fuel cell system (hydrogen consumption model) are also required to develop the energy management strategy. Therefore, they are presented in this part followed by the description of the basis optimization method.

#### 3.4.3.1 Drive train model

As in the case of the optimization for the sizing procedure, the energy management strategy needs to know the electric power demanded by the vehicle during the cycle. Such information is provided by a backward model of the drive train, which transforms the speed profile (drive cycle) in power profile. The equations, static maps and calculations that represent this backward model are the same as used in the optimization for the sizing procedure (eqs. (3.3), (3.5) and (3.6)).

#### 3.4.3.2 Battery model

In order to perform fast calculations, the battery model is a simple one with emphasis on the dynamics of the state of energy $SoE$:

$$SoE = 100\left(\frac{\varepsilon}{\varepsilon_{max}}\right); \quad \varepsilon = \int P_{batt}dt \tag{3.29}$$

#### 3.4.3.3 Fuel cell system consumption model

The approach used to obtain this model was different from the one in the sizing procedure. For this energy management strategy, the calculation of the hydrogen consumption should be simplified in order to be adapted to embedded applications, which leads to choose a simple analytical model that relates the hydrogen consumption to the power delivered by the fuel cell system. This fuel cell system representation also requires to consider that all the state variables (pressures, temperatures, etc.) are controlled and regulated on their optimal values.

Different authors [75, 115] have shown that the equivalent hydrogen consumption rate can be represented by a quadratic function $g(P_{FC})$ (3.30), where $P_{FC}$ is the power delivered by the fuel cell system. This work uses the same quadratic approximation to represent the fuel cell system consumption.

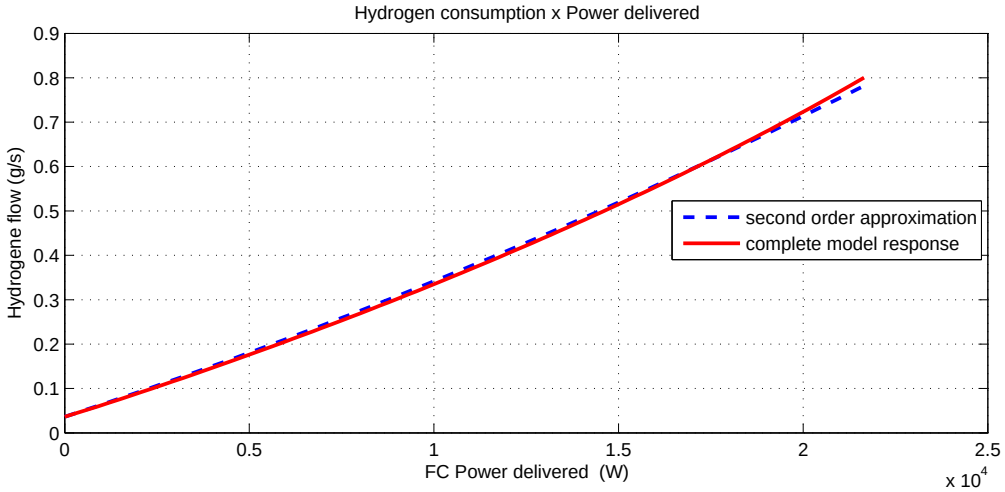


**Figure 3.13:** Typical equivalent hydrogen consumption map for a fuel cell system

$$g(P_{FC}) = a_1 P_{FC}^2 + a_2 P_{FC} + a_3 \tag{3.30}$$

The figure 3.13 shows an example of this approximation compared with the response of a model that considers the dynamics of each subsystem (Gerard [64]). The hydrogen consumption rate represents the amount of hydrogen used in the fuel cell reaction and an equivalent consumption resulting from the conversion of the auxiliaries electric energy in hydrogen.

#### 3.4.3.4 Optimization method

The optimization method, used to construct an algorithm compatible to online applications, must be able to solve in real time the optimization problem (5.29), with a solution that approximates the global optimization response. It is also desired that the method could solve an optimization problem that includes the dynamic of the fuel cell system without too much computational efforts. This requirement leads to the adoption of another global optimization method instead of the dynamic programming. In this work the online energy management strategy is derived from the Pontryaguins' Maximum Principle (PMP). The characteristics of this method presented in the following aids to justify the choice according to the desired objective.

**Pontryaguins Maximum Principle** The PMP is part of the variational methods used to optimize a process. Variational methods are applicable when it is possible to assess the variation of the criterion according to the change in control. The basic idea is to characterize the optimal control $u^*$ by the fact that a control $u = u^* + u$ must give a

higher criterion as $\mathbf{J} = \mathbf{J}^* + \mathbf{J} > \mathbf{J}^*$. Expressing $\mathbf{J}$ in terms of $u$, it can be expected to find characterizations of $u^*$.

In terms of implementation, the minimization of the criterion $\mathbf{J}$ for a system with a dynamics given by (3.31) is made by the calculation of the co-states $\lambda_i$ for each dynamic constraint. The equation (3.32) represents this integration.

$$\dot{x} = f\left(x\left(t\right), u\left(t\right), t\right),\ x\left(t_0\right) = x_0 \tag{3.31}$$

$$min_{x(t),\,u(t)}\mathbf{J}\left(u\right) = \int_0^{t_f} \left\{g\left(x\left(t\right), u\left(t\right), t\right) + \lambda\left[\dot{x} - f\left(x\left(t\right), u\left(t\right), t\right)\right]\right\} dt \tag{3.32}$$

The solution using this new criterion is obtained by calculating the Pontryaguins function, called as well as the Hamiltonien [39] (equation 3.33). The optimal control $u^*$ at time $t$ is obtained by the optimization condition $\mathcal{H}_u\left(x, u, t\right) = 0$.

$$\mathcal{H}\left(x, u, \lambda, t\right) = \lambda.f\left(x, u, t\right) - g\left(x, u, t\right) \tag{3.33}$$

When $g$ is convex and $f$ is linear, $\mathcal{H}$ is concave. This optimality condition corresponds to a maximum of $\mathcal{H}$. In the case of the consumption criterion, the sign of the Hamiltonian constraint is therefore reversed to obtain Pontryagin minimum.

However, the optimal solution do not depends only on $\mathcal{H}_u\left(x, u, t\right) = 0$. A set of three conditions must be satisfied (3.34), which does take into account the dynamics of the system in the optimization process.

$$\mathcal{H}_u\left(x, u, t\right) = 0\,;\ \dot{x} = \mathcal{H}_\lambda\,,\ \dot{\lambda} = -\mathcal{H}_x \tag{3.34}$$

In the case of the optimization for the FCHEVs, the cost function $g(x, u, t)$ is a simplified quadratic function (3.30) that represents the overall hydrogen equivalent consumption of the fuel cell system. Concerning the dynamics, different authors considers only the $SoE$ dynamics (3.29). This consideration allows to obtain a convex Hamiltonien and a possible global optimization. Equation 5.31 represents the Hamiltonien obtained under these assumptions using the power balance ($P_{vehtot} = P_{FC} + P_{batt}$) to change the variables in the cost function. In this function, the power demanded by the vehicle is considered as a known information, which leads to adopt $P_{batt}$ as the new control variable.

$$\mathcal{H}\left(\varepsilon, P_{batt}, \lambda\right) = g\left(P_{vehtot} - P_{batt}\right) - \lambda\left(P_{batt}\right) =$$

$$= a_1 P_{batt}^2\left(t\right) - \left(2a_1\left(P_{vehtot}\left(t\right)\right) + a_2\right).P_{batt}\left(t\right) + \cdots \tag{3.35}$$

$$\cdots \left(a_1\left(P_{vehtot}\left(t\right)\right)^2 + a_2\left(P_{vehtot}\left(t\right)\right) + a_3\right) - \lambda\left(P_{batt}\right)$$

Appling the three conditions on (5.31), an optimal profile of $P_{batt}^*$ is obtained. $P_{batt}^*$ depends on the known variable $P_{vehtot}$ and the co-state $\lambda$ (6.7). The condition $\dot{\lambda} = -\mathcal{H}_\varepsilon$ shows that the co-state has a constant profile during the entire cycle ($\lambda = cte$), but it does not indicate its value. In general, $\lambda$ is related to the knowledge of the drive cycle in order to obtain the boundary condition ($SoE\left(0\right) = SoE\left(t_f\right)$). Therefore, assuming that the information of the entire drive cycle is not available in real time, the presence of $\lambda$ in $P_{batt}^*$ calculation represents a limitation for on line applications.

$$\frac{\partial \mathcal{H}}{\partial P_{batt}} = 0 = 2aP_{batt}^*\left(t\right) - \left(2a\left(P_{vehtot}\left(t\right)\right) + b\right) - \lambda \Rightarrow$$

$$\Rightarrow P_{batt}^*\left(t\right) = \frac{\lambda + \left(2a\left(P_{vehtot}\left(t\right)\right) + b\right)}{2a} \tag{3.36}$$

Despite the mentioned limitation, this approach provides an mathematical solution that is useful to the development of an optimization method well adapted for on line applications and that takes into account other dynamics involved in the fuel cell system.

## 3.5 Conclusion of the chapter

The technology of the fuel cell vehicles still presents limitations in several levels, which avoids its insertion in the market. Considering this context, our work proposes to deal with technical limitations that are defined in terms of the following objectives:

- Optimal sizing of the elements that compose the fuel cell vehicle
- Optimal energy management strategy, including the fuel cell system dynamics and its durability

This particular chapter presented and defined the necessary elements to accomplish the steps that lead to reach the two established objectives. These elements were represented by the models of the vehicle's components and optimization tools. As the objectives require the adoption of different model levels and optimization methods, these tools were described according to their purposes:

**Optimal Sizing** In order to develop a sizing procedure, the steps that compose it require the adoption of drive train, fuel cell system and battery models adapted to the assigned goals: design or validation. In the design part, the drive train elements and the energetic elements (fuel cell system and battery) are sized using different approaches. The first ones (drive train elements) are based on the technical specifications, while the others (ful cell system and battery) are based on the optimization of the energy management (hydrogen consumption). Therefore, the models used for the two task differs in terms of assumptions made and modeling approaches, as presented in the chapter. Besides, the sizing of the fuel cell system and battery is performed using an approach that applies the global optimization method called Dynamic Programming in order to minimize a chosen criterion (hydrogen consumption). In the validation part, the dimension obtained must be verified according to the technical specifications, which requires a model of the vehicle capable to represent its dynamic and static responses.

**Development of Energy Management Strategy** Concerning the synthesis of the online optimal energy management strategy (EMS), its development must consider the inclusion of the fuel cell system dynamics in the optimization problem. Thus, a dynamic model of FC system is presented in this chapter in order to aid in the definition of this new constraint. This model will be used for the validation of a control law, which is responsible to improve the performance of the fuel cell system and to simplify the inclusion of its dynamics in the optimization algorithm. The conception of the energy management strategy also requires the adoption of other models that indicate the power required to accomplish the mission (vehicle and powertrain models) and the energy aspects of the battery (State of Energy) and fuel cell system (hydrogen consumption).

The last element necessary to the development of the EMS is the method used to perform the optimization. Maximum Pontryaguin's Principle was defined as the basis of the EMS that will be developed in the chapter 5. According to the characteristics described in this chapter, this principle shows to be adapted to include the new dynamics and to propose an analytical resolution for the optimization problem, which are important advantage compared with the dynamic programming approach.

In the next chapters the presented objectives will be developed and the elements described in this chapter will be useful during the processes.

# Chapter 4

# Fuel Cell Hybrid Electric Vehicle Sizing

**Abstract**

In this chapter, it will be proposed a sizing methodology for a fuel cell hybrid vehicle. The methodology combines technical specifications, optimizations theory, mobility aspects and economical analysis in order to define the size of the most important parts of the vehicle (powertrain and power sources).

## 4.1 Introduction

In the context of the vehicles, the last years shown that the recent technologies introduced new functionalities for the vehicle. Acting in different application fields, they provide improvements of the economy, performance, comfort and even in new concepts such as connectivity. In order to reach this development level, it was necessary a breakthrough in several processes involved in the design of the new type of vehicles. Topics as hybridization rate, zero emission drive mode and eco-driving were or are still part of design studies and discussions.

Being an element of the design process, the vehicle sizing has required in recent years a special attention from the automobile constructors. In the FCHEV particular case, the development context indicates that the sizing process can contribute to permit this technology to reach an equivalent maturity level as the hybrid vehicles present in the market so far. A sizing procedure specific for the FCHEV application can improve the hydrogen consumption and even its durability. However, the new functionalities introduce extra requests to the sizing and behave as open issues. The chapter 2 presented the most representative functionalities introduced by the hybrids architectures as:

- Micro hybrid

- Mild hybrid
- Full hybrid
- Plug-in hybrid
- Range extender

Nowadays, the three last topics are the most discussed by the community interested in the fuel cell vehicle development. Therefore, the main objective of the chapter is to present the development of a sizing methodology for the hybrid fuel cell vehicle, considering its features and contributions. Initially, the issue of sizing for a hybrid architecture is studied by the approaches already used, highlighting their requirements and characteristics. An analysis of the sizing characteristics for the three most studied functionalities (full hybrid, plug-in hybrid and range extender) is also performed in this initial part of the chapter, followed by the definition of the type of vehicle adopted in this work (reference vehicle) and the technical specifications (performance requirements) used in the sizing procedure of the elements

In the sequence, the optimal sizing approach is developed with a description of all its steps and results. Combining performance requirements, optimization and other criteria, the method presented in this chapter propose a systematic approach to obtain the optimal dimensions of the main elements in the vehicle.

## 4.2 FCHEV Sizing methods: state of art, concepts and basic requirements

### 4.2.1 State of art

The sizing methodology oriented for hybrid vehicles is a subject that has been tackled by several authors. Moore and Lovins [90] studied the new technology of vehicles with an special attention to the hybrid ones. In their research, the choice about the size of the elements in the vehicle's powertrain must meet a set of requirements obtained from technical specifications that are adapted for the type of vehicle. Among these specifications there are criteria about performance, drivability and degraded modes.

Other authors also justified the importance of technical specifications in the sizing process, but they included extra conditions and methods related to the optimization potential presented in the hybridization.

- Assanis et al. [17] adopted a method that performs an exhaustive research of the powertrain best dimension in terms of consumption. Such method tests the several combinations of powertrain elements and chooses the one that presents the minimal consumption. The approach presents drawbacks associated to the calculation effort necessary and especially to the local minimization obtained.

- den Tillaart [47] proposed to work with all the hybrid architectures using a different optimization method to each architecture, which complicates the evaluation of the results because the methods can not be directly compared.

- Scordia presented in [106] his proposition of sizing method for hybrid electric/ ICE vehicles. Applying this method for different architectures (series, parallel and power-split), he chose a global optimization method to perform the sizing of the battery, electric and ICE. The dynamic programming method was used to optimize the consumption of the vehicle either in charge sustaining or in charge depleting mode, defining as well the dimensions of the elements.

Regarding the applications in the fuel cell vehicle domain:

- Yu et al. [131] performed the sizing of a vehicle having fuel cell system, batteries and ultracapacitors with the function to deliver power to the traction elements. The authors represented the dimensioning problem as a minimization of a cost function composed by several criteria, such as energy consumption and battery lifetime. This combination is made by subjective weighting parameters.

- Wu et al. [126] applied an approach that implements an iterative and evolutionary algorithm to obtain the optimal sizing for a fuel cell/battery vehicle. The algorithm applied is called parallel chaos optimization algorithm and it behaves as a meta-heuristic approach, which can not guarantee the convergence of the solution nor the global minimization.

Differently from the mentioned FCHEV sizing approaches, our work proposes to ally technical specifications to global optimization methods in order to compose a systematic sizing process. However, these two components should be adapted to the available hybridization functionalities. Considering this, in the sequence is presented an overview of the requirements and methods for the full hybrid, plug-in hybrid and range extender functionalities.

### 4.2.2 Sizing requirements related to the hybrid functionalities

**Full hybrid** In this functionality the batteries have the power assistance function, which means that the total energy at the end of a mission should come from the hydrogen. Therefore, the charge sustaining mode is implemented in the optimization algorithm as a constraint ($SoE_{initial} = SoE_{final}$). Such power assistance function of the battery also affects the definition of the technical specifications by the inclusion of a specific degraded mode. Considering a situation where the battery can not be used (defect or weak energy level), some of its functions like power boost are no more available, letting the fuel cell system alone in the traction function and possibly limiting the performances or the drivability. Such situation can be observed in a drive condition with slope. In order to tackle this operation mode, it is normally included a requirement where this type of drive condition can be performed using only one power supply element (fuel cell system in our case). For instance, Toyota [12] advises $105\,km/h$ with $5\,\%$ slope as the degraded mode requirement.

**Plug-in hybrid** In this functionality the vehicle uses two types of energy (hydrogen and electricity) due to the fact that the embedded batteries can be externally recharged and depleted (until a certain limit) during the vehicle operation. Such characteristic hinders the optimization process because the cost function to be minimized by the optimization algorithm must associate the hydrogen and the electric energy of the battery by the translation to a common quantity. The monetary cost or the pollutant emissions (released during the hydrogen and electricity production) would be the best choices, but the related numbers are not easily available due to the uncertainty in cost and emissions brought by the mix of existing production process. Despite this inconvenient, the two power sources are able to meet the performance and drivability requirements, not needing to integrate degraded mode in the technical specifications. However, a battery autonomy range (distance traveled using battery to power the vehicle) replaces the aforementioned constraint.

**Range extender** As mentioned in chapter 2, this functionality defines the battery as the main element in the electric power delivery function. Thus, this element has a size (energy capacity) compatible to full electric vehicle applications. In this context, the fuel cell system only works to recharge the battery, giving an extra autonomy range to the vehicle. The optimization involved can be derived from the plug-in hybrid with an extra constraint that avoids the traction directly using the power delivered by the fuel cell system. Normally, the extra drive range provided by the fuel cell system is present

in the technical specification for vehicles with this functionality, which is used to define the power and hydrogen capacity of the fuel cell system.

Among these functionalities, our work is intended to size a full hybrid FCHEV using optimization methods and technical specifications for a given platform (type of vehicle). In the sequence, the reference platform (vehicle) is presented followed by the description of the specifications that will be used.

### 4.2.3 Reference Vehicle

In the design process, the vehicle platform can be chosen by selecting one of the two choices:

- Adoption of a reference vehicle commercially available

- Adoption of a new platform oriented for the particular application

Even if the second option represent the best option for a new technology, it requires more effort in the development of the elements that compose the platform. This drawback is overcome in the first option, where it presents the advantage to allow the utilization of the known characteristics associated to the already existing elements, serving as a basis for the definition of the technical specifications.

This work uses an existing vehicle with light-duty characteristics chosen as the reference. It should be able to meet the demands of ordinary drivers in different drive conditions. Thus, the vehicle must have performance characteristics that permits to accomplish either urban or highway paths.

Having all the necessary features to perform the requirements about the types of missions, a Renault Clio II 1,5L Dci model (figure 4.1) was selected as the reference platform (vehicle).


**Figure 4.1**: Reference Vehicle: Renault Clio 2 1,5L Dci

Table 4.1 presents the main characteristics in the technical specification of the chosen vehicle [48].

| **Dimensions** | |
|---|---|
| Height | $142\,cm$ |
| Length | $381\,cm$ |
| Width | $164\,cm$ |
| Weight | $1034\,kg$ |
| **Engine** | |
| Type of Engine | $In\,line\,4\,Cylinders$ |
| Energy (fuel) | $Diesel$ |
| Power | $65Hp\,(50\,kW)\,at\,4000\,rpm$ |
| Torque | $160\,Nm\,at\,2000\,rpm$ |
| **Chassis** | |
| Cx | 0.35 |
| Tire type | $176/65\,TR14\,(Radius:\,23\,cm)$ |

**Table 4.1**: Technical data of reference vehicle

By these technical characteristics, this vehicle is capable to reach the performance levels described in table 4.2 [1].

| **Performance** | |
|---|---|
| $Max.Speed$ | $160\,km/h$ |
| $time\ for: 0 \rightarrow 100\,km/h$ | $14.3\,s$ |
| $400\,m\ start \rightarrow stop$ | $19.5\,s$ |
| $1000\,m\ start \rightarrow stop$ | $36.2\,s$ |

**Table 4.2:** Performance of the reference vehicle

In order to adopt the aforedescribed platform as a reference for the sizing of the new powertrain, a numerical model of this vehicle is used. The model integrates the VEHLIB modeling tool and was created and validated using experimental results obtained from tests on a real Renault Clio II 1.5L Dci. As stated in the last chapter, VEHLIB has a focus on the energy consumption analyses, meaning that some inherent dynamics of the vehicle were simplified.

Despite the importance of the performance index in table 4.2, it is necessary to take into account other index adapted to the new technologies involved in the electrical powertrain.

The next section develops a set of technical specifications that represents a combination of the reference vehicle performances index and the new requirements that includes the technologies involved.

### 4.2.4 Technical Specifications

The set of the technical specifications, to which the new types of vehicles are submitted, are normally based on statements and specifications made by institutions or groups specialized in the subject. In the case of vehicles having new powertrain and new types of energy embedded, the Partnership for a New Generation Vehicles (PNGV) indicates a set of technical specifications and performance requirements [90].

The PNGV document is very often adopted for sizing works, as in the case of Wu et al. in [126]. Table 4.3 shows the main technical references of the document for hybrid vehicles.

| Constraints | Description |
|---|---|
| Acceleration time | 0–97 km/h $\leqslant$ 12.2 s |
| | 64–97 km/h $\leqslant$ 5.3 s |
| | 0–137 km/h $\leqslant$ 23.4 s with hybrid traction |
| | 0–48.3 km/h $\leqslant$ 5 s with motor-only traction |
| Gradeability | 88.5 km/h at 6.5% grade |
| | for 1200 s with the SoC (State of Charge) range of 20%–70% |
| Maximum speed | $\geqslant$ 145 km/h |

**Table 4.3:** PNGV hybrid vehicle performance requirements [126]

As can be noticed in table 4.3, the PNGV only establishes minimal performance limits that a general vehicle must meet. Consequently, a new set of specifications is defined for our specific case. This appropriates the informations of the work performed by Desbois-Renaudin et al. [48] in agreement with the data in the tables 4.3 and 4.2. Such composition aggregates the typical drive conditions presents in Europe roads (with a highlight in France) with the minimal limits imposed by the PNGV and the inherent performances of the reference vehicle.

The performance index that compose the technical specifications are shown in table 4.4.

| Constraints | Description |
|---|---|
| Acceleration time | 0–100 km/h $\leqslant$ 13 s |
| | 80–120 km/h $\leqslant$ 20 s |
| | 30–60 km/h $\leqslant$ 6 s |
| Gradeability | 0-10 km/h in 2s at 20% grade |
| | with the SoC (State of Charge) range of 20–70 % |
| Maximum speed (vehicle) | $\geqslant$ 145 km/h |
| Maximum speed (FC mode) | $\geqslant$ 110 km/h at 5% grade |

**Table 4.4:** FCHEV requirements

These specifications are mainly used to define the criteria to be applied in the sizing of the powertrain. However, it exists an index related to the fuel cell system that characterizes a fuel cell traction mode (all the traction power is due to the FCS).

In the next section, it is shown how the data of the table 4.4 are used in the proposed sizing methodology.

## 4.3 Sizing Methodology

The objective of the methodology described in this section is to accomplish, using a systematic approach, the sizing of the main elements in the powertrain and in the hybrid system of the vehicle. The definitions of the element's dimensions are related to the minimum and maximum limits of each component (power, torque, energy, etc). The elements and their main variables that are submitted to this sizing process are:

1. Electric motor
    a) Maximum rotational speed
    b) Maximum/ Minimum torque: same value with different signs (+ traction and - braking)
    c) Maximum/ Minimum power: same value with different signs (+ traction and - braking)
2. Mechanical Power transmission
    a) Reduction gain
3. Fuel Cell System
    a) Minimum / Maximum Power
4. Battery Pack
    a) Minimum / Maximum Capacity
    b) Minimum / Maximum power

Most of the variables are subjected to one or more aspects of the technical specifications (table 4.4). Nevertheless, for the fuel cell system and the battery pack the sizing methodology is not restricted to the adoption of the technical specifications.

The methodology is summarized with the structure presented in figure 4.2. Each step of the process is described in the sequence.

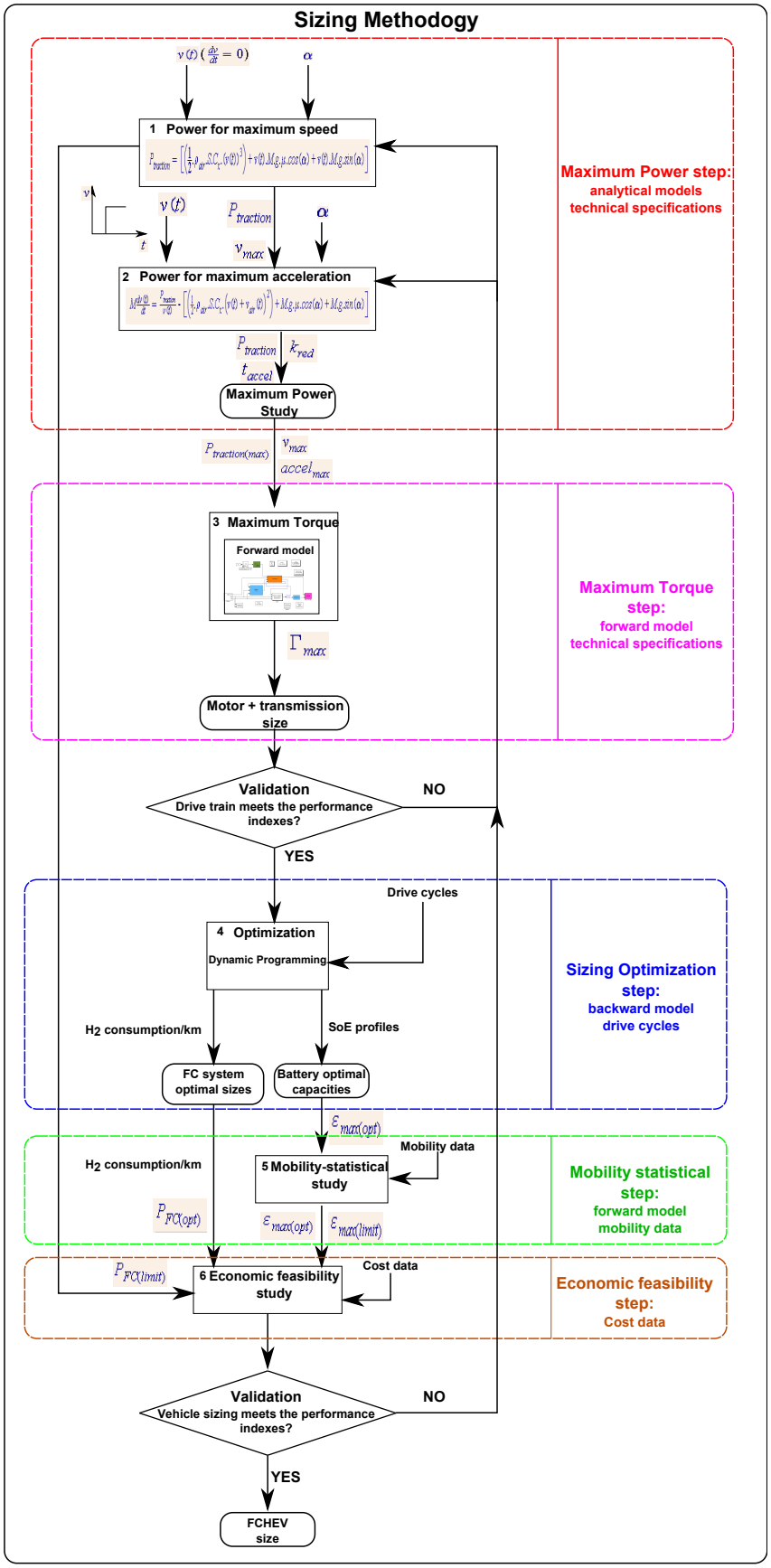


**Figure 4.2:** Sizing methodology structure

### 4.3.1 Maximum Power Step

First part of the process deals with the definition of the maximum traction power needed for the vehicle. Power requirements concerning the specifications about the maximal speed and acceleration (table 4.4) are indicated to the definition of the power capacity of the electric motor. However, before tackling the sizing task of this element, it is necessary to present the most important characteristics of the electric motor technology used in this work.

**Electric Motor** A synchronous motor technology is adopted in this work. This technology presented an outstanding performance in hybrid applications, such as in the Toyota Prius [10, 5, 76]. Moreover, this type of motor presents a good relationship between the maximum power and the mass of the motor ($kW/kg$). In general, this technology indicates a value about $2.7\,kW/kg$ [76] for the range of the selected application (light-duty vehicle).

In VEHLIB a quasi-static model represents the characteristics of the motor. A consumption analyses can be performed by using a map that represents the losses in the motor related to torque and rotational speed (figure 4.3).

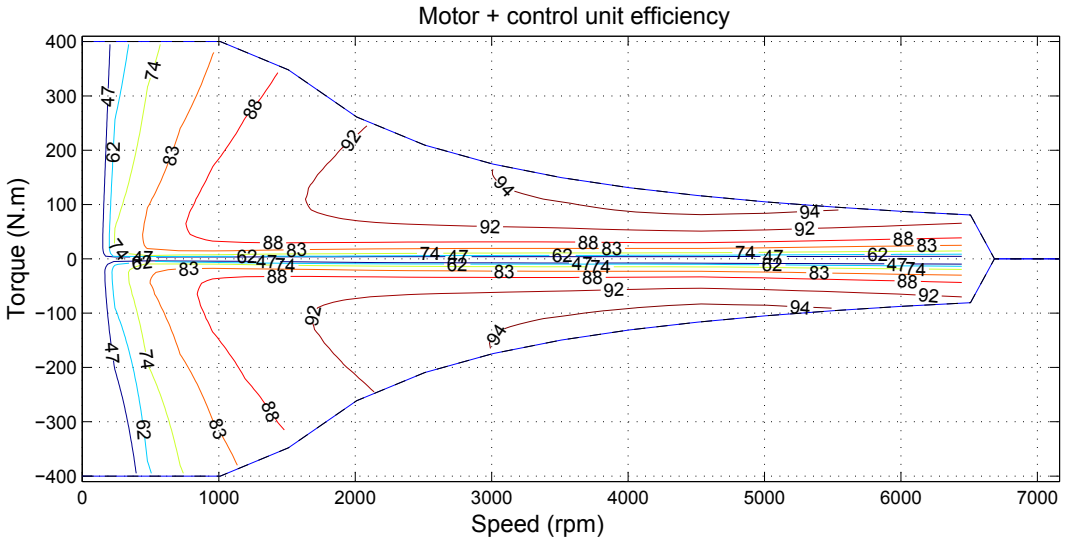


**Figure 4.3:** Electric motor map VEHLIB

Ideally, the behavior of the operating envelope of a electric motor map presents two main regions: Maximum/Minimum torque and Maximum/ Minimum power (figure 4.4). The two variables have constant profiles on their respective regions in the map.

The maximum torque can be obtained up to a base rotational speed $\omega_{base}$, while the maximum power can be obtained in the range of $\omega_{base}$ and the maximum rotational speed $\omega_{max}$. In this work, the maximum rotational speed is established as $5900\,rpm$ in order to comply with the technology of the base model.

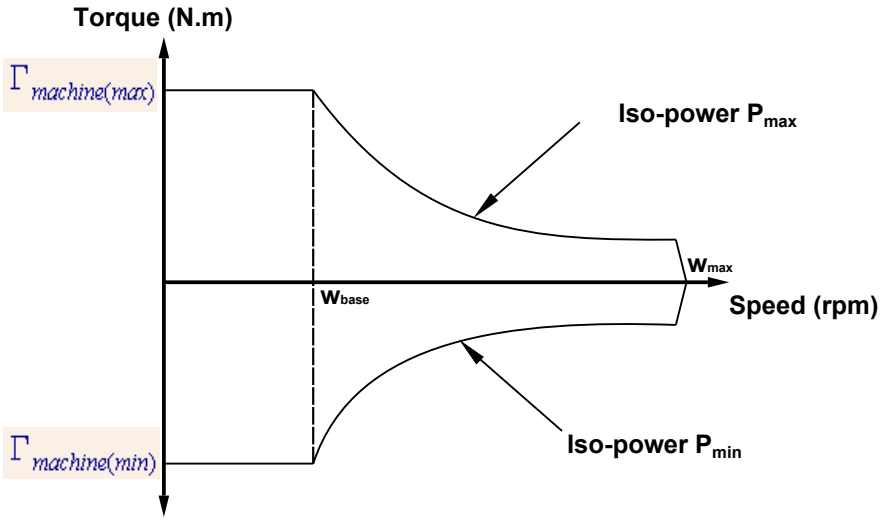


**Figure 4.4:** Ideal electric motor map

#### 4.3.1.1 Methodology to obtain the maximum power

The blocks 1 and 2 in figure 4.2 relate respectively the maximum speed and accelerations (time to execute the task) to the different values of the traction power.

**Block 1 : Maximum speed** Analytically, the vehicle can be defined by the dynamic force balance stated in equation 2.3 of chapter 2. Aiming to obtain an analytic relationship between the traction power and the vehicle speed, a changing in $F_{traction}$ variable allows to introduce $P_{traction}$ in the force balance (equation 4.1).

$$M\frac{dv(t)}{dt} = F_{traction} - F_{resistance};\ F_{traction} = \frac{P_{traction}}{v(t)}$$

$$M\frac{dv(t)}{dt} = \frac{P_{traction}}{v(t)} - \left[\left(\frac{1}{2}.\rho_{air}.S.C_x.\left(v\left(t\right)+v_{air}\left(t\right)\right)^2\right) + M.g.\mu.cos\left(\alpha\right) + M.g.sin\left(\alpha\right)\right] \tag{4.1}$$

Considering that the maximum speed of the vehicle $v_{max}$ is accomplished with a maximum traction power $P_{traction\,max}$ in steady state ($\frac{dv}{dt} = 0$) and ignoring the air speed ($v_{air} = 0$), the equation 4.1 becomes the desired relation between the maximum traction power $P_{traction\,max}$, the maximum speed $v_{max}$ and the slope angle $\alpha$ (equation 4.2).

$$P_{traction\,max} = \left[\left(\frac{1}{2}.\rho_{air}.S.C_x.\left(v_{max}\right)^3\right) + v_{max}.M.g.\mu.cos\left(\alpha\right) + v_{max}.M.g.sin\left(\alpha\right)\right] \quad (4.2)$$

Through this equation, it is possible to find the maximum traction power value for different maximum speed values.

Imposing the two speed requirements (vehicle maximum speed and vehicle maximum speed in fuel cell mode) present in the FCHEV technical specification (table 4.4), the traction power necessary by the vehicle to reach each maximum speed can be calculated analytically.

Figure 4.5 illustrates the obtained power/speed relation. As can be seen, the adoption of a electric motor allows to obtain a maximum speed of $162\,km/h$ with $42\,kW$ of embedded traction power. Concerning the first information about the fuel cell system dimension, the figure 4.5 shows that a fuel cell system with $30\,kW$ of maximum power can reach the speed requirements established ($110\,km/h\,@\,5\,\%\,slope$). This power value represents a minimal limit for the rated power of the fuel cell system.

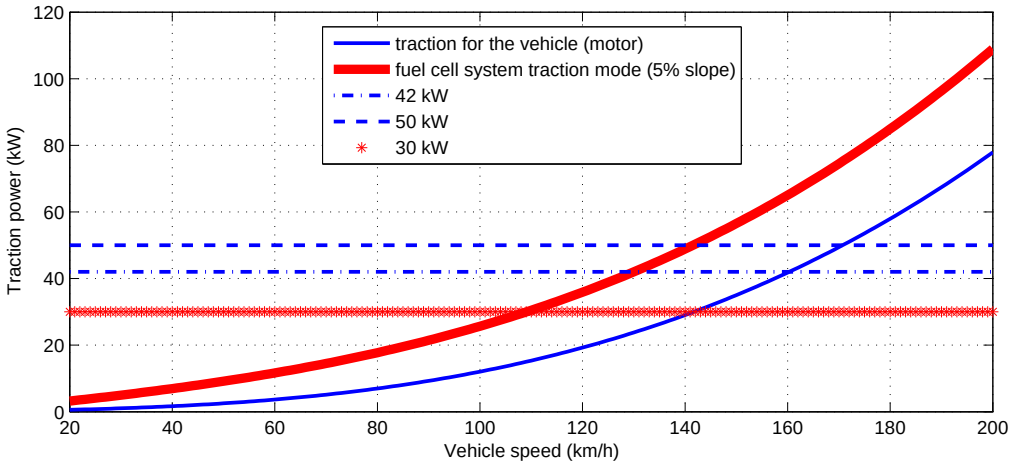


**Figure 4.5:** Traction power x maximum speed for the vehicle

**Block 2 : Acceleration** Performance index related to the accelerations in the table 4.4 permits to augment the analysis about the maximal traction power.

The time necessary to execute the acceleration tasks are obtained by simulating the three conditions on the analytical model in equation 4.3. These values of time determine the acceleration capacity of the vehicle for different conditions.

Figure 4.6 shows the diagram that represents the procedure used to obtain the acceleration time vs maximum traction power.

$$M\frac{dv(t)}{dt} = F_{traction} - \left[\left(\frac{1}{2}.\rho_{air}.S.C_x.\left(v\left(t\right)+v_{air}\left(t\right)\right)^2\right) + M.g.\mu.cos\left(\alpha\right) + M.g.sin\left(\alpha\right)\right]$$

$$\begin{cases} F_{traction} = \frac{k_{red}.\Gamma_{traction\,max}}{R_{wheel}} \left(max\,torque\,region\right) \\ F_{traction} = \frac{P_{traction}}{v(t)} \left(max\,power\,region\right) \end{cases} \tag{4.3}$$

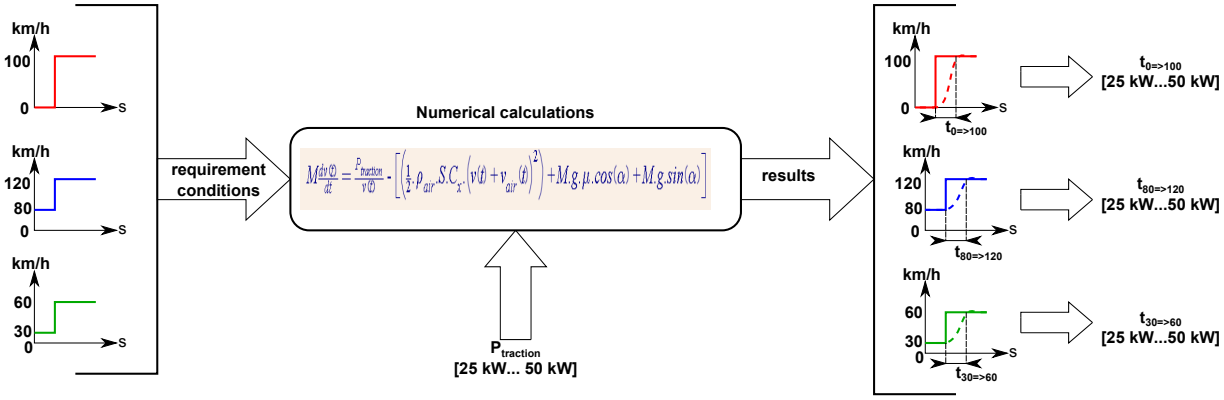


**Figure 4.6:** Diagram for the acceleration index

As the maximum traction torque ($\Gamma_{traction\,max}$) and the gear reducer gain ($k_{red}$) must be used in this step to solve the dynamic equation in 4.3. The initial value of $\Gamma_{traction\,max}$ was chosen from the electric motor map (fig. 4.4), while the reduction gear gain is obtained by a calculation using the rotational speed ratio between the primary and secondary of the reduction gear.

Transforming the longitudinal maximal speed of the vehicle $v_{max}$ in maximal rotational speed at the secondary $\Omega_{wheel(max)}$ (equation 4.4) and considering the maximal rotational speed at primary $\Omega_{motor(max)}$as $5900\,rpm$, the reduction ratio $k_{red}$ can be calculated by the equation 4.5.

$$\Omega_{wheel(max)} = v_{max}.R_{wheel} \tag{4.4}$$

$$\Omega_{motor(max)} = k_{red}.\Omega_{wheel(max)} \tag{4.5}$$

The transmission ratio value obtained from this calculation is 3.42.

Afterwards, the several configurations of the electric motor, according to the different power characteristics, are obtained by a homothetic transformation from the initial motor torque vs speed static map (4.4) that presents $27\,kW$ of max power.

To perform the homothetic transformations it was considered the same technology for all the different power results. Other assumptions made were based in the work of Desbois-Renaudin et al. [48]:

- The efficiencies are kept for the same technology, no matter the considered power of the motor;
- The motor inertia changes proportionally to its power

Such hypothesis leads to define a homothetic rate $k_{homothetic}$ related to the maximum power desired to the electric motor and the maximum power of the reference motor (4.6) that is applied to the torque, losses and inertia of the motor. However, the maximum rotational speed is maintained at the same value ($5900\,rpm$).

$$k_{homothetic} = \frac{P_{max\,motor}}{P_{max\,reference}} \tag{4.6}$$

Applying this approach permited to built motor static maps to represent powers from $27\,kW$ up to $50\,kW$. Thereafter, these static maps were used in the procedure illustrated in (4.6), which generated the results of figure (4.7).

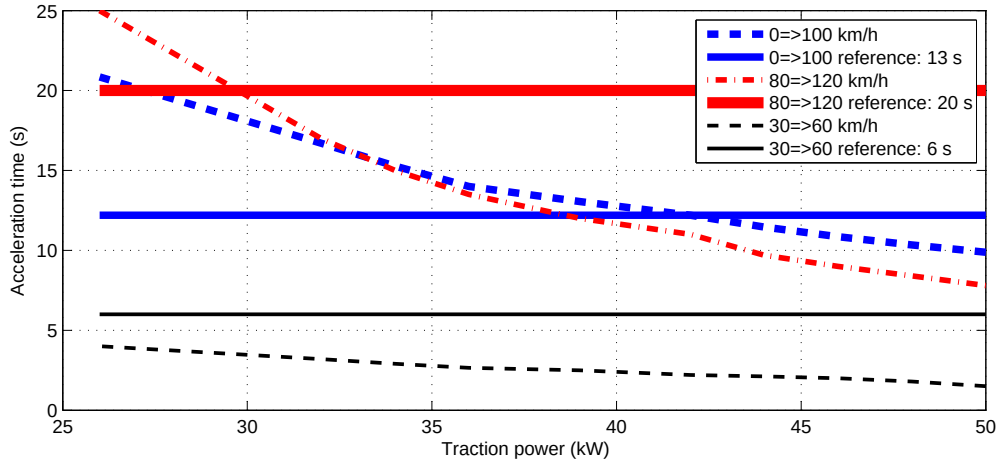


**Figure 4.7:** Time x Power for the accelerations requirements

The analysis of the results shows that, out of all the acceleration criteria, the first criterion ($0 \Longrightarrow 100\,km/h$) is the most constrained one. The constraint that specifies an acceleration time equal or lower than $13\,s$ is achieved only for traction power values higher or equal to $43\,kW$. Considering that the transmission presents an efficiency of $97\,\%$, the minimal traction power delivered by the motor to meet this acceleration requirement

is about $44\,kW$. As this value is in accordance with the maximum speed requirement ($P_{max\,motor} \geqslant 42\,kW$), it is retain as the maximum traction power of the vehicle.

Next step refers to the maximum torque, which is sized using the requirement of gradeability.

### 4.3.2 Maximum Torque Step

This part of the process is about the determination of the maximum traction torque and the validation of the mechanical transmission reduction gain.

The reduction ratio obtained in the previous step is verified verified by submitting the vehicle to the gradeability requirement (table 4.4). This is performed by simulation of the gradeability index using the vehicle dynamic model (4.3) and the parameters related to the elements of the powertrain and vehicle.

The results of the simulation indicate that the value of the reduction gain enables the achievement of the gradeability requirement, applying a maximum traction torque $\Gamma_{motor(max)}$ of $260\,Nm\,@\,350\,rpm$ at electric motor level.

### 4.3.3 Drive train validation step

After the definition of the motor (maximum/ minimum torque and power) and the transmission ration, it is necessary to verify if the drive train proposed is capable to meet the the performance requirements contained in the technical specifications.

Using the longitudinal dynamic model of the vehicle, the reduction gear model and the obtained electric motor representation (static map + inertia), the performance index are imposed to the vehicle and the results show that the sizing results permits to accomplish the performance requirements.

### 4.3.4 Conclusions about the drive train sizing

Throught the obtained results, the elements of the powertrain (motor + mechanic power transmission) are dimensioned according to its macroscopic energetic characteristics. Besides, a lower limit for the fuel cell system maximal power is known, which transforms the maximal speed in fuel cell mode to a FCS power constraint. Table 4.5 summarizes the obtained results.

| Variable | Value |
|---|---|
| $v_{max}(km/h)$ | 162 |
| $\Omega_{motor(max)}\ (rpm)$ | 5900 |
| $P_{motor(max)}\ (kW)$ | 44 |
| $P_{FCS(max)}\ (kW)$ | $\geqslant 30$ |
| $\Gamma_{motor(max)}\ (Nm)$ | 260 |
| $k_{red}$ | 3.42 |
| $k_{vehicle}$ | $27.4\,(km/h)/1000\,rpm$ |
| $\eta_{red}\ (\%)$ | 97 |

**Table 4.5:** Powertrain parameters

Analyzing the summary of results in (4.5) it can be seen that the electric motor presents a reasonable power level while the fuel cell system presents maximum power that gets close to this level. The fuel cell system traction mode is responsible for this result, which does not means the best commitment between cost and performance of the vehicle.

The remaining elements in the sizing process are the components of the hybrid system (FCS and battery). They are sized using an approach based on the optimization of the energy consumption, mobility analysis and economic aspects. The next step presents the optimization part.

### 4.3.5 Optimization step

The hybridization present in the chosen architecture requires a more complex methodology in the process of the FCS and battery sizing, such that the final configuration reduces the energy consumption.

Different types of solutions were already adopted for this problem. Using intelligent methods, such as artificial neural networks, Jain et al. [74] proposed a multi-objective approach for the components sizing in hybrid vehicles.

A sizing approach based on drive cycles and energy management strategy using fuzzy logic was proposed by Ravey et al. [100]. This has as objective to find a configuration that minimizes the hydrogen consumption in a fuel cell hybrid truck. The result indicates a better downsizing possibility of the fuel cell system.

Florian Duprez [51] developed a sizing methodology for a hybrid system (ICE + battery) in a boat. This adopts the optimizations principles of the Dynamic Programming,

which are inserted in a main algorithm. Despite the complexity of the problem, an optimal solution was obtained for the energy management of the boat and it was transported to the sizing of the components.

Associating Dynamic Programming and artificial neural networks, Julien Scordia [106] presented an optimal sizing procedure for different architectures of hybrid vehicles. The dimensions of the elements were well adapted to the energy management proposed in his work.

The choice of global optimization methods made by different authors is justified by the offline characteristic of the sizing process. As a good candidate for the optimization task, the Dynamic Programming method (introduced in the last chapter) is chosen to perform the optimization of the hydrogen consumption.

#### 4.3.5.1 Optimization process

The entire optimal procedure is developed in the block 4 of the figure 4.2. Different drive cycles, previous sizing results and a range of power capacity and energy capacity (respectively to FCS and battery) are the inputs of the process, while the hydrogen consumption for each FCS + battery combination is the output. Figure 4.8 illustrates the structure of the process.

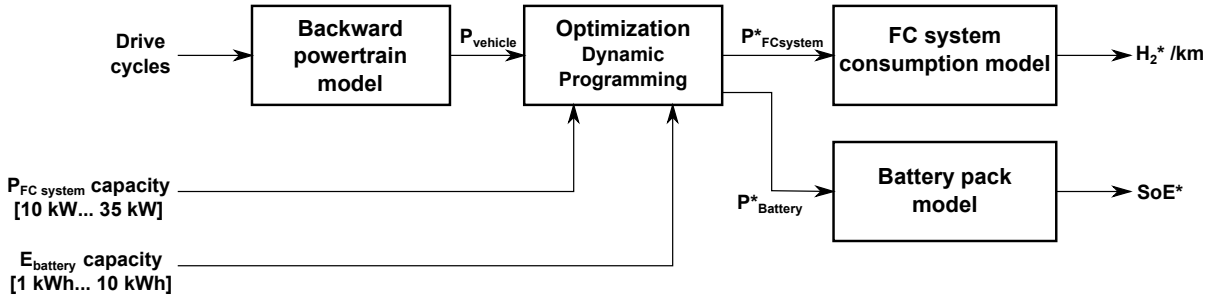


**Figure 4.8:** Optimal sizing structure

In order to perform this optimization, the backward vehicle model is used, which allows to obtain the electric power required by the vehicle to carry out the speed profile imposed.

As the FCS and the battery chosen capacities are linked to the total mass of the vehicle, the increase of the embedded power or energy capacity requires more electric power to perform the drive cycle.

The possible capacities used for the battery are presented in the table 4.6.

| **Energy** ($kWh$) | 1 | 2 | 3 | 4 | 5 | 6 | 7 | 8 | 9 | 10 |
|---|---|---|---|---|---|---|---|---|---|---|
| **N° elements** | 120 | 240 | 400 | 520 | 680 | 800 | 920 | 1080 | 1200 | 1320 |
| **Mass** ($kg$) | 10.3 | 20.6 | 34.4 | 44.8 | 58.6 | 68.9 | 79.3 | 93 | 103.4 | 113.7 |

**Table 4.6:** Battery capacity values

If the pack should have a nominal voltage of $128\,V$, where each element of the pack has a nominal voltage of $3.2\,V$. Therefore, the pack presents a physical configuration with $N$ parallel branches composed by 40 elements in series (figure 4.9).

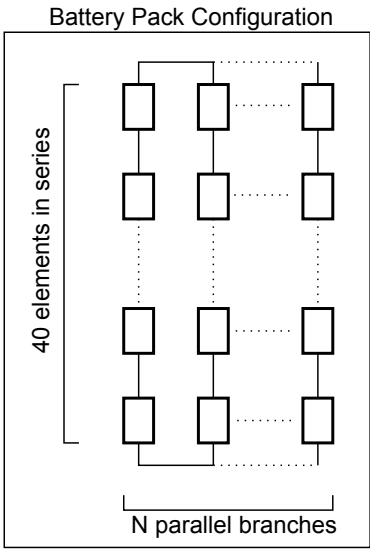


**Figure 4.9:** Battery pack configuration

An assumption was made about the fuel cell system mass evolution. It states that there is a linear evolution of the entire system mass with respect of the number of the cells. The equation 4.7 shows this relation, where $\varphi_1$ and $\varphi_2$ were obtained by interpolation of data granted by CEA. They represent a ratio mass/power for the entire system (fuel cell + auxiliaries + connections) close to $2.3\,kg/kW$.

$$M_{sysFC} = \varphi_1 N_{cell} + \varphi_2 \tag{4.7}$$

Table 4.7 shows the different configurations of the fuel cell system used in the process.

| **Max. Power** ($kW$) | 10 | 15 | 20 | 25 | 30 | 35 |
|---|---|---|---|---|---|---|
| **N° Cells** | 110 | 164 | 218 | 273 | 328 | 382 |
| **Mass** ($kg$) | 23 | 34.5 | 46 | 57.5 | 69 | 80.5 |

**Table 4.7:** Fuel cell system power configurations

Dynamic programming method is implemented in the optimization block of the figure 4.8 and is used to solve the optimization problem stated in chapter 3.

The optimization algorithm is capable to calculate the optimal power profiles of fuel cell system $P^*_{FC}$ and battery $P^*_{batt}$ related to a complete drive cycle. These optimal profiles minimize the hydrogen consumption and ensure the constraints of the optimization problem.

The equivalent hydrogen consumption of the fuel cell system and the profile of the state of the energy $SoE$ of the battery are calculated imposing their respective optimal power profiles on energy consumption models. The $SoE$ profile is particularly important to verify the constraint $SoE_{initial} = SoE_{final}$, indicating that all the energy is delivered from the hydrogen.

At the end of the optimization process, the results lead to define the optimal size of the FCS and battery.

#### 4.3.5.2 Optimization conditions and results

As presented in figure 4.8, the optimization process is always related to a certain drive condition. Such drive condition is represented by the drive cycles (speed profiles) imposed to the vehicle and can represent either normalized drive profiles or real ones based on the measurements and recordings made in real vehicles. In our work, speed profiles with real characteristics are chosen in the optimization process. Normally, these types of drive cycles reflects the driver behaviors when driving in urban, extra-urban and highway conditions. The three profiles, used in this work, are present in the appendix 1. However, these types of drive conditions are not adopted with the same frequence by the drivers. According to the type of travelled path, transportation objectives and the limitation of the drive laws (maximum speed limitation), some of drive cycles are favored than the others. In the context of this work, the transportation characteristics of duty-light vehicles in France are used to compose the sizing optimization.

**Transportation context in France** In 2008 a research about mobility was demanded by the French government [4]. The informations present in the data base of this research

deal with different aspects of the population mobility, including the types of transport, distances, frequencies, etc.

In this part of the process, this set of statistical data is used to analyze and cover the existent gaps present in the sizing results.

Out of all the data, some information are particularly useful for the objectives of this part. They correlate the requirements of the population mobility with the energy range of a fuel cell hybrid vehicle:

- Types of displacements (drive cycles)
- Distance travelled per displacement

Regarding the type of displacement using light-duty vehicles, the research characterizes two types of drive cycles as the most representatives: urban and extra-urban. They were identified according to their average speed and the type of the route (city, between cities, rural, etc.)

Considering the total of data related to the type of the route for a driver in a light-duty vehicle, the results of the mobility research show a proportion of 28 % of urban drive routes and 72 % of extra-urban drive routes, as can be seen in the figure 4.10.

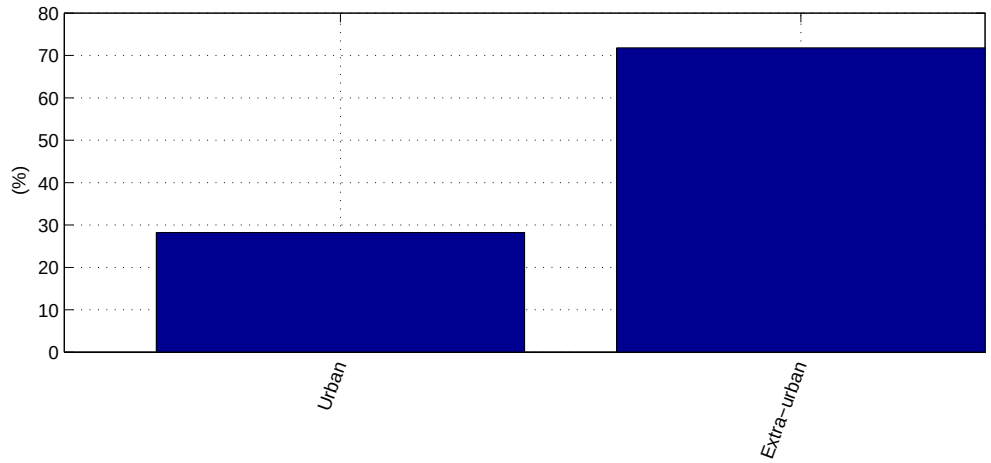


**Figure 4.10:** Proportion of each type of route

The data about the most frequent travelled distance are presented in figure 4.11. They indicate that for extra-urban routes the range from 5 to 10 $km$ is the most frequent while for urban routes the range from 2 to 5 $km$ is the most covered. Table 4.8 indicates the average distances for each type of route.

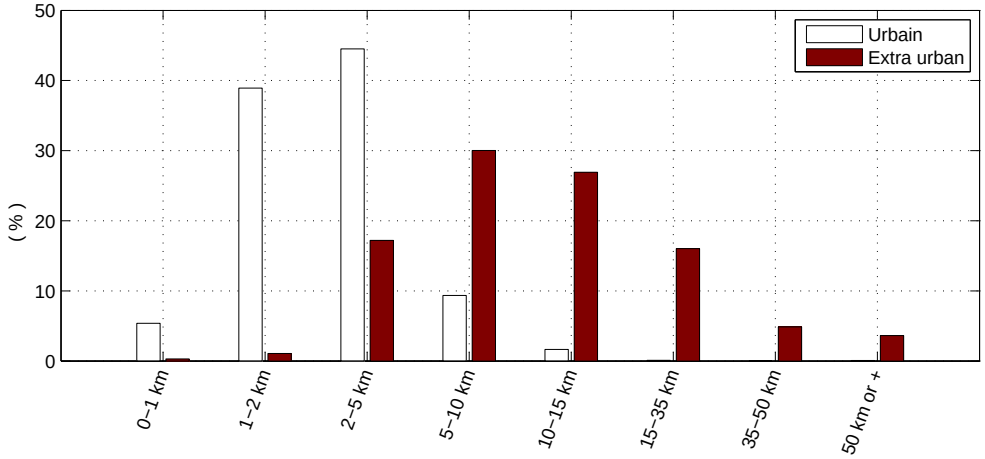


**Figure 4.11:** Travelled distance distribution for a single travel

| Cycle | Average travelled distance (km) |
|---|---|
| Urban | 2.87 |
| Extra-Urban | 14.5 |

**Table 4.8:** Average distance for each type of cycle

Even if these data do not define the drive cycles to be used in the optimization process, they can guide the analysis about the sizing coherence of the optimization results and the mobility context in France.

**Optimization results** Three drive cycles were imposed to the optimization algorithm (DP). These drive cycles are presented in appendix 1 and have urban, extra-urban and highway characteristics.

The power profiles of these cycles, obtained from the backward model, are presented in the figures 4.12 to 4.14.

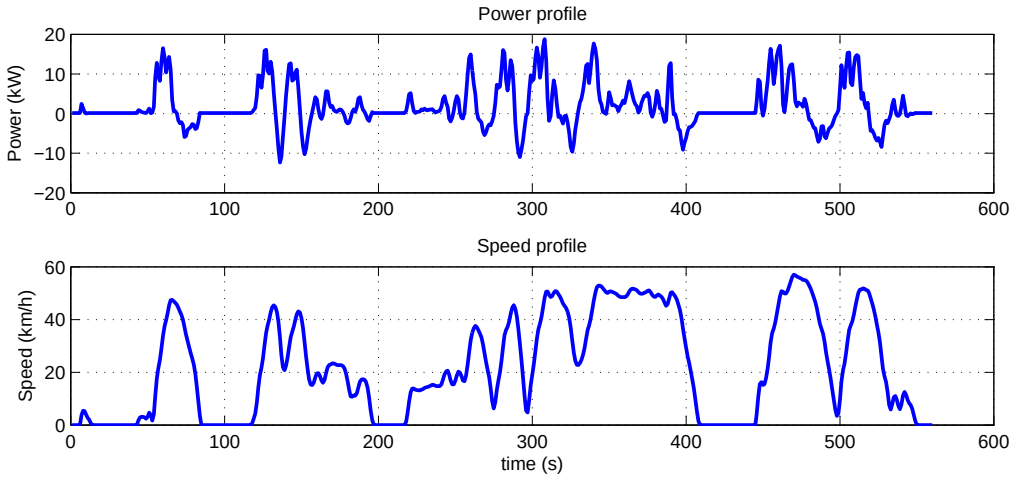


**Figure 4.12**: HYZURB- Urban cycle: power and speed profile

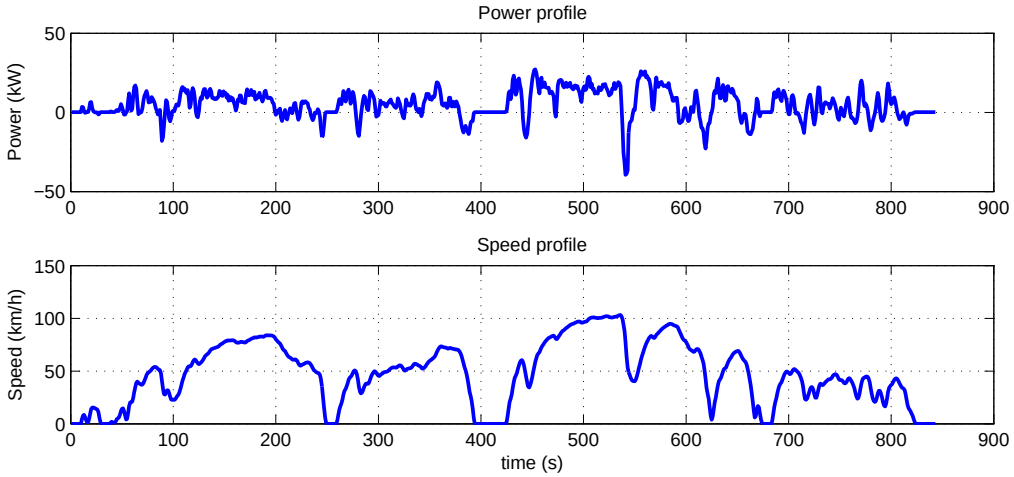


**Figure 4.13**: HYZROUT-Extra-urban cycle: power and speed profile

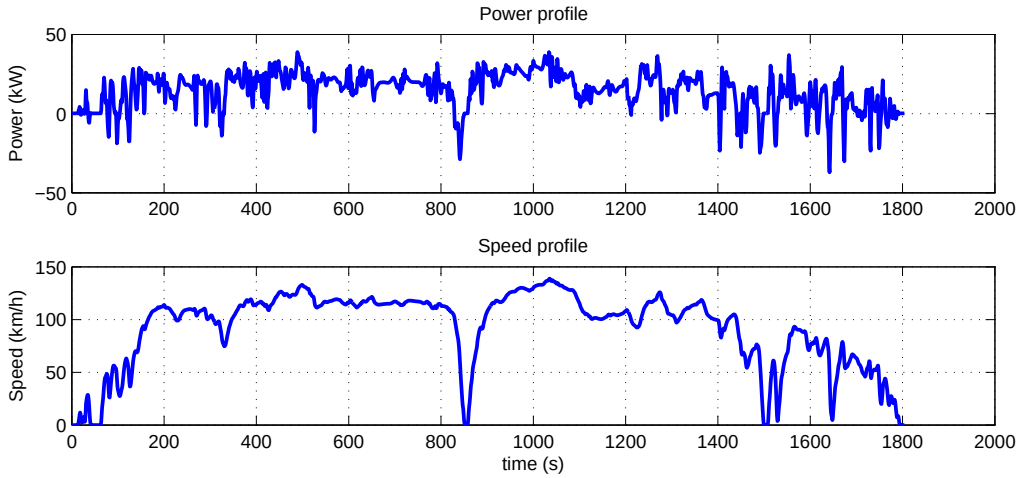


**Figure 4.14:** HYZAUTO-Highway cycle: power and speed profile

The hydrogen consumption related to each cycle and to each combination of FCS and battery is used to develop a parametric study. This study intends to find the best hybrid configuration in terms of hydrogen consumption.

In this sizing step, some assumptions are made:

- The efficiency of the fuel cell system DC/DC converter is considered constant as 95 %.
- The battery charge and discharge efficiency have the the same constant value of 90 %.
- The electric motor has a simetric behavior in terms of torque and power ($\Gamma_{motor(max)} = \Gamma_{motor(min)}$, $P_{motor(max)} = P_{motor(min)}$), allowing to apply the minimal power during recovery braking procedures.

Figure 4.16 presents the results for the urban drive cycle.

For this cycle, a hybrid configuration composed by $15\,kW$ of fuel cell system and $3\,kWh$ of battery pack shows be the best option.

As can be noticed, for fuel cell systems with less or more than $15\,kW$ there is an over-consumption effect.

For lower values, there is less consumption of the auxiliaries and a reduced mass of the FC system. However, the optimal power profile $P^*_{FC}$ requires to operate at a value closer to its maximum power, where the efficiency is lower than its best value. Thus, the reductions in the mass and in the consumption of the auxiliaries do not compensate the losses in the fuel cell stack.

For a fuel cell system with a power capacity higher than the optimal, the increasing on the mass and specially on the auxiliaries' consumption leads to the noticed over-consumption.

Concerning the batteries capacities, two aspects of the pack are important in the definition of the optimal value: embedded mass and capacity to recover the energy during braking procedures.

For packs with less than $3\,kWh$ there is a lower embedded mass, but the recovery capacity (recharge) is not enough to store all the available energy during the braking operations. This braking kinetic energy that is not stored can not be transformed in traction energy later. Such situation leads to use hydrogen when the traction is necessary instead of the possible recovery energy.

In the case of battery packs with a capacity greater than $3\,kWh$, the embedded mass causes the over-consumption. A configuration with more than $3\,kWh$ will not bring more gain in efficiency because the cycle do not provides more energy to be recovered. Consequently, when the battery capacity increases there is no compensation of the mass increasing by the energy recovering.

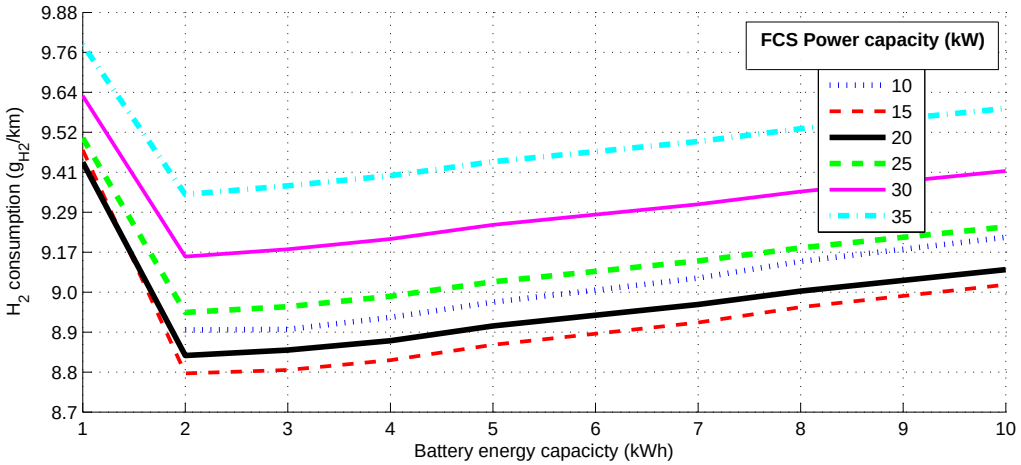


**Figure 4.15:** Sizing study of battery and FC system for urban cycle

The results obtained when the extra-urban drive cycle was imposed to the vehicle shown a minimum consumption for a hybridization with $35\,kW$ of fuel cell system and $5\,kWh$ for the battery (figure 4.16). Through the results of the fuel cell system dimensions, it is possible to verify that the economy in hydrogen obtained adopting a $35\,kW$ FCS has almost no difference from the adoption of $25\,kW$, leading to choose this last configuration as the best in terms of performance/cost commitment.

The effects explained for the previous case are still valid for this cycle, but the power profile required by the vehicle leads to another optimal combination.

The decoupling effect of the hybrid series architecture allows to the fuel cell system to adopt an optimal power behavior that tends to follows the average value of the cycle power profile. Therefore, due to the higher average power of this drive cycle (compared with the urban one), a fuel cell system with higher power capacity would be more adapted to deliver the power with better efficiency and reduced hydrogen consumption.

Compared with the last drive cycle, the capacity obtained for the battery pack increased due to the potential in terms of energy recovery available in this cycle.

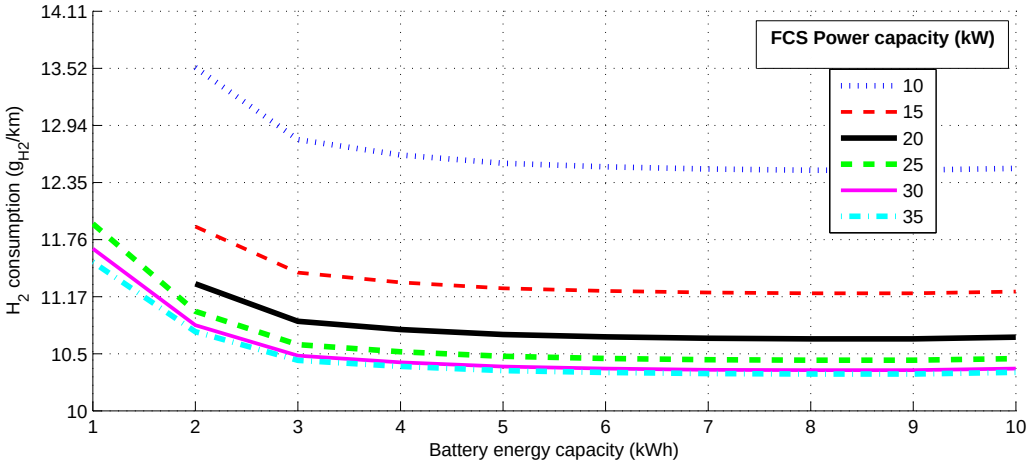


**Figure 4.16:** Sizing study of battery and FC system for extra-urban cycle

For a drive cycle with highway characteristics, the results of the optimization shown a saturation in the value of the maximum power of the fuel cell system ($35\,kW$) and an augmented energy capacity of the battery pack up to $6\,kWh$.

The increase of $1\,kWh$ (compared to the result for extra-urban cycle) in the battery capacity is again justified by the energy recovery capacity during braking procedures. For values greater or equal to $6\,kWh$ the system is able to recover enough energy to compensate the losses with the augmentation of the embedded mass.

Concerning the fuel cell system, a value of $35\,kW$ do not necessarily represent the best value. The increase of the maximum power could lead to a reduction in the consumption. Nevertheless, it can be seen in (4.17) that the performance gains become weaker with the increasing of the maximum power. Moreover, the adoption of higher values of maximum power would lead to obtain a relation between the maximum power of the fuel cell system and the maximal traction power of the vehicle ($P_{FC}/P_{veh}$) close to $90\,\%$, compromising

the hybridizing and downsizing ideas proposed in this work. Hence, a value of $35\,kW$ is kept as reference for this cycle.

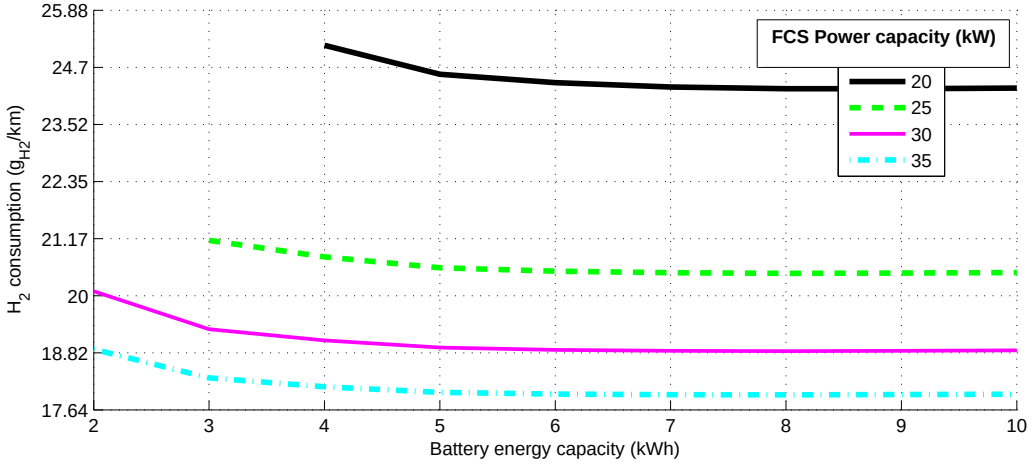


**Figure 4.17:** Sizing study of battery and FC system for highway cycle

Table 4.9 summarizes the best results for the three cycles.

| **Cycle** | **FC system max power** $(kW)$ | **Battery energy capacity** $(kWh)$ |
|---|---|---|
| Urban | 15 | 3 |
| Extra-Urban | 25 | 5 |
| Highway | 35 | 6 |

**Table 4.9:** Results of the optimization process

As the fuel cell system power constraint in the table 4.5 limits the value of the maximum power to values greater or equal to $30\,kW$, a fuel cell system capable to deliver $35\,kW$ is the only available solution among the results of the optimization process. However, another criterion should be applied to verify if the gain in hydrogen economy compensate the extra cost related to a more powerfull fuel cell system.

Concerning the battery size, the optimization results are not able to define the its energy capacity. The three different battery capacities in table 4.9 must to be submitted to other criterions in order to determine the final battery sizing. The next step in the sizing process proposes the inclusion of the mobility aspects in order to aid in the definition of the battery pack dimension

### 4.3.6 Mobility statistical step

In the proposed analysis, the information of a distance travelled by a common driver is linked to the energy capacity of the battery. Considering in this work that the vehicle can operate in a battery traction mode (present in a plug-in hybrid functionality), the distance travelled in this mode would define the capacity of the battery pack.

In this analysis, the data of travelled distance of urban and extra-urban drive cycles present in French transportation research are used. Nevertheless, the distance value can not be well defined using only the data of the figure 4.11.

In order to identify how a certain distance would satisfies the two types of drive cycles, the same data of the figure 4.11 are presented again in the figure 4.18 using a cumulated representation.

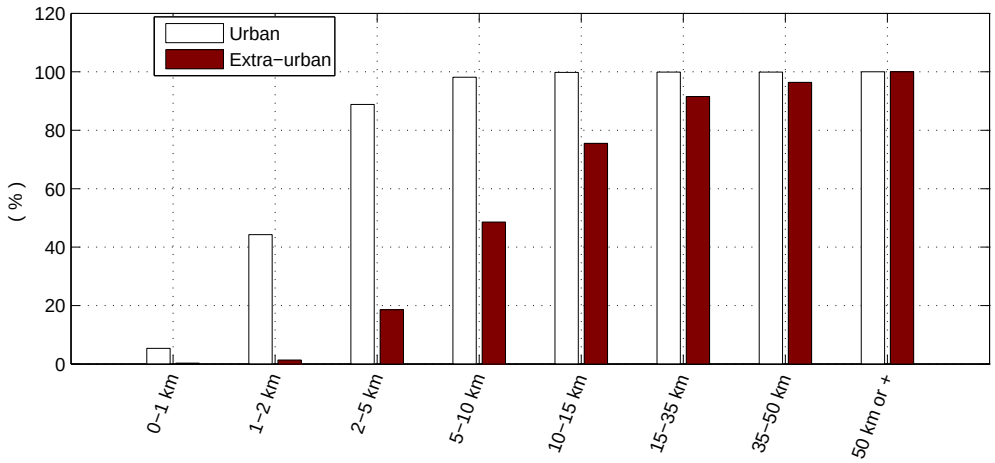


**Figure 4.18:** Cumulated travelled distance distribution for a single travel

As can be seen, a travelled distance of $15\,km$ can meet almost all the urban paths and more than $60\,\%$ of the extra-urban ones.

Using this distance as the reference and keeping the $SoE$ limits of the optimization problem, the proposition made here states that $40\,\%$ of the total energy capacity of the battery pack ($\Delta SoE = 40\,\%$) is sufficient to accomplish a distance of $15\,km$.

The definition of the amount of energy required for this task is obtained by simulating the drive conditions on the forward vehicle model.

Drive condition is represented by a drive cycle that is a series composition of the urban and the extra-urban drive cycles of the figures 4.12 and 4.13 with the same proportion presented in fig. (4.10). The final travelled distance is close to $15\,km$ ($14.7\,km$).

Simulation results indicate that the amount of energy necessary to accomplish the mission is $1.7\,kWh$ with 25 % for urban and 75 % for extra-urban drive cycles. Therefore, the total energy capacity of the pack ($SoE = 100\,\%$) is $4.25\,kWh$, which represents that the battery should have at least this capacity value to perform the battery mode functionality.

After the determination of the minimal limit of the battery size, an economical approach finishes the definition of the battery pack and fuel cell system dimension.

### 4.3.7 Economic feasibility step

The previous steps in the battery and FCS sizing process lead to obtain the optimal results in table 4.9 and the sizing constraints in 4.10.

| Sizing variable | Constraint | Criterion used to define the constraint |
|---|---|---|
| $min\left(P_{FC\,(max)}\right)$ | $\geqslant 30\,kW$ | Fuel cell system drive mode |
| $min\left(\varepsilon_{Batt\,(max)}\right)$ | $\geqslant 4.25\,kWh$ | Battery drive mode |

**Table 4.10:** FCS and Battery sizing constraints

This part of the methodology is intended to define the FCS and battery pack dimansions through the comparison of the reduction in terms of hydrogen consumption with the cost related to the choice of a certain energy capacity of the battery pack and maximal FCS power capacity. In order to do this comparison, the variables units should be transformed to a common base, which is the cost in euros.

The cost data were obtained from the DOE indications [92] and from the article of Xu et al. [128], published in 2012 that develops a sizing study of a hybrid fuel cell bus. Two values are specially important for our study:

- FCS cost: $56\,€/kW$ (DOE)
- Battery cost: $496\,€/kWh$
- Hydrogen Cost: $2.28\,€/kg$

**Battery sizing** The reference value for the total capacity of the battery is the same obtained in the previous step ($4.25\,kWh$). The values to be compared with this reference are the results of the optimization process that observes the constraint obtained in the mobility study ($\varepsilon_{batt} \geqslant 4.25\,kWh$):

- $5\,kWh$ for extra-urban drive cycles
- $6\,kWh$ for highway drive cycles

The viability to add $0.75\,kWh$ and $1.75\,kWh$ to the reference value is verified in terms of the hydrogen savings (in euros) necessary to compensate the cost of the extra capacities.

In the extra-urban context, the optimal consumption for a $4.25\,kWh$ configuration is about $10.5\,g_{H_2}/km$, while the best configuration in terms of hydrogen consumption ($5\,kWh$) requires $10.3\,g_{H_2}/km$. Transforming the consumption difference in monetary values, it is obtained $0.0005\,€/km$. This means that it would be necessary more than $990,000\,km$ to compensate the cost of an extra $0.75\,kWh$ ($496\,€$). Taking into account that a fuel cell hybrid vehicle has a target of life time that represents approximately $241,000\,km$ ($150,000\,miles$ according to DOE [92]), the reduction in hydrogen consumption do not justifies the adoption of a $5\,kWh$ battery.

For highway drive cycles, the difference in cost consumption between the reference and the best result of the optimization process ($6\,kWh$) is $0.001\,€/km$. This leads to require a life time that allows to reach approximately $992,000\,km$ to compensate the cost of extra $1.75\,kWh$, indicating a scenario as unjustifiable as the previous one.

It can be concluded that the distance range criterion, defined by the battery traction mode, is a determinant factor on the definition of the battery's energy capacity due to the high cost of this component.

**Fuel cell system sizing** In the case of the fuel cell system, the reference value given by the fuel cell drive mode constraint ($30\,kW$). As the optimization results in tab. (4.9) presents only one value that respect the fuel cell system power constraint ($P_{FC(max)} \geqslant 30\,kW$), the hydrogen economy obtained adopting this FCS dimension ($35\,kW$) is compared with the cost related to the $5\,kW$ increased (compared with the reference).

The highway optimization results presents a value of $18.9\,g_{H_2}/km$ as the optimal consumption for a $4.25\,kWh$ of battery and $30\,kW$ of fuel cell system configuration, while the consumption obtained for the same battery capacity and $35\,kW$ of FCS is $17.8\,g_{H_2}/km$. The monetary difference indicates an economy of $0.0025\,€/km$ by using a $35\,kW$ FCS instead of $30\,kW$. Considering that the extra cost involved must be compensate by the hydrogen savings, it would be necessary $112,000\,km$ to achieve this objective. This value represents about $46\,\%$ of the target distance ($241,000\,km$), which means that this scenario ($P_{FC(max)} = 35\,kW$) is economically feasible.

It can be concluded that the hydrogen savings obtained using a larger fuel cell system can compensate the cost of the extra embedded power, for a highway scenario, before

the end of life of the vehicle. Therefore, a fuel cell stack of $35\,kW$ is considered as the chosen dimension for this work.

### 4.3.8 Validation of the sizing

The dimensions of the fuel cell system and battery impacts the mass of the vehicle, which can affect the vehicle performances. Thus, the mass associated to these elements are integrated in the vehicle dynamic model and the performances in the technincal specifications are verified if they are reached.

This validation step indicated that the inclusion of the FCS and battery combination defined in the previous step in the vehicle still allows the vehicle to meet the assigned performance indexes, validating the size obtained.

## 4.4 Conclusions of the chapter

In this chapter, the models and optimization tools described previously were used in the conception of a sizing methodology for a fuel cell hybrid electric vehicle. Such methodology started with the definition of the reference vehicle and its characteristics.

The performances index of the reference vehicle provided an initial idea of the FCHEV functional requirements. However, the final set of the specifications and technical requirements was obtained combining the performances index of the reference vehicle and new index that reflect the technological contribution brought by this transportation solution. The total content of the functional requirements allowed to size the main elements of the powertrain (electric motor and mechanical power transmission).

Regarding the elements of the hybrid system (fuel cell system and battery pack), it was applied a specific procedure that uses the concepts of global optimization. This procedure lead to obtain the best combinations of FCS and battery pack in terms of reduction in hydrogen consumption for typical drive cycles: urban, extra-urban and highway. This part of the sizing methodology defined the FCS dimension and presented the better options for the battery pack.

In order to define the energy capacity of the battery, it was first used an approach based on the population mobility. In the sequence, it was effectuated an analysis of the economical cost about the choice of the battery capacity and the reduction in the hydrogen consumption.

The data in the table 4.11 summarize the final sizing of the vehicle.

| | | |
|---|---|---|
| Electric motor | $P_{max}$ $(kW)$ | 44 |
| | $\Gamma_{max}$ $(N.m)$ | 260 |
| | $\Omega_{max}$ $(rpm)$ | 5900 |
| Mechanical transmission | $k_{red}$ | 3.42 |
| | $\eta_{red}$ $(\%)$ | 97 |
| FC system | $P_{max}$ $(kW)$ | 35 |
| Battery | $\varepsilon_{max}$ $(kWh)$ | 4.25 |

**Table 4.11:** Size of the vehicle elements

Analyzing the results about the elements in the hybrid system, the FCS presents a ratio $P_{FCS(max)}/P_{motor(max)}$ with a value that is close to the indicated by vehicle constructors such as Daimler (80 %) [120]. Regarding the battery, it was obtained an energy capacity higher than the value indicated by the same constructor in its Class B hydrogen model ($1.4\,kWh$). This difference is due to two factors:

- Presence of a battery traction mode (allowing to drive the vehicle in zero-emission zone) that imposes an energetic condition in the sizing process.
- Lower capacity of the battery to deliver and recover power ($10\,C$ and $-3\,C$) compared with the data indicated by the constructor ($24\,C$ and $-7.2\,C$) [120].

In the next chapter, the sizing obtained is incorporated in the models and in the optimization problem with the objective to develop an optimal energy management strategy for online applications.

# Chapter 5

# Online energy management strategy

**Abstract**

In this chapter, the energy management of the FCHEV is defined in order to solve an optimization problem that includes the dynamics of the fuel cell system. This non-linear dynamics is changed with the adoption of a control strategy that linearizes the fuel cell system dynamics.

Optimal power split strategy is designed using optimization principles combined with predictive approach. An online algorithm represents the local optimization solution for the constrained hydrogen minimization problem.

## 5.1 Introduction

Despite the presence of hybrid vehicles on the market, the energy management required for this kind of vehicles is still an open problem. Several studies have dealt with this topic proposing solutions that uses different methods, but there is no consensus of the method that is the most adapted. Besides, the way to treat with this problem differs from authors to authors, which means that the assumptions made will differentiate the approaches. For instance, in the FCHEV particular case, the fuel cell system dynamics is often ignored in the solutions using optimizations methods as presented in chapter 3. Nevertheless, this dynamics is still considered as technological drawback that should be overcome, being approached in this work as a main objective such that it would be included in the energy management strategy.

Another concern of the energy management methods is about its applicability for a problem that requires online responses without too much computation time and memory capacity, such as the vehicle applications. For our specific problem, the optimizations

methods presented in the chapter 3 have shown the ability to solve the typical optimization problem for a FCHEV, but the non causal characteristics of their implementations avoid the applicability for problems addressed to real time systems, such as the hybridization in the vehicle. Therefore, this chapter's goal is to propose an online optimization algorithm capable to solve an optimization problem as stated in the chapter 3 and that includes the dynamics of the fuel cell system in its constraints. In order to achieve these goals, an outline is used to development process.

The dynamics of the fuel cell system have been presented in the first part of the chapter. This representation is obtained from the dynamic equations of the main elements that compose the system.

Afterwards a control strategy is applied to the fuel cell system in order to control the state variables and to linearize the dynamics. The controller's performance is verified applying it on the validation dynamic fuel cell system model introduced in chapter 3. Thereafter, the control law is tested in the real fuel cell system that integrates the PROSPAC prototype (appendix B), where the perormance of the proposed control law is compared to other strategies frequently used in the automotive applications.

A simplification performed by application of the control law allows to include this new dynamics as a constraint in the optimization problem, which is presented in the sequence of the chapter.

Based on an algorithm that allies the Pontryaguin's maximum principle with a predictive approach, a local optimization algorithm is designed and tested by comparing their results with a global optimization method.

The algorithm is tested and validated by simulations and experimental campaigns. During the testing procedure, several types of cycles are used to confirm the validity of the strategy. Different speed and altitude profiles permit to validate the algorithm robustness to maximize the energy recovery under different conditions.

## 5.2 Fuel Cell System Dynamics

Composed by several elements in different subsystems, the fuel cell system has its dynamics determined by a complex set of interactions among the stack, the different subsystems and the dynamic evolutions of the external environment.

These interactions can associate state variables with different dynamic behaviors, which lead to undesired effects. Such undesired effects are often present in the case of multi-physical systems. For the specific case of the fuel cell system, several harmful effects result from the possible different dynamics.

In this work, the dynamics of the fuel cell system is represented by the dynamics of the subsystems that are the most constrained, meaning the dynamics that can more often generate some harmful effect for the stack. Therefore it is necessary a first overview of the most representatives harmful effects for the fuel cell stack.

Out of the numerous harmful effects, two particular ones have the special attention due to their common presence in normal operations and their important degradation results: hydrogen and oxygen starvation.

Thounthong et al. [114] shown the effects caused by hydrogen starvation in the stack during an electric load demand. The failure to feed the stack with hydrogen as fast as the electrical demand, is responsible for different undesirables effects to the system. Beside the losses in the fuel cell stack performance observed with the time, hydrogen starvation causes irreversible degradation effects in different parts of the stack leading to a reduction of the life time [105, 114, 125].

On the cathode side, the lack of oxygen during electrical demands imposes the fuel cell stack to operate in a condition that also affects the performance and the characteristics of the stack. This oxygen starvation was discussed by different authors. Gerard et al. [65] presented the effects of the oxygen starvation on the different characteristics of the fuel cell. Schimittinger et al. [105] highlighted the importance of this phenomenon among the types of harmful phenomena that can happen during an operation of the fuel cell system.

Even though hydrogen starvation can produces highly degradation effects, oxygen starvation is considered the phenomenon that defines the dynamics of the fuel cell system due to the control effort necessary to avoid it.

As the oxygen starvation results from a failure in the interaction between the electric and air supply subsystem, more precisely, between the current demand and the oxygen flow in the fuel cell active layer sites.

Compared to the components of the electric subsystem (DC/DC converter), the elements present in the air supply subsystem have a slower dynamics (air compressor valve, etc.). Consequently, the dynamics of the air supply subsystem is considered to represent the fuel cell system dynamics.

Being also considered by other authors [24, 120, 98] as the most representative dynamic of the system, the air subsystem dynamics has a non linear characteristics. Equations 3.17, 3.14 and 3.23 of the chapter 3 show that the dynamics is represented by the non-linear equations of the compressor, cathode capacity and pressure control valve. In these dynamic equations, the control of the compressor and the valve should regulate the air stoichiometry (air flow) and the cathode pressure in order to assure a good reaction.

The application of control strategies would allows a regulated and stable behavior of the output variables to be obtained. This subject is presented in the following section.

## 5.3 Air circuit control

A control strategy for the air supply subsystem must be implemented such that the stoichiometry (ratio of the input oxygen flow over the reacted oxygen flow) is maintained around a constant desired value, whatever the power demand is. Moreover, the control of the oxygen flow should be coupled to the regulation of the pressure in the cathode, keeping a pressure equilibrium between cathode and anode.

The command of the motor-compressor in the air group is the way to regulate the stoichiometry, but it should deal with an important barrier that is the nonlinear characteristics of the components of the air supply subsystem (compressor, valves, capacity volume, transport phenomena) [119, 120].

Several authors dealt with this subject with different approaches. Tekin et al. [112] adopted the fuzzy logic with particle swarm approach to control the motor compressor; Grujicic et al. [69] applied static and dynamic feedfoward control techniques for the air flow control. Nonlinear approaches using passivity, sliding mode and prediction control techniques were developed in [108, 109, 119] respectively. Theses approaches obtained good results in terms of oxygen flow.

However, the works mentioned previously assume that the anode pressure follows the cathode pressure value. This means that the cathode pressure is not regulated around a desired value and it changes according to the control. Therefore, in order to maintain the pressure equilibrium between cathode and anode, a fast electro-valve is required to control the anode pressure and to adapt its setpoint with the real time value of the cathode pressure [13, 91].

In order to tackle this problem and to implement a robust solution for the control of the air supply system, this work proposes a non linear control design that enables stoichiometry and pressure control to be coupled. Hence, the oxygen stoichiometry and the cathode pressure are controlled at the same time, keeping the variables close to their desired values. Moreover, the proposed control solution must preserve the stack performance and its durability during all the operation.

The control design is based on the differential flatness theory [58]. According to this theory, if flat outputs exist, it is possible to obtain the full control of all the system state variables and to impose the system to track desired trajectories as imposed on these flat outputs.

Differential flatness strategy is designed using a simplified fuel cell system model and is firstly tested using the dynamic model of the fuel cell system introduced in chapter 3 and after implemented and tested in the real fuel cell system (PROSPAC).

### 5.3.1 Control Model

A simplified model of the air supply system has been designed based on the respective model used in the hybrid system model (chapter 3). Some assumptions are made to reduce the model complexity and dimension:

- Operation in gas phase only (no multiphase flow).
- The humidifier is represented only by its equivalent pressure drop without dynamics and transport phenomena.
- The transport phenomena inside the fuel cell are not taken into account. Therefore, diffusion through the membrane is not taken into account (no gas crossover or water transport).
- The temperature inside the fuel cell is homogeneous and perfectly controlled.
- The cathode is represented by a global volume and a pressure drop from the inlet to the outlet (figure 5.1).

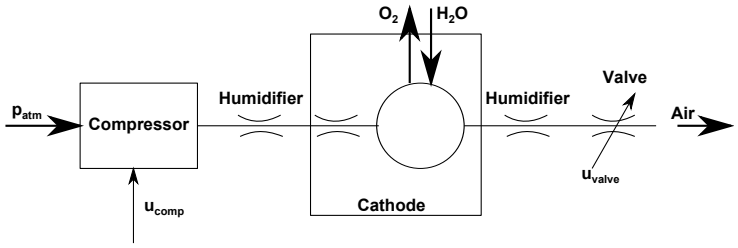


**Figure 5.1**: Simplified model of air supply subsystem

The compressor air flow results from the compressor characteristics in a nonlinear stationary condition model (5.1). The parameters $a$, $b$, $\psi_1$ and $\psi_2$ are obtained by fitting the experimental characteristics of the real compressor operating in the fuel cell working domain.

$$q_{cp} = \left(a\omega^2 + b\omega\right)\left\{\frac{\psi_1}{\psi_2} - \frac{1}{\psi_2\left[1 - \left(\frac{p_{sm}}{p_{atm}} - 1\right)^{\frac{\gamma-1}{\gamma}}\right]}\right\} \tag{5.1}$$

Finally, the model used for the control synthesis is given by equation 5.2.

$$\begin{cases} \frac{d\omega}{dt} = \frac{1}{J}\left(\alpha.u_{mot} - \frac{C_p T_{atm}}{\omega \eta_{cp}}\left[\left(\frac{p_{sm}}{p_{atm}}\right)^{\frac{\gamma-1}{\gamma}} - 1\right] q_{cp}\left(\omega, p_{sm}\right) - \varphi\omega\right) \\ \frac{dp_{cath(out)}}{dt} = \frac{RT_{cath}}{V_{cath} m_{molar}}\left(q_{cp}\left(\omega, p_{sm}\right) - q_{O_2} + q_{H_2O} - q_{valve}\right) \\ \dot{x}_{valve} = \frac{1}{\tau_{valve}}\left(-x_{valve} + k_{valve} u_{valve}\right) \end{cases} \tag{5.2}$$

Values of the parameters in equations 5.1 and 5.2 are presented in appendix C.

The outputs to be controlled are the cathode outlet pressure $p_{cath(out)}$ and the compressor air flow $q_{cp}$. However, there is a coupling between these two variables, which leads to implement a non-linear control strategy to decouple the outputs, linearize the system and thereafter apply a classical control strategy for the equivalent linear system.

### 5.3.2 Proposed Control Strategy

A non linear control strategy called differential flatness [58] is applied to the non linear system presented previously. This control strategy permits to define the control inputs $u$ directly from the desired output trajectories $y$ and its derivatives.

In comparison with other approaches, the differential flatness strategy permits to compensate the known non-linearities of the system, setting a trajectory for the flat outputs and ensuring performance for the system. However, a stabilization feedback loops are required to ensure robustness to the system. The theory that defines this control strategy is briefly presented, followed by its implementation.

#### 5.3.2.1 Differential flatness theory

According to Fliess et al. [58, 59], given a non linear system such as 5.3, if all the states $x_i$ can be expressed as functions of the outputs and their derivatives, the system in 5.3 is defined to be differentially flat and admits the flat output $y$ defined as in 5.4.

$$\dot{x} = f\left(x, u\right);\ x \epsilon \Re^n;\ u \epsilon \Re^m; \tag{5.3}$$

$$\begin{cases} y = [y_1, y_2, y_3, ..., y_m]^T \; ; \; y \epsilon \Re^m \\ \\ \qquad\qquad with \\ \\ y = \phi\left(x, \dot{u}, ..., u^{(\theta)}\right) \end{cases} \tag{5.4}$$

The state variables and the input variables can be written as in 5.5.

$$\begin{cases} x = f_1\left(y, \dot{y}, ..., y^{(\kappa)}\right) \\ \\ u = f_2\left(y, \dot{y}, ..., y^{(\kappa+1)}\right) \end{cases} \tag{5.5}$$

Where $\theta$ and $\kappa$ are a finite number of derivatives. The summation of the relative degree of each output must have the same value as the system characteristic index [73].

#### 5.3.2.2 Implementation of the differential flatness control strategy

In order to implement the differential flatness control strategy in 5.2, the states ($\omega$, $p_{cath(out)}$ and $q_{valve}$) and the inputs ($u_{mot}$ and $u_{valve}$) should be function of the flat output $y_1$ and $y_2$. Therefore, choosing the flat outputs as $\omega$ and $p_{cath(out)}$, two states are directly the flat outputs, while the controls ($u_{mot}$ and $u_{valve}$) and the other state ($x_{valve}$) are developed in sequence.

Considering the dynamic model of the air supply subsystem (5.2) with a simplified representation performed by the adoption of the functions $f_i$ as in (5.6). The compressor air flow $q_{cp}$ is represented function of $\omega$ and $p_{cath(out)}$ due to the transformation that can be done from the cathode outlet pressure $p_{cath(out)}$ to the supply manifold pressure $p_{sm}$ by the application of the pressure drops in the cathode and humidifier $k_{hu} + k_{FC}$. In accordance with the model presented in chapter 3, the contribution of the pressure valve flow $q_{valve}$ in the cathode pressure dynamics is represented by two functions ($f_5$ and $f_6$) that are dependent on $x_{valve}$ and $p_{cath(out)}$. The cathode outlet pressure $p_{cath(ou)}$ appears in the functions due the application of the pressure drop in the humidifier $k_{hu}$ that transforms the valve inlet pressure to $p_{cath(out)}$.

$$\begin{cases} \frac{d\omega}{dt} = f_1(u_{mot}) + f_2\left(\omega, p_{cath(out)}\right) + f_3(\omega) \\ \frac{dp_{cath(out)}}{dt} = f_4\left(\omega, p_{cath(out)}, q_{O_2}, q_{H_2O}\right) + f_5\left(x_{valve}, p_{cath(out)}\right) + f_6\left(p_{cath(out)}\right) \\ \dot{x}_{valve} = f_7(x_{valve}) + f_8(u_{valve}) \end{cases} \tag{5.6}$$

Derivating the first flat output $y_1$and changing the state variables $\omega$ and $p_{cath(out)}$ by the flat outputs $y_1$ and $y_2$ in (5.6), the control input $u_{mot}$ is obtained from the first equation of the model as:

$$u_{mot} = f_1^{-1}(\dot{y}_1 - f_2(y_1, y_2) - f_3(y_1)) \tag{5.7}$$

Equation (5.7) shows that $u_{mot}$ depends on the flat outputs and its derivatives ($\dot{y}_1$, $y_1$ and $y_2$), defining an initial characteristic index $\rho_1 = 1$.

Derivating the second flat output $y_2$ and replacing the function $f_5$ by a more detailed representation(5.8), in accordance with $q_{valve}$ model, the state variable can be represented in (5.9).

$$f_5(x_{valve}, y_2) = x_{valve}.f_9(y_2) \tag{5.8}$$

$$x_{valve} = \frac{\dot{y}_2 - f_4(y_1, y_2, q_{O_2}, q_{H_2O}) - f_6(y_2)}{f_9(y_2)} \tag{5.9}$$

As can be noticed, $x_{valve}$ depends on the flat outputs, their derivatives, $q_{O_2}$ and $q_{H_2O}$. These two last elements are not considered as state variables, but as known disturbances which are estimated from the FC reaction according to the desired supplied current. Therefore, the three state variables confirm the adoption of the assigned flat outputs. However, it is necessary to verify if the control of the pressure valve also meets this requirement.

In order to obtain $u_{valve}$, the flat output $y_2$ is derivated twice as presented in (5.10), where $x_{valve}$ is replaced by the function $f_{10}$ to simplify the representation.

$$\begin{aligned} \ddot{y}_2 = \frac{d}{dt}(f_5(y_1, y_2, q_{O_2}, q_{H_2O})) + \dot{x}_{valve} f_9(y_2) + \cdots \\ \cdots + f_{10}(\dot{y}_2, y_1, y_2, q_{O_2}, q_{H_2O}) \frac{d}{dt}(f_9(y_2)) + \frac{d}{dt}(f_6(y_2)) \end{aligned} \tag{5.10}$$

Replacing $\dot{x}_{valve}$ by its equation in (5.6), the control $u_{valve}$ is represented by the equation (5.11).

$$u_{valve} = f_8^{-1}\left(\frac{\ddot{y}_2 - \frac{d}{dt}\left(f_5\left(y_1, y_2, q_{O_2}, q_{H_2O}\right)\right) - f_{10}\left(\dot{y}_2, y_1, y_2, q_{O_2}, q_{H_2O}\right)\frac{d}{dt}\left(f_9(y_2)\right)}{f_9(y_2)} \cdots \right. \\ \left. \cdots + \frac{\frac{d}{dt}\left(f_6(y_2)\right)}{f_9(y_2)} - f_7\left(f_{10}\left(\dot{y}_2, y_1, y_2, q_{O_2}, q_{H_2O}\right)\right)\right) \tag{5.11}$$

$u_{valve}$ equation also shows its depence only on the flat outputs, their derivatives, the known disturbances and their derivatives, indicating that the chosen outputs ($\omega$ and $p_{cath(out)}$) are suitable to become the flat outputs.

Consequently, according to [58, 59], the system is differentially flat, admits the flat outputs $y_1$ and $y_2$ and permits a stable inversion to define the control inputs. Besides, the characteristc index $\rho_2$ of the cathode pressure dynamics equals 2 leads to obtain the characteristic index of the system equals 3 ($\rho_{system} = \rho_1 + \rho_2 = 3$), indicating that the dynamics resulted from the control strategy do not present a residual part.

After the confirmation about the existence of the flat outputs, a trajectory generation should be done for them. The output $p_{cath(out)}$ has as desired trajectory a stationary profile ($p^d_{cath(out)} = cte$), where the value is the same at the anode pressure, assuring a balance pressure between cathode and anode.

The definition of the motor speed desired trajectory $\omega^d$ begins with the assignment of the desired air flow in the fuel cell stack (5.12). This is directly dependent to the desired current trajectory $i^d_{FC}$ (eq. 5.12), which is a known variable controlled in the electric subsystem (DC/DC converter). This air flow is supplied by the compressor ($q^d_{air} = q^d_{cp}$) and is function of two variables: desired supply manifold pressure $p^d_{sm}$ and compressor speed $\omega^d$ (eq. 5.13). In equation 5.13, $p^d_{sm}$ is obtained by the equation 5.14 that takes into account the pressure drop at the fuel cell stack and the humidifier ($k_{FC}$ and $k_{hu}$). Therefore, in order to obtain $\omega^d$, the quadratic equation 5.15, obtained from 5.12, 5.13 and 5.14, must be solved. According to the equation 5.15, the motor speed desired profile $\omega^d$ is function of $i^d_{FC}$ and $p^d_{cath(out)}$.

$$q^d_{air} = \frac{St_{O_2}}{\chi_{O_2}} \frac{N_{cell} i^d_{FC}}{4F} \tag{5.12}$$

$$q^d_{cp} = \left(a\left(\omega^d\right)^2 + b\omega^d\right)\left\{\frac{\psi_1}{\psi_2} - \frac{1}{\psi_2\left[1 - \left(\frac{p^d_{sm}}{p_{atm}} - 1\right)^{\frac{\gamma-1}{\gamma}}\right]}\right\} \tag{5.13}$$

$$p^d_{sm} = p^d_{cath(out)} + \left(q^d_{air}\right)^2\left(k_{hu} + k_{FC}\right) \tag{5.14}$$

$$\left(a\left(\omega^d\right)^2+b\omega^d\right)\left\{\frac{\psi_1}{\psi_2}-\frac{1}{\psi_2\left[1-\left(\frac{p^d_{cath(out)}+\left(\frac{St_{O_2}}{\chi_{O_2}}\frac{N_{cell}i^d_{FC}}{4F}\right)^2(k_{hu}+k_{FC})}{p_{atm}}-1\right)^{\frac{\gamma-1}{\gamma}}\right]}\right\}\cdots$$
$$\cdots-\frac{St_{O_2}}{\chi_{O_2}}\frac{N_{cell}i^d_{FC}}{4F}=0 \tag{5.15}$$

Concerning the valve behavior, the trajectory of its pressure difference $\Delta p_{valve}$, used to calculate the mass flow $q_{valve}$, is given from equation 5.16.

$$\Delta p_{valve}=p^d_{cath(out)}-k_{hu}q^2_{valve}-p_{atm} \tag{5.16}$$

Therefore, applying this equation in the valve mass flow equation (3.22 in chapter 3), the new value of $q_{valve}$ is given by the resolution of the quadratic equation 5.17. The solution is given by equation 5.18 ensures that for all $x_{valve}\geqslant 0$ and $p^d_{cath(out)}\geqslant p_{atm}$ there is a $q_{valve}\geqslant 0$. The presence of the displacement in the valve control law integrates the content of its mechanical characteristics that approximates to the physic behavior.

$$q^2_{valve}-\left[\frac{\left(\zeta_1x_{valve}+\zeta_2\right)^2}{1+k_{hu}\left(\zeta_1x_{valve}+\zeta_2\right)^2}\left(p^d_{cath(out)}-p_{atm}\right)\right]=0 \tag{5.17}$$

$$q_{valve}=\left(\zeta_1x_{valve}+\zeta_2\right)\sqrt{\frac{\left(p^d_{cath(out)}-p_{atm}\right)}{1+k_{hu}(\zeta_1x_{valve}+\zeta_2)^2}} \tag{5.18}$$

The system 5.19 presents the new dynamic of the air group, where the constants are replaced by $c_i$ (to simplify the notation), $f_{comp}$ calculates the air desired flow supplied by the compressor ($q^*_{cp}$) and $f_{valve}$ calculates the desired air flow passing across the valve ($q^*_{valve}$).

$$\begin{cases}\frac{dy_1}{dt}=c_1.u_{mot}-c_2\frac{1}{y^d_1}\left[\left(\frac{y^d_2+f_{comp}\left(y^d_1,y^d_2\right)(c_3)}{p_{atm}}\right)^{\frac{\gamma-1}{\gamma}}-1\right]f_{comp}\left(y^d_1,y^d_2\right)-c_4y^d_1\\ \\ \frac{dy_2}{dt}=c_5\left(f_{comp}\left(y^d_1,y^d_2\right)-q_{O_2}+q_{H_2O}-f_{valve}\left(x_{valve},y^d_2\right)\right)\\ \\ \frac{dx_{valve}}{dt}=\frac{1}{c_6}\left(-x_{valve}+c_7u_{valve}\right)\end{cases} \tag{5.19}$$

The first control variable $u_{mot}$ is claculated in 5.20, where $W_1$ is the new input that replaces the term $\frac{dy_1}{dt}$.

$$u_{mot} = \frac{W_1 + c_2 \frac{1}{y_1^d}\left[\left(\frac{y_2^d + f_1\left(y_1^d, y_2^d\right)(c_3)}{p_{atm}}\right)^{\frac{\gamma-1}{\gamma}} - 1\right] f_{comp}\left(y_1^d, y_2^d\right) + c_4 y_1^d}{c_1} \tag{5.20}$$

As mentioned before, the second control variable is calculated in two steps. The first derivative of the flat output $y_2$ allows to calculate $q_{valve}$ (equation 5.21) and using this result in 5.17 the value of $x_{valve}$ is obtained as in 5.22.

$$q_{valve} = \left[f_{comp}\left(y_1^d, y_2^d\right) - q_{O_2} + q_{H_2O} - \frac{1}{c_5}\frac{dy_2^d}{dt}\right] = f_{valve}\left(x_{valve}, y_2^d\right) \tag{5.21}$$

$$x_{valve} = \frac{1}{\zeta_1}\left[\frac{q_{valve}\left(y_1^d, y_2^d, \dot{y}_2^d, q_{O_2}, q_{H_2O}\right)}{\sqrt{y_2^d - k_{hu} q_{valve}\left(y_1^d, y_2^d, \dot{y}_2^d, q_{O_2}, q_{H_2O}\right) - p_{atm}}} - \zeta_2\right] \tag{5.22}$$

As can be noticed, it is necessary to compute the first derivative of the desired output trajectory $y_2^d$ to find the value of $x_{valve}$. In our case the value of the first derivative is zero because the desired trajectory for the outlet cathode pressure is a constant value.

Finally, the second control input $u_{valve}$ is obtained from the second derivative of the flat output $y_2$ (5.23). In 5.23, the first derivative of $q_{valve}$ is calculated using the equation 5.18. It presents the terms of $x_{valve}$ and $\dot{x}_{valve}$ that are respectively replaced by 5.22 (calculated previously) and the dynamic equation of the valve. Therefore, the control variable $u_{valve}$ is presented in 5.24, where $x_{valve}$ is replaced by a function $f_{x\,valve}\left(y_1^d, y_2^d, \dot{y}_2^d, q_{O_2}, q_{H_2O}\right)$ to simplify the presentation and $W_2$ is a new input that replaces the term $\frac{d^2 y_2}{dt^2}$.

$$\frac{d^2 y_2^d}{dt^2} = c_5\left[\dot{f}_{comp}\left(y_1^d, y_2^d\right) - \dot{q}_{O_2} + \dot{q}_{H_2O} - \dot{q}_{valve}\right] \tag{5.23}$$

$$u_{valve} = \frac{f_{x\,valve}}{c_7} + \left\{\frac{\frac{1}{c_5}W_2 - \dot{f}_{comp} + \dot{q}_{O_2} - \dot{q}_{H_2O}}{k_{hu}\zeta_1\left(\zeta_1 f_{x\,valve} + \zeta_2\right) - \frac{\left[k_{hu}^2 \zeta_1 (\zeta_1 f_{x\,valve} + \zeta_2)^3 + \zeta_1\left(y_2^d - p_{atm}\right)\right]}{\sqrt{k_{hu}^2 (\zeta_1 f_{x\,valve} + \zeta_2)^4 - 4\left[(\zeta_1 f_{x\,valve} + \zeta_2)^2\left(y_2^d - p_{atm}\right)\right]}}}\right\} \tag{5.24}$$

In the sequence, the effects of these control laws in the system dynamics are presented.

#### 5.3.2.3 New Dynamics of the System

A new open loop structure of the system is obtained as the result of the proposed control laws. This consists of an integrator chain as can be seen in (5.25).

$$\begin{cases} \dot{Z}_1^d = W_1 \\ \dot{Z}_2^d = Z_3^d \\ \dot{Z}_3^d = W_2 \end{cases} \tag{5.25}$$

For the new linear system in 5.25 it is possible to apply classic control approaches. The state space representation in (5.26) allows to apply a state feedback ($U = -KX$) to assure the stability.

$$\begin{gathered} \begin{bmatrix} \dot{Z}_1^d \\ \dot{Z}_2^d \\ \dot{Z}_3^d \end{bmatrix} = \begin{bmatrix} 0 & 0 & 0 \\ 0 & 0 & 1 \\ 0 & 0 & 0 \end{bmatrix} \begin{bmatrix} Z_1^d \\ Z_2^d \\ Z_3^d \end{bmatrix} + \begin{bmatrix} 1 & 0 \\ 0 & 0 \\ 0 & 1 \end{bmatrix} \begin{bmatrix} W_1 \\ W_2 \end{bmatrix} = \dot{X} = AX + BU \\ \begin{bmatrix} Y_1 \\ Y_2 \end{bmatrix} = \begin{bmatrix} 1 & 0 & 0 \\ 0 & 0 & 1 \end{bmatrix} \begin{bmatrix} Z_1^d \\ Z_2^d \\ Z_3^d \end{bmatrix} = Y = CX \end{gathered} \tag{5.26}$$

Assigning the poles positions as $(-10, 10i)$, $(-10, -10i)$ and $(-50, 0i)$, there is a guarantee that the system is stable. The $K$ matrix obtained from this pole positioning is:

$$K = \begin{bmatrix} 50 & -10.57 & -0.63 \\ -0.72 & 200.18 & 20 \end{bmatrix} = \begin{bmatrix} K_1 \\ K_2 \end{bmatrix} \tag{5.27}$$

The final linear system with its control is given in (5.28).

$$\begin{cases} \dot{Z}_1^d = W_1 = y_1^d - \left(50.y_1 - 10.57.Z_2^d - 0.63.y_2\right) \\ \dot{Z}_2^d = Z_3^d \\ \dot{Z}_3^d = W_2 = y_2^d - \left(-0.72.y_1 + 200.18.Z_2^d + 20.y_2\right) \end{cases} \tag{5.28}$$

#### 5.3.2.4 Control Structure

Figure 5.2 presents the control structure proposed where the systems $\sum_i$ are defined as:

- $\sum_1$: calculated air flow that must be delivered to the stack (equation 5.12).
- $\sum_2$: calculated desired trajectory of the supply manifold pressure (equation 5.14).
- $\sum_3$: desired motor speed (inversion of the equation 5.1).
- $\sum_4$: control law for the motor-compressor (equation 5.20).
- $\sum_5$: control law for the pressure valve (equation5.24).
- $\sum_6$: motor-compressor (first equation of system 5.2).
- $\sum_7$: cathode of the fuel cell (second equation of system 5.2).
- $\sum_8$: pressure valve (third equation of system 5.2).

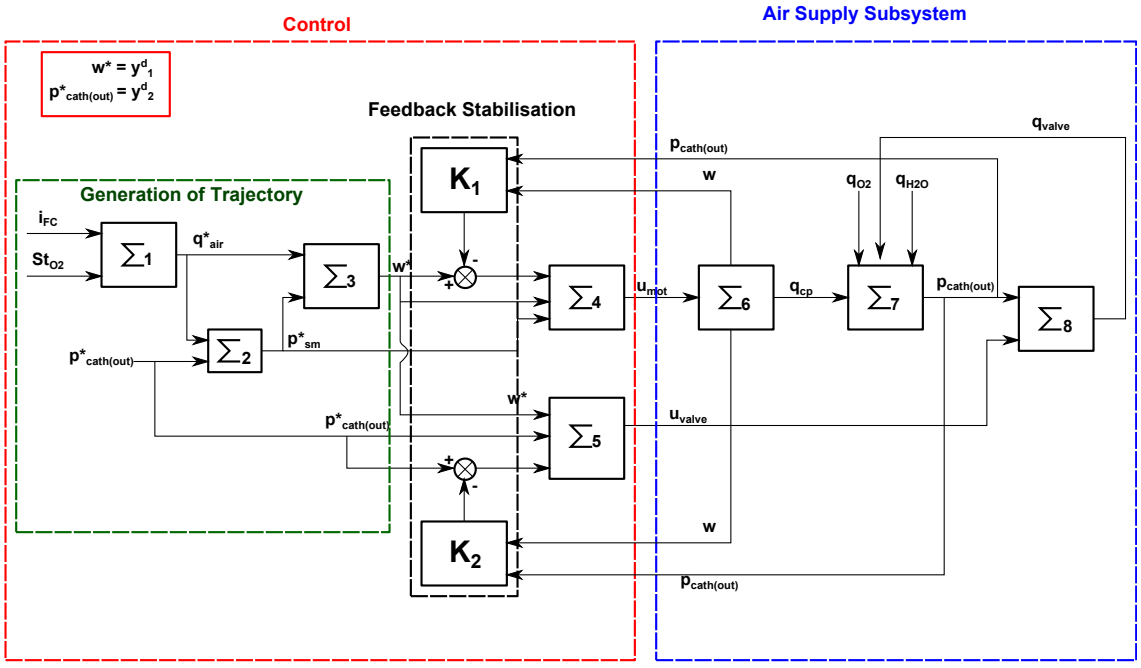


**Figure 5.2:** Control block structure

### 5.3.3 Simulation Results

In order to verify the efficiency of the control law a first study in simulating is done using the dynamic model introduced in chapter 3. The conditions applied in this case are:

- Oxygen stoichiometry (reference = 1.8).
- Cathode outlet pressure (reference=1.2 bar).
- Compressor speed profile.
- Pressure valve behavior.

These variables were obtained from the hybrid system model when it is submitted to a power profile defined in figure 5.3.

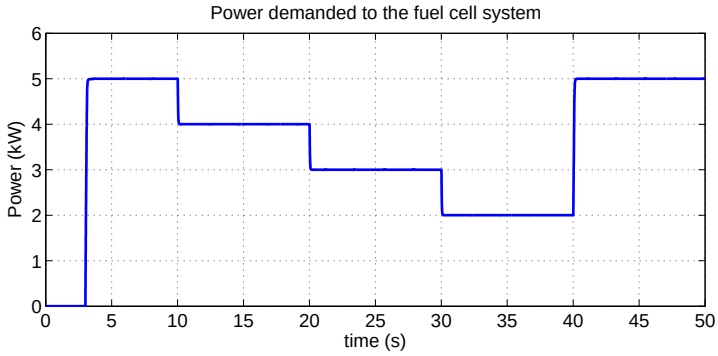


**Figure 5.3:** Electrical power profile demanded to the fuel cell

Figures in 5.4 present the behavior of the above-mentioned variables when the system is subjected to the power profile of the figure 5.3.

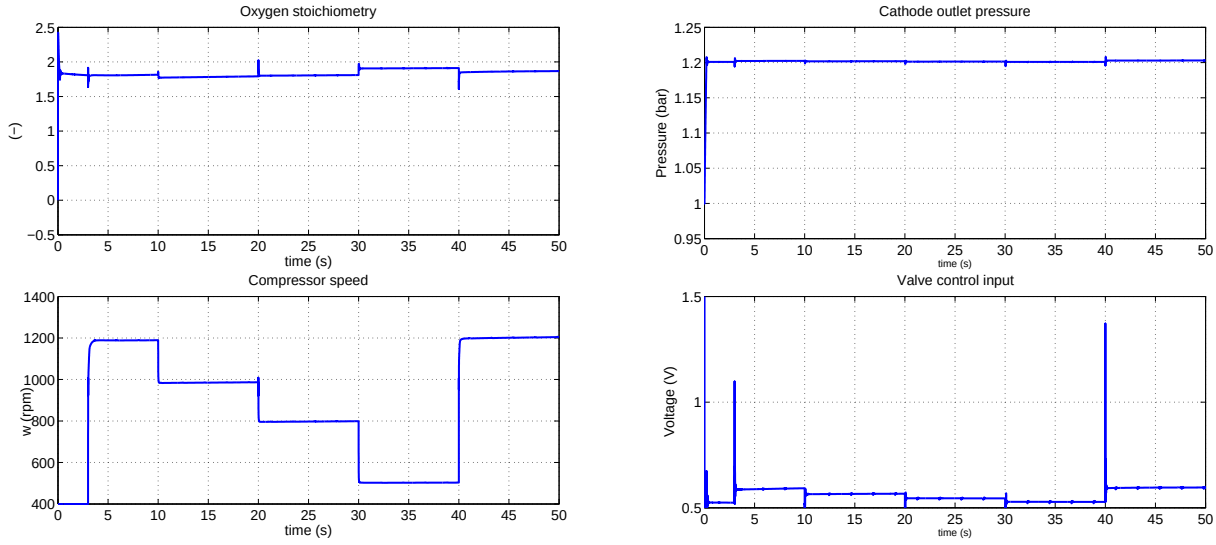


**Figure 5.4:** Results of the simulation- air system variables

Despite the steps in the power demanded profile, the oxygen stoichiometry and the outlet pressure present responses close to the reference values. Observing in details the

valve control input (figure 5.5), it is possible to verify that the derivatives in the control law ($\dot{q}_{O_2}$, $\dot{q}_{H_2O}$ and $\dot{f}_{comp}\left(y_1^d, y_2^d\right)$) will compensate the low dynamics of the valve during the fast transients. This avoids important pressure drops on the cathode outlet. Moreover, the figure 5.5 shows that the disturbance created by the periodic purge procedure in the anode is compensated by an action in the valve control in order to reject this perturbation in the cathode pressure profile.

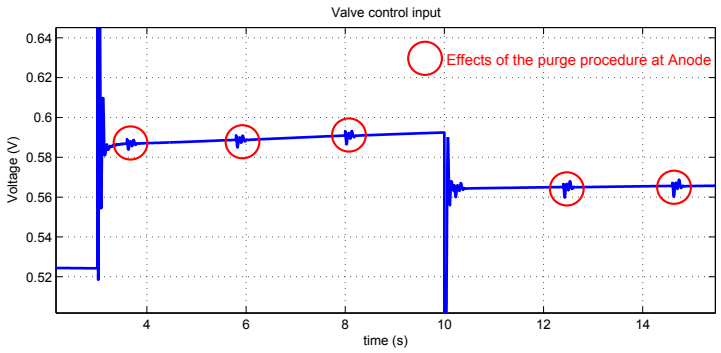


**Figure 5.5:** Pressure valve control input during the transients and disturbances

Concerning the small transient effects present in the pressure and stoichiometry responses, they do not represent a harmful consequence for the fuel cell, as it can be seen from the cell voltage evolution (figure 5.6).

The cell voltage follows the demanded power profile, which means that the fuel cell state conditions allow to deliver a rated power without a significant voltage drop at the cell level. Thus, even when the maximum power was demanded, the cell voltage remains close to $0.7\,volts$.

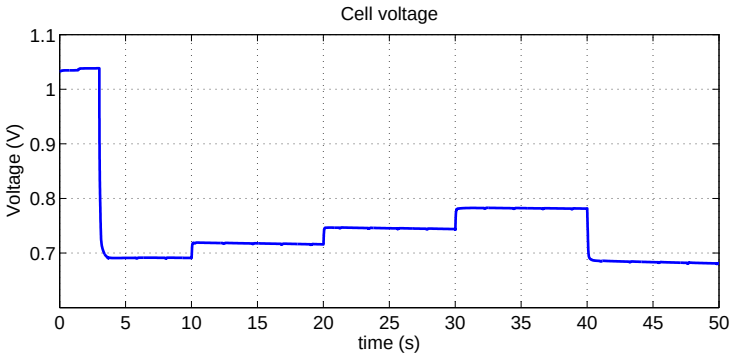


**Figure 5.6:** Cell voltage

The compressor speed shows a behavior that follows the power demanded without high oscillations or large overshoot. This is very satisfying in terms of the speed control.

The compressor control, coupled with the control valve, avoids as well the choked flow regime at the compressor, since the pressure ratio has a value greater than the critical regime ($\Pi_{critic} = 0.52$) during all the operation.

Nevertheless, this coupled control, linked also to the dynamic operational conditions, could affect the durability of the stack directly or indirectly by its effects on different internal variables, such as oxygen molar fraction, cell voltage and membrane humidification, for instance [110].

In terms of degradation, the result of oxygen molar fraction presents a non-homogeneous distribution inside the stack (figure 5.7), however the minimal level assures the operational conditions of the stack without losses in the performance, as presented by the cell voltage response (figure 5.6). In order to obtain a better distribution, a control law that takes into account the geometry inside the stack should be applied.

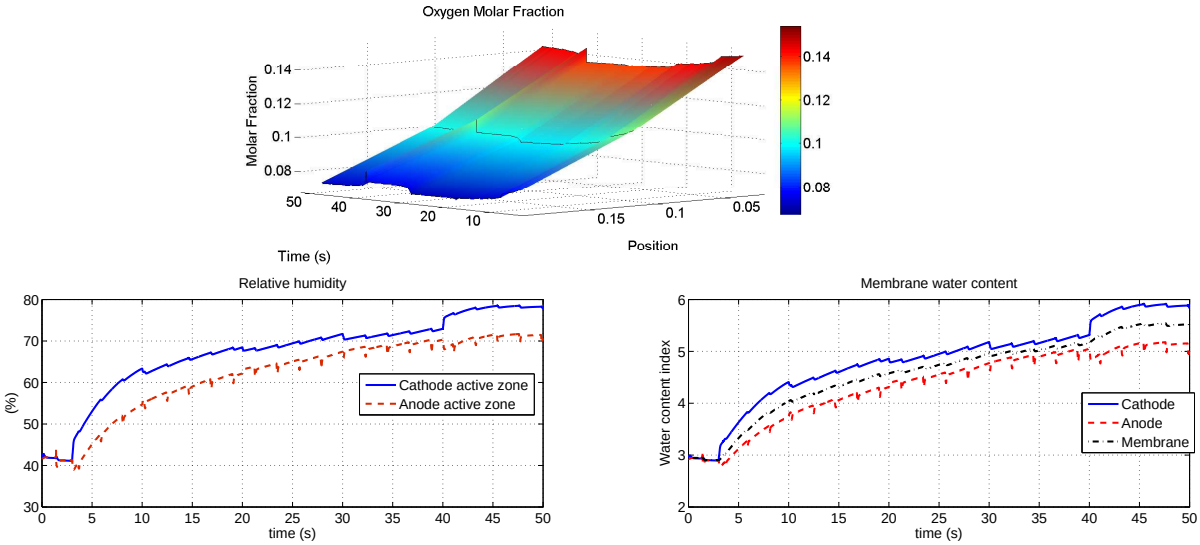


**Figure 5.7:** Fuel cell internal variables

The control law shows good results in the regulation of the air circuit variables and fuel cell voltage response; however, it is important to observe if there is no side effect on other important state variables, such as the humidity in the fuel cell stack. As a variable dependent on a passive element (humidifier), the relative humidity is indirectly subjected to actions on the other state variables. Therefore, even if the control of this variable is out of the scope of this work, the relative humidity in the fuel cell is observed in order to assure that the air subsystem control law does not create an undesired effect on it.

During the operation, the humidity remains acceptable ($>50\%$) at anode and cathode (figure 5.7) and converge towards an equilibrium level at the end of the cycle, which reflects the good water contents of the membrane (figure 5.7). This avoids degradation

effects due to membrane dryness. One can be observed the presence of small oscillations in the humidity response, which are related to the purge in the anode. The purge procedure reduces the humidity in the anode active zone, creating an instantaneous water transport from the cathode active zone to the anode active zone through the membrane, which explains the phenomenon at the three levels (cathode active zone, membrane and anode active zone).

### 5.3.4 Results in Real Fuel Cell System

The performance of the control law is tested in the real fuel cell system contained in PROSPAC (appendix B). The reference for the oxygen stoichiometry is 2, for the cathode outlet pressure is 1.2 *bar* and for the stack temperature measured on the cooling liquid at stack's outlet is 60 °C. The most important variables to be observed are:

- Compressor speed profile.
- Cathode pressure profile.

A current demanded profile in figure 5.8 was imposed to the fuel cell system, in order to verify the response of three control strategies:

- Classical approach using two PID control loops (figure 5.9)
- Dynamic prepositioning control strategy (figure 5.10)
- Flat control strategy (figure 5.2)

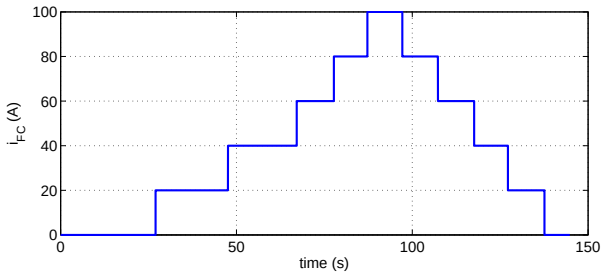


**Figure 5.8**: Demanded current profile

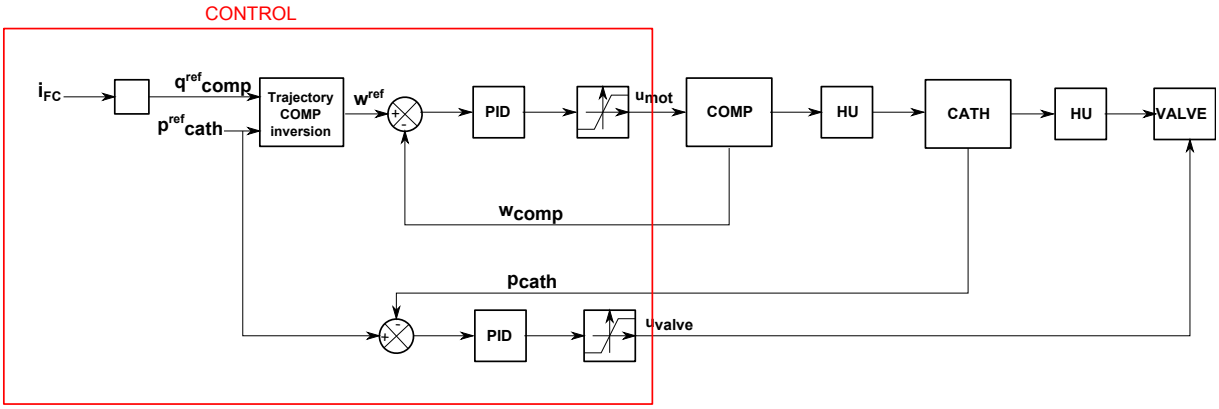


**Figure 5.9**: 2PID control block

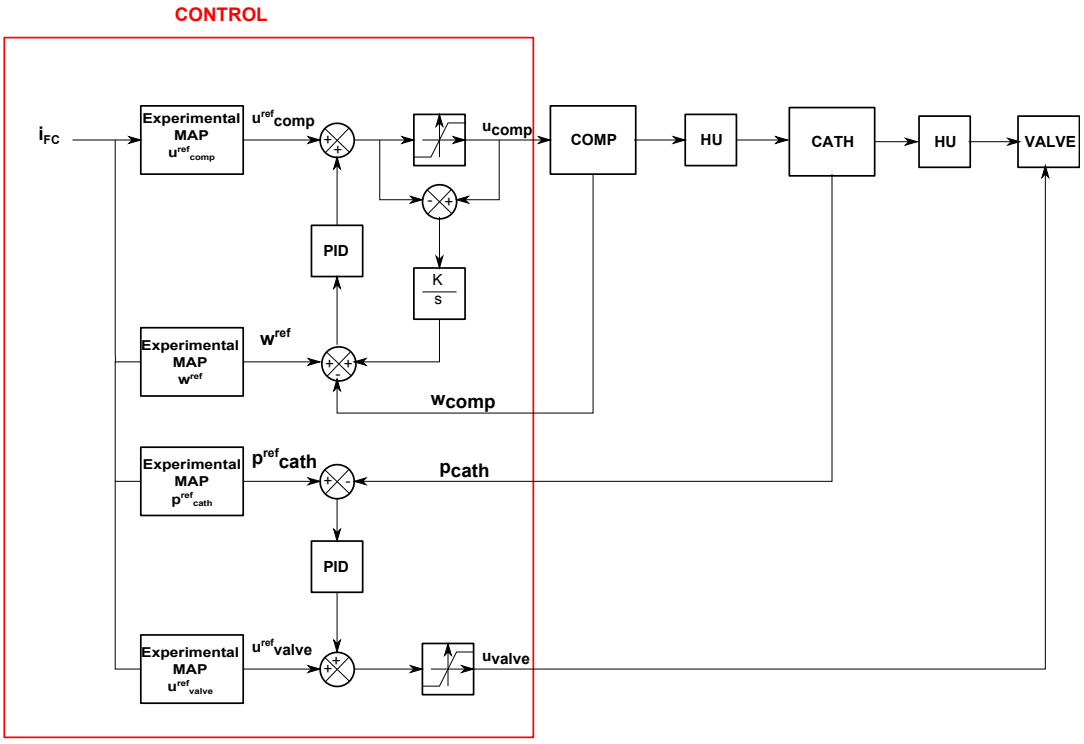


**Figure 5.10**: Dynamic prepositioning control block

The speed and pressure responses in figures 5.11 and 5.12 shows the good tracking performances of the flat control strategy. As it can be seen, the flat control strategy provides a better response time than the prepositioning strategy and its decoupling property avoids the interference of one variable on the other, as it is observed for the PID strategy.

The performance of the flat control strategy has influence on the fuel cell stack response. Figure 6.5 illustrates the voltage and power response for this control strategy

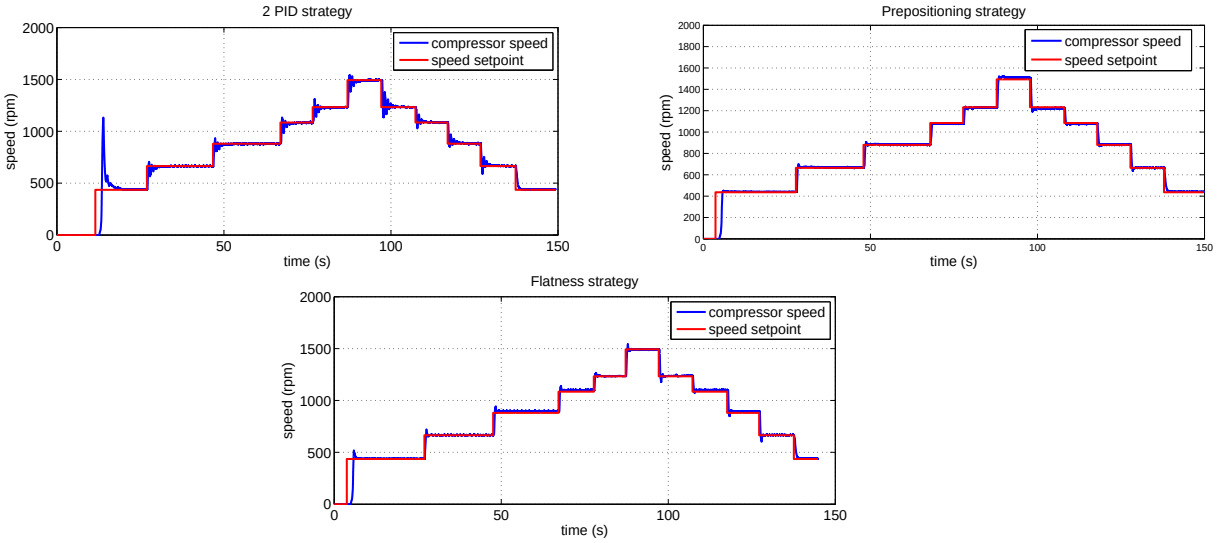


**Figure 5.11**: Compressor speed for the control strategies

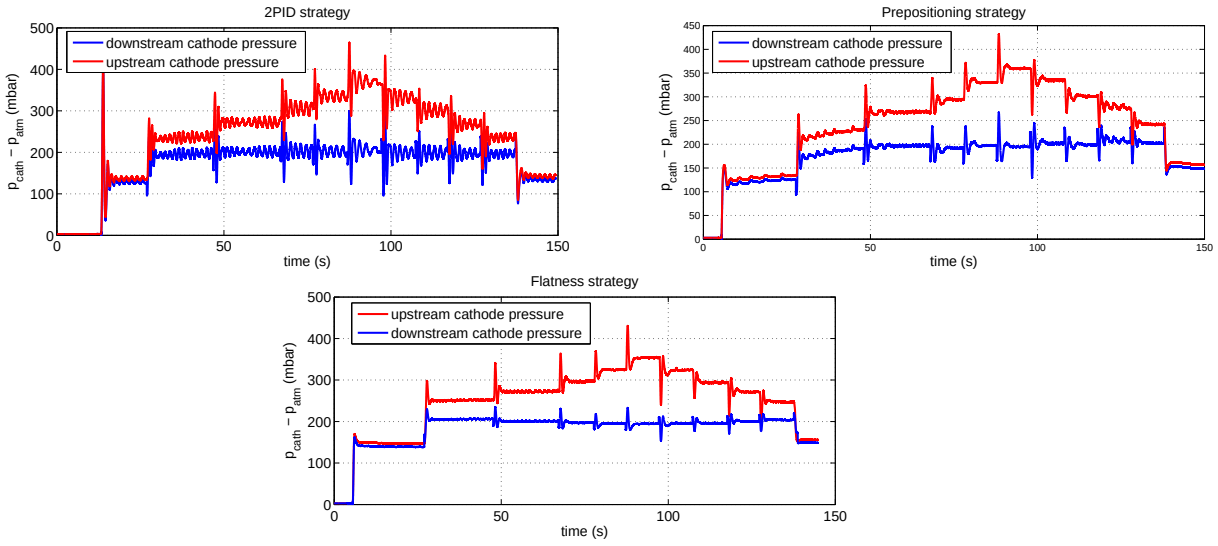


**Figure 5.12**: Cathode pressures for the control speed strategies

when a current is demanded from the system. As in the simulation results, the voltage remains at an acceptable level without strong oscillations, even for high values of power.

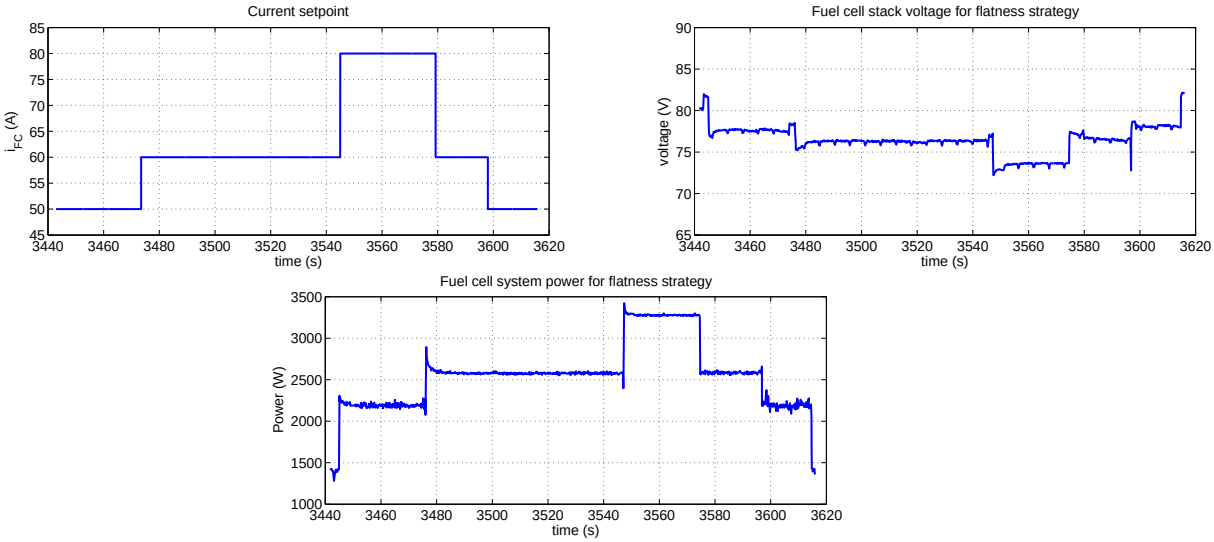


**Figure 5.13:** Fuel cell stack electrical response- flatness strategy

### 5.3.5 Conclusion on the air supply subsystem control

The non linear control strategy applied to the complex dynamics of the air subsystem provided good dynamic responses in different levels of the system. Compared with classical solutions adopted, the flat control strategy offered a stabilization of the dynamics with a controllability and stability obtained from its decoupling property.

Regarding the application for vehicles, the results shown a response time lower than $300\,ms$ to reach the demanding setpoints, which is perfectly adapted to the range of the FCHEV applications that requires a response time from one to a couple of seconds.

Moreover, the control strategy enables to represent the fuel cell system by an equivalent linear model in the energy management process. In the next section, the linearized dynamics given in 5.25 is introduced in the energy management optimization problem and used to the definition of a online optimization method.

## 5.4 New Optimization problem and predictive online energy management strategy

### 5.4.1 Optimization problem

The optimization problem stated in the chapter 3 is changed in order to take into account the new equivalent dynamic for the fuel cell system as developed in the last section (5.30).

This requires the proposed solutions to consider the fuel cell system dynamics in 5.25 as a constraint to be respected during the power split definition process.

$$\begin{cases} Cost\,Minimization: \\ J\left(P_{FC}^{*}\right) = min_{P_{FC}^{*}} \int_{0}^{t_f} g\left(P_{FC}\left(t\right)\right).dt \\ P_{FC}^{*} = argminJ\left(P_{FC}\left(t\right)\right) \\ \hline Constraints: \\ P_{batt\,min}\left(-3C\right) \leq P_{batt} \leq P_{batt\,max}\left(10C\right) \\ P_{FC\,min}\left(0kW\right) \leq P_{FC} \leq P_{FC\,max}\left(35kW\right) \\ SOE_{min}\left(40\%\right) \leq SOE \leq SOE_{max}\left(80\%\right) \\ Boundary\,condition: \\ SOE\left(0\right) = 60\% = SOE\left(t_f\right) \end{cases} \tag{5.29}$$

$$\begin{cases} \dot{\varepsilon} = f_1\left(P_{batt}\right) = -P_{batt} \\ \dot{\omega} = f_2\left(W_1\right) = W_1 \\ \dot{p}_{cath} = f_3\left(W_2\right) = W_2 \end{cases} \tag{5.30}$$

In order to solve this problem with an online approach, it is proposed a new optimization method.

### 5.4.2 Online predictive energy management method

When the complete driving cycle is unknown, the optimization problem can not be solved at once. Thus, a new approach based on the Pontryaguin's Minimum Principle (PMP) [39, 21] allied with a predicting horizon approach is proposed in this work.

This method deals with the constraints over the cycle, compromising as less as possible the optimization step.

Appling the PMP, the optimization problem in (5.29) can be solved using the Hamiltonien formulation (5.31). In this equation, the power balance was applied, such that the control inputs are defined as $P_{batt}$, $W_1$ and $W_2$.

$$\mathcal{H}\left(\varepsilon, \omega, p_{cath}, P_{batt}, W_1, W_2, \lambda_1, \lambda_2, \lambda_3\right) =$$

$$g\left(P_{vehtot} - P_{batt}\right) + \lambda_1 f_1\left(P_{batt}\right) + \lambda_2 f_2\left(W_1\right) + \lambda_3 f_3\left(W_2\right) = \tag{5.31}$$

$$g\left(P_{vehtot} - P_{batt}\right) - \lambda_1\left(P_{batt}\right) + \lambda_2 W_1 + \lambda_3 W_2$$

The optimal solution is obtained applying the conditions in (5.32)[39, 122, 21].

$$\begin{cases} \dot{\varepsilon} = \frac{\partial \mathcal{H}}{\partial \lambda_1};\ \dot{\omega} = \frac{\partial \mathcal{H}}{\partial \lambda_2};\ \dot{p}_{cath} = \frac{\partial \mathcal{H}}{\partial \lambda_3} \\ -\dot{\lambda}_1 = \frac{\partial \mathcal{H}}{\partial \varepsilon}; -\dot{\lambda}_2 = \frac{\partial \mathcal{H}}{\partial \omega};\ -\dot{\lambda}_3 = \frac{\partial \mathcal{H}}{\partial p_{cath}} \\ \frac{\partial \mathcal{H}}{\partial P_{batt}} = 0;\ \frac{\partial \mathcal{H}}{\partial W_1} = 0;\ \frac{\partial \mathcal{H}}{\partial W_2} = 0 \end{cases} \tag{5.32}$$

The conditions about the derivatives of the co-states $\lambda_n$ show that they are constants ($\dot{\lambda}_n = 0$), while the minimization of $\mathcal{H}$ according to the control inputs deliver the optimal power profile of the battery $P^*_{batt}$ and the values of the co-states $\lambda_2$ and $\lambda_3$ (6.7):

$$\begin{gathered}\frac{\partial \mathcal{H}}{\partial P_{batt}} = 0 = 2a_1 P^*_{batt}(t) + (2a_1 (P_{vehtot}(t)) + a_2) - \lambda_1 \Rightarrow \\ \Rightarrow P^*_{batt}(t) = \frac{\lambda_1 - (2a_1 (P_{vehtot}(t)) + a_2)}{2a_1} \\ \frac{\partial \mathcal{H}}{\partial W_1} = 0 = \lambda_2 \\ \frac{\partial \mathcal{H}}{\partial W_2} = 0 = \lambda_3\end{gathered} \tag{5.33}$$

An analytic function represents the optimal profile $P^*_{batt}$, which depends on the known variable $P_{vehtot}$ and the constant co-state $\lambda_1$. In general, $\lambda_1$ is related to the knowledge of the drive cycle in order to obtain the boundary condition ($SoE(0) = SoE(t_f)$). Therefore, assuming that the information of the entire drive cycle is not available, the presence of $\lambda_1$ in $P^*_{batt}$ calculation represents a limitation for online applications. To overcome this limitation, a predictive strategy is adopted to define the value of $\lambda_1$.

#### 5.4.2.1 Predictive approach

Isolating $\lambda_1$ in the response of the optimization problem (equation 5.34) and knowing that it has a constant value during the drive cycle, a finite horizon can be applied to equation 5.35.

$$P^*_{batt}(t) = \frac{\lambda_1 - (2a_1 (P_{vehtot}(t)) + a_2)}{2a_1} \tag{5.34}$$

$$\lambda_1 = 2a_1 P^*_{batt} + (2a_1 (P_{vehtot}(t)) + a_2) \tag{5.35}$$

Considering a time horizon $t_h$ and a calculation time step $\triangle t$, the sum of $\lambda_1$ over $t_h$ is:

$$\sum_{j=t}^{t+t_h} \lambda_1 = \frac{t_h}{\triangle t}\lambda_1 = \left(\sum_{j=t}^{t+t_h} (P_{batt}(j)).2a_1\right) - \sum_{j=t}^{t+t_h} (2a_1 (P_{vehtot}(j)) + a_2) \tag{5.36}$$

Hence, $\lambda_1$ is calculated in 5.37.

$$\lambda_1 = \frac{2a_1 \left(\left(\sum_{j=t}^{t+t_h} (P_{batt}(j))\right) - \sum_{j=t}^{t+t_h} P_{vehtot}(j)\right)}{\left(\frac{t_h}{\Delta t}\right)} + a_2 \tag{5.37}$$

Where the distributions $\sum_{j=t}^{t+t_h}(P_{batt}(j))$ and $\sum_{j=t}^{t+t_h} P_{vehtot}(j)$ are calculated differently:

**$P_{vehtot}$ distribution:** Observing equation 5.37, it can be seen that the time ordered prediction to the future power $P_{vehtot}$ is not necessary. Therefore, it is not important to know when a specific power demand will be done. Using this observation, this proposed method makes a simple hypothesis that the distribution of $P_{vehtot}$ during a predicted finite horizon is assumed as the same of the last finite horizon ($\sum_{j=t}^{t+t_h} P_{vehtot}(j) = \sum_{i=t-t_h}^{t-1} P_{vehtot}(j)$). Despite the simplicity, this prediction represents a valid and computational efficient prediction approach, according to Bernard et al. in [75].

For this application, the finite horizon is applied as a sliding window of time. Thus, at every $\triangle t$ there is a new value of $P_{vehtot}$ distribution to be used in the algorithm. A certain amount of memory is necessary to store the values of $P_{vehtot}$ in the past time window $t_h$, nevertheless it does not represent a strong drawback compared to the application of the Dynamic Programming.

**$P_{batt}$ distribution:** The calculation of $P_{batt}$ distribution is made considering that the $\lambda_1$ profile will bring the battery $SoE$ to its reference value ($SoE_{reference}$) at the end of the predicted horizon $t_h$ ($SoE(t+t_h) = SoE_{reference}$). Consequently, a change of variable can be done such that $SoE$ information appears in the $\lambda_1$ calculation. Replacing the term $\sum_{j=t}^{t+t_h}(P_{batt}(j))$ by $\varepsilon_{max}.\triangle SoE_{desired}/\triangle t$, the calculation of $\lambda_1$ is obtained from 5.38.

$$\lambda_1 = \frac{2a_1\left(\frac{\Delta SoE_{desired}.\varepsilon_{max}}{\Delta t} - \sum_{i=t-t_h}^{t-1} P_{vehtot}(i)\right)}{\left(\frac{t_h}{\Delta t}\right)} + a_2 \tag{5.38}$$

Instead of using the difference between $SoE_{reference}$ and $SoE(t)$ to represent the $\Delta SoE_{desired}$ target, a PI (proportional + integrator) controller is applied, which increases the robustness against the presence of noise in the $SoE$ measurement and uncertainties in the battery model.

The gains ($k_p$ and $k_i$) of the PI controller are obtained using a pole placement procedure. For this objective, the dynamic system is composed by the battery dynamics ($SoE$ calculation) and the control part (equation 5.34), where $\lambda_1$ is replaced by (5.38). Figure 5.14 presents the control block diagram.

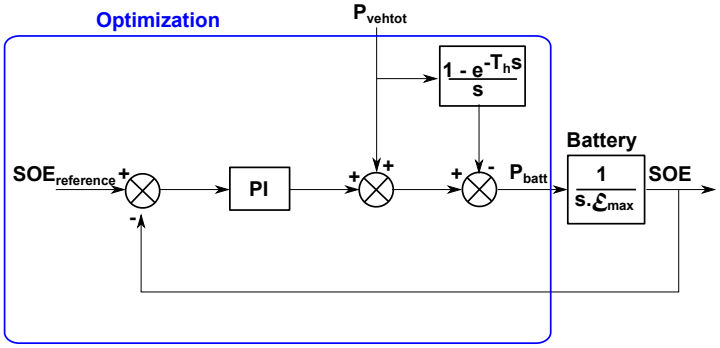


**Figure 5.14:** Control block diagram

Applying the Pade approximation [99] for the presented time delay, the block diagram of figure 5.14 can be represented by the equation (5.39). The aim of this control procedure is to place the poles in the stable region without vanishing $P_{vehtot}$ component.

$$SoE = \frac{P_{vehtot}}{\varepsilon_{max}} \left[ \frac{t_h s^2+2s-4}{t_h s^3+(2+t_h k_p)s^2+(2k_p+t_h k_i)s+2k_i} \right] + SoE_{reference} \left( \frac{k_p s+k_i}{s^2+k_p s+k_i} \right) \tag{5.39}$$

With a prediction horizon of $150\,s$, the values of $k_p$ and $k_i$ are respectively 0.087 and 0.0014, giving the poles positions at $(-0.0567, 0)$, $(-0.0213, 0)$, $(-0.0213, 0)$, $(-0.004, 0)$ and $(-0.004, 0)$. This prediction horizon value affects the calculus of $\lambda_1$ and the optimization results. In our work a brief parametric study about the duration of the prediction horizon was performed, which indicated that there is a value adapted to each type of cycle. Figure (5.15) shows the results for a extra-urban drive cycle, where the value of $150\,s$ presented the best performance in terms of hydrogen consumption. However, for different drive cycles it was found other values of $t_h$, indicating that that this subject still needs a better analysis, such as the identification of the drive cycle to adapt the predictive horizon duration.

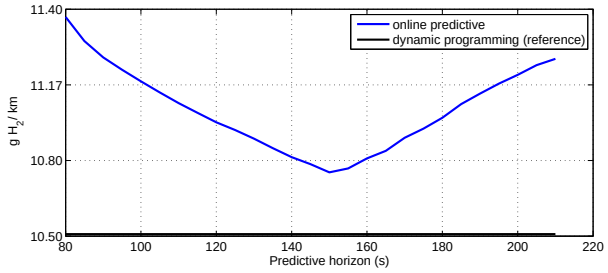


**Figure 5.15:** hydrogen consumption vs prediction horizon

Introducing the PI controller in the $\lambda_1$ calculation, it becomes:

$$\lambda_1 = \frac{2a_1\left(\frac{\left[k_p\left(SoE_{reference}-SoE(t)\right)+k_i\int\left(SoE_{reference}-SoE(t)\right)dt\right].\varepsilon_{max}}{\Delta t}-\sum_{i=t-t_h}^{t-1}P_{vehtot}\left(i\right)\right)}{\left(\frac{t_h}{\Delta t}\right)}+a_2 \tag{5.40}$$

The last variable to be defined in (5.40) is the $SoE_{reference}$. It has a dynamic profile, differently from several authors that adopt the $SoE_{reference}$ fixed in the middle of the $SoE$ operational range. This permits to increase the entire system efficiency, taking advantage of the kinetic and potential energy.

The main idea is related to the fact that when the vehicle has a non zero positive speed, the amount of kinetic energy can be partially recovered during the braking operations. Consequently, in this situation the vehicle can optimize the energy recovering increasing the $SoE$ region by the reduction of the $SoE_{reference}$ value.

The same concept is used for the potential energy. $SoE_{reference}$ reduces when the vehicle passes to a higher altitude, which means that it will have an adapted $SoE$ region to maximize the braking recovering energy, compensating the potential energy barrier to reach the current altitude.

Otherwise, when the vehicle is in a lower altitude level (compared with the reference), the potential energy to get down in the level can be stored in the battery due to the recovering braking. In this case, $SoE_{reference}$ has a higher value when the level is lower than the reference. To return to the reference level, it is necessary to overcome the potential energy barrier, which will be done by the previous energy stored in the battery.

Allied with a fixed reference value ($SoE_0$), the two aforementioned components ($SoE_{kinetic}$ and $SoE_{potential}$) define the $SoE_{reference}$ function (equation 5.41).

$$SoE_{reference} = SoE_0 - SoE_{kinetic} - SoE_{potential} \tag{5.41}$$

The value of $SoE_0$ is given by the stationary desired value ($SoE\left(0\right) = 60\,\%$) and brings the power assistance mode ($SoE\left(0\right) = SoE\left(t_f\right)$) to the $SoE_{reference}$ function . $SoE_{kinetic}$ is obtained from the equation 5.42, where $\eta_{braking\,chain}$ is the efficiency of the vehicle braking chain, $v\left(t\right)$ is the current vehicle speed and $v_{max}$ is maximum speed.

$$\begin{aligned} SoE_{kinetic} &= \left(SoE_{max}-SoE_{min}\right)\eta_{braking\,chain}\frac{Kinectic\,Energy(v(t))}{Kinectic\,Energy(v_{max})} = \\ &= \left(SoE_{max}-SoE_{min}\right).\eta_{braking\,chain}\frac{\left(v(t)\right)^2}{\left(v_{max}\right)^2} \end{aligned} \tag{5.42}$$

$SoE_{potential}$ is calculated in 5.43, where $h\left(t\right)$ is the vehicle current level, $h_{ref}$ is the reference level, $h_{max}$ is the maximum level and $h_{min}$ is the minimum level.

$$SoE_{Potential} = (SoE_{max} - SoE_{min})\,\eta_{braking\,chain}\frac{Potential\,Energy\left(h(t)-h_{ref}\right)}{Potential\,Energy(h_{max}-h_{min})} = \\ = (SoE_{max} - SoE_{min})\,.\eta_{braking\,chain}\frac{\left(h(t)-h_{ref}\right)}{(h_{max}-h_{min})} \tag{5.43}$$

The figure 5.16 presents the entire solution integrated with the physical part. $P^*_{FC}$ is the optimal control applied, obtained from $P_{vehtot} - P^*_{batt}$.

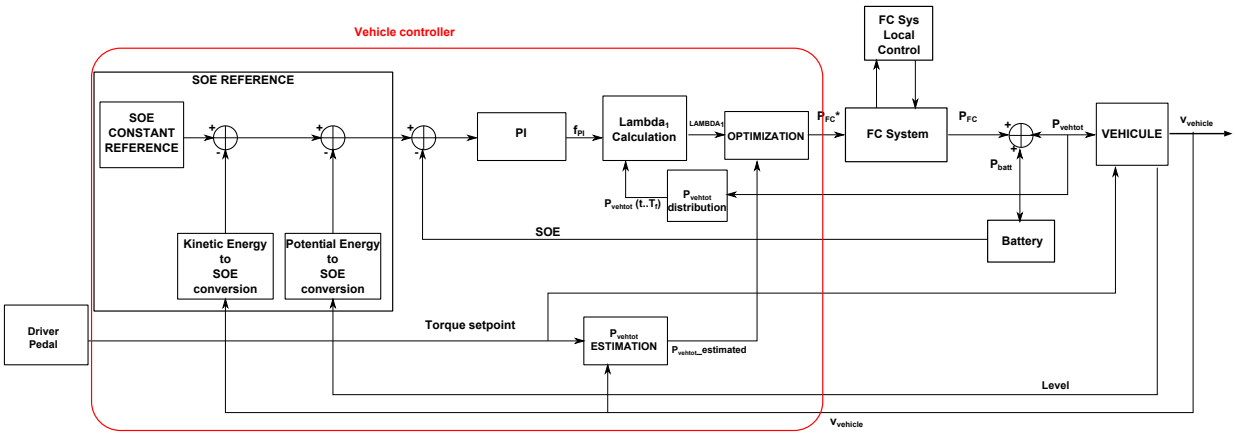


**Figure 5.16**: Optimization control block

Despite the several functionalities integrated around the optimization process, the structure remains flexible to enlarge the domain of the optimization solution through the inclusion of different constraints. Furthermore, due to the analytical characteristic, the final solution calculates a new optimal power value at each time step using a low computational effort and low amount of memory.

The next section present the simulation and experimental results of the the proposed energy management strategy.

## 5.5 Optimization Results

### 5.5.1 Results from the optimization applied in the model

The backward vehicle model is used in this tests, where the urban, extra-urban and highway drive cycles of the appendix A were imposed. The altitude profiles in the cycles are constant and equal to zero.

Results obtained from the predictive optimization method were compared with the Dynamic Programming results in order to verify how close to the global optimization this method is.

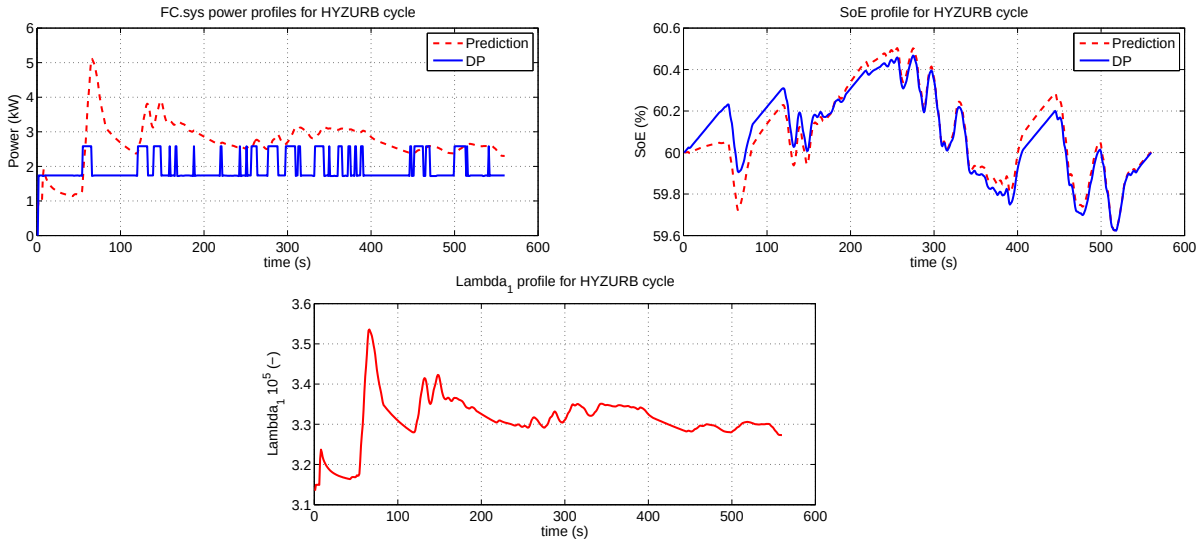


**Figure 5.17:** Urban cycle optimization results

Figure 5.17 presents the results for the urban drive cycle. As can be noticed, the power profiles of fuel cell system for the two optimization methods are different due to the drive cycle prediction made. As expected, this result shows that the on line prediction method gives a sub optimal response when compared with the DP method.

Despite this difference, the hydrogen consumption obtained from the on line prediction method ($16.2\,g_{H_2}/km$) is close to the value of the DP method ($16.1\,g_{H_2}/km$). As the fuel cell system has a large power region with good efficiency, neither the power nor the consumption are the most appropriate variables to evaluate the optimality level of the response. Therefore, the $SoE$ profile was used to verify how close the sub optimality is to the global optimality.

The similarity of the $SoE$ profiles in figure 5.17, shows that the proposed online method has a sub optimality that is close to the DP global optimality, with the advantages of the low time consumption, memory allocation and no need of knowledge of the entire drive cycle (time causality).

Concerning the $\lambda_1$ profile, it adapts its value according to the predicted $SoE$ and the power demanded drive cycle ($P_{vehtot}$), without important losses in terms of optimization.

The same analysis can be extended for the others drive cycles, as can be seen in terms of hydrogen consumption (table 5.1) and profiles of power and $SoE$ (figures 5.18 and 5.19).

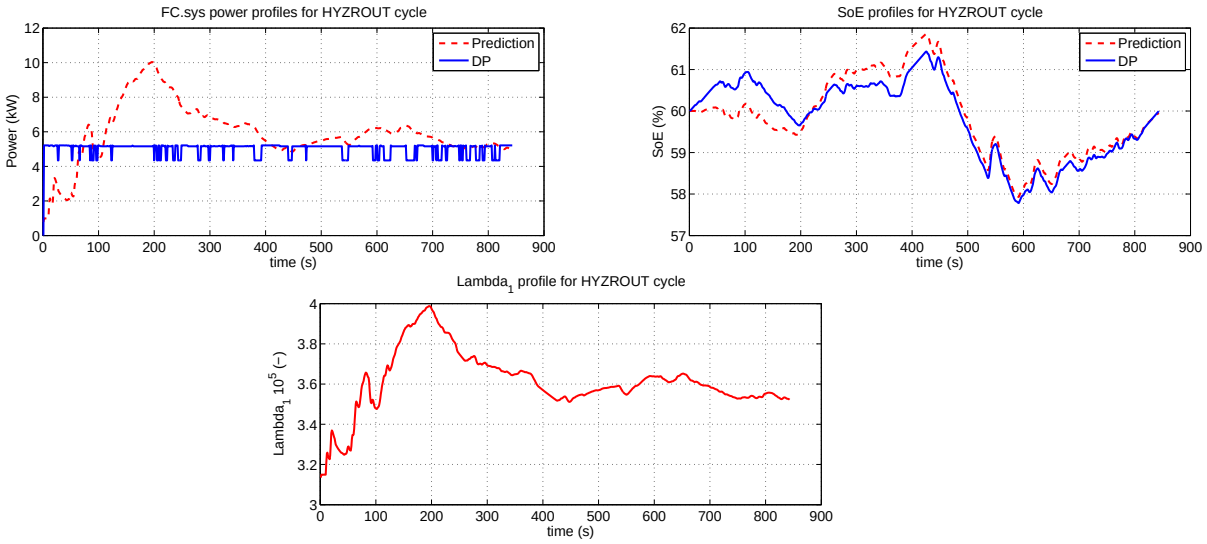


**Figure 5.18:** Extra-urban cycle optimization results

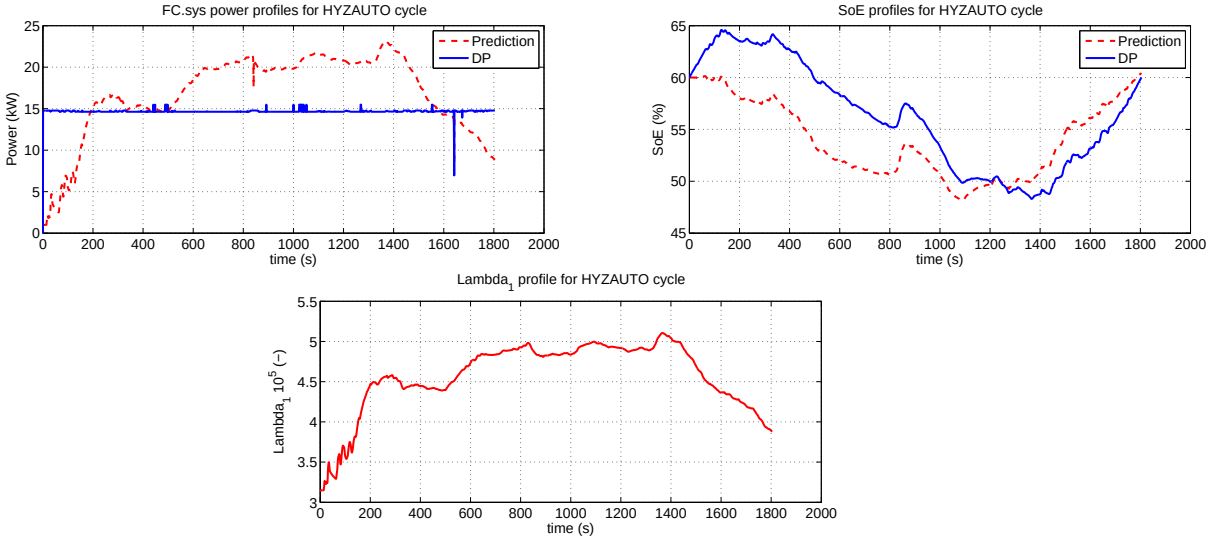


**Figure 5.19:** Highway cycle optimization results

In order to verify the effect of a drive profile including gradation in the optimization process, a real drive cycle with mountain profile was applied to the methods (appendix A). Figure 5.20 presents the grade profile of this cycle.

For this simulation, the limits of $SoE$ were changed to [20 % 80 %] to allow a better convergence for the DP method.

Figure 5.21 presents the profiles of $P_{FC}$, $SoE$ and $\lambda_1$. The information about the grade changes the $SoE_{reference}$ in the proposed algorithm, which leads to a result very close to what is obtained with the DP method. Furthermore, the difference in hydrogen

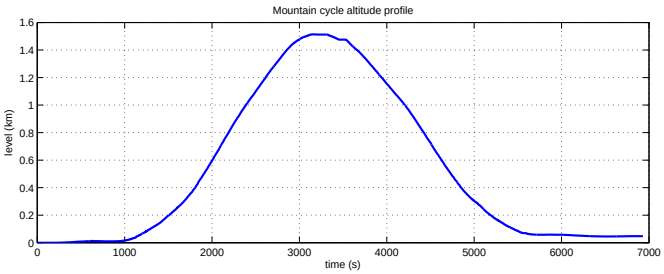


**Figure 5.20**: Mountain cycle level profile

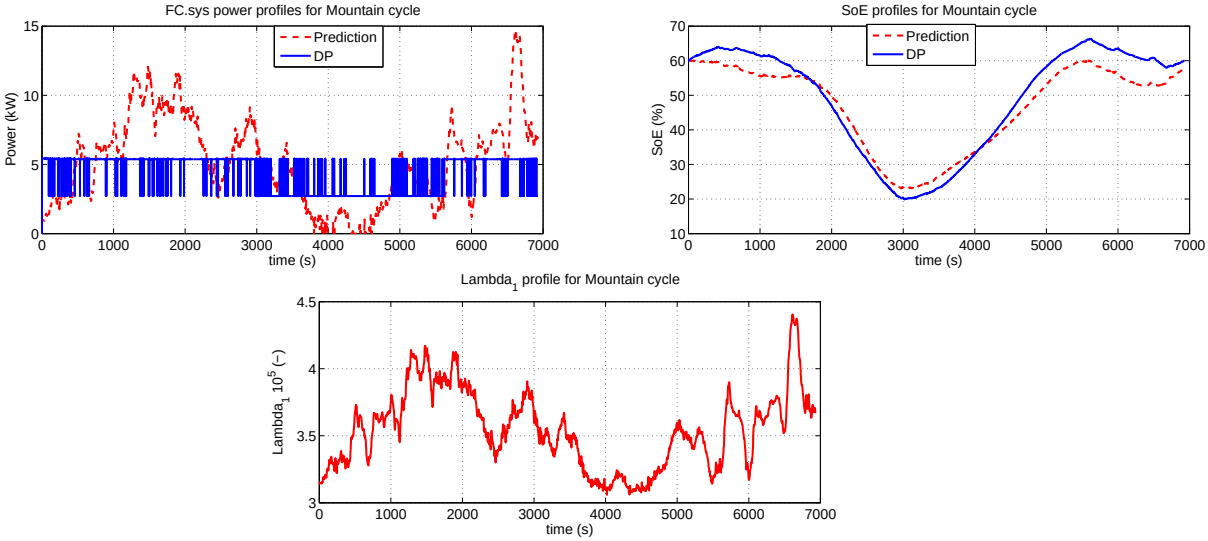


**Figure 5.21**: Mountain cycle optimization results

consumption between the two methods (table 5.1) justifies the use of the online prediction method for real time embedded applications.

| Cycle\Method | Dynamic Programming | On line predicitive |
|---|---|---|
| Urban | 9.7 | 9.8 |
| Extra-Urban | 10.5 | 10.6 |
| Highway | 18.1 | 18.8 |
| Mountain | 8.8 | 9.0 |

**Table 5.1**: Hydrogen consumption in $\frac{g_{H_2}}{km}$

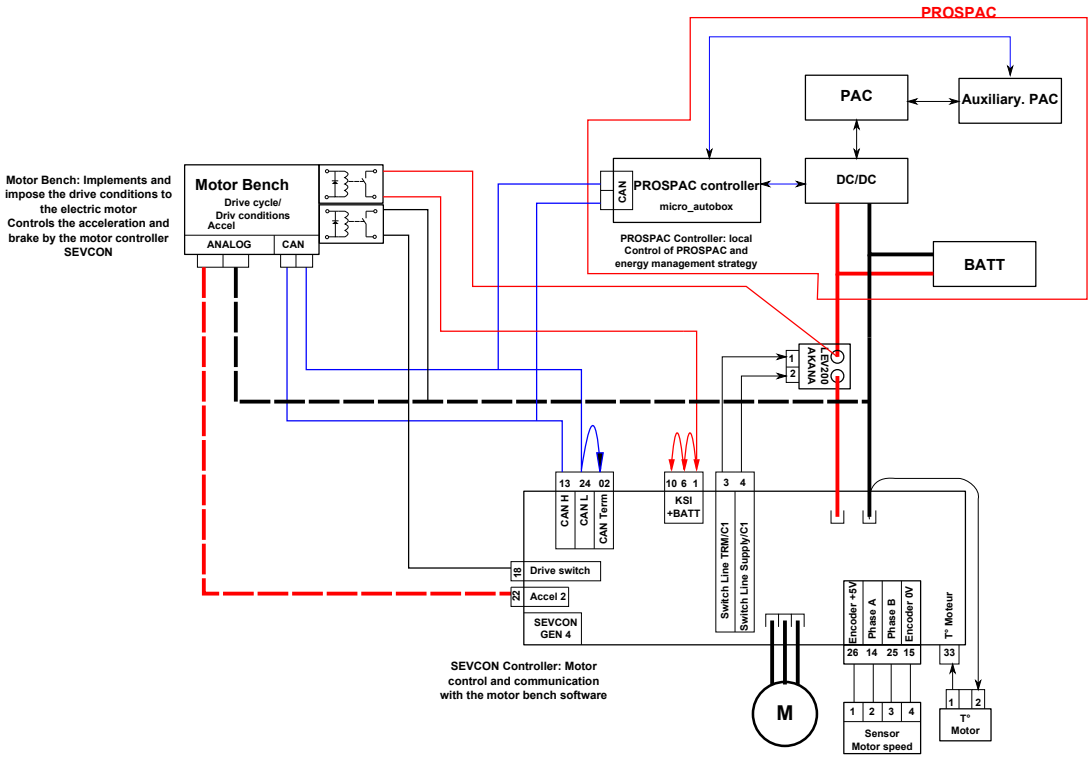


**Figure 5.22**: Experimental test structure

## 5.5.2 Experimental tests of the optimization algorithm

In order to verify the applicability of the energy management strategy proposed, a down-scale FCHEV was implemented using the PROSPAC prototype, a electric motor test bench and an electric motor.

### 5.5.2.1 Experimental structure

The fuel cell system and battery in PROSPAC are responsible to deliver the power demanded by a $8\,kW$ electric motor. The vehicle characteristics and drive conditions are imposed to the motor by the test bench structure. Figure (5.22) illustrates this assembly.

The motor bench controls the motor speed simulating the drive behavior in the vehicle. This control is made by imposing an acceleration setpoint (driver pedal) to the motor controller in order to follow a given speed profile (speed control). Besides, the motor bench also simulates the drive conditions and efforts, which means that in the dynamic equation of the vehicle (2.8), the mass and resistant efforts are simulated by the motor bench using a mechanical charge (electric motor). Therefore, the losses in rolling and aerodynamics are calculated by the motor bench and the related torque is applied against the motor.

In order to adapt the model of the vehicle to the elements present in the test structure, a scale factor of 10 was applied to the mass of the vehicle, its frontal surface $S_{vehicle}$ and air penetration coefficient $C_x$ (table 5.2). This reduces the maximum traction power of the motor to $4.5\,kW$. Despite the symmetric assumption made during simulation tests about the features of motor model ($P_{motor(max)} = -P_{motor(min)}$), in the experimental test campaign, the minimal power of the motor (regenerative power) was limited to $-2\,kW$ to guarantee the maximum recharge of the battery at $-1\,C$, as required in PROSPAC specifications.

| | |
|---|---|
| mass of the vehicle $(kg)$ | 100 |
| $S_{vehicle}.C_x$ | 0.07 |

**Table 5.2:** Vehicle experimental parameters

PROSPAC prototype is responsible to provide the power to the electric motor and auxiliaires. The total power is obtained from the combination of the fuel cell system and battery, where the sharing between them is made by the energy management strategy (EMS) embedded in the PROSPAC controller (DSPACE platform). The EMS controls the power provided by the fuel cell system through the command of the DC/DC converter. Furthermore, the PROSPAC controller regulates and controls the operation of the fuel cell system elements (compressor, valves, etc).

#### 5.5.2.2 Developed tests

In the developed tests, the extra-urban drive cycle is imposed by the motor bench to the motor. The objectives established are to validate the functioning of the proposed strategy and to analyze the potential about the optimization of the hydrogen consumption. Three energy management strategies were applied in this test:

- Dynamic Programming: the implementation was made imposing an optimal FCS power profile obtained by simulation to the real system.
- Predictive online energy management strategy: the same algorithm used for simulation was adapted and applied to the real system, with a time prediction of $150\,s$.
- Rule based strategy: an algorithm created by the PROSPAC designer that aims to keep the $SoE$ controlled close to $50\,\%$. In this method, the informations of $SoE$, demanded power $P_{vehtot}$ and the state conditions of the fuel cell stack (pressures, flows and temperatures) define the power delivered by the fuel cell system $P_{FC}$.

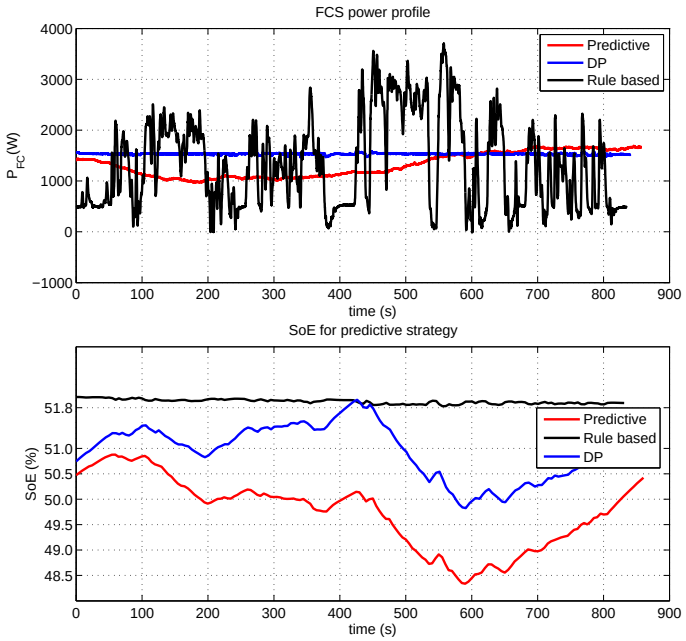


**Figure 5.24:** Fuel cell system power and battery $SoE$ profiles for the EMS strategies

The state conditions operate as security constraints to limit the power delivered by the fuel cell, while $SoE$ and $P_{vehtot}$ determine the power split. The main objective of this method is to perform an energy management where the battery is only responsible for the peak power and high frequencies, being the responsibility of the fuel cell system to deliver the main power and to keep the $SoE$ stable around 50 % (recharge the battery).

Figure (5.23) presents the power profile demanded by the motor and the auxiliaries.

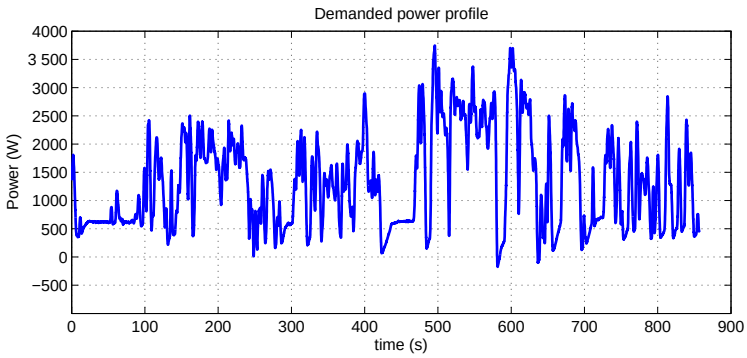


**Figure 5.23:** Demanded Power profile

The fuel cell system power and $SoE$ profiles for the three strategies are presented in figure (5.24).

While the rule base strategy tracks the demanded power, the predictive online method tends to approach the dynamic programming value. The existing difference between the DP and predictive is caused by the choice about the duration of the predictive horizon and its initials values, which requires a certain time to converge towards the best solution.

Figure (5.25) shows the consumptions for the three strategies as function of the $\Delta SoE$. These consumptions were estimated by the current relationship in (2.21), meaning that the losses in the purge procedures were neglected.

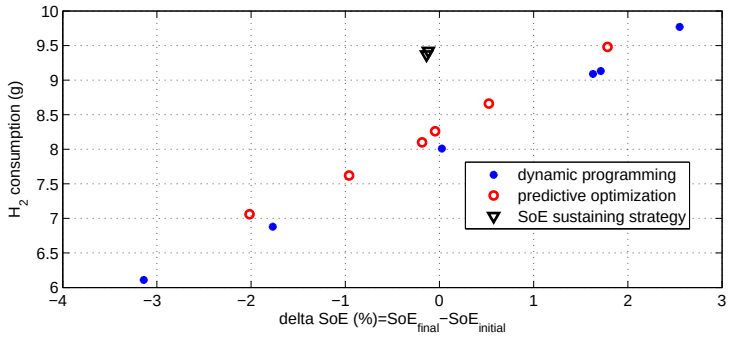


**Figure 5.25:** Hydrogen consumption vs $\Delta SoE$ for the EMS strategies

The results show that the predictive online method presented an optimization performance close to the dynamic programming one, while the rule based strategy with $SoE$ sustaining characteristics shows an overconsumption compared to the other methods. This indicates that, in contrast with the predictive online approach, the $SoE$ sustaining method (Rule Based) does not takes advantage of the braking recovery energy in the $SoE$ control, spending more hydrogen to accomplish the mission.

## 5.6 Conclusions of the chapter

The main objective of this chapter was focused on the synthesis of an online algorithm for the FCHEV energy management. In order to achieve this goal, different subjects were discussed leading to a development chain to compose the final solution.

As this work proposes a solution of the energy management that takes into account the dynamics of the fuel cell system, the first part of the chapter analyses the fuel cell system considering the dynamic effects of the interactions between the several subsystem that compose it.

Using the information of the most harmful effects created from the failure of the interactions and the dynamics of the elements, it is defined the air supply subsystem as the one having the dynamics to represent the fuel cell system dynamics.

To assure optimal operating points for the fuel cell, a non linear control law using the differential flatness theory is applied to the non-linear dynamics of the air supply subsystem. Cathode outlet pressure and oxygen stoichiometry are the considered flat outputs to be controlled, where the control inputs are the air compressor velocity and the pressure valve controls.

The control law is firstly applied to the detailed fuel cell system model, leading to good results in terms of desired trajectory tracking and behavior of the other internal states of the fuel cell stack. Afterwards, the designed flatness control strategy is applied to the real fuel cell system present in PROSPAC prototype. These results are compared with the results of two other classical control methods. Among the three methods, the flatness control strategy presented a better performance than the others with a more stable profile of pressure and stoichiometry. Furthermore, this control strategy allowed the air supply subsystem with its control to be taken as equivalent to a very simple linear model.

Integrated in the optimization problem, the new fuel cell system dynamic represented an additional new dynamic constraint that the optimal solution must respect in the process of the optimal power split definition.

In order to propose an online solution for the new optimization problem, a predictive energy management method is developed based on one hand on the theory of the Pontryaguin's Maximum Principle and on the other hand on the predictive control using a sliding horizon window to find out the power demands of the cycle.

Thanks to the fuel cell control linearization, an analytic solution of the optimal power split can be calculated in real time. Finally, the battery $SoE$ is adjust to maximize the recovery of kinetic and potential energy involved in the braking procedure.

The performance of the algorithm is verified applying different drive cycles and comparing the results to a global optimization method. Dynamic Programming method is used as reference, where the hydrogen consumption and the profiles of the fuel system power and state of energy of the battery are the variables to be compared. The analysis of the results showed that the proposed algorithm is a sub optimal solution that approaches nearly the global optimization, without requiring the prior knowledge of the drive cycle. The applicability and the performance potential of the proposed method were verified by experimental tests. Using a real fuel cell and battery system to power a scaled vehicle and drive train, the results of the online predictive strategy were compared with the dynamic programming and a rule based ($SoE$ sustaining) ones. The advantages of the proposed method obtained in the simulation steps were confirmed in the experimental tests, showing that the method can approach the global optimization results.

The advantages brought from the adoption of this energy management strategy permits to obtain a flexible control structure, which can be adapted to receive new constraints for the optimization problem. Therefore, in the next chapter, the issue of the fuel cell system durability is presented and is included in the optimization problem and in the energy management strategy.

# Chapter 6

# Optimal energy management strategy including fuel cell durability constraint

**Abstract**

In this chapter, the durability of the fuel cell system is considered in order to limit the effect of bad decisions on FC aging due to the energy management strategy. The objective here is to propose an energy management strategy under durability constraint. The irreversible degradation mechanisms are studied emphasizing the dynamic of mechanisms that lead to the reduction of the performance and of the time-of-life of the fuel cell system. A dynamic mode that represent these phenomena and a model is used in the optimization problem as a new constraint. Optimization structure introduces the fuel cell State-of-Health $SoH$ control, compromising as less as possible the other constraints and the hydrogen consumption.

## 6.1 Introduction

The durability aspect of the fuel cell system is one of the main challenges to upscale fuel cell commercialization. In the FCHEV context, the automobile constructers are facing this challenge as a high-priority matter. They apply development efforts in several areas such as materials and systems. Aiming to contribute to this discussion, this chapter intends to include this issue in the energy management strategy.

In order to achieve this objective, is required to first study the concepts and characteristics involved in the fuel cell durability issue. Regarding the time of life definitions and the performance index that indicate it, the first part of the chapter establishes the background needed to understand to the phenomena and operation modes related to the degradation mechanisms. This part is composed by a definition of a fuel cell end of life

performance, the operation modes and mechanisms present in the degradation process, and a state of art of the methods used in the diagnostics of the fuel cell state of health ($SoH$).

Considering the presented background, a simplified degradation model is adopted based on works performed in CEA. The model relates a degradation rate to the power demands and the state conditions imposed to the fuel cell during operation. Additionally, the model supposes to determine the state of health of the fuel cell, which will be important in the optimization process.

As a part of the dynamic representation of the system, this model is integrated as a dynamical constraint in initial the optimization problem and the optimization algorithm presented in the previous chapter is extended to take into account this new constraint. In order to take into account the durability aspect, the optimization criteria is modified and includes the target time of life of the fuel cell (EoL).

The final optimization structure aggregates constraints and cost functions that are related with the hydrogen consumption, battery $SoE$ and fuel cell State of Health ($SoH$).

## 6.2 Important concepts and requirements about durability in a FCHEV

As a promising technology for energy applications, the hydrogen fuel cell has several advantages compared with conventional solutions (ICE, gas, etc). However, it is not yet a mature technology, which makes it not ready to be competitive with the other options. One particular aspect is about the durability of the fuel cell stack. Despite the fast improvements of the materials and systems involved, the fuel cell stacks are still presenting a lifetime that does not reach the assigned targets.

According to the type of application, the durability targets stated by the US Department of Energy (DOE) [92] are different. For stationnary applications it is demanded $40000\,hrs$ of operating hours. For transport applications, the DOE indicates that the fuel cell stack should assure a time of life of $5000\,hrs$ in order to be adapted to the market in 2015.

In this work, we are interested in the targets for the transport application. Even if the recent announcements of the automobile constructors indicates that the durability goal has been reached and the FCHEV is ready to be inserted in the market (depending on the hydrogen structure), the scientific publications only present values that reach the half of the target ($2500\,hrs$). Therefore, our work deals with the durability of the fuel

cell system, and specially the fuel cell stack, as an open and major issue. The durability is a complex subject that must be firstly approached by a definition of the fuel cell end of life ($EoL$) concept.

The $EoL$ of a fuel cell stack is related to its inability to assure basic operations or/and to guarantee a minimal performance. Thus, the end of life of a fuel cell stack can be defined by the observation of a failure or a certain loss in performance.

**Failure** The occurrence of any failure normally imposes a condition to the user that impedes the operation of the fuel cell (for example a membrane failure). In the case of a FCHEV it leads to a need of a complex and unexpected maintenance to bring the system back to its normal operational conditions. This represents the most undesired situation and should be prevented in advance to avoid any harmful effect. In order to detect these events, some fault detection methods have already been developed [129, 57, 101]. Through the observation of the measured variables of the fuel cell, a fault can be predicted and prevented in a certain range of probability.

**Loss in performance** Differently from the failure case, the reversible or irreversible losses in the fuel cell performance lead to a degraded mode that implies overconsumption (efficiency) or reduction of the power capacity. Figure 6.4 [64] shows the effects of the loss in performance with the time in the polarization curve for a fuel cell stack composed by 5 cells. As can be noticed, the aging effect causes degradation in the performance of the cell, which means that a old stack needs a higher amount of hydrogen than a new stack, in order to provide the same power. Despite the undesirable behavior of the FCHEV, the loss in performance does not stop the basic operational capability of the system.

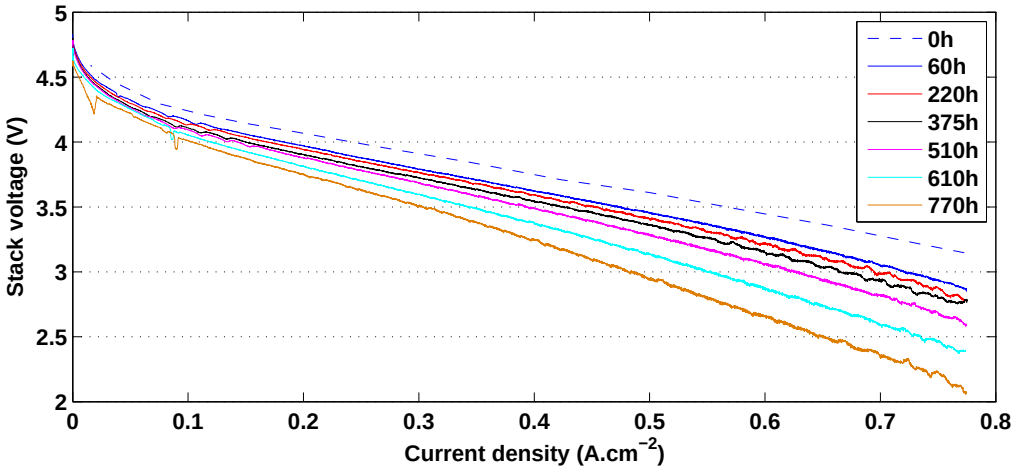


**Figure 6.1**: Polarization curves for a fuel cell stack (5 cells) in different life times [64]

The loss in performance is adopted in this work to evaluate the durability of the fuel cell. However, it must be defined how to evaluate the performance (performance index) and its minimal acceptable limit at which some specifications of the vehicle, including the technical ones are still guaranteed.

Some performance indexes are defined to indicate the end of life of a fuel cell stack. In the FCHEV particular case, Pei et al. [95] used the information of the cell voltage to analyze the end of life of a stack for a bus application. Their proposition outlines that a fuel cell stack is considered at its *EoL* when its rated power capacity is decreased leading to reduction of 10 % in the cell voltage (fig. 6.2). Such situation represents that the fuel cell stack can not guarantee the traction functions of the vehicle (electric power). Such analysis allows to include the losses of fuel cell efficiency, which causes an increase of hydrogen consumption to perform the same task (same power delivered). Furthermore, the loss in voltage is related also to the reduction of the maximum power of the stack and consequently to the ability to accomplish some technical requirements of the vehicle.

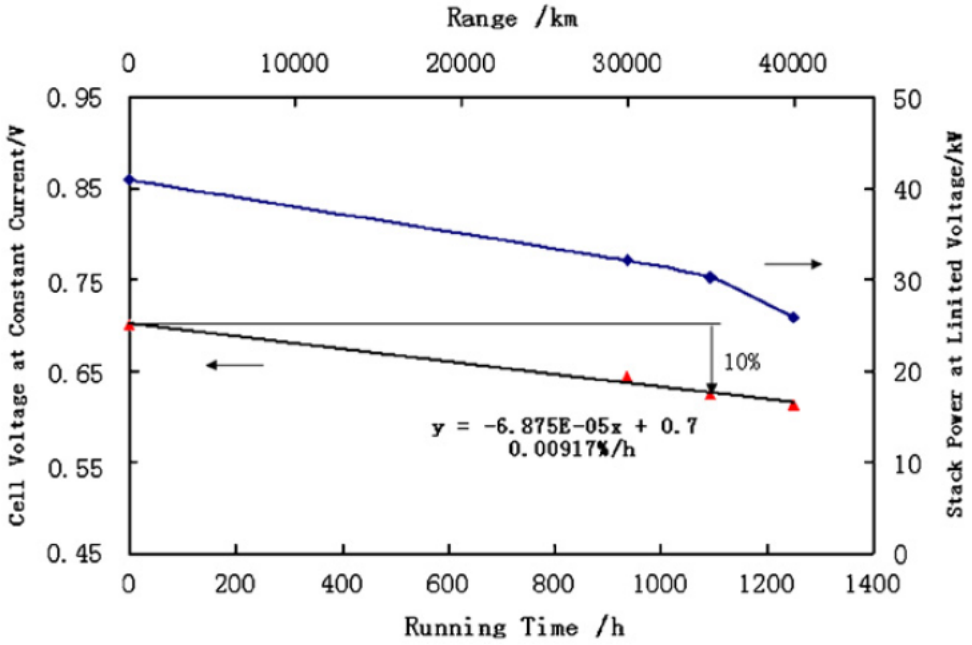


**Figure 6.2:** Durability index [95]

In the study of Pei et al. [95], the causes for these losses in performance are due to the operational conditions imposed to the stack. A vehicle application demands operation modes that can induce degradation phenomena in the fuel cell stack characteristics and response. In the sequence, the FC degradation is tackled by the presentation of the most degrading operation modes and the degradation mechanisms triggered during each mode.

Moreover, the diagnostic methods used to observe the FC degradation are outlined by a brief state of the art.

## 6.3 Degradation of FC in a FCHEV: Operation modes, degradation mechanisms and diagnostic methods

The typical operation modes of a vehicle present a combination of power profile that combine dynamical, stationary, low power and high power features. Maximum speed, acceleration and start/stop conditions are examples of the technical requirements imposed by the vehicle to the powertrain. Such requirements reach also the fuel cell system, leading it to be subjected to conditions that can cause reversible or irreversible degradation effects.

### 6.3.1 Vehicle operating modes and their degradation mechanisms

At the time, the operational modes considered as the most important in the FC aging context are:

**Cold start** A start up from subzero temperatures is a procedure that the fuel cells embedded in vehicles are submitted. However, when the fuel cell is operated at subfreezing temperatures, the water generated at the cathode will tend to form ice that can result in a loss in performance of the fuel cell.

According to Yang et al. 130, this operation affects the durability of the Membrane Electrode Membrane (MEA) by the occurrence of degradation mechanisms. Yang et al. 130 stated that the cold start has found three principal degradation mechanisms:

- Interfacial delamination between the cathode catalyst layer and membrane,
- Cathode catalyst layer pore collapse and densification
- Pt area loss due to particle ripening and dissolution in PFSA ionomer.

The ice formation in the cathode generates these mechanisms that lead to a reduction in the electrochemical surface area in addition to the membrane resistance increasing [25]. As a side effect, it is obtained a worse quality reaction (less electrochemical surface) and more losses in the membrane.

**Start/Stop** Being subjected to ordinary drive conditions, a vehicle must have the possibility to perform start/stop procedures very often. In this operation, it is demanded a dynamic power profile and consequently a dynamic flow of fuel. This induces a transient condition in which the distribution of the fuel in the cell is not homogeneous and the proportion of $H_2/air$ drives a reverse current in some parts of the cell [25]. Moreover, this can cause a carbon corrosion on the supports of the electrodes and the collapse of the Pt catalyst layer [111]. Another problem created by this operation mode is about the dissolution of platinum in the membrane [38]. As a result, starting and stopping the fuel cell can induce considerable losses in its performance due to the reduction of the catalyst layer.

**Idling** The idling condition present in the vehicle operation requires that the fuel cell stack operates at its high potential and no current. It can induce performance loss caused in part by a loss of electrochemically active surface area [36]. In this loss of surface area, the platinum dissolution plays a major role, especially of the cathode catalyst, where high potentials are encountered [123, 132]. The dissolved platinum can be clustered with other platinum particles (forming larger particle) or diffuse in inaccessible parts of the MEA. Furthermore, according to [125] the OCV (Open Circuit Voltage) condition present in this mode promotes the occurrence of peroxide ($HO^{\bullet}$) and hydroperoxide ($HOO^{\bullet}$) radicals, which are considered to be responsible for chemical attack on the membrane and catalyst [27], affecting the performance and damaging the cell.

**Load changing** Load changing operation or load cycling operation is a mode that is often present in the vehicles due the dynamic drive profiles usually required by the drivers. This dynamics in the load profile affects the performance of the fuel cells by the modification in the catalyst layer. Platinum sintering and dissolution are the degrading mechanisms triggered by this operation mode. The reduction in the catalyst surface compromises the electrochemical reaction and then the performance of the cell. The possible occurrence of reverse current can also generate carbon support corrosion, which acts in the reduction of the catalyst layer by the dissolution of the platinum.

**High power load** A technical specification of maximum speed requires to the vehicle to maintain a rated traction power which is provided by the powertrain elements. Depending on the power split strategy adopted, it may be required from the fuel cell system to provide its maximum power for a long duration. Such behavior causes an increase of the heat flow created by the fuel cell stack and a humidity that depends on the balance

of production of water related to the power delivered and the dryness caused by the high temperature. These aspects are linked to the degradation effects associated to the performance of the cells. A high temperature and a possible low humidity can change the membrane resistivity. Besides, the temperature can also impact on others parts of the cell, such as the GDL [25]. The GDL degradation acts on the water diffusion, influencing related degradation mechanisms and leading to losses in performance.

Even if degradations are unavoidable, the degradation rate can be limited with a specific design of the components and using mitigating strategies. Concerning the mitigating strategies, several authors proposed different strategies for each degradation mechanisms, but without considering the drawbacks brought by the vehicular applications. The embedded characteristic imposes strong constraints to implement the proposed strategies. For example, Borup et al. 25 indicated that to avoid the increase of loss of GDL hydrophobicity it would be better to use sparging nitrogen instead of air during shut-down procedures, but the space and application automobile constraint avoids the inclusion of a nitrogen vessel in the vehicle.

Consequently, other works considered different approaches to deal with the limitation of the degradation rate, our work also intends to contribute to this subject. Nevertheless, the control of the degradation needs the knowledge of the degradation state of the fuel cell stack. Thus, a diagnostic method should be used to observe and apply the control strategies to minimize the degradation. In the sequence this subject is presented in a brief state of art.

### 6.3.2 Diagnostic methods for the fuel cell stack durability

All the aforementioned vehicle operating modes are responsible by a degradation contribution in the decay of the fuel cell time of life. Pei et al. 95 determined experimentally each contribution, allowing to observe the evolution of the degradation of the stack in realtime. However, such approach needs an important number of experimental tests in a long duration in a real FCHEV to characterize these durability decay rate. The structure necessary to perform these test campaigns is out of the scope of our work. Therefore, in this work, the State of Health $SoH$ of a fuel cell stack is measured by the observation of variables and intrinsic phenomena, such as the active surface value (catalyst layer), membrane resistivity, etc.

The phenomena related to each degradation mechanism cannot be observed separately, they present strong interactions that are difficult to isolate them. Moreover, as a multi-physic, multi-scale and multi-variable complex system, the fuel cell system remains a real challenge in terms of diagnostics. The definition of the State of Health ($SoH$) of

the fuel cell is dependent on the knowledge of inner variables which are not available for measurements, especially in mobile applications. Different diagnostics and observation methods for this purpose have been proposed in the literature. In the sequence an overview of the methods is presented.

The challenge to rebuild the non observed inner states is faced by the researchers using several approaches that sometimes combine signal processing theory, measurements, dynamic modeling and artificial intelligence.

Kim et al. [78] studied the durability of the fuel cell using a pattern recognition approach. Based on the measurement of the fuel cell voltage, the authors applied a behavior model-based method that uses the Hamming neural network [87]. This is intended to indentify a fuel cell output voltage among the known profiles that reflect the time of life of a typical fuel cell. The information used to verify the degradation state of the cell is its composed resistance (activation and concentration). The estimated value is compared to the new and aged fuel cell values in order to define its state of health. Despite the facility of implementation of this approach, it method needs an important amount of good quality data, which sometimes can not be assured.

Using an approach that applies the signal processing theory, Bethoux et al. [22] proposed to estimate the fuel cell impedance by the measurements of the voltage and current at different frequencies. Therefore, an AC signal is added to the main input signal (current), which includes a frequency component to the output signal. Using the Fresnel framework, the amplitude and the phase of the impedance are obtained; This allows the parameters values of the fuel cell equivalent electric model to be calculated. The state of health of the fuel cell is evaluated according to the equivalent resistance of the cell. To be embedded in a realtime system, the calculations required by this procedure should be performed with a dynamics of the degradation control, which can require an important calculation capacity. Besides, this method needs add a high frequency signal to the main current demand, which is not simple for a final application, such as a FCHEV.

Kurtz et al. [81] considered the specific problem of the diagnostic of the water management in the fuel cell. Due to the inability to identify the related phenomena from the polarization curve, their approach used the impedance of the fuel cell. Electrochemical Impedance Spectroscopy (EIS) was the tool adopted to measure this variable and allowed to distinguish the membrane conductivity, kinetics and mass transport limitations. Through the EIS results, the authors can detect in advance possible faults in terms of water management. As can be noticed, this method needs a structure that is difficult to apply for embedded application and is mainly used to fault detection.

Lee et al. [72] dealt with the durability subject by a lifespan approach. They proposed

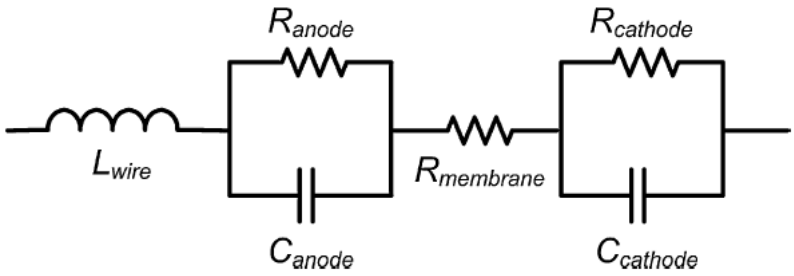


**Figure 6.3:** Fuel cell equivalent circuit [72]

a method that uses the EIS to fit the values of the parameters presented in a equivalent model. This model is composed by inductances, resistances and capacities that represent the characteristics of the elements in the cell (figure 6.3). Such approach focus on the effect of performance drop due to the cathode catalyst loss, which means that the changes in the resistance and capacity of the cathode indicate the state of health of the cell. As most of diagnostic methods, this one also needs equipments that limit the implementation for online embedded applications.

As noticed by the presented methods, they are oriented to identify one type of phenomena (humidity, catalyst loss, membrane resistivity), considering that the other ones are not affecting the diagnostic. Another major inconvenient is about the lack in knowledge of the interactions between the input variables (current, voltage, pressures, temperature, humidity, etc) and the degradation index, which is composed by several effects. This avoids to create a model that could be inverted to discover the effect of each state variable in the degradation result.

The research in this area continues and tends to converge towards methods adapted to the requirements and constraints of the FCHEV applications; however, the diagnostic method is an open problem so far.

This work do not have the objective to propose a method, but the importance of the diagnostic to achieve the stated objective (optimal energy management including durability constraint) leads to consider the $SoH$ as an available information, independently of the applied diagnostic method.

In order to develop an energy management strategy that includes the fuel cell durability, the $SoH$ information is not the only durability information required. The durability aspect is included in our optimization process as a new dynamic constraint as well. Therefore, a model that represents the fuel cell stack degradation dynamics is necessary. In this work, such model (degradation dynamics) is obtained based on the results of the work made by [102]. Next section presents the approach used to define the degrada-

tion dynamic of the fuel cell stack, followed by the optimization problem including such dynamic as a constraint.

## 6.4 Fuel cell stack degradation dynamic model and optimization problem for EMS application

### 6.4.1 Degradation dynamic model

Several models designed for study the degradation of PEMFC are available in the litterature. Out of all, the ones adopting phenomenological approach present the advantage to mainly use physical aspects in the construction of the model. This simplifies the understanding of the results, but they normally need a powerful calculation platform to solve the model. For the aimed application, the degradation model should be related to the loss in fuel cell performance and be easily calculated to be implemented in the energy management algorithm. Thus, this calculation requirement avoids the use of complex models.

The approach chosen in this work designs the degradation dynamics of a fuel cell stack according to the results of models simulations. The degradation mechanisms of the fuel cell (loss in active surface, carbon corrosion, etc.) are observed when harmful conditions are imposed to the model (power cycling, high power, etc). Besides, degradation result highlights its influence on the performance instead of the failure.

Robin et al. [102] performed a study about the degradation of fuel cell submitted to automotive conditions and requirements, which is well adapted to meet our stated objective. Their approach was based on the use of models developed in CEA (Commissariat à l'Energie Atomique) that delivers either informations about the FC performance and element's degradation levels. The required interactions between the system and the fuel cell are achieved combining two different models [102].

Due to the difference in the models, an indirect coupling procedure is used (more information can be found in [102]). This needs some additional assumptions in order to make compatible the two models:

- Ideal response of the auxiliary of the fuel cell system
- Open Circuit Voltage (OCV) is not considered in the possible operation modes
- Start/Stop cycles are not considered
- Carbon corrosion is neglected

- Membrane degradation is neglected

- Otswald ripening is neglected

This set of assumptions leads to adopt the cathode Pt surface degradation as the mechanism to be observed and to be considered as the one representing the aging of the fuel cell. Pt surface has an influence on the cell performance, where a new cell (high surface) presents a better performance than a aged one (low surface). Figure 6.4 and 6.5 illustrates these relationships in terms of voltage and power response.

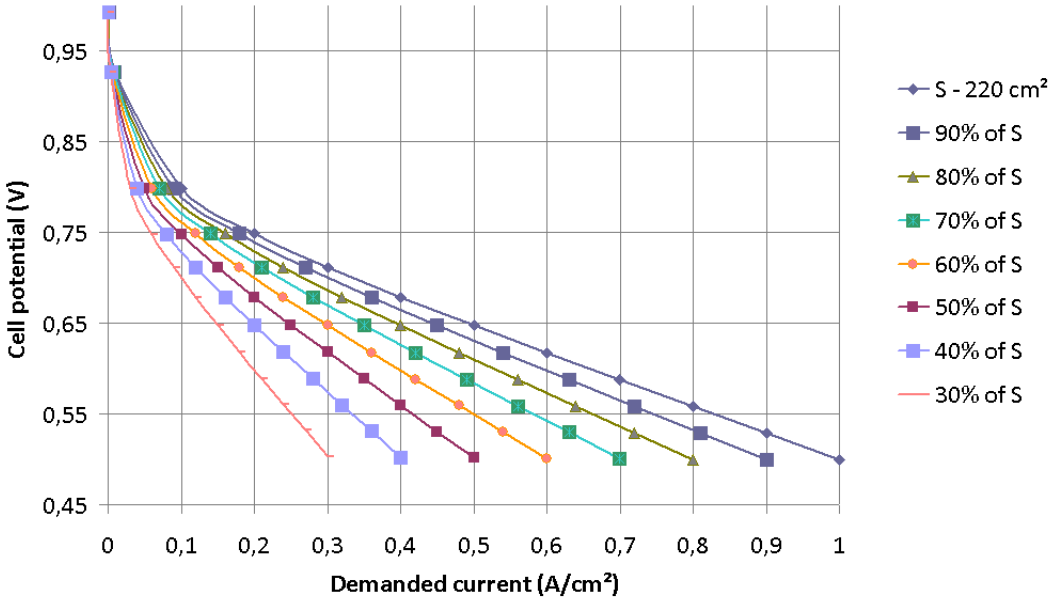


**Figure 6.4:** Polarization curves for different active surface values [102]

The figure 6.6 presents the results obtained from the coupling approach. The results represent were obtained imposing stationary values for each variable (current, temperature, pressure, relative humidity, $O_2$stoichimetry and $H_2$ stoichiometry) until the $EoL$ of the fuel stack. Lifetime reference is related to a considered operating condition. As the models were not validated experimentally, the results only indicate trends of the behaviors.

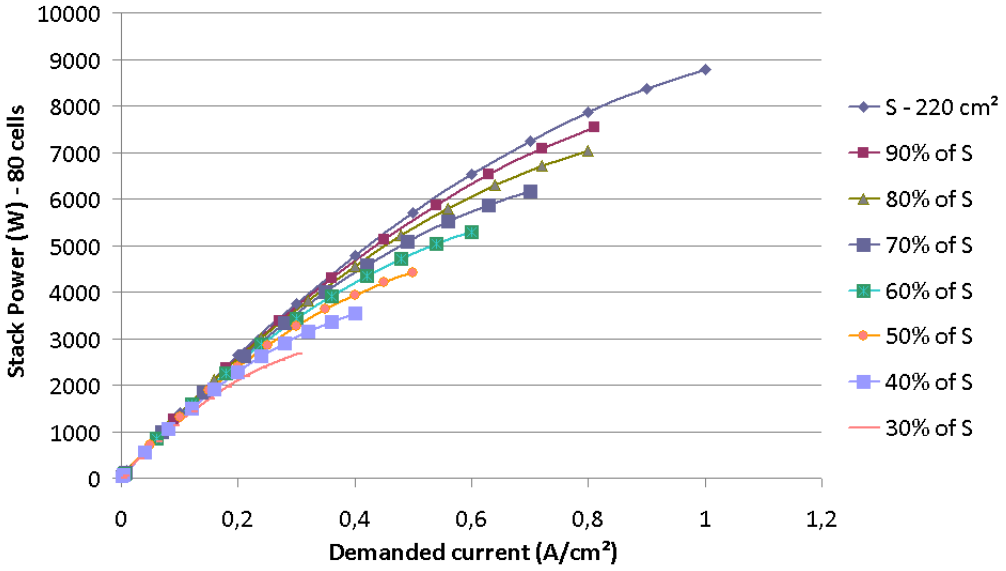


**Figure 6.5**: Fuel cell stack power response for different active surface values [102]

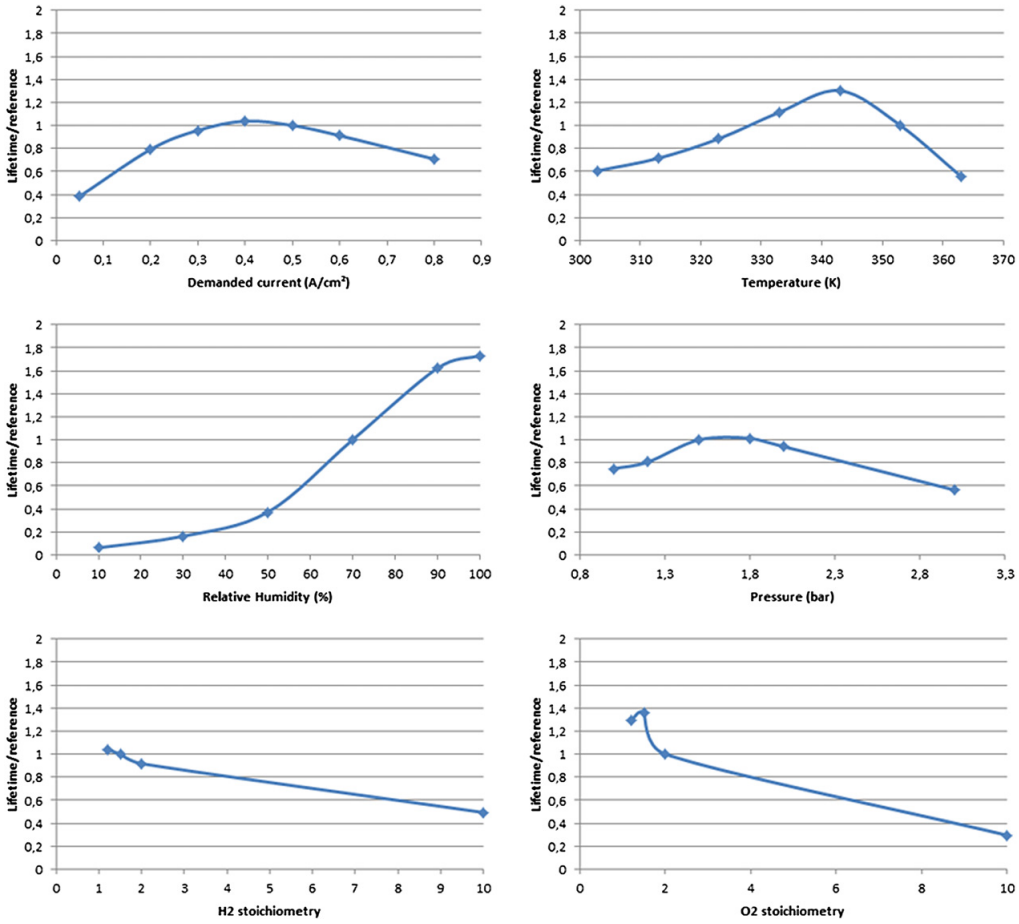


**Figure 6.6**: Lifetime results [102]

Figure 6.6 shows the existence of an value for each variable that results in the maximum of the time of life. A temperature regulated at 70 °C, a pressure of 1.7 $bar$

The temperature optimal value at 343 $K$ indicates that the reactions are favored by a high temperature, but the values higher than the optimal tends to disturbs the water distribution in the fuel cell core and dries the membrane.

It is known that a low current makes the fuel cell to operate close to the OCV triggering undesired degradation effects in the catalyst layer, while high current values is stressing the fuel cell components.

The relative humidity shows a profile where the increasing of its value is followed by an improvement of the lifetime. As the only degradation mechanism taken into account is the cathode Pt surface degradation, the high $H_r$ values (100 %) other degradation mechanisms (e.g. carbon corrosion) do not create degradation effects as they usually do.

Concerning the pressure, the optimum values are located between 1.5 and 1.8 $bar$. According to the author, a low pressure tends to compromise the reaction kinectics, while a high pressure interfere the distribution of reactant gas flows in the cell, reducing the lifetime.

$O_2$ stoichiometry profile illustrates an optimum at 1.5, which is justified by the fact that a low stoichiometry is insufficient to satisfy the reaction rate, while high stoichiometry increases the cathodic pressure and decreases the relative humidity, reducing the fuel cell lifetime

Differently from the other variables, $H_2$ has no influence on the fuel cell durability (considering only the Pt surface degradation). This result is explained by the fact that the anodic conditions were neglected.

Except for the $H_2$ stoichiometry, the regulation of the state variables at their best operation values can minimize the degradation rate of the fuel cell stack. This regulation can be obtained by an implementation of a control strategy at a fuel cell system level. In this work, the degradation dynamics of the fuel cell is obtained considering that the state variables are regulated at their reference values. Nevertheless, as the objective is to define a optimal power split that considers the durability in the strategy, the current is a control variable and is not regulated at its reference value. The definition of its value is given by the energy management strategy.

Despite the lack of precision, the results give good indications to build the degradation dynamic model. This enables, the relationship to be constructed between the active surface degradation rate and the current delivered is the basis to construct the degradation model. As the control variable in the energy management strategy is the power delivered by the fuel cell system, the surface degradation rate vs. current is transformed

in order to implement the power as the control variable. Using the same data of 6.6, it is constructed a relationship between the active surface degradation rate and the power delivered by the fuel cell system. Figure 6.7 shows the degradation dynamics which was defined (equation 6.1).

This curve reflects the current behavior in terms of degradation mechanisms, where a low power tends to submit the fuel cell stack to a OCV condition (undesired in terms of degradation of Pt surface), while a high power stress the fuel cell components. For a fuel cell stack of 90 cells, a minimum of degradation rate is obtained at $5.5\,kW$ and the profile can be approximated by a quadratic function as in the equation 6.1.

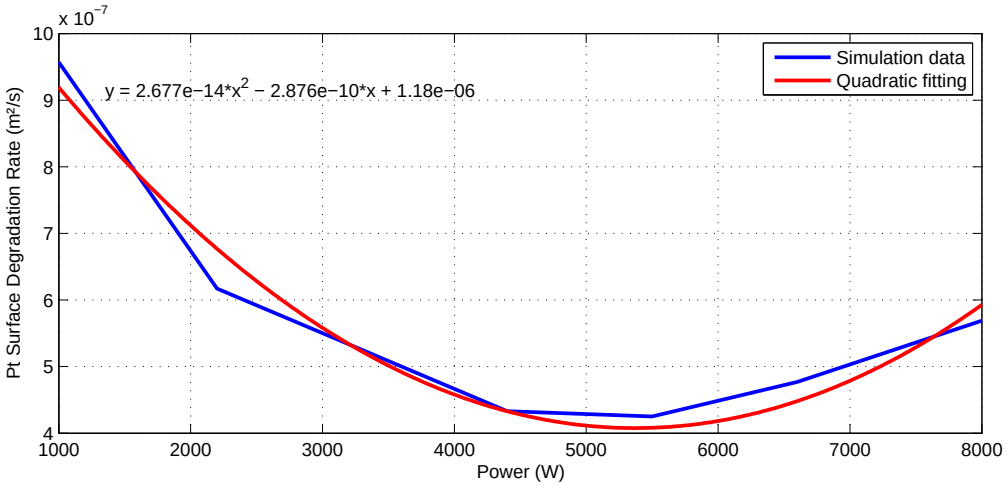


**Figure 6.7**: Active Surface degradation rate x FCS power delivered

$$\frac{dS}{dt} = f_2\left(P_{FC}\right) = b_1 P_{FC}^2 + b_2 P_{FC} + b_3 \tag{6.1}$$

In (6.1), $S$ is the current value of the equivalent active surface area. This equivalent surface area considers that the specific cathode Pt surface is equivalent to the active cell surface. $P_{FC}$ is power delivered and the parameters $b_i$ are obtained by a quadratic fitting of the result in figure 6.7.

Active surface dynamics in (6.1) not only allows to include it in the optimization problem, but also leads to the definition of the fuel cell State of Health $SoH$. Then equation 6.2 defines the $SoH$ indicator, where $S_{tot}$ $(220\,cm^2)$ is the initial value of the surface.

$$SoH\,(\%) = 100.\frac{S}{S_{tot}} \tag{6.2}$$

Both equation 6.1 and 6.2 must be integrated in the optimization problem to establish new constraints concerning the fuel cell system durability.

### 6.4.2 Optimization problem with durability constraint

Due to the durability constraints of (6.1), the new optimization problem (6.3) enables a solution of optimal power split to be calculated, that takes into account the durability constraints.

$$
\begin{cases}
Cost\,Minimization: \\
J\left(P_{FC}^{*}\right) = min_{P_{FC}^{*}} \int_{0}^{t_f} g\left(P_{FC}\left(t\right)\right).dt \qquad where\, g(P_{FC}) = a_1 P_{FC}^{2}\left(t\right) + a_2 P_{FC}\left(t\right) + a_3 \\
P_{FC}^{*} = argmin J\left(P_{FC}\left(t\right)\right) \\
\hline
Constraints: \\
P_{batt\,min}\left(-3\,C\right) \leq P_{batt} \leq P_{batt\,max}\left(10\,C\right) \\
P_{FC\,min} \leq P_{FC} \leq P_{FC\,max} \\
SoE_{min}\left(40\,\%\right) \leq SoE \leq SoE_{max}\left(80\,\%\right) \\
Boundary\,condition: \\
SoE\left(0\right) = 60\,\% = SoE\left(t_f\right) \\
SoH \geq SoH_{min} \quad for\, t \leq t_{EoL}
\end{cases}
\tag{6.3}
$$

$$\begin{cases} \dot{\varepsilon} = f_1(P_{batt}) = -P_{batt} \\ \dot{\omega} = f_2(W_1) = W_1 \\ \dot{p}_{cath} = f_3(W_2) = W_2 \\ \dot{S} = f_4(P_{FC}) = b_1 P_{FC}^2 + b_2 P_{FC} + b_3 \end{cases} \tag{6.4}$$

The $SoH$ boundary condition in (6.3) requires the definition of its minimal value $SoH_{min}$, which defines the end of life of the fuel cell stack. This minimal value is related to the performance index presented in section 2. Furthermore, the same boundary condition do not only indicate the limit value but also the time scale when it could happens $t_{EoL}$ (end of life). Such characteristic requires a solution able to deal with different time references at the same problem. This means, the presence of an instantaneous reference related to the hydrogen consumption ($g(P_{FC}(t))$), a cycle duration related to the $SoE$ boundary condition and the lifetime duration associated to the $SoH$ boundary condition.

In the sequence is defined the limits of the new constraints ($S$ and $SoH$), either at the $EoL$ ($SoH$ value at $EoL$) and during the fuel cell stack lifetime ($SoH$ limit profile).

### 6.4.3 $SoH$ limits for the optimization problem

In section 2 the performance limit were defined in terms of end of life of a fuel cell system as a loss of 10 % in voltage at a rated power delivered. Because the variable that represents the degradation is the active surface area, the $EoL$ index should be translated in terms of $S$.

Previous sections explained that the reduction in the active surface is always followed by a reduction in the performance. Consequently, it is possible to determine the value of active surface area that gives a loss of 10 % in the voltage for a FC system rated power ($5\,kW$).

The procedure to define this surface imposes a rated power and different values of $S$ for the fuel cell stack in fuel cell system model of the chapter 3. Therefore, the cell voltage value is observed for different surface values when the stack delivers the rated power. When the voltage presents a reduction in 10 % compared with the value of a

new stack (initial active surface value), the related surface value is chosen to define the minimal limit. Figure (6.8) illustrates the process.

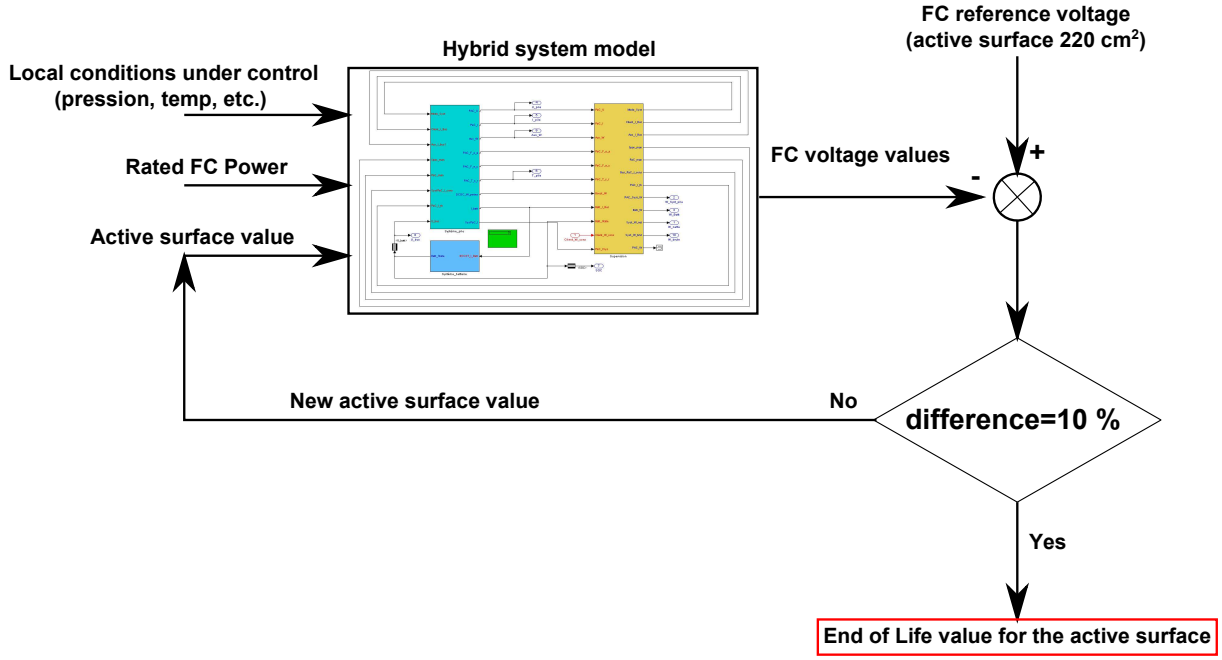


**Figure 6.8:** Method used to obtain the limit active surface area value

The set of voltage results indicates that for a loss about 20 % of active surface area, the cell presents a voltage value 10 % smaller than the value for a total surface area ($220\,cm^2$). Therefore, when the value of the active surface area reaches 80 % of its initial value, we can consider that the fuel cell stack achieved the end of life.

Such value of limitation is adopted by Robin et al. [102] as well. Their choice is justified by the fuel cell stack capacity to deliver enough power to meet the transport requirements and specifications.

Using the degradation dynamics (6.1), the lower boundary of the fuel cell $SoH$ and equivalent active surface ($176\,cm^2$ for an initial value of $220\,cm^2$) give the durability condition of the fuel cell system that will be integrated in the optimization problem.

In order to be adapted to the automobile targets, our work considers that the $SoH_{min}$ is reached at the desired lifetime assigned by the DOE [92], which means that $SoH \geq 80\,\% \quad for\, t \leq 5000\,hrs$. However, this condition do not provide information about the limit profile of $SoH$ before the $EoL$. This allows the power split strategy to degradate the fuel cell stack since the beginning of life and reach the $SoH_{min}$ before the $EoL$, which can not be sustained due to the existence of a minimum degradation rate, no matter the power value chosen. To avoid this situation, it is proposed the definition of a $SoH$

limit profile that determines a $SoH$ boundary to be avoided by the energy management strategy. $SoH_{limit}$ profile evolutes in the time and reaches its end of life value (80 %) when the fuel cell stack accomplishes a desired lifetime of 5000 $hrs$. This is a limit for the $SoH$ that separates the allowed area over it from the avoidable area under it. The profile proposed is supposed by default linear, which does not means that it could not have another shape. Figure 6.9 illustrates the proposed profile.

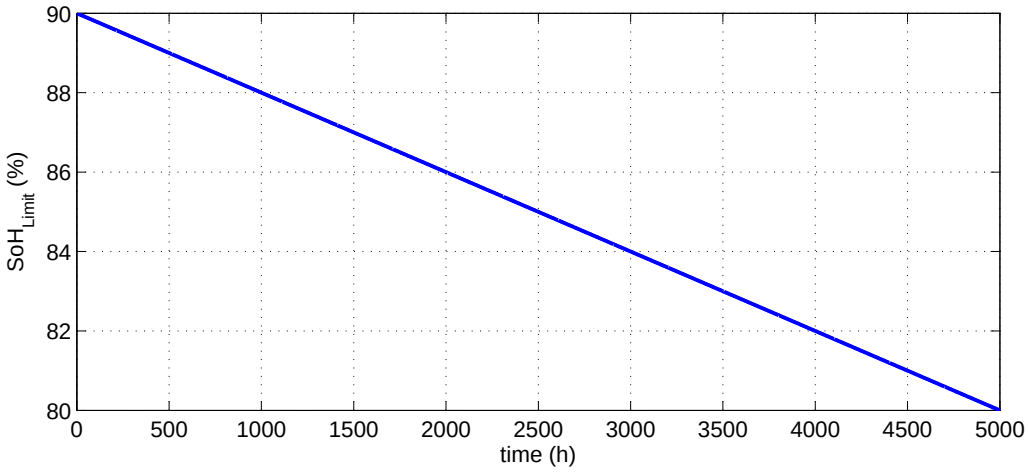


**Figure 6.9:** $SoH_{limit}$ proposed profile

In the next section this profile is used by an optimal energy management strategy to solve the optimization problem stated.

## 6.5 Optimal energy management strategy with durability constraints

As introduced in the previous chapter, the optimization problem is solved using the Pontryaguin's Maximum Principle (PMP) [39]. Using the Hamiltonian function (6.5) that includes the degradation dynamics, the optimal power split can be calculated applying again the three conditions (6.6).

$$\mathcal{H}\left(\varepsilon,\omega,p_{cath},P_{batt},W_1,W_2,\lambda_1,\lambda_2,\lambda_3,\lambda_4\right)=$$

$$g\left(P_{vehtot}-P_{batt}\right)+\lambda_1 f_1\left(P_{batt}\right)+\lambda_2 f_2\left(W_1\right)+\lambda_3 f_3\left(W_2\right)+\lambda_4 f_4\left(P_{FC}\right)=$$

$$=\left(a_1+\lambda_4 b_1\right)\left(P_{vehtot}-P_{batt}\right)^2+\left(a_2+\lambda_4 b_2\right)\left(P_{vehtot}-P_{batt}\right)+\cdots \tag{6.5}$$

$$\cdots\left(a_3+\lambda_4 b_3\right)-\lambda_1 P_{batt}+\lambda_2 W_1+\lambda_3 W_2$$

$$\begin{cases}\dot{\varepsilon}=\frac{\partial\mathcal{H}}{\partial\lambda_1};\ \dot{\omega}=\frac{\partial\mathcal{H}}{\partial\lambda_2};\ \dot{p}_{cath}=\frac{\partial\mathcal{H}}{\partial\lambda_3};\ \dot{S}=\frac{\partial\mathcal{H}}{\partial\lambda_4}\\ -\dot{\lambda}_1=\frac{\partial\mathcal{H}}{\partial\varepsilon};-\dot{\lambda}_2=\frac{\partial\mathcal{H}}{\partial\omega};\ -\dot{\lambda}_3=\frac{\partial\mathcal{H}}{\partial p_{cath}};\ -\dot{\lambda}_4=\frac{\partial\mathcal{H}}{\partial S}\\ \frac{\partial\mathcal{H}}{\partial P_{batt}}=0;\ \frac{\partial\mathcal{H}}{\partial W_1}=0;\ \frac{\partial\mathcal{H}}{\partial W_2}=0\end{cases} \tag{6.6}$$

The $\lambda_n$ derivative conditions indicates that they have constant values ($\dot{\lambda}_n=0$) while the condition about the derivative of the Hamiltonian with respect to the control inputs ($P_{batt}$, $W_1$ and $W_2$) present the following results:

$$\frac{\partial\mathcal{H}}{\partial P_{batt}}=0=2\left(a_1+\lambda_4 b_1\right)P^*_{batt}\left(t\right)-\left(2\left(a_1+\lambda_4 b_1\right)\left(P_{vehtot}\left(t\right)\right)+\left(a_2+\lambda_4 b_2\right)\right)-\lambda_1\Rightarrow$$

$$\Rightarrow P^*_{batt}\left(t\right)=\frac{\lambda_1+\left(2(a_1+\lambda_4 b_1)(P_{vehtot}(t))+(a_2+\lambda_4 b_2)\right)}{2(a_1+\lambda_4 b_1)}$$

$$\frac{\partial\mathcal{H}}{\partial W_1}=0=\lambda_2$$

$$\frac{\partial\mathcal{H}}{\partial W_2}=0=\lambda_3 \tag{6.7}$$

Optimization result in (6.7) leads to an algebraic relation between the power demanded by the vehicle and the co-states $\lambda_1$ and $\lambda_4$. As in the previous chapter, $P_{vehtot}$ is a known information and $\lambda_1$ is calculated using the predictive approach as previously. Despite the presence of $\lambda_4$ in the $P^*_{batt}$ equation, it was considered that its influence in the calculation of $\lambda_1$ can be neglected. This assumption is based on the difference in time scales of $\lambda_1$ and $\lambda_4$. While $\lambda_1$ is calculated using a prediction of hundreds of seconds, the co-state $\lambda_4$ has a dynamics adapted to the hours scale. Therefore, in a prediction of $\lambda_1$ the value of $\lambda_4$ is considered constant.

Concerning the calculation of $\lambda_4$, it has to be performed such that it is possible to partially control the fuel cell system $SoH$ by the power setpoint established through the energy management strategy. Some similar approaches are already applied for a battery $SoE$ control. Thritschler et al. [115], Kessels [113] and [80] are examples of this type of implementation. They use a $SoE$ or $SoC$ reference value and the measurements of these variables to calculate the co-state value, which is performed by a feedback control strategy, as in figure 6.10. Such control permits to the $SoE$ or $SoC$ to follows their references during the drive cycle, assuring the power assistance mode of the battery.

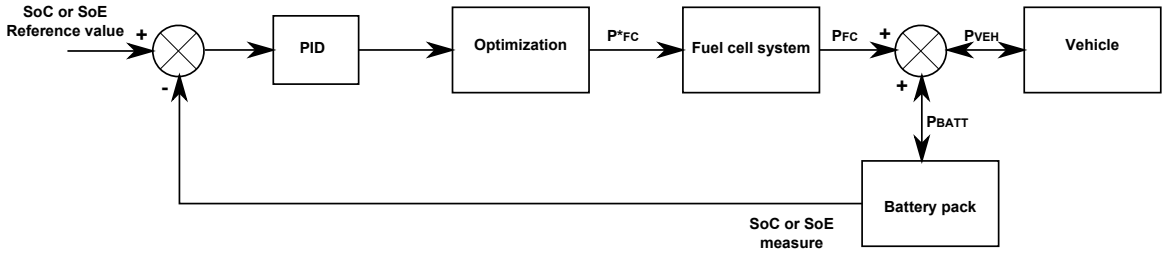


**Figure 6.10:** $SoE$ or $SoC$ control block diagram

However, we do not want that the $SoH$ has a reference value to be followed. As indicated in the last section, the $SoH$ has a limit profile that evolutes in time (fig. 6.9), so it has to avoid this limit during the entire lifetime. Therefore, the control strategy for the calculation of $\lambda_4$ must only maximize the positive difference value between the $SoH$ to its limit value $SoH_{limit}$.

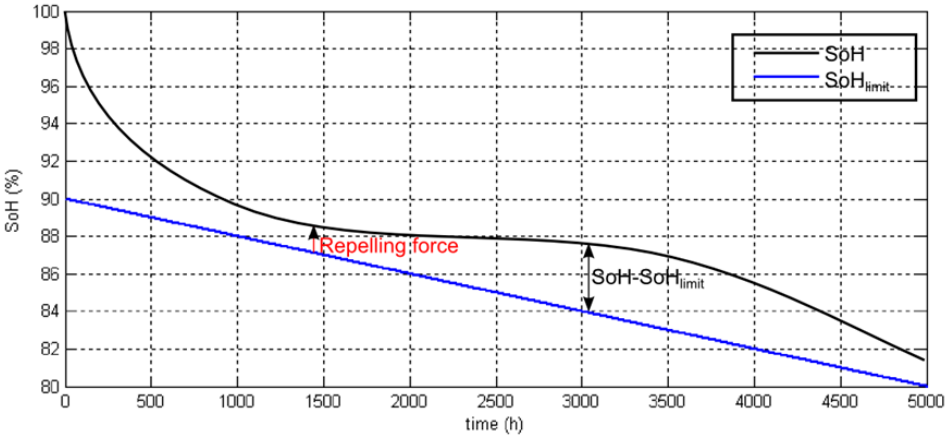


**Figure 6.11:** $SoH_{limit}$ profile

This $SoH$ control works as a repelling force linked to the difference between $SoH\,(t)$ and $SoH_{limit}\,(t)$ (fig. 6.11). As the smaller is the difference the greater is the force, otherwise the force tends to zero.

Somehow, this force is related to the value of $\lambda_4$ and its calculation uses an exponential function such as:

$$\lambda_4 = f_5\left(\triangle SoH\left(t\right)\right) = \frac{k_1}{e^{k_2(\triangle SoH(t))} - 1}; \quad \triangle SoH\left(t\right) = SoH\left(t\right) - SoH_{limit}\left(t\right) \tag{6.8}$$

Where $k_1$ and $k_2$ are constants.

Figure 6.12 shows the behavior of this gain function. As can be observed, as closer to the limit the $SoH\left(t\right)$ is, as greater the $\lambda_4$ value is. While $\lambda_4$ can be neglected when $\triangle SoH\left(t\right)$ presents a important value (it means the fuel cell degradations are not accelerated).

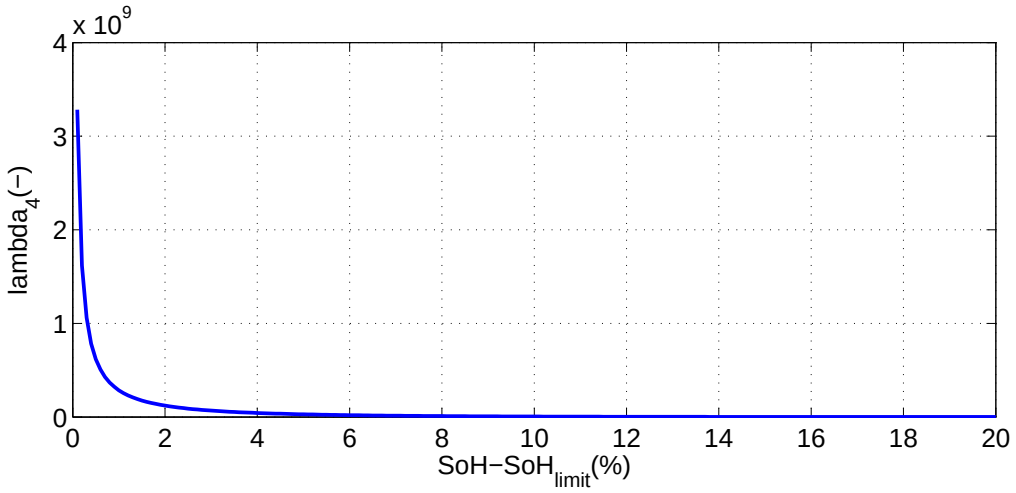


**Figure 6.12:** $\lambda_4$ in function of $\triangle SoH\left(t\right)$

The implementation of the $SoH$ control turns the optimization structure to the one presented in figure 6.13.

The final solution of the optimization problem presents a commitment between the minimization of the hydrogen consumption and the warranty that the durability constraint is controlled. It is expected that this association modify the best operational point (in terms of hydrogen consumption) when $SoH$ is close to its limit, leading to adopt the a lower degradation rate and increasing the hydrogen consumption.

In the next section, the optimization structure proposed is tested under different $SoH$ conditions for a real automotive environment (drive cycle).

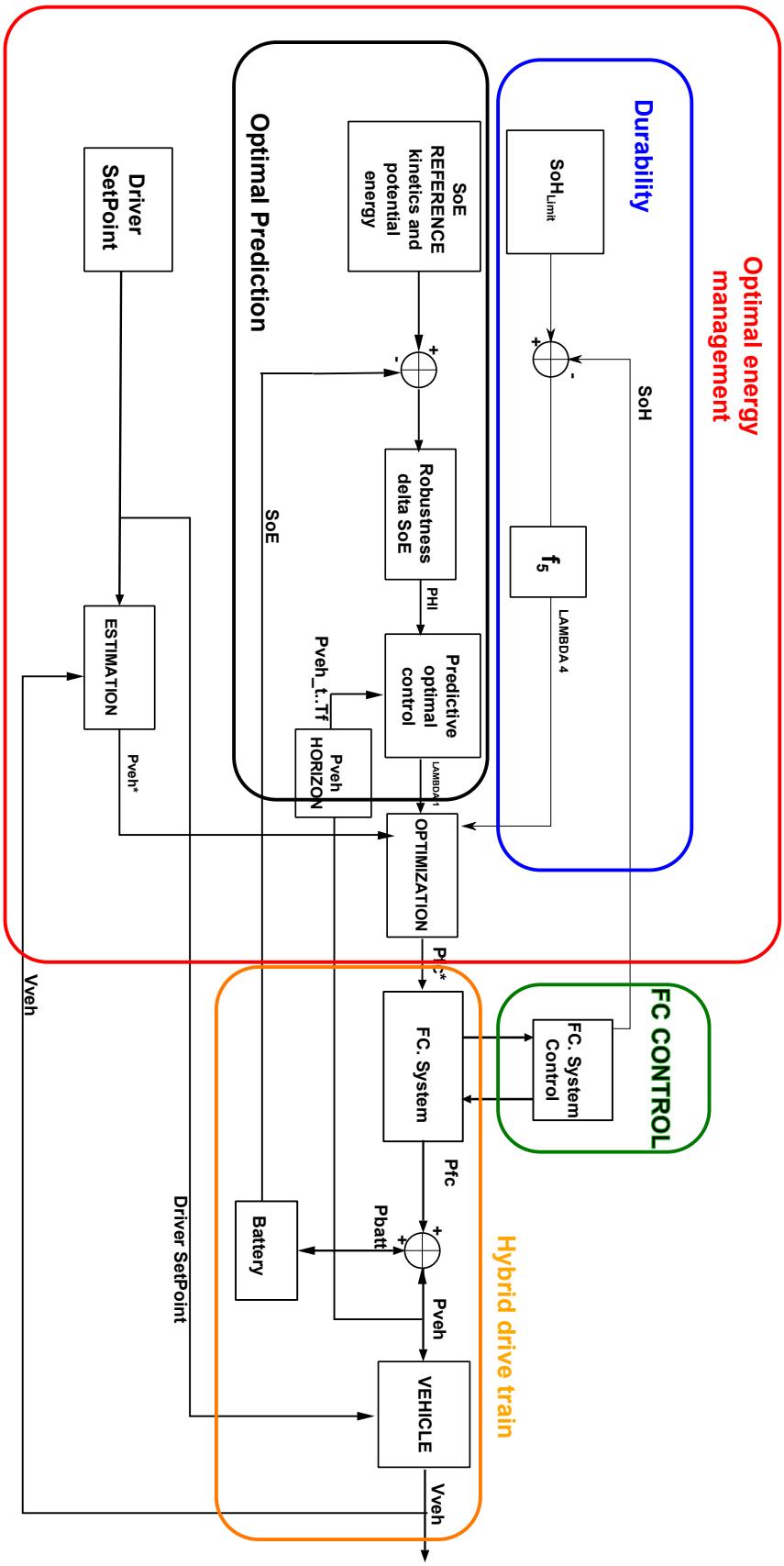


**Figure 6.13:** New optimization structure including $SoH$ control

## 6.6 Optimization results

The optimization solution is applied to the model that represents the real system PROSPAC composed by fuel cell system of $5\,kW$ and a $2\,kWh$ battery . In order to verify the effect of the state of health in the energy management, three initial conditions are imposed: $\triangle SoH\,(t) = 1\,\%$; $\triangle SoH\,(t) = 5\,\%$; $\triangle SoH\,(t) = 10\,\%$ ($\triangle SoH\,(t) = SoH\,(t) - SoH_{limit}\,(t)$).

Extra-urban drive cycle (appendix A) is imposed to the system. Power profile related to this cycle, which is required from the hybrid system, is shown in figure 6.14.

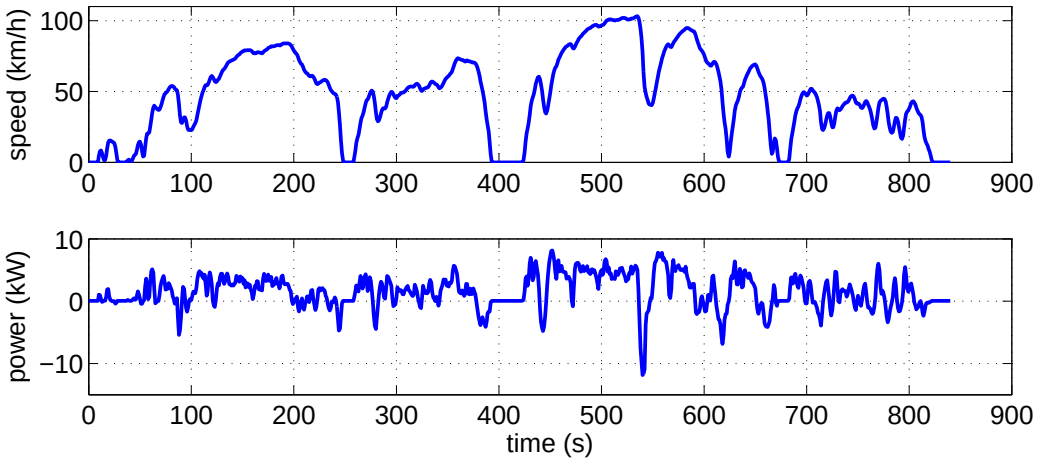


**Figure 6.14:** Drive Cycle

When this power profile is imposed to the hybrid system, the energy management strategy replies with three different fuel cell system power profile related to each $\Delta SoH$, as can be seen in figure 6.15.

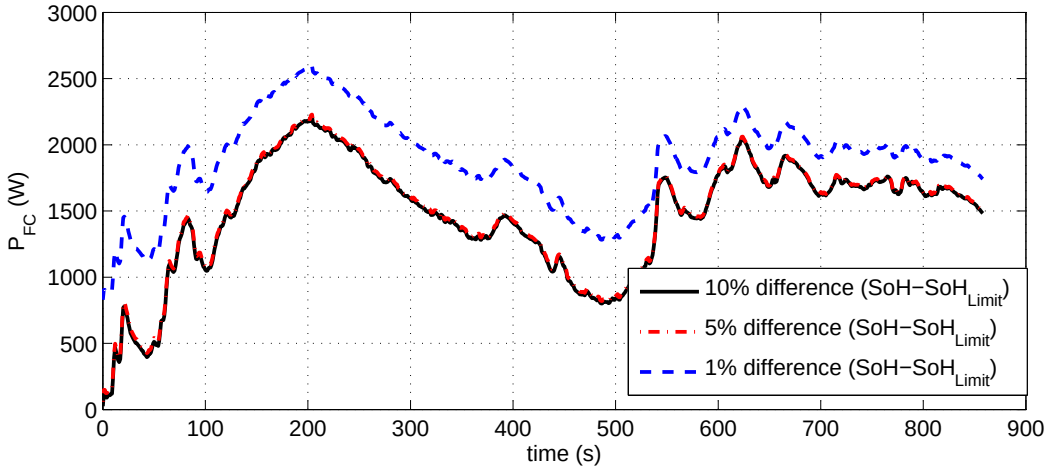


**Figure 6.15**: FC system power profile

When the fuel cell has a high degradation (small $\triangle SoH$), the energy management increases the power delivered by the fuel cell in order to reach a less critical region in terms of degradation. However, there are some points where the FC system power decreases due to the effect of the $SoE$ constraint. When the $SoE$ value deviates from its reference, this constraint becomes more important and reduces the effect of the durability constraint (figure 6.16).

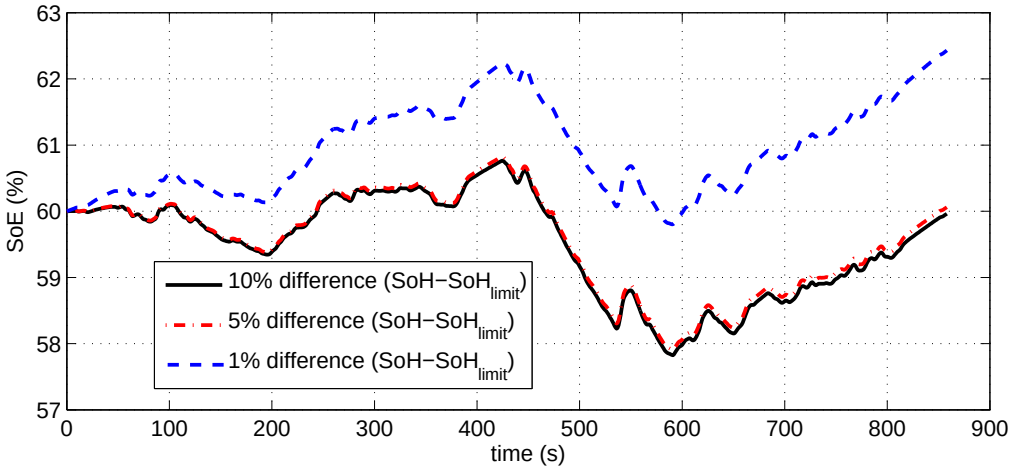


**Figure 6.16**: $SoE$ profile

The results in terms of active surface losses are presented in table 6.1. Active surface losses are represented as percentage of the total allowed. This total is considered as 20 % of the initial surface area ($220\,cm^2$); thereby, a reduction of $44\,cm^2$ represent the total of losses allowed.

| $\triangle SoH\,(t_0)$ (%) | 100. $\frac{surface\,losses\left(cm^2\right)}{44\,cm^2}$ (%) | consumption ($\frac{g_{H_2}}{km}$) |
|---|---|---|
| 10 | 0.0502 | 11.9 |
| 5 | 0.0495 | 12.1 |
| 1 | 0.0431 | 13.3 |

**Table 6.1**: Active surface losses and hydrogen consumption

It can be noticed a reduction in the degradation when the $\triangle SoH\,(t_0)$ goes from 10 to 5 %, which is followed by a slight increase in the hydrogen consumption.

Nevertheless, an important relative reduction in terms of surface degradation is obtained when the initial condition is $\triangle SoH\,(t_0) = 1\,\%$. The reduction in surface degradation of almost 16 % (compared to $\triangle SoH\,(t_0) = 10\,\%$) is followed by an expected increase in terms of hydrogen consumption (11 %) that is not completely lost in the process, but also converted and stored in the battery pack.

## 6.7 Conclusion of the chapter

The development of energy management strategy for FCHEV is again studied in this chapter, but with a different approach. Keeping all the characteristics of the solution given in the previous chapter, the power split has been changed such that the durability aspect of the fuel cell system is included and considered in the optimization process as a constraint.

These durability aspects of the fuel cell system are firstly presented in the chapter by the definition of the durability criteria adopted and how it is related to the performance of the fuel cell. Based on studies made by other authors, the loss in voltage was chosen as the performance index that can indicate the end of life of the fuel cell stack. As this information is directly related to the efficiency, the loss of 10 % in the cell voltage for a rated power delivered indicates an efficiency level that disqualifies it for the vehicle applications.

The different operation modes imposed by the automotive application would lead the fuel cell to reach this end of life level too early. Requirements such as start/stop and load cycling are examples of type of vehicle requirements. However, they represent conditions in the vehicle level that are related to several phenomena within the fuel cell stack. The understanding of the causes and effects of theses phenomena is necessary as a background before including the durability aspect in the optimal energy manage-

ment strategy. Therefore, the chapter introduced a brief review of the most important degradation mechanisms and which components of the fuel cell that are affected.

As important as the knowledge of the degradation mechanisms is the diagnosis of the fuel cell state of health $SoH$. Such information allows to follow the performance of the fuel cell and to propose actions that reduce degradation. Several methods used to evaluate the $SoH$ are existing in the literature. They adopt approaches based on different identification tools. Examples of identification methods are presented and it can be concluded that despite the evolution in diagnostic of the fuel cell, this subject still needs some developments before being integrated in realtime applications, such as FCHEV. Nevertheless, $SoH$ measurement is considered as an available and reliable information to control the fuel cell degradation.

Then, a fuel cell degradation model is introduced to represent the specific phenomenon of loss in the cathode catalyst activity, which is represented by a reduction in the active surface area of the fuel cell. Using the study developed by Robin et al. [102], a degradation rate of the active surface in function of the power delivered by the system is used as the degradation dynamic model of the fuel cell. This dynamic equation allows the $SoH$ to be calculated and two new constraint to the optimization (degradation dynamics and limit of $SoH$) to be defined. Concerning the last one, its limiting value is related to the fuel cell end-of-life, which is given in terms of cell voltage degradation limit. Then, it required a transformation of the voltage loss into active surface reduction. We show that such translation indicated a 20 % of equivalent active surface reduction has to be integrated as the $SoH$ final limitation at the end of life.

The integration of the new durability constraints in the optimization problem developed in the previous chapter, but taking into account the new constraints. A new structure is proposed as the solution, where a $SoH$ control is implemented to avoid its oncoming to a low limit profile. Such profile defines an available region during all the fuel cell stack life, which tends to assure a time of life target value.

A reasonable commitment between the consumption and durability is observed as the results of the optimization method for different degradation conditions. The algorithm shows a capacity to handle with the two tasks needing a low calculation capacity and memory, which are important characteristics for a vehicle application.

The energy management strategy developed in this chapter show its potential by the simulation results; however, they must be considered as trends and not quantitative results. An experimental approach would be desired to verify these qualitative results, but the equipments and required structure were not part of the scope of this work.

# Chapter 7

# General Conclusion

Transport sector presents a context that demands from the available transport ways ever more performance and especially less pollutants emissions. The environmental constraints has pushed up the development of new suitable solutions with different energetic approaches. According to the characteristics of the region, the vehicular technologies are oriented towards the most available sources of energy. Ethanol and GPL are some examples of the energy options used to replace the petrol for conventional vehicles. Although the acceptation of these new types of energy vectors, several studies presented that is necessary a breakthrough not only in the energy source but also in the powertrain of the vehicles.

Therefore, the adoption of electrical powertrain has been often adopted by automobile constructors either to integrate hybrid vehicles or in the full electric vehicles. In the first option the hybridization allows to reduce the petrol consumption and pollutants emissions. Meanwhile, the full electric vehicle represent, at first sight, a perfect solution as it does not uses directly fuel; however, the price of the battery, distance range and recharge time are still drawbacks of this technology.

Despite the recent commercialization of hybrid and full electric vehicle, they represent solutions that compose the set of options available. As a complementary solution, the Fuel Cell Hybrid Electric Vehicles (FCHEV) has been subjected of research and developments of research centers and automobile constructors.

Considered as a promising option, this solution allies the good efficiency to the drive range and "clean" features. However, even if some automakers announced the commercialization of FCHEV for 2015, this technology has not reached a maturity and stability level to be compared with the available options in the market. Even if advances have been obtained, high cost, difficult energy management and low durability are still barriers to the full adoption of the hydrogen fuel cell technologies embedded in the vehicles. In

order to contribute to the efforts applied to the development of the FCHEV, this work performed a study of different functionalities related to the existing drawbacks. They are grouped in three main subjects:

- FCHEV optimal sizing
- Online optimal energy management strategy
- Consideration of the durability aspects (degradation) in the energy management strategy

In the outline of the development chain, firstly a tool basis was created to achieve the objectives. It is composed by a set of optimization tools and models adapted to the different elements of the fuel cell hybrid electric vehicle. Matlab/Simulink environment was adopted to the developments.

Concerning the main objectives of this thesis, the optimal sizing was the first to be dealt. Such task was intended to obtain the best configuration of the vehicle's elements in order to meet a set of technical specifications and minimizing the hydrogen consumption. Moreover, population mobility and economical aspects were also included in this sizing procedure. Adopting a systematically approach, the sizing procedure was performed in four steps:

- Technical requirement: The vehicle powertrain was sized to meet a set of technical requirements composed by specifications based on a typical vehicle capability and also on the technological features imposed by the new elements included in the vehicle. The sizing of the powertrain elements resulted in a configuration that keeps the drivability for a typical user and integrated the new functionalities brought by the new technologies embedded.
- Optimization: The hybridization contained in the architecture provides an extra degree of freedom, which can be used to optimize the hydrogen consumption during a mission. Such reduction is obtained by optimizing the power split between the fuel cell system (FCS) and the battery pack at the time. Even if this optimization process is mostly used to define the energy management strategy, an optimal sizing of the FCS and battery can be obtained as well for a given mission (drive cycle). The results of this step indicated the best combinations of FCS max power and battery energy capacity in terms of hydrogen consumption. During this optimization process, several aspects were took into account, such as the mass of the systems, the energy consumption of FCS auxiliaries and the battery pack capacity to deliver and recover power.

- Mobility aspects: The distance range of the vehicle was submitted to the requirements of the population mobility aspects. Based on statistical data about the population displacement, a bound of the battery energy capacity was assigned. Such capacity is related to the ability of the vehicle to accomplish a most frequent distance range in a battery traction mode.

- Economical aspects: The economical point of view was applied in the last part of the sizing procedure. This economical analysis aimed to verify the interest in the increasing of the hybridization performance (reduction of hydrogen consumption) when comparing to the cost of the new dimension of the system. The results indicate that the cost of the battery pack extra capacity is not compensated by the economy in hydrogen consumption during all vehicle's life, while the savings in hydrogen can justify the extra-cost of a more powerful fuel cell system.

To summarize the optimal sizing work, the proposed method presents a systematic approach that allies different and complementary tasks useful to determine the capacities of the main elements of the vehicle power train and hybrid system. Furthermore, the results of the hybridization sizing process of indicate the following remarks:

- According to the type of drive cycle and constraints adopted in the optimization problem, the optimal configuration presents different results.

- The increasing in mass and energy consumption of FCS and battery should be compensated by an increase of the hybrid system performance, which is not always the case.

- The battery pack power recovery capacity is more effective than the power delivery capacity in the optimization of the hydrogen consumption.

- The cost of the battery is hardly compensated by the gain in performance of the system, which means that it limits the adoption of the best configurations (in terms of hydrogen consumption).

In the sequence, the subject dealt was the development of an optimal online energy management strategy (EMS). Differently from the global optimization tool used in the sizing procedure, this EMS is oriented to online embedded applications, such as the vehicle ones. Moreover, the proposed online optimization method includes the dynamics of the fuel cell system, which is normally neglected in the literature.

Concerning this EMS subject, the contribution of this work might be divided in two parts:

- Fuel cell system dynamics: Considered as a limiting factor for vehicle applications, the dynamics of the fuel cell system was included in the constraints of the optimization problem. Therefore, it was necessary to define and develop the dynamical model that represents the main fuel cell system behavior. As the most constrained subsystem in the FCS and presenting a non-linear dynamics that could be responsible for some harmful effects, the air supply subsystem had its dynamic behavior modeled to represent the fuel cell system dynamics. In order to deal with this dynamics, a non-linear control law using the differential flatness theory was applied to regulate the most important state variables: oxygen flow and cathode pressure. This control strategy has been validated though simulations (with a dynamic FCS model) and tests on real hybrid FC system. Besides, such control simplified the dynamics to an integrator chain, leading to an easier inclusion of it in the optimization problem.

- Predictive online energy management strategy: Requiring an optimization approach better adapted for the vehicle applications than global optimization methods such as Dynamic Programming or Pontryaguin's Maximum Problem (PMP), the energy management strategy to be embedded in the FCHEV was developed using an optimization method that aggregates the PMP theory and a predictive approach. This predictive component is responsible to fill the gap of the unknown information related to the drive cycle imposed to the vehicle. The prediction adopts a sliding horizon of power demanded and integrates the information of battery's state of energy ($SoE$), allowing to obtain the power assistance mode ($SoE\left(t_{initial}\right) = SoE\left(t_{final}\right)$). Another improvement provided by this proposed optimization strategy concerns the energy recovery during braking procedures. Adapting the reference of the $SoE$ according to the speed and altitude of the vehicle, the battery is prepared to recover the maximum of the kinetic and potential energy available during braking, leading to an optimization in the hydrogen consumption.

The analysis of the simulation and experimental optimization results showed that even though the algorithm presents a local optimization, it has the ability to approximate the global optimization results. Furthermore, the proposed solution is capable to calculate the power split in an analytical way and demanding a small amount of memory, which represents an overcome of the global solution drawbacks and an important feature to be highlighted.

Durability aspect was the last subject dealt in this work. As made with the fuel cell dynamics, the degradation dynamics was integrated in the optimization problem as a

constraint. This was effectuated using a model that indicates the fuel cell degradation rate in function of the power demanded. Such degradation rate is observed though the losses at the fuel cell active surface area and enables the definition of the State-of-Health $SoH$ variable. Combining the consumption criterion, battery $SoE$ constraint and durability constraints, it was created three different time scales in the optimization problem that mixes instantaneous conditions to drive cycle durations ($SoE$ constraint) and time of life aspects (fuel cell system durability). Therefore, it was required an adoption of a $SoH$ boundary profile, where this profile changes in time up to reach the fuel cell's end-of-life. To respect this boundary profile, a $SoH$ control is integrated in the solution of the optimization problem, such that it assures an assigned lifetime of the fuel cell.

Even if the results represent only trends, it was noticed that the expected commitment between hydrogen consumption, $SoE$ and $SoH$ constraints was presented in the results. This indicates that although the lack of accuracy, the results lead to consider the proposed optimization structure adapted to the give consistent responses and to allow the evolution of the constraints complexity.

The results and developments presented in this document opened the perspectives for future research and developments. Out of all the possibilities, three applications fields are closely related to this thesis work:

**Drive cycle identification methods:** Global optimization methods and specially the proposed online predictive optimization method emphasized the importance of the knowledge about the drive cycle. The differences between the local optimization results and global optimization ones could be reduced using a better estimation about the type of the drive cycle imposed to the vehicle. Consequently, it can increase the performance of the vehicle even in realtime applications.

Such estimation must represent the main characteristics of the drive conditions and should be provided during the driving operation. This type of research has been developed for several applications using different approaches, such as GPS data analysis, statistical analysis and intelligent methods for pattern recognition.

**Control and observation of the fuel cell state variables:** As already mentioned, the fuel cell response is affected by the conditions imposed to its state variables. Being a multivariable system, a more elaborated control strategy would be a better option to obtain a regulation of the variables in a integrated way. This means a control strategy that aggregates the dynamics of each subsystem to define commands to be applied on the actuators. The interest of such proposition is related to obtain a better performance

of the fuel cell system (energetic gain) and a better control of the degradation rate. Considering these two topics, our work open the prespectives for developments on the control of the fuel cell state variables, as was performed for the air supply subsystem variables. As presented in the chapter 6, the other state variables (temperature, humidity, etc) are also important in the durability and performance of the fuel cell system, but their related dynamics require the use of more advanced control laws for stabilization and optimization.

Despite the developments and researches conducted in this area, it is still considered an open research field. Some of the most difficulties to advance in this topic are about the several application domains required in the development:

- Modeling
- Parametric identification
- Observation and reconstruction of state variables (software sensors)
- Control strategies (linear and non-linear)

These requirements indicate the need to perform a multi-domain interaction represented by commom efforts of different experts (controls, electrochemical, modeling, system design, etc.).

**Fuel cell diagnostics:** In order to deal with the fuel cell system durability issue, an understanding of the degradation mechanisms and their measurements are very important. All this diagnostic process can be used to understand the degradation and evaluate the state of health of the fuel cell system. Moreover, either through the fault detection or by the estimation about the dynamic performance evolution, the diagnostic methods can offer reliability to the fuel cell system and aid in the control of the degradation process.

Nevertheless, the characteristics of the related areas demand research levels from the nano scale up to the system level, which involves the adoption of models and measurement systems not completely adapted to be coupled and to be embedded in realtime systems. At the time, numerous efforts are been made to overcome these drawbacks, but research groups still faces gaps about the degradation process informations and diagnostic implementation that could be filled adopting multiscale modeling approaches, adapted measurement systems and identification methods to indicate the dynamical behavior of the fuel cell degradation.

# Bibliography


[1] Performance renault clio. URL http://www.autotitre.com/fiche-technique/Renault/Clio/II/1.5dCi. 82

[2] Daimler fcev, . URL http://www2.mercedes-benz.com.au. 14

[3] Daimler fcev performance, . URL https://www.daimler.com. 14

[4] Enquete nationale transports et deplacement 2008. URL http://www.statistiques.developpement-durable.gouv.fr/transports/r/transport-voyageurs-deplacements.html. xxiv, 96

[5] Technologie des voitures electrices et hybrides. URL http://www.expert-ve.fr/moteur-onduleur-ve.html. 87

[6] Ford fcev. URL http://media.ford.com. 12

[7] Gm fcev. URL http://gm-volt.com. 12

[8] Hyundai fcev, . URL http://www.hyundai.com.au. 13

[9] Performance hyundai, . URL http://www.autocar.co.uk. 13

[10] Toyota prius i-tech. URL http://www.toyota.com.au/prius/specifications/i-tech. 87

[11] R.K. Ahluwalia and X. Wang. Rapid self-start of polymer electrolyte fuel cell stacks from subfreezing temperatures. *Journal of Power Sources*, 162:502–512, 2006. 19

[12] Kimura Akihiro, Abe Tetsuya, and Sasaki Shoichi. Drive force control of a parallel-series hybrid system. *JSAE review*, 20:337–341, 1999. 80

[13] Ahmed Al-Durra, Stephen Yurkovich, and Yann Guezennec. Study of nonlinear control schemes for an automotive traction pem fuel cell system. *International Journal of Hydrogen Energy*, 35:11291–11307, 2010. 112

[14] Michel André. The artemis european driving cycles for measuring car pollutant emissions. 7th international symposium, highway and urban pollution. In *The science of the total environment. Special issue*, 2002. 49

[15] M. André. Driving pattern analysis and driving cycles - European Development of Hybrid Technology approaching Zero Emission Mobility (HYZEM). Technical Report 9709, INRETS LEN, 1997. 49

[16] Alireza Askarzadeh and Alireza Rezazadeh. Artificial neural network training using a new efficient optimization algorithm. *Applied Soft Computing*, 13:1206–1213, 2013. 53

[17] D. Assanis, G. Delagrammatikas, and R. Fellini. An optimization approach to hybrid electric propulsion system design. *Journal of Mechanic of Structures and Machines*, 27:393–421, 2000. 79

[18] Y. Ates, O. Erdinc, M. Uzunoglu, and B. Vural. Energy management of an fc/uc hybrid vehicular power system using combined neural networks-wavelet transform based strategy. *International Journal of Hydrogen Energy*, 35(2):774–83, 2010. 53, 54

[19] Patricia Baptista, Mario Tomas, and Carla Silva. Plug-in-hybrid fuel cell vehicle market penetration scenarios. *International Journal of Hydrogen Energy*, 35:10024–10030, 2010. 13, 33

[20] Nuno Bento. *La transition vers une economie de l'hydrogène: infrastructures et changement technique*. PhD thesis, Université de Grenoble, 2010. 1, 2, 3

[21] J. Bernard, S. Delprat, F. N. Buchi, and T. M. Guerra. Fuel cell hybrid vehicles: Global optimization based on optimal control theory. *International review of electrical engineering*, 1(3), 2006. xxi, xxvii, 130

[22] O. Bethoux, M. Hilairet, and T. Azib. A new on-line state-of-health monitoring technique dedicated to pem fuel cell. In *Industrial Electronics, 2009. IECON '09. 35th Annual Conference of IEEE*, pages 2745–2750, 2009. doi: 10.1109/IECON.2009.5415422. 152

[23] E. Bideaux, J. Laffite, A. Derkaoui, W. Marquis-Favre, S. Scarvarda, and F. Guillemard. Design of a hybrid vehicle powertrain using an inverse methodology. *Journal Européen des Systèmes Automatisés*, 40:279–290, 2006. 49

[24] Benjamin Blurnier. *Modelisation de moto-compresseurs en vue de la gestion de l air dans les systemes pile a combustible - simulation et validation experimentale.* PhD thesis, Universite de Technologie de Belfort-Montbeliard, 2007. 40, 111

[25] Rod Borup, Michael Inbody, John Davey, David Wood, Fernando Garzon, Jose Tafoya, Jian Xie, and Susan Pacheco. Fy 2004 program report. Technical report, DOE Hydrogen Program, 2004. 149, 150, 151

[26] Shelley Brown. *Diagnosis of the Lifetime Performance Degradation of Lithium-Ion Batteries: Focus on Power-Assist Hybrid Electric Vehicle and Low-Earth-Orbit Satellite Applications.* PhD thesis, KTH, Applied Electrochemistry, 2008. 29, 31

[27] Felix N. Buchi, Bhuvanesh Gupta, Otto Haas, and Gunther G. Scherer. Study of radiation-grafted fep-g-polystyrene membranes as polymer electrolytes in fuel cells. *Electrochimica Acta*, 40(3):345 – 353, 1995. ISSN 0013-4686. doi: 10.1016/0013-4686(94)00274-5. URL `http://www.sciencedirect.com/science/article/pii/0013468694002745`. <ce:title>Polymer electrolyte fuel cells</ce:title>. 150

[28] Denis Candusso. *Hybridation du groupe electrogene a pile a combustible pour l alimentation d un vehicule electrique.* PhD thesis, Institut National Polytechnique de Grenoble, 2002. 33, 36

[29] Ricardo Sales Cardoso, Enver Doruk Ozdemir, and Ludger Eltrop. Enviromental and economic assessment of international ethanol trade options for the german trasnport sector. *Biomass and Bioenergy*, 36:20–30, 2012. 2

[30] S. Caux, W. Hankache, M. Fadel, and D. Hissel. On-line fuzzy energy management for hybrid fuel cell systems. *International Journal of Hydrogen Energy*, 35:2134–2143, 2010. 53

[31] Fuel cell Today. The fuel cell industry review. Technical report, Fuel cell Today, 2012. 11, 15, 20

[32] M. Ceraolo. New dynamical models of lead-acid batteries. *IEEE Transactions on Power Systems*, 15:1184–1190, 2000. 29

[33] C. C. Chan. The state of the art of electric, hybrid and fuel cell vehicles. *Proceedings of the IEEE*, 95:N 4, 2007. 2, 19

[34] C. C. Chan, Y. S. Wong, Alain Bouscayrol, and Keyu Chen. Powering sustainable mobility: Roadmaps of electric, hybrid and fuel cell vehicles. *Proceedings of the IEEE*, 2009. 2

[35] C. C. Chan, Alain Bouscayrol, and Keyu Chen. Electric, hybrid and fuel-cell vehicles: Architectures and modeling. *IEEE Transaction on Vehicular Technology*, 59:N 2, 2010. 23

[36] Xuan Cheng, Zheng Shi, Nancy Glass, Lu Zhang, Jiujun Zhang, Datong Song, Zhong-Sheng Liu, Haijiang Wang, and Jun Shen. A review of {PEM} hydrogen fuel cell contamination: Impacts, mechanisms, and mitigation. *Journal of Power Sources*, 165(2):739 – 756, 2007. ISSN 0378-7753. doi: 10.1016/j.jpowsour.2006.12.012. URL `http://www.sciencedirect.com/science/article/pii/S0378775306025304`. <ce:title>IBA - {HBC} 2006</ce:title> <ce:subtitle>Selected papers from the {INTERNATIONAL} {BATTERY} {ASSOCIATION} & {HAWAII} {BATTERY} {CONFERENCE} 2006 Waikoloa, Hawaii, {USA} 9-12 January 2006</ce:subtitle>. 150

[37] European Commission. Hydrogen energy and fuel cells. Technical report, European Commission, 2003. 11

[38] Romain Coulon. *Modélisation de la dégradation chimique de membranes dans les pile à combustibles à membrane électrolyte polymère.* PhD thesis, Université de Grenoble, 2012. 150

[39] Jean Christophe CULIOLI. *Introduction à l'Optimisation.* Ellipses, 1994. xviii, xx, 54, 60, 74, 130, 162

[40] Ramon da Fonseca, Eric Bideaux, Mathias Gerard, Bruno Jeanneret, Ali Sari, and Matthieu Desbois-Renaudin. Dimensionnement optimal des elements energetiques d'un vehicule hybride a pile a combustible. *JCGE (Conference jeunes chercheurs en genie electrique)*, 2011. 8

[41] Ramon da Fonseca, Eric Bideaux, Bruno Jeanneret, Mathias Gerard, Matthieu Desbois-Renaudin, and Ali Sari. Energy management strategy for hybrid fuel cell vehicle. *In proceedings at Control, automation and systems (ICCAS), 2012 12th*, pages 485–490, 2012. 9

[42] Ramon da Fonseca, Eric Bideaux, Mathias Gerard, Bruno Jeanneret, Matthieu Desbois-Renaudin, and Ali Sari. Hybrid fuel cell vehicle energy management includ-

ing dynamic and durability constraints. *FDFC (Fundamentals and Development on Fuel Cells)*, 2013. 9

[43] Ramon Naiff da Fonseca, Eric Bideaux, Mathias Gerard, Bruno Jeanneret, and Matthieu Desbois-Renaudin. Hybrid electric system for an hydrogen fuel cell vehicle and its energy management. *SAE- Society of Automobile Engineers*, DOI: 10.4271/2012-01-1226, 2012. 8

[44] Ramon Naiff da Fonseca, Eric Bideaux, Mathias Gerard, Bruno Jeanneret, Matthieu Desbois-Renaudin, Ali Sari, and Didier Buzon. Flatness control strategy for the air subsystem of a hydrogen fuel cell system. *ASCC (Asian Control Conference)*, 2013. 9

[45] Ramon Naiff da Fonseca, Eric Bideaux, Mathias Gerard, Bruno Jeanneret, Matthieu Desbois-Renaudin, and Ali Sari. Control of pemfc system air group using differential flatness approach: validation by a dynamic fuel cell system model. *Applied Energy*, 2013 (in review). 9

[46] S. Delprat, J. Lauber, T.M. Guerra, and J. Rimaux. Control of a parallel hybrid powertrain: optimal control. *IEEE Transactions on Vehicular Technology*, 53:872–881, 2004. 55

[47] E. Van den Tillaart. Matador: Management tool for the assessment of driveline technologies and research, chapter subtask 2.4: Test methods. soc correction methods for hevs. *TNO Automotive*, 2000. 79

[48] Matthieu Desbois-Renaudin, Julien Scordia, Rochdi Trigui, Francois Badin, Bruno Jeanneret, Cedric Plasse, and Jean-Francois Sarrau. Vehicules hybrides thermiques-electriques. etude parametrique de l'architecture hybride parallele. rapport final d'etude. Technical report, INRETS, 2004. 82, 84, 91

[49] Arnaud Devie. *Caracterisation de l usage des batteries Lithium-Ion dans les vehicules electriques et hybrides. Application a l etude du vieillissement et de la fiabilite*. PhD thesis, Universite Claude Bernard Lyon 1, 2012. xiv, 28, 30, 31

[50] Nuclear Engineering Division. Tecnical assessment of cryo-compressed hydrogen storage tank systems for automotive applications. Technical report, Argonne National Laboratory, 2009. 16

[51] Florian Dupriez-Robin. *Dimensionnement d'une propulsion hybride de volier, basé sur la modélisation par les flux de puissance*. PhD thesis, Université de Nantes, 2010. 49, 93

[52] A. Emadi, K. Rajashekara, S. S. Williamson, and S. M. Lukic. Topological overview of hybrid electric and fuel cell vehicular power systems architectures and configurations. *IEEE Transaction on Vehicular Technology*, 54:763–770, 2005. 20

[53] O. Erdinc and M. Uzunoglu. Recent trends in pem fuel cell-powered hybrid systems: Investigation of application areas, design architectures and energy management approaches. *Renewable and Sustainable Energy Reviews*, 14:2874–2884, 2010. 4, 13, 19

[54] O. Erdinc, B. Vural, and M. Uzunoglu. A wavelet-fuzzy logic based energy management strategy for a fuel cell/battery/ultra-capacitor hybrid vehicular power system. *Journal of Power Sources*, 194(1):369–80, 2009. 53

[55] O. Erdinc, B. Vural, M. Uzunoglu, and Y. Ates. Modeling and analysis of an fc/uc hybrid vehicular power system using a wavelet-fuzzy logic based load sharing and control algorithm. *International Journal of Hydrogen Energy*, 34(12):5223–33, 2009. 53

[56] Y. Eren, O. Erdinc, H. Gorgun, M. Uzunoglu, and B. Vural. A fuzzy logic based supervisory controller for an fc/uc hybrid vehicular power system. *International Journal of Hydrogen Energy*, 34(20):8681–94, 2009. 53

[57] T. Escobet, D. Feroldi, S. de Lira, V. Puig, J. Quevedo, J. Riera, and M. Serra. Model-based fault diagnosis in {PEM} fuel cell systems. *Journal of Power Sources*, 192(1):216 – 223, 2009. ISSN 0378-7753. doi: 10.1016/j.jpowsour.2008.12.014. URL `http://www.sciencedirect.com/science/article/pii/S0378775308023288`. <ce:title>CONAPPICE 2008, Zaragoza, Spain, 24-26 September 2008</ce:title>. 147

[58] M. Fliess, J. Lévine, Ph. Martin, and P. Rouchon. Flatness and defect of nonlinear systems: Introductory theory and examples. *International Journal of Control*, 61:1327–1361, 1995. xxv, 112, 114, 117

[59] Michel Fliess, Jean Lévine, Philippe Martin, and Pierre Rouchon. A lie-backlund approach to equivalence and flatness of nonlinear systems. *IEEE Transactions on Automatic Control*, 44:922–937, 1999. xxv, 114, 117

[60] Adrian Florescu. *Gestion optimise des flux energetiques dans le vehicule electrique*. PhD thesis, Universite de Grenoble, 2012. 20, 24, 27

[61] Dawei Gao, Zhenhua Jin, and Qingchun Lu. Energy management strategy based on fuzzy logic for a fuel cell hybrid bus. *Journal of Power Sources*, 185:311–317, 2008. 53

[62] Y. Gao and M. Ehsani. Hybrid electric vehicle: Overview and state of the art. *IEEE ISIE*, 2005. 26

[63] David Gargett. Transport energy futures: long-term oil supply trends and projections. Technical report, Bureau of Infrastructure, Transport and Regional Economics (BITRE), 2009. 2

[64] Mathias Gerard. *Etude des interactions pile/systeme en vue de l optimisation d un generateur pile a combustible: Interactions coeur de pile/ compresseur; - Interactions coeur de pile/ convertisseur*. PhD thesis, Universite de Franche-Conte, 2010. xxix, 35, 39, 40, 67, 73, 147

[65] Mathias Gerard, Jean-Philippe Poirot-Crouvezier, Daniel Hissel, and Marie-C'ecile Pera. Oxygen starvation analysis during air feeding faults inpemfc. *International Journal of Hydrogen Energy*, 35:12295–12307, 2010. xxv, 111

[66] R. Glises, D. Hissel, F. Harel, and M. C. Pera. New design of a pem fuel cell air automatic climate control unit. *Journal of Power Sources*, 150:78–85, 2005. 42

[67] Garth Joni Govidan. World energy outlook 2010. Technical report, France OECD Publishing, 2010. xi, 1, 2

[68] UK H2 Mobility Group. Uk h2 mobility. synopsis of phase 1 results. Technical report, UK H2 Mobility Group, 2013. 13

[69] M. Grujicic, K.M. Chittajallu, E.H. Law, and J.T. Pukrushpan. Model-based control strategies in the dynamic interactions of air supply and fuel cell. *Proceedings of the Institution of Mechanical Engineers, Part A: Journal of Power and Energy*, 218:487–499, 2004. 112

[70] Gargeth E. Haslam, Joni Jupesta, and Govidan Parayil. Assessing fuel cell vehicle and the role of policy in japan, korea and china. *International Journal of Hydrogen Energy*, 37:14612–14623, 2012. 4, 11

[71] Jenn-Jiang Hwang. Sustainability of hydrogen pathways for fuel cell vehicle applications. *Renewable and Sustainable Energy Reviews*, 19:220–229, 2013. 4, 11, 15

[72] Ju hyung Lee, Jong-Hak Lee, Woojin Choi, Kyung-Won Park, Hee-Young Sun, and Jae-Hyuk Oh. Development of a method to estimate the lifespan of proton exchange membrane fuel cell using electrochemical impedance spectroscopy. *Journal of Power Sources*, 195(18):6001 – 6007, 2010. ISSN 0378-7753. doi: 10.1016/j.jpowsour.2010.02.054. URL http://www.sciencedirect.com/science/article/pii/S0378775310003137. <ce:title>Selected Papers Presented at 4th International Conference on Polymer Batteries and Fuel Cells</ce:title>. 152, 153

[73] Alberto Isidori. *Nonlinear control systems*. Springer, 1995. 115

[74] M. Jain, C. Desai, N. Kharma, and S.S. Williamson. Optimal powertrain component sizing of a fuel cell plug-in hybrid electric vehicle using multi-objective genetic algorithm. In *Industrial Electronics, 2009. IECON '09. 35th Annual Conference of IEEE*, pages 3741–3746, 2009. doi: 10.1109/IECON.2009.5415111. 93

[75] J.Bernard, S.Delprat, T.M.Guerra, and F.N.Buchi. Fuel efficient power management strategy for fuel cell hybrids powertrains. *Control Engineering Practice*, 18:408–417, 2010. xxvii, 55, 72, 132

[76] Y. Kano and T. Mano. Design of slipring-less winding excited synchronous motor for hybrid electric vehicle. In *Electrical Machines and Systems (ICEMS), 2012 15th International Conference on*, pages 1–5, 2012. 87

[77] Saida Kermani. *Gestion energetique des vehicules hybrides: de la simulation a la commande temps reel*. PhD thesis, Universite de Valenciennes et du Hainaut Cambresis, 2009. xxvii, 24, 29

[78] Jonghoon Kim, Inhae Lee, Yongsug Tak, and B.H. Cho. State-of-health diagnosis based on hamming neural network using output voltage pattern recognition for a {PEM} fuel cell. *International Journal of Hydrogen Energy*, 37(5):4280 – 4289, 2012. ISSN 0360-3199. doi: 10.1016/j.ijhydene.2011.11.092. URL http://www.sciencedirect.com/science/article/pii/S0360319911025900. <ce:title>Portable Fuel Cells Fundamental and Applications (ISPFC2010)</ce:title>. 152

[79] Donald E. Kirk. *Optimal Control Theory An Introduction*. Dover Publications, Inc, 2004. 61

[80] Michiel Koot, J. T. B. A. Kessels, Bram de Jager, W. P. M. H. Heemels, P. P. J. van den Bosch, and Maarten Steinbuch. Energy management strategies for vehicular electric power systems. *IEEE transactions on vehicular technology*, 54, 2005. 164

[81] Timo Kurz, Alex Hakenjos, Jerome Kramer, Mario Zedda, and Carsten Agert. An impedance-based predictive control strategy for the state-of-health of {PEM} fuel cell stacks. *Journal of Power Sources*, 180(2):742 – 747, 2008. ISSN 0378-7753. doi: 10.1016/j.jpowsour.2008.02.062. URL `http://www.sciencedirect.com/science/article/pii/S0378775308004515`. 152

[82] Jérôme Lachaize. *Etude des stratégies et des structures de commande pour le pilotage des systèmes énergétiques à Pile à Combustible (PAC) destinés à la traction.* PhD thesis, L'Institut National Polytechinique de Toulose, 2004. 63

[83] Chun-Yan Li and Guo-Ping Liu. Optimal fuzzy power control and management of fuel cell/battery hybrid vehicles. *Journal of Power Sources*, 192:525–533, 2009. 53

[84] G. Liu, J. Zhanga, and Y. Sun. High frequence decoupling strategy for the pem fuel cell hybrid system. *International Journal of Hydrogen Energy*, 33(21):6253–61, 2008. 54

[85] A. Gilbert McCoy, L. Todd, and J. G. Douglass. Energy-efficient electric motor selection handbook. Technical report, The Bonneville Power Administration, US Department of Energy, 1993. 26

[86] Will McDowall. Technology roadmaps for transition management: The case of hydrogen energy. *Tecnological Forecasting & Social Change*, 79:530–542, 2012. 2, 4, 18

[87] I. Meilijson, E. Ruppin, and M. Sipper. A single-iteration threshold hamming network. *IEEE Transactions on Neural Networks*, 6:261–266, 1995. 152

[88] Victor Mester. *Conception Optimale Systémique des Composants des Chaînes de Traction Electrique.* PhD thesis, Ecole Centrale de Lille, 2007. 49, 57

[89] Maxime Montaru. *Contribuition a l evaluation du vieillissement des batteries de puissance utilisees dans les vehicules hybrides selon leurs usages.* PhD thesis, Institut Polytechinique de Grenoble, 2009. 20, 30

[90] Timothy C. Moore and Amory B. Lovins. Vehicle design strategies to meet and exceed pngv goals. *SAE Technical Paper*, 1995. xxi, 78, 83

[91] Yoshiaki Naganuma, Kota Manabe, Hiroyuki Imanishi, and Yasuhiro Nonobe. Control system for sensing the differential pressure between air and hydrogen in a pefc. *SAE Technical Paper*, 2012. 112

[92] U;S. Department of energy. The department of energy hydrogen and fuel cells program plan. Technical report, U. S. Department of Energy, 2011. xi, 4, 13, 14, 15, 16, 17, 18, 20, 33, 105, 106, 146, 161

[93] ONU. World population to 2300. Technical report, Organisation des Nations Unies, 2004. 1, 2, 20

[94] M.D. Paster, R.K. Ahluwalia, G. Berry, A. Elgowainy, S. Lasher, K. McKeneey, and M. Gardiner. Hydrogen storage technology options for fuel cell vehicles: Well-to-wheel costs, energy efficiencies and greenhouse gas emissions. *International Journal of Hydrogen Energy*, 36:14534–14551, 2011. 16, 17

[95] Pucheng Pei, Qianfei Chang, and Tian Tang. A quick evaluating method for automotive fuel cell lifetime. *International Journal of Hydrogen Energy*, 33(14):3829 – 3836, 2008. ISSN 0360-3199. doi: 10.1016/j.ijhydene.2008.04.048. URL `http://www.sciencedirect.com/science/article/pii/S036031990800476X`. <ce:title>TMS07: Symposium on Materials in Clean Power Systems</ce:title>. xxviii, xxix, 148, 151

[96] Jean-Philippe Poirot-Crouvezier. *Modelisation dynamiques des phenomenes hydrauliques, thermiques et electriques dans un groupe electrogene a pile a combustible destine a l application automobile*. PhD thesis, INPG, 2000. 34, 36, 37, 70

[97] DV Prokhorov. Toyota prius hev neurocontrol and diagnostics. *Neural Networks*, 21(2-3):458–65, 2008. 53

[98] Jay Tawee Pukrushpan, Anna Stefanopoulou, and Huei Peng. Modeling and control for pem fuel cell stack system. *In Proc. American Control Conference*, 2002. 111

[99] N. N. Puri and D.P. Lan. Stable model reduction by impulse response error minimization using michailov criterion and pade's approximation. *Journal of Dynamics Systems, Measurement and Control*, 110:389–394, 1988. 133

[100] A. Ravey, N. Watrin, Manfeng Dou, D. Bouquain, and A. Miraoui. Energy-source-sizing methodology for hybrid fuel cell vehicles based on statistical description of driving cycles. *Vehicular Technology, IEEE Transactions on*, 60(9):4164–4174, 2011. ISSN 0018-9545. doi: 10.1109/TVT.2011.2158567. 93

[101] Luis Alberto M. Riascos, Marcelo G. Simoes, and Paulo E. Miyagi. On-line fault diagnostic system for proton exchange membrane fuel cells. *Journal of Power Sources*, 175(1):419 – 429, 2008. ISSN 0378-7753. doi: 10.1016/j.jpowsour.2007.09.010. URL http://www.sciencedirect.com/science/article/pii/S0378775307017715. 147

[102] Christophe Robin, Mathias Gerard, Alejandro A. Franco, and Pascal Schott. Multi-scale coupling between two dynamical models for {PEMFC} aging prediction. *International Journal of Hydrogen Energy*, 38(11):4675 – 4688, 2013. ISSN 0360-3199. doi: 10.1016/j.ijhydene.2013.01.040. URL http://www.sciencedirect.com/science/article/pii/S0360319913000979. xxix, xxx, 153, 154, 155, 156, 161, 170

[103] P. Rodatz, G. Paganelli, A. Sciarretta, and L. Guzzella. Optimal power management of an experimental fuel cell/supercapacitor-powered hybrid vehicle. *Control Engineering Practice*, 2005. 55

[104] M. Safari and C. Delacourt. Aging of a comercial graphite/ lifepo4 cell. *Journal of The Electrochemical Society*, 158:A1123–A1135, 2011. 31

[105] Wolfgang Schmittinger and Ardalan Vahidi. A review of the main parameters influencing long-term performance and durability of {PEM} fuel cells. *Journal of Power Sources*, 180(1):1 – 14, 2008. ISSN 0378-7753. doi: 10.1016/j.jpowsour.2008.01.070. URL http://www.sciencedirect.com/science/article/pii/S0378775308001924. 111

[106] Julien Scordia. *Approche systématique de l'optimisation du dimensionnement et de l'élaboration des lois de gestion d'énergie de véhicules hybrides*. PhD thesis, Université Heny Poincaré - Nancy 1, 2004. xviii, 54, 60, 79, 94

[107] C. Sueur and G. Dauphin-Tanguy. Bond-graph approach for structural analysis of {MIMO} linear systems. *Journal of the Franklin Institute*, 328(1):55 – 70, 1991. ISSN 0016-0032. doi: 10.1016/0016-0032(91)90006-O. URL http://www.sciencedirect.com/science/article/pii/001600329190006O. 49

[108] R. Talj, R. Ortega, and M. Hilairet. Modeling and control of the air supply system of pem fuel cells. *Fundamentals and Developments of Fuel Cells (FDFC) conference*, 2008. 112

[109] R. Talj, R. Ortega, and M. Hilairet. Second order sliding mode control of the motocompressor of a pem fuel cell air feeding system, with experimental validadtion. *Industrial Electronics, 2009. IECON '09. 35th Annual Conference of IEEE*, pages 2790–2795, 2009. xxv, 112

[110] Yong Tang, Wei Yuan, Minqiang Pan, Zongtao Li, Guoqing Chen, and Yong Li. Experimental investigation of dynamic performance and transient responses of kw-class pem fuel cell stack under various loads changes. *Applied Energy*, 87:1410–1417, 2012. 124

[111] Akira Taniguchi, Tomoki Akita, Kazuaki Yasuda, and Yoshinori Miyazaki. Analysis of electrocatalyst degradation in {PEMFC} caused by cell reversal during fuel starvation. *Journal of Power Sources*, 130(1-2):42 – 49, 2004. ISSN 0378-7753. doi: 10.1016/j.jpowsour.2003.12.035. URL `http://www.sciencedirect.com/science/article/pii/S0378775304000096`. 150

[112] Mestan Tekin, Daniel Hissel, Marie-C'ecile Pera, and Jean-Marie Kauffmann. Energy consumption reduction of a pem fuel cell motor-compressor group thaks to efficient control laws. *Jornal of Power Sources*, 156:57–63, 2006. 112

[113] Johannes Theodorus and Bernard Anna Kessels. *Energy Management for Automotive Power Nets*. PhD thesis, Technische Universiteit Eindhoven, 2007. 164

[114] P. Thounthong and P. Sethakul. Analysis of a fuel starvation phenomenon of a pem fuel cell. In *Power Conversion Conference - Nagoya, 2007. PCC '07*, pages 731–738, 2007. doi: 10.1109/PCCON.2007.373048. 111

[115] P. J. Thritschler, S. Bacha, E. Rullière, and G. Husson. Energy management strategies for an embedded fuel cell system on agricultural vehicles. *ICEM 2010. 19th International Conference Electrical Machines*, 2010. 72, 164

[116] R. Trigui, B. Jeanneret, and F. Badin. Systemic modelling of hybrid vehicles in order to predict dynamic performance and energy consumption- building the vehlib library of models. *Revue Recherche Transports Securite*, 83:129–150, 2004. 24, 48

[117] Philipp Tritschler. *Optimisation de l architecture electrique et gestion d energie pour un systeme a pile a combustible embarquee dedie a l application agricole*. PhD thesis, Universite de Grenoble, 2010. 17, 22, 27, 33, 36, 55

[118] M. Uzunoglu and MS. Alan. Modeling and analysis of an fc/uc hybrid vehicular power system using a novel wavelet based load sharing algorithm. *IEEE Transaction on Energy Conversion*, 23(1):263–72, 2008. 54

[119] Ardalan Vahidi, Anna Stefanopoulou, and Huei Peng. Current management in a hybrid fuel cell power system: A model-predictive control approach. *IEEE Transactions on Control Systems Technology*, 14:1047–1057, 2006. 41, 68, 112

[120] Massimo Venturi, Jochen Sang, Andreas Knoop, and Gerald Hornburg. Air supply system for automotive fuel cell application. *SAE Technical Paper*, 2012. 41, 108, 111, 112

[121] Massimo Venturi, Jochen Sang, Andreas Knoop, and Gerald Hornburg. Air supply system for automotive fuel cell application. *SAE Technical Paper*, 2012. xxv

[122] Emmanuel Vinot, Rochdi Trigui, and Bruno Jeanneret. Optimal management of electric vehicles with hybrid storage system. *in Proc. IEEE VPPC- Vehicle power and propulsion conference, Lile, France.*, pages 1 – 6, 2010. xviii, 54, 130

[123] Masahiro Watanabea, Kazunori Tsurumib, Takayuki Mizukamia, Toshihide Nakamurab, and Paul Stonehartc. Activity and stability of ordered and disordered co-pt alloys for phosphoric acid fuel cells. *Jounal of the Electrochemical Society*, 141 (10): 2659–2668, 1994. 150

[124] K. Wipke, S. Sprik, J. Kurtz, T. Ramsden, C. Ainscough, and G. Saur. National fuel cell vehicle learning demonstration fuinal report. Technical report, National Renewable Energy Laboratory - NREL, 2012. 4

[125] Jinfeng Wu, Xiao Zi Yuan, Jonathan J. Martin, Haijiang Wang, Jiujun Zhang, Jun Shen, Shaohong Wu, and Walter Merida. A review of pem fuel cell durability: Degradation mechanisms and mitigation strategies. *Journal of Power Sources*, 184: 104–119, 2008. 54, 111, 150

[126] Xiaolan Wu, Binggang Cao, Xueyan Li, Jun Xu, and Xiaolong Ren. Component sizing optimization of plug-in hybrid electric vehicles. *Applied Energy*, 88:799–804, 2010. 79, 83, 84

[127] Liangfei Xu, Jianqiu Li, Jianfeng Hua, Xiangjun Li, and Minggao Ouyang. Optimal vehicle control strategy of a fuel cell/ battery hybrid city bus. *International Journal of Hydrogen Energy*, 34:7323–7333, 2009. 55

[128] Liangfei Xu, Minggao Ouyang, Jianqiu Li, Fuyuan Yang, Languang Lu, and Jianfeng Hua. Optimal sizing of plug-in fuel cell electric vehicles using models of vehicle performance and system cost. *Applied Energy*, 103(0):477 – 487, 2013. ISSN 0306-2619. doi: 10.1016/j.apenergy.2012.10.010. URL http://www.sciencedirect.com/science/article/pii/S0306261912007143. 105

[129] Quan Yang, A. Aitouche, and B.O. Bouamama. Fault detection and isolation of pem fuel cell system by analytical redundancy. In *Control Automation (MED), 2010 18th Mediterranean Conference on*, pages 1371–1376, 2010. doi: 10.1109/MED.2010.5547857. 147

[130] X. G. Yang, Y. Tabuchi, F. Kagami, and Chao-Yang Wang. Durability of membrane electrode assemblies under polymer electrolyte fuel cell cold-start cycling. *Journal of The Electrochemical Society*, 155:B752–B761, 2008. 149

[131] Zhihong Yu, Donald Zinger, and Anima Bose. An innovative optimal power allocation strategy for fuel cell, battery and supercapacitor hybrid electric vehicle. *Journal of Power Sources*, 196(4):2351 – 2359, 2011. ISSN 0378-7753. doi: 10.1016/j.jpowsour.2010.09.057. URL http://www.sciencedirect.com/science/article/pii/S0378775310016630. 79

[132] Yunfeng Zhai, Huamin Zhang, Danmin Xing, and Zhi-Gang Shao. The stability of pt/c catalyst in h3po4/pbi {PEMFC} during high temperature life test. *Journal of Power Sources*, 164(1):126 – 133, 2007. ISSN 0378-7753. doi: 10.1016/j.jpowsour.2006.09.069. URL http://www.sciencedirect.com/science/article/pii/S0378775306020568. 150

[133] X. Zhang, CC. Mi, A. Masrur, and D. Daniszewski. Wavelet-transform-based power management of hybrid vehicles with multiple on board energy sources including fuel cell, battery and ultracapacitor. *Journal of Power Sources*, 185(2):1533–43, 2008. 54

# Appendix A

# Drive Cycles

The drive cycles used in this work are presented in this appendix :

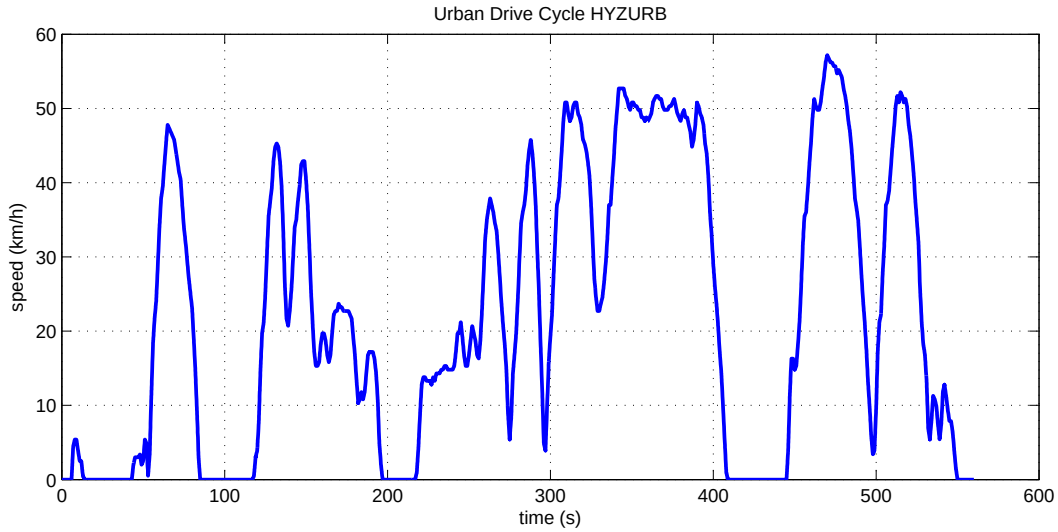


**Figure A.1**: Urban cycle HYZURB

**Urban Drive cycle: HYZURB**

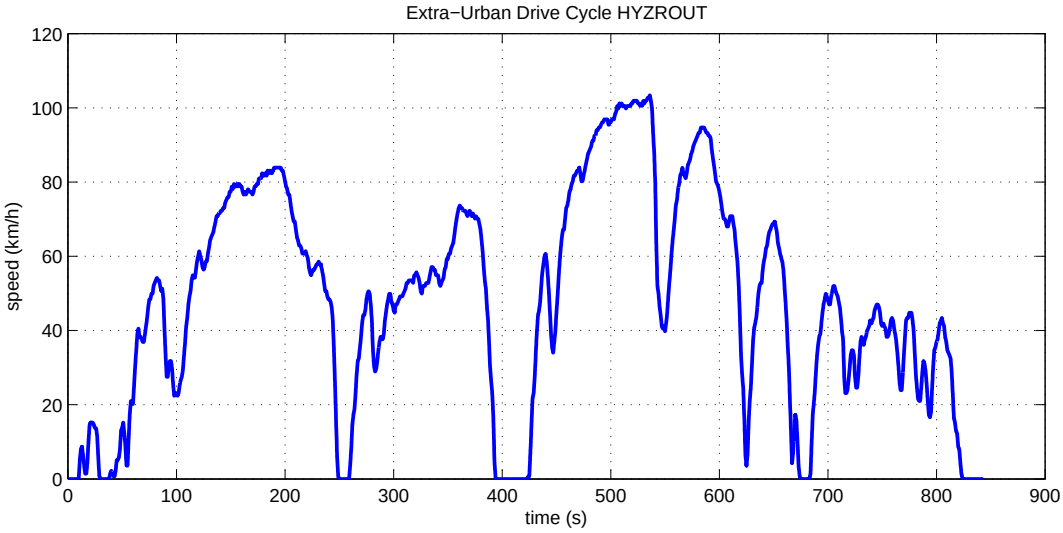


**Figure A.2**: Extra-Urban Cycle HYZROUT

### Extra-urban Drive cycle: HYZROUT

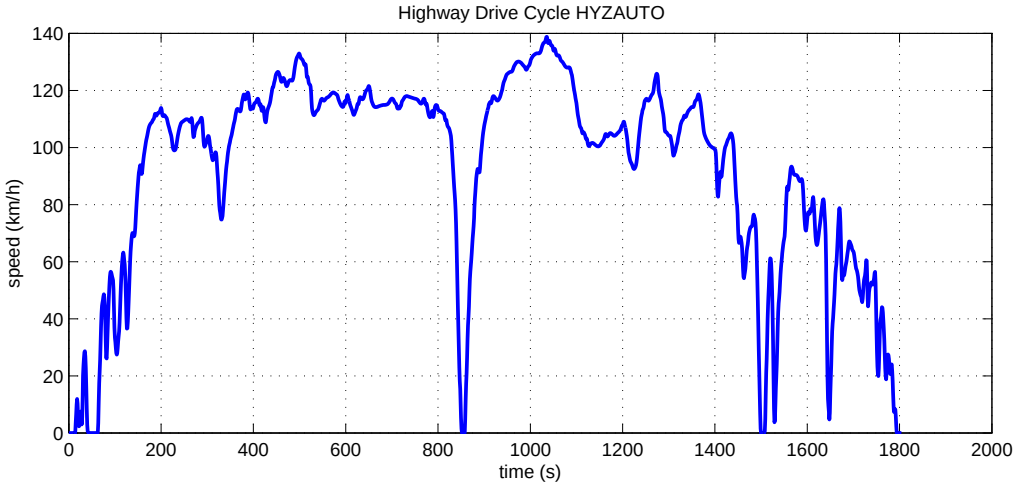


**Figure A.3**: Highway Cycle HYZAUTO

### Highway Drive cycle: HYZAUTO

### Mountain Drive cycle: Grenoble-Chamrousse path

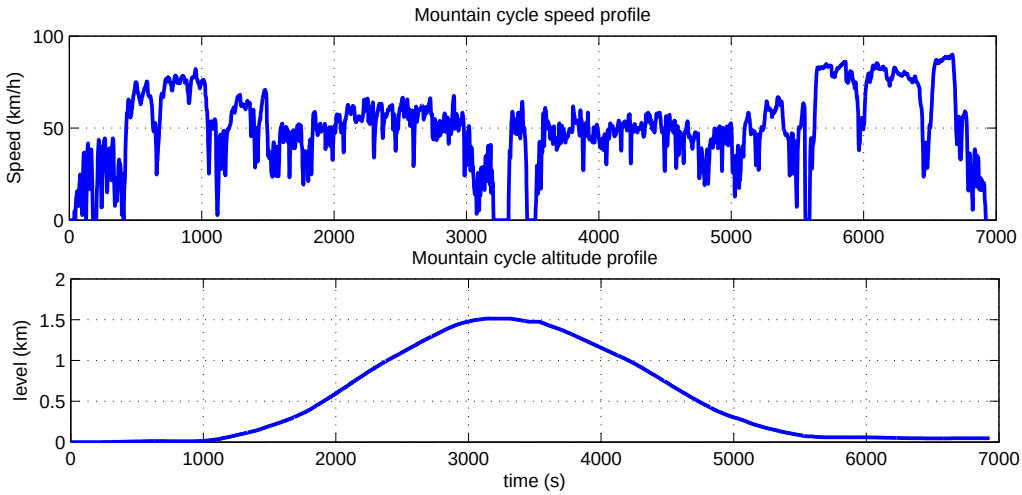


**Figure A.4:** Mountain cycle level profile

# Appendix B

# PROSPAC Prototype

This appendix presents a description of real hybrid system (FC system + battery) prototype. It is used for the development of dynamic models, control law design and tests, and energy management.

The PROSPAC system (figure B.1) is a mobile electric generator system. It can delivers a net power of $5kW$. Besides, the system should respond to the following overload characteristics:

- 100% ($5kW$) in steady state
- 110% during 10 minutes
- 125% during 60 seconds

**Figure B.1**: PROSPAC prototype

The main elements that compose the system and their characteristics are:

**Fuel cell system** The stack embedded in PROPAC is composed of 90 cells and its voltage can vary from 62V to 100V depending on its operating conditions. The nominal operating point (maximum power of the stack) is at $62V$ $105A$ and $6.5kW$.

Pure hydrogen at $1.2\,bar$ is used in the stack with a dead-end configuration. The pressure and flow control at the anode is made by a servovalve that uses the anode inlet pressure information to control the hydrogen flow towards the stack. A purge procedure is done aiming to eliminate the nitrogen and water in liquid state, possibly present in the anode chamber.

On the cathode side, a compressor ensures the air feeding. The air, initially filtered, is compressed and sent to a humidifier, where it is enriched with water vapor before entering the cathode. At the outlet of the cathode, the air depleted in oxygen and rich in water vapor is introduced into the secondary of the humidifier. Coordinated with the

compressor, the valve at the outlet of the humidifier allows to effectuate the pressure control.

The cooling circuit is composed by a pump, a radiator and a thermovalve. The cooling liquid (de-ionized water) cross the stack and pass through the thermovalve. This element has the function to direct the liquid flow in function of the liquid temperature. This procedure is made passively and progressively using a simple strategy:

1. When the temperature of the cooling liquid is lower than $60°C$, the flow is aspirated by the pump and driven towards the hydrogen heater before to get into stack again.

2. When the temperature of the cooling liquid is higher than $70°C$, the flow is driven to a heat exchanger (for a possible heat recover) and afterwards to a ventilated radiator to evacuate the heat. Then, the liquid follows the aforementioned path.

3. When the temperature value is in between $60°C$ and $70°C$, the thermovalve remains in a state where it is partially opened for the two mentioned circuits.

**Batteries** Two battery packs of $24V$ are embedded in the PROSPAC system. They have technology $LiFePO_4$ and were developed by CEA. In this series hybrid configuration, the batteries aims to guarantee the start-up procedure of the FC system and to perform the hybridization in the power split procedure.

Each battery pack has a capacity of $1kWh$, constituting $2kWh$ in total. The operation voltage value is $48V$ in discharge mode and $58V$ for a 100% charged.

**DC/DC converter** A buck converter is used as the interface between the fuel cell stack and the voltage bus (where the batteries are located). The input voltage range is from $60V$ to $100V$, while the output voltage is around $55V$. This converter presents a maximum power of $6.5kW$ in the input at steady state and with a minimum efficiency of 90% when its in the zone between $74V$ $35A$ to $62V$ $105A$.

**Control and supervision** The PROSPAC system is entirely controled in an autonomous and automatic way by a DSPACE fast prototyping device of type microautoboxII. This device ensures the management of all the auxiliaries of the system during all the functioning phases, which are composed by:

- Stopped mode
- Battery mode

- Fuel cell system start-up
- Fuel cell system nominal state
- Hybrid management for the entire system
- Stop procedure of the fuel cell system
- Security stop procedure of the fuel cell system
- Urgency stop procedure

The communication between the auxiliaries and the sensors is done by analogical signals, digital signals and two CAN bus.

# Appendix C

# Parameters of the air supply subsystem

| | | | |
|---|---|---|---|
| $p_{atm}$ | 1 $bar$ | $\varphi$ | 0.0000385 $Nm.rpm^{-1}$ |
| $a$ | 0.0081 | $R$ | 8.31 $Pa.m^3.mol^{-1}.K^{-1}$ |
| $b$ | 0.59 | $V_{cath}$ | 0.00008 $m^3$ |
| $\psi_1$ | 15.3 | $T_{cath}$ | 348 $K$ |
| $\psi_2$ | 15.5 | $\tau_{valve}$ | 0.1 $s$ |
| $\gamma$ | 1.4 | $\zeta_1$ | 9 |
| $J$ | $32.10^{-6}$ $kg.m^2$ | $\zeta_2$ | -4.5 |
| $\alpha$ | 3.45 $Nm.V^{-1}$ | $N_{cell}$ | 80 |
| $C_p$ | 1 $kJ.kg^{-1}.K^{-1}$ | $F$ | 96400 $C.mol^{-1}$ |
| $T_{atm}$ | 300 $K$ | $St_{O_2}$ | 1.8 |
| $\eta_{cp}$ | 0.75 | $\chi_{O_2}$ | 0.21 |
| $k_{hu}$ | 0.0084 $bar.m^{-3}h$ | $k_{FC}$ | 0.008 $bar.m^{-3}h$ |
| $m_{molar}$ | 18 $g/mol$ | $k_{valve}$ | 9 $mm/V$ |

**Table C.1**: Parameters values for the control model

.

# Folio Administratif
# Thèse soutenue devant l'Institut National des Sciences Appliquées de Lyon

**Nom** : NAIFF DA FONSECA **Date de soutenance** : 10/10/13

**Prénoms** : Ramon

**Titre** :Optimization of the Sizing and Energy Management Strategy for a Hybrid Fuel Cell Vehicle Including Fuel Cell Dynamics and Durability Constraints

**Nature** : Doctorat **Numéro d'ordre** :

**Ecole doctorale** : Electronique, Electrotechnique, Automatique

**Spécialité** : Energie et Systémes

**Résumé**: L'hydrogène à travers de l'utilisation des piles à combustible (PAC), est de plus en plus considéré comme une option énergétique possible au secteur des transports grace à ces caractéristiques fonctionnelles. Cependant, la technologie liée à la mise en oeuvre de véhicules alimentés par une pile à combustible n'a pas encore atteint le niveau de maturité requis. Ainsi, ce travail propose de traiter certaines de ces limitations qui existent encore. Plus précisément, trois thèmes représentent les objectifs de ce travail. Le premier thème est abordé à travers l'élaboration d'une méthodologie de dimensionnement adapté à un véhicule hybride à la pile à combustible. Dans une approche systématique, le dimensionnement proposée combine les exigences de performance présents dans les spécifications techniques du véhicule, les algorithmes d'optimisation, l'analyse de la mobilité de la population et la viabilité économique de la conception.

Le deuxième objectif établi a été développé à l'aide d'une approche d'optimisation de la répartition de puissance entre la batterie et le système PAC. Par l'adoption d'une méthode d'optimisation globale combinée à une stratégie de commande prédictive et l'inclusion de la dynamique du système PAC, un algorithme de gestion d'énergie pour des applications de temps réel a été conÃ§u.

Enfin, la durabilité de la pile à combustible a été incluse dans ce travail par l'intégration de sa dynamique de dégradation dans le problème d'optimisation lié à la gestion d'énergie. Cette dynamique représente une contrainte à prendre en considération lors de la répartition de puissance entre le système PAC et la batterie.

**Mots-clés** : Hydrogen, Fuel Cell Vehicle, Optimal Energy Management, Optimal Sizing, Fuel Cell Durability, Non Linear Control

**Laboratoire de Recherches** : AMPERE, UMR CNRS 5005

**Directeur de Thèse** : Eric BIDEAUX

**Président du Jury** : XXXXXXXXXXXXX

**Composition du Jury** Alexandre TROFINO, Christophe TURPIN,Rachid OUTBIB, Luc LORON, Denis CANDUSSO, Eric BIDEAUX, Mathias GERARD, Bruno JEANNERET, Loic BOUILLO,Matthieu DESBOIS-RENAUDIN and Ali SARI